Machine Learning Applied to Prediction of Pavement Performance under Cold Conditions

by

Yunyan Huang

A thesis submitted in partial fulfillment of the requirements for the degree of

Doctor of Philosophy
in
Civil (Cross-Disciplinary)

Department of Civil and Environmental Engineering

University of Alberta

ABSTRACT

Pavements in cold regions face challenging environmental conditions, including prolonged periods of extreme cold, frost heave, and freeze-thaw cycles during late winter and early spring. These factors contribute to premature damage, reduced service life, and increased maintenance costs for cold region pavements. Previous studies have shown that these issues are primarily influenced by environmental factors rather than traffic loads, necessitating specific research for cold region pavements. To address these challenges, a full-scale Integrated Road Research Facility (IRRF) test road was constructed in Edmonton, Alberta, Canada to investigate the impact of the environment on pavement structures and the long-term performance of insulation materials.

Accurately predicting pavement temperature and moisture content within the base and subgrade layers is crucial for assessing the load-bearing capacity and overall performance of cold region pavements. Traditional approaches, including numerical and statistical models, often lack suitability for cold regions or provide limited predictions within the asphalt layer. In this research, artificial intelligence techniques, specifically machine learning models, were employed to predict pavement temperature and moisture content under cold conditions. Environmental data collected from the IRRF test road, along with weather information from a local weather station, were utilized to develop and train the machine learning models. These models exhibited higher accuracy compared to existing models in the literature, showcasing their potential for improved pavement performance prediction.

To investigate the long-term effects of different embankment and insulation materials, Falling Weight Deflectometer (FWD) tests were conducted on the IRRF test road. The FWD test results were analyzed to evaluate structural capacity changes in various sections after five years of operation. Test sections with embankments backfilled with a mixture of tire-derived

aggregate and soil, as well as sections insulated with bottom ash, demonstrated performance comparable to conventional sections, exhibiting lower loss in load-bearing capacity.

Additionally, machine learning models were employed to enhance road management practices. Specifically, they were utilized to estimate the start and end dates of spring load restrictions and winter weight premium. By replacing fixed dates with dynamic predictions derived from frost and thaw depths, road management can become more adaptive and responsive.

In conclusion, artificial intelligence, specifically machine learning, presents a practical and robust method for predicting pavement temperature and moisture content at various depths, thereby enhancing pavement performance assessment. Furthermore, these models can be utilized to improve road management by providing accurate predictions for the timing of seasonal policies. The development of pavement temperature and moisture content prediction models requires a comprehensive dataset incorporating pavement measurements, moisture data, and relevant weather information.

PREFACE

This thesis is an original work by Yunyan Huang and is presented in a paper format. In all the papers, I am the principal investigator and responsible for the data collection, analysis and interpretation of results, and draft manuscript preparation. My supervisor, Dr. Bayat, professionally designed and managed the research program and was the corresponding author. **Chapter 4** has been published as Huang, Y., Molavi Nojumi, M., Hashemian, L. and Bayat, A., 2021. Performance evaluation of different insulating materials using field temperature and moisture data. Transportation Research Record, 2675(9), pp.595-607. **Chapter 5** has been published as Huang, Y., Molavi Nojumi, M., Hashemian, L. and Bayat, A., 2023. Evaluation of a Machine Learning Approach for Temperature Prediction in Pavement Base and Subgrade Layers in Alberta, Canada. Journal of Transportation Engineering, Part B: Pavements, 149(1), p.04022076. **Chapter 6** has been submitted to the Journal of Applied Remote Sensing in 2023. **Chapter 7** has been published as Huang, Y., Molavi Nojumi, M., Ansari, S., Hashemian, L. and Bayat, A., 2023. Evaluation of machine learning approach for base and subgrade layer temperature prediction at various depths in the presence of insulation layers. International Journal of Pavement Engineering, 24(1), p.2180640. **Chapter 8** has been published as Huang, Y., Molavi Nojumi, M., Ansari, S., Hashemian, L. and Bayat, A., 2023. Evaluating the use of machine learning for moisture content prediction in base and subgrade layers. Road Materials and Pavement Design, pp.1-19. **Chapter 9** has been submitted to the Journal of Testing and Evaluation in 2023. **Chapter 10** has been published as Huang, Y., Molavi Nojumi, M., Hashemian, L. and Bayat, A., 2023. Structural Capacity of Sections Constructed with Different Waste and Recycled Embankment and Insulation Materials at the IRRF Test Road after Five Years of Operation. Transportation Research Record, p.03611981231159874. **Chapter 11** has been submitted to the Journal of the Transportation Research Board.

DEDICATION

To

my parents, my husband

and

my children

ACKNOWLEDGEMENTS

I would like to express my sincere gratitude to my supervisor, **Dr. Bayat**, for his invaluable guidance, support, and encouragement throughout my thesis research. His insightful comments, constructive feedback, and unwavering commitment have been essential in shaping my academic and personal development.

I would also like to extend my thanks to my committee members, **Dr. Hashemian** and **Dr. Pulisci**, for their insightful feedback and constructive criticism that helped me improve my thesis significantly. Their guidance and support have been crucial in my academic journey.

I am grateful to **Dr. Molavi Nojumi**, **Dr. Ansari**, and **Dr. Moghaddam**, for their support and encouragement throughout my academic career. Their knowledge and expertise have been invaluable in shaping my understanding of the subject matter and improving the quality of my research.

Finally, I would like to thank my colleagues and friends, Farshad Kamran, Manjunath Basavarajappa, Amirhossein Ghasemirad, Mohamed Saleh, Thomas Johnson and all the others, for their unwavering support, love, and encouragement throughout my academic journey. Their support has been essential in keeping me motivated and focused on my goals.

Thank you all for your support and encouragement, and for making my academic journey a memorable and rewarding experience.

TABLE OF CONTENTS

Abstract ii

Preface iv

Dedication v

Acknowledgements vi

Table of Contents vii

List of Tables xiv

List of Figures xvii

Chapter 1. Introduction 1

1.1. Statement of the Problem 1

1.2. Research Objectives 3

1.3. Research Hypothesis 4

1.4. Research Methodology 4

1.5. Structure of Dissertation 9

1.6. Correlation between Different Chapters 11

Chapter 2. Literature Review 14

2.1. Environmental Factors for pavement Performance 15

2.1.1. Pavement Temperature 15

2.1.2. Moisture Content 17

2.2. Bottom Ash 20

2.3. Seasonal Polices for Road Management 23

2.4. Existing Models for Pavement Performance Prediction and Management 25
2.4.1. Pavement Temperature Prediction Models 25
2.4.2. Moisture Content Prediction Model.....26
2.4.3. Spring Load Restrictions and Winter Weight Premiums Dates Prediction Models 29
2.5. Application of Artificial Intelligence for Prediction Performance in Road.....32
2.6. FWD Test.....34
Chapter 3. The Integrated Road Research Facility Test Road 37
3.1. Instruments.....40
3.2. Data Availability.....41
Chapter 4. Long-term Analysis of Environmental Factors Variations in the Test Sections 46
4.1. Abstract.....46
4.2. Introduction.....47
4.3. Background.....50
4.4. Data Collection and Analysis.....54
4.4.1. Control Section 54
4.4.2. Bottom Ash Section 57
4.4.3. Polystyrene Section.....60
4.5. Discussion.....63
4.6. Conclusions.....71

4.7. Recommendations for Future Work....73
4.8. Acknowledgments....74
Chapter 5. Application of Machine Learning Model in Temperature Prediction of Unbonded Material Layers....75
5.1. Abstarct....75
5.2. Introduction....76
5.3. Description of the IRRF Test Road Facility....81
5.4. Procedure for Model Development....83
5.4.1. Data Availability....84
5.4.2. Machine Learning Algorithms....85
5.4.3. Sensitivity Analysis....85
5.4.4. Training Data and Model Validation....89
5.5. Comparison of Machine Learning Models with Conventional Model....91
5.6. Conclusions and Recommendations....99
Chapter 6. Multi-depth Temperature Prediction....102
6.1. Abstract....102
6.2. Introduction....103
6.3. Data Collection....107
6.4. Model Development....108
6.4.1. Data Availability....111
6.4.2. Sensitivity Analysis....111

6.4.3. Model Validation 116
6.5. Comparison of Performance Between ML Models and Existing Models 118
6.5.1. Average Daily Temperature 118
6.5.2. Minimum Daily Temperature 123
6.5.3. Maximum Daily Temperature 128
6.6. Conclusions 132
Chapter 7. Temperature Prediction at the Presence of Insulating Materials 134
7.1. Abstract 134
7.2. Introduction 135
7.3. Procedure for Model Development 138
7.3.1. Data Availability 141
7.3.2. Statistical Analysis of Pavement Temperature 144
7.3.3. Machine Learning Algorithms 147
7.3.4. Sensitivity Analysis 149
7.3.5. Validation of the Model 152
7.4. Comparison of the Machine Learning Results with a Statistical Model 154
7.5. Discussion 162
7.6. Conclusions 163
Chapter 8. Evaluating the Use of Machine Learning for Moisture Content Prediction in Base and Subgrade Layers 166
8.1. Abstract 166

8.2. Introduction 167
8.3. Description of the IRRF Test Road Facility 171
8.4. Model Development 173
8.4.1. Data Availability 176
8.4.2. Sensitivity Analysis 177
8.4.3. Model Validation 181
8.5. Comparison of Machine Learning Results with an Existing Model 185
8.6. Limitations of the Proposed Model 190
8.7. Conclusion 192
Chapter 9. Model Development for Simultaneous Prediction of Temperature and Moisture Content 194
9.1. Abstract 194
9.2. Introduction 195
9.3. The Integrated Road Research Facility Test Road 199
9.4. Methods 201
9.4.1. Algorithms 205
9.4.2. Statistical Analysis of Pavement Temperature and Moisture Content 205
9.4.3. Model Development 206
9.5. Results and Discussion 210
9.5.1. Average Daily Pavement Temperature Prediction 211
9.5.2. Average Daily Moisture Content Prediction 214

9.5.3. Limitation of the Proposed ANN Model 218
9.6. Conclusions....219
Chapter 10. Changes in Structural Capacity after Five Years of Operation....221
10.1. Abstract....221
10.2. Introduction....222
10.3. Integrated Road Research Facility Test Road....225
10.4. Falling Weight Deflectometer Testing....228
10.5. Environmental Factors....229
10.6. Results and Discussion....231
10.6.1. Deflection Bowls....231
10.6.2. Maximum Deflection....232
10.6.3. Back-Calculated Subgrade Modulus....234
10.6.4. Back-Calculated Effective Modulus of Pavement....237
10.6.5. Structural Number....239
10.6.6. Analysis of Variance....240
10.7. Summary and Conclusions....241
Chapter 11. Applicaion of the Machine Learning Model to Determine Spring Load restrictions and Winter Weight Premium....246
11.1. Abstract....246
11.2. Introduction....247
11.3. Machine Learning Model Development....250

11.4. Air Temperature 255
11.5. Comparison of Measured and Estimated Frost and Thawing Depths 257
11.6. Moisture Content Variation of Base and Subgrade 259
11.7. Discussion 261
11.7.1. Actual Start and End Dates of WWP and SLR 261
11.7.2. Observed Moisture Content at the Start and End of the Day for WWP and SLR 263
11.7.3. Limitations of the Machine Learning Models 264
11.8. Conclusion 265
Chapter 12. Conclusions and Reconmmendations 268
12.1. Conclusions 268
12.2. Academic and Industry Contributions 271
12.2.1. Academic Contributions 271
12.2.2. Industry Contributions 272
12.3. Limitations 273
12.4. Recommendations 274
Bibliography 276

LIST OF TABLES

Table 1-1: Research objectives in chapters 5 to 9.....12

Table 2-1: Spring load restrictions dates in some Canadian provinces (Canada Cartage Group of Companies, 2021).....24

Table 3-1: Temperature data availability for different pavement test sections. 44

Table 3-2: Availability of moisture content data for the control section. 45

Table 4-1: Properties of materials used in integrated road research facility test road construction. 52

Table 4-2: Thermal characteristics of integrated road research facility test road. 64

Table 4-3: Comparison of rates of temperature change of test sections with control section for different layers. 66

Table 4-4: Moisture content and change ratio. 70

Table 5-1: Data availability for machine learning analysis. 85

Table 5-2: Machine learning algorithms used for temperature prediction. 86

Table 5-3: Correlation coefficients for climatic and time-dependent parameters. 87

Table 5-4: Impact of contributing parameters on the model performance. 90

Table 5-5: Performance of different machine learning algorithms for temperature prediction in GBC and subgrade layers.....91

Table 5-6: Comparison of the performance of machine learning and literature model from Heydinger (2003). 95

Table 5-7: Comparison of accuracy of temperature prediction in winter for machine learning model and conventional predictive model (Heydinger, 2003) given in Equation 5-1.....96

Table 6-1: Data availability for development of ML models. 111

Table 6-2: Correlation coefficients of air temperature, solar radiation, relative humidity, wind speed, and day of the year with subgrade temperature. 112

Table 6-3: Results of Machine learning model for different combinations of input parameters. 114

Table 6-4: Comparison of performance between ML models and literature models for prediction of average daily asphalt and soil temperature (Asefzadeh et al., 2017; Heydinger, 2003b). 121

Table 6-5: Comparison of performance between ML models and existing models for prediction of minimum daily asphalt and soil temperature (Asefzadeh et al., 2017; Mohseni, 1998). ..126

Table 6-6: Comparison of performance between ML models and existing models for prediction of maximum daily asphalt and soil temperature (Asefzadeh et al., 2017). 128

Table 7-1: Properties of materials used in insulation sections. 143

Table 7-2: Temperature data availability for the pavement test sections (BA and PS). 144

Table 7-3: Statistical analysis results were collected from two insulation sections. 146

Table 7-4: The influence of parameter inclusion on model performance. 151

Table 7-5: Machine learning training and testing results. 153

Table 7-6: Comparison of the performance of machine learning and statistical model models. 162

Table 8-1: Availability of VWC data for training and validation datasets to use in development of machine learning models. 177

Table 8-2: Impact of parameters on model performance. 180

Table 8-3: Summary of machine learning model training and test comparison results.....182

Table 8-4: Performance comparison at different depths.....187

Table 9-1: Availability of data for model development.....200

Table 9-2: Statistical parameters for pavement temperature and moisture content.....206

Table 9-3: ANN model's training results.....209

Table 9-4: Performance of different algorithms for predicting pavement temperature and moisture content.....210

Table 9-5: Pavement temperature performance comparison between ANN and the statistical model.....213

Table 9-6: Moisture content prediction performance comparison between ANN and the statistical model 218

Table 10-1: Back-calculated subgrade moduli for the various IRRF test road sections.....236

Table 10-2: Back-calculated effective moduli of the pavement for the various sections.....238

Table 10-3: Structural numbers of the various sections.....240

Table 10-4: Analysis of variance results for the integrated road research facility test road..241

Table 11-1: Grain size distribution of GBC and subgrade soil used in IRRF test road.....253

Table 11-2: Performance of the ML model developed.....255

Table 11-3: Measured and estimated start and end dates of WWP. 262

Table 11-4: Measured and estimated start and end dates of SLR.....262

LIST OF FIGURES

Figure 1-1: The research flowchart 5

Figure 2-1: Conceptual pavement stiffness variations due to freezing and thawing (Salour, 2015) 15

Figure 2-2: Graphical illustration of the five temperature quintiles used in the MEPDG to determine HMA-mixture properties for load-related distresses (AASHTO, 2008) 17

Figure 2-3: Temperature-dependent unfrozen water contents in soils of different grain sizes (a) and in sandy soil with different contents of kaolinite (b) and montmorillonite (c) clay (Chuvilin et al. 2020) 19

Figure 2-4: Insulated materials used in the IRRF test road (a) polystyrene board and (b) bottom ash 21

Figure 2-5: Subgrade moisture content and rainfall (Hedayati and Hossain 2015). 28

Figure 2-6: Subgrade resilient modulus and soil moisture content (Haghi 2019) 28

Figure 2-7: Decisions regarding Spring Load Restrictions guided by freezing and thawing depth forecasts (Baïz et al., 2008; Bao et al. 2019, 2021) 32

Figure 2-8: Arrangement of FWD equipment and sensor positions during field testing 35

Figure 3-1: (a) Test and control sections in the IRRF test road and (b) the cross-section of the IRRF test road 39

Figure 3-2: Particle size distribution in (a) granular base course layer and (b) subgrade layer 40

Figure 4-1: Cross section of pavement layers and as-built depth of thermistors and moisture probes 51

Figure 4-2: Moisture content variation at a depth of 0.48 m (in granular base course layer) and precipitation over time (2015 data) 54

Figure 4-3: Daily ambient temperature and average daily temperature from sensors installed in the base layer and the subgrade layer (control section) 55

Figure 4-4: Temperature variation with depth in the control section of the Integrated Road Research Facility test road 56

Figure 4-5: Volumetric water content (VWC) and temperature in the control section: (a) depth of 0.8 m and (b) depth of 1.8 m 57

Figure 4-6: Daily ambient temperature and average temperature recorded at sensors installed in base layer (depth 0.72 m) and subgrade layer (depth 1.80 m) in Integrated Road Research Facility test road section insulated with bottom ash 58

Figure 4-7: Temperature variation along depth across pavement structure in the bottom ash section 58

Figure 4-8: Volumetric water content (VWC) and temperature in the bottom ash test section measured at a depth of 1.8 m 60

Figure 4-9: Variation in daily ambient temperature and average temperature over time at various depths in the 10 cm polystyrene test section 61

Figure 4-10: Temperature variation along depth across pavement structure in the 10 cm polystyrene section 62

Figure 4-11: Change of Volumetric water content (VWC) and temperature in the 10 cm polystyrene section at depths of (a) 0.8 m and (b) 1.8 m 62

Figure 4-12: Maximum frost depths for test sections from February 2017 to January 2018 ..68

Figure 4-13: Temperature and volumetric water content (VWC) at a depth of 1.8m (subgrade) for control section, bottom ash test section, and polystyrene test section 70

Figure 5-1: IRRF test road pavement structure, showing the location of TDRs embedded in the GBC and subgrade layers.....82

Figure 5-2: Particle size distribution in (a) GBC layer and (b) subgrade layer 83

Figure 5-3: Procedure for developing machine learning predictive models.....84

Figure 5-4: GBC temperature versus (a) air temperature; (b) solar radiation; (c) precipitation; and (d) day of the year 89

Figure 5-5: Comparison between measured and predicted pavement temperatures at depths of (a) 0.5 m; (b) 0.7 m; (c) 0.8 m; (d) 1.8 m; and (e) 2.7 m 94

Figure 5-6: Comparison of temperature predictions using (a) machine learning; and (b) Equation 5-5 temperature data at a depth of 0.50 m 97

Figure 6-1: Cross-section of the test road indicating the location of TDRs and thermistors.108

Figure 6-2: Model building flow chart.....110

Figure 6-3: Relationship between average daily subgrade temperature (°C) and (a) average daily air temperature (°C), (b) average daily solar radiation (W/m^2), (c) average daily relative humidity (%), (d) average daily wind speed (km/hr), and (e) day of the year.....113

Figure 6-4: Model validation for (a) average daily temperature, (b) minimum daily temperature, and (c) maximum daily temperature 117

Figure 6-5: Comparison of the measured and predicated values (using ML model) of average daily road temperature at depths of (a) 0.02 m, (b) 0.09 m, (c) 0.17 m, (d) 0.25 m, (e) 0.50 m, (f) 0.70 m, (g) 0.80 m, (h) 1.80 m, and (i) 2.70 m 120

Figure 6-6: Comparison of predicted and measured average daily temperature for the (a) parametric model (Heydinger, 2003b) and (b) statistical model (Asefzadeh et al., 2017) with the Exponential GPR model.....123

Figure 6-7: Comparison of the measured and predicted minimum daily temperature at depths of (a) 0.02 m, (b) 0.09 m, (c) 0.17 m, (d) 0.25 m, (e) 0.50 m, (f) 0.70 m, (g) 0.80 m, (h) 1.80 m, and (i) 2.70 m.....125

Figure 6-8: Comparison of the predicted minimum daily temperatures and measured minimum daily temperature for (a) statistical model(Asefzadeh et al., 2017b), (b) SHRP (Mohseni, 1998), and (c) C-SHRP (Mohseni, 1998).....126

Figure 6-9: Comparison of the measured and predicted maximum daily road temperature at a depth of (a) 0.02 m, (b) 0.09 m, (c) 0.17 m, (d) 0.25 m, (e) 0.50 m, (f) 0.70 m, (g) 0.80 m, (h) 1.80 m, and (i) 2.70 m.....131

Figure 6-10: Comparison of predicted and measured maximum daily temperature for ML model and statistical model (Asefzadeh et al., 2017) 132

Figure 7-1: Procedure for developing machine learning predictive models.....140

Figure 7-2: Schematic illustration of the pavement cross-section at the IRRF test road for test sections containing BA and PS insulation layers.....142

Figure 7-3: Pavement temperature at a depth of 1.4 m versus (a) air temperature, (b) solar radiation, (c) precipitation, and (d) day of the year 151

Figure 7-4: Comparison of measured and predicted temperature in the bottom ash section for depths of (a) 0.72 m, (b) 1.40 m, (c) 1.85 m, (d) 2.83 m, and (e) 3.36 m.....157

Figure 7-5: Measurements and predicted temperature in the polystyrene section for depths of (a) 0.64 m, (b) 0.80 m, (c) 1.80 m, (d) 2.25 m, and (e) 3.25 m.....159

Figure 7-6: Pavement temperature predicted using the machine learning model and statistical model in the (a) BA and (b) PS sections.....161

Figure 8-1: Pavement structure and location of time-domain reflectometers installed in the base and subgrade of the IRRF test road.....172

Figure 8-2: Grain size distribution of the granular base course and subgrade soil used in the construction of the IRRF test road.....173

Figure 8-3: Procedure for implementing predictive machine learning models 174

Figure 8-4: Visualisation of moisture content data (depth 0.7 m) correlations with (a) pavement temperature, (b) precipitation, and (c) day of the year 178

Figure 8-5: Average daily soil moisture content predicted results comparison at (a) 0.5 m, (b) 0.7 m, (c) 0.8 m, (d) 1.8 m, and (e) 2.7 m.....184

Figure 8-6: Predicted versus measured moisture content in five different depths. 185

Figure 8-7: Comparison of measured average daily volumetric moisture content and VWC results based on the machine learning model and a literature model (semi-logarithmic function developed by Teltayev and Suppes (2019) based on initial moisture content and temperature) at depths of (a) 0.5 m, (b) 0.7 m, (c) 0.8 m, and (d) 1.8 m. 189

Figure 9-1: Cross-section of pavement layers and location of TDR embedded in the base and subgrade layers.....199

Figure 9-2: Grain size distribution of the (a) granular base course and (b) subgrade soil.....201

Figure 9-3: Flowchart for training models to predict pavement temperature and moisture content.....202

Figure 9-4: The neural network diagram used in this model development 204

Figure 9-5: Correlation between inputs and outputs at a depth of 0.50 m (a) moisture content vs. air temperature, (b) moisture content vs. day of the year, (c) pavement temperature vs. air temperature, and (d) pavement temperature vs. day of the year 208

Figure 9-6: Results of the model with Levenberg-Marquardt algorithm (a) training results, (b) validation results, (c) test results, and (d) overall results 209

Figure 9-7: Average daily pavement temperature predicted results comparison at (a) 0.5 m, (b) 0.7 m, (c) 0.8 m, and (d) 1.8 m 213

Figure 9-8: Pavement temperature predicted using (a) the ANN model and (b) the statistical model 214

Figure 9-9: Average daily moisture content predicted results comparison at (a) 0.5 m, (b) 0.7 m, (c) 0.8 m, and (d) 1.8 m 217

Figure 10-1: Test and control sections in the Integrated Road Research Facility test road...226

Figure 10-2: Cross-section of the Integrated Road Research Facility test road showing test and control sections and sensor placement 227

Figure 10-3: Variation in pavement temperature with depth in the (a) insulation section and (b) tire section 230

Figure 10-4: Pavement moisture content with depth for CS2 230

Figure 10-5: Deflection measured by all nine geophones for tire embankment sections backfilled with tire-derived aggregate (TDA) from passenger and light-truck tires (PLTT), TDA from off-the-road (OTR), and PLTT/soil mixture, as well as the control section (CS1) August 20 2020 231

Figure 10-6: Deflection measured by all nine geophones for sections containing different insulation layers (bottom ash, 10 cm polystyrene [Poly-10], and 5 cm polystyrene [Poly-5], as well as the control section) for August 20 2020 232

Figure 10-7: Maximum deflection D_0 measured 0 mm from the load plate.....233

Figure 10-8: Maximum deflection D_9 measured 1800 mm from the load plate.....234

Figure 11-1: (a) Cross-section of the IRRF test road, and (b) CS 650 TDR 252

Figure 11-2: Procedure for developing machine learning predictive models (Huang et al., 2023a; Huang et al., 2023).....255

Figure 11-3: (a) Average daily air temperature and (b) average monthly air temperature...257

Figure 11-4: Measured and estimated frost and thaw depths from 2013 to 2014 and 2016 to 2017.....259

Figure 11-5: Average daily moisture content variation in the pavement structure from (a) 2013 to 2014 and (b) 2016 to 2017.....261

CHAPTER 1.INTRODUCTION

1.1. STATEMENT OF THE PROBLEM

In cold regions, pavements are subject to harsh environmental conditions including long periods of extremely low air temperature, frost heave, and freeze-thaw cycles during late winter and early spring. In winter, the air temperature drops sharply resulting in pavement temperatures falling below 0°C, the freezing point of water. Ice lenses form in the base and subgrade layers, which can result in differential frost heave in the pavement structure. Frost heave negatively affects the road's ride quality. Temperatures increase in the late winter or early spring, and ice lenses turn into liquid water again. However, as the pavement temperature rises from top to bottom, the sublayer remains in a frozen state with low permeability; the subgrade layer begins to accumulate water, and the moisture content of the soil reaches the maximum value, resulting in the pavement's bearing capacity to fall to the minimum value (Bayat, 2009). Both unbound pavement materials and thin pavements are susceptible to moisture content, and higher moisture content in the thawing period can lead to lower load capacity (Bayat, 2009; Salour, 2015). To safeguard pavements during the thawing period, seasonal policies like spring load restrictions (SLR) and winter weight premiums (WWP) have been implemented in northern American regions. Nevertheless, these policies adhere to fixed dates each year for imposing restrictions, irrespective of the actual structural capacity of the pavement (Asefzadeh et al., 2016). Pavements in cold regions generally exhibit premature damage, have shorter service lives, and incur higher maintenance costs, among other issues (Tighe et al., 2006), and those problems cannot be addressed by studies conducted in warm regions.

Pavement temperature and moisture content are two environmental parameters that have been shown to dominate the material properties of pavement and its structural capacity (Bayat, 2009;

Salour, 2015). Thus, a better understanding of the environmental factors within the pavement structures could improve road management. A full-scale Integrated Road Research Facility (IRRF) test road was constructed in Edmonton, Alberta, Canada to investigate the environmental factors within pavement structures and the long-term performance of insulation materials. Sensors were installed at multiple depths to monitor the environmental factors within the pavement structure.

Insulation layers have long been employed as a standard method to safeguard pavement structures from extreme cold conditions. In contemporary pavement construction, an environmentally friendlier insulation material, known as bottom ash, has also found its place. Bottom ash, a byproduct of coal combustion in electricity generation, primarily comprises silica, alumina, and iron. Nevertheless, the exploration of bottom ash's utility as an insulation layer for safeguarding the subgrade against frost heave in cold regions only commenced about two decades ago (Hashemian and Bayat, 2016). Previous studies have demonstrated that bottom ash can effectively shield the subgrade from freezing (Haghi et al., 2014, 2016, 2018). Nevertheless, the long-term implications of bottom ash on moisture content fluctuations within the subgrade layer and variations in structural capacity remain largely unexplored.

Artificial intelligence techniques, specifically machine learning models, have increasingly gained attention in pavement performance prediction. Machine learning models have been applied to predict the pavement temperature within the asphalt layer (Gungor and Al-Qadi, 2018; Molavi Nojumi et al., 2022; Qiu et al., 2020; Solaimanian and Kennedy, 1993) and the soil moisture content for agricultural applications. Therefore, artificial intelligence techniques should be a practical option to help understand the pavement temperature and moisture content within pavement structures under cold conditions.

In summary, a thorough examination of the existing literature in this domain underscores the following primary gaps that demand attention and resolution:

- Long-term performance and effects of the bottom ash on moisture content and structural capacity are unknown.
- Existing prediction models only focus on estimating the pavement temperature within the asphalt layer.
- No temperature prediction model has yet taken the insulated layers into account.
- No existing prediction model can predict base and subgrade layers' moisture content in cold regions for the whole year.
- The start and end dates of the SLR and WWP are fixed dates every year.

1.2. RESEARCH OBJECTIVES

The primary objective of this study was to examine variations in environmental factors affecting pavement structures and utilize machine learning to predict these factors, particularly in cold conditions such as those found in Edmonton. We utilized years of Falling Weight Deflectometer (FWD) test results to assess the variations in structural capacities of the test road. The application of the machine learning model aimed to enhance road network management and determine the commencement and conclusion dates of seasonal policies, specifically SLR and WWP.

To accomplish this goal, the following tasks were set out to be achieve:

- Qualify the long-term performance and effects of the bottom ash on moisture content and structural capacity.
- Develop machine learning models for pavement temperature prediction.
- Develop pavement temperature prediction models tailored for special pavement structures.
- Assess the structural capacity changes of the IRRF test road after five years of operation.

- Utilize machine learning models to optimize road management practices by directly predicting the commencement and conclusion dates of spring load restrictions and winter weight premiums based on frost and thaw depths.

1.3. RESEARCH HYPOTHESIS

Based on the detailed research objectives, the following hypotheses were devised for examination within the scope of this research:

- Bottom ash can protect the subgrade layer from freezing and have a positive influence on the structural capacity.
- The variation in moisture content within base and subgrade layers is strongly impacted by environmental factors.
- Pavement temperature prediction can be achieved by utilizing factors such as air temperature, solar radiation, and the day of the year.
- Prediction of moisture content in base and subgrade layers is possible through consideration of air temperature, precipitation, and the day of the year.
- The test section insulated by the bottom ash layer demonstrates superior performance compared to the conventional section, exhibiting significantly higher structural capacities following years of operational testing.
- Machine learning models can accurately determine the commencement and conclusion dates of SLR and WWP by frost and thaw depths, offering a valuable tool for optimizing road management practices.

1.4. Research Methodology

Figure 1-1 is the flowchart of this research. This research was divided into three phases.

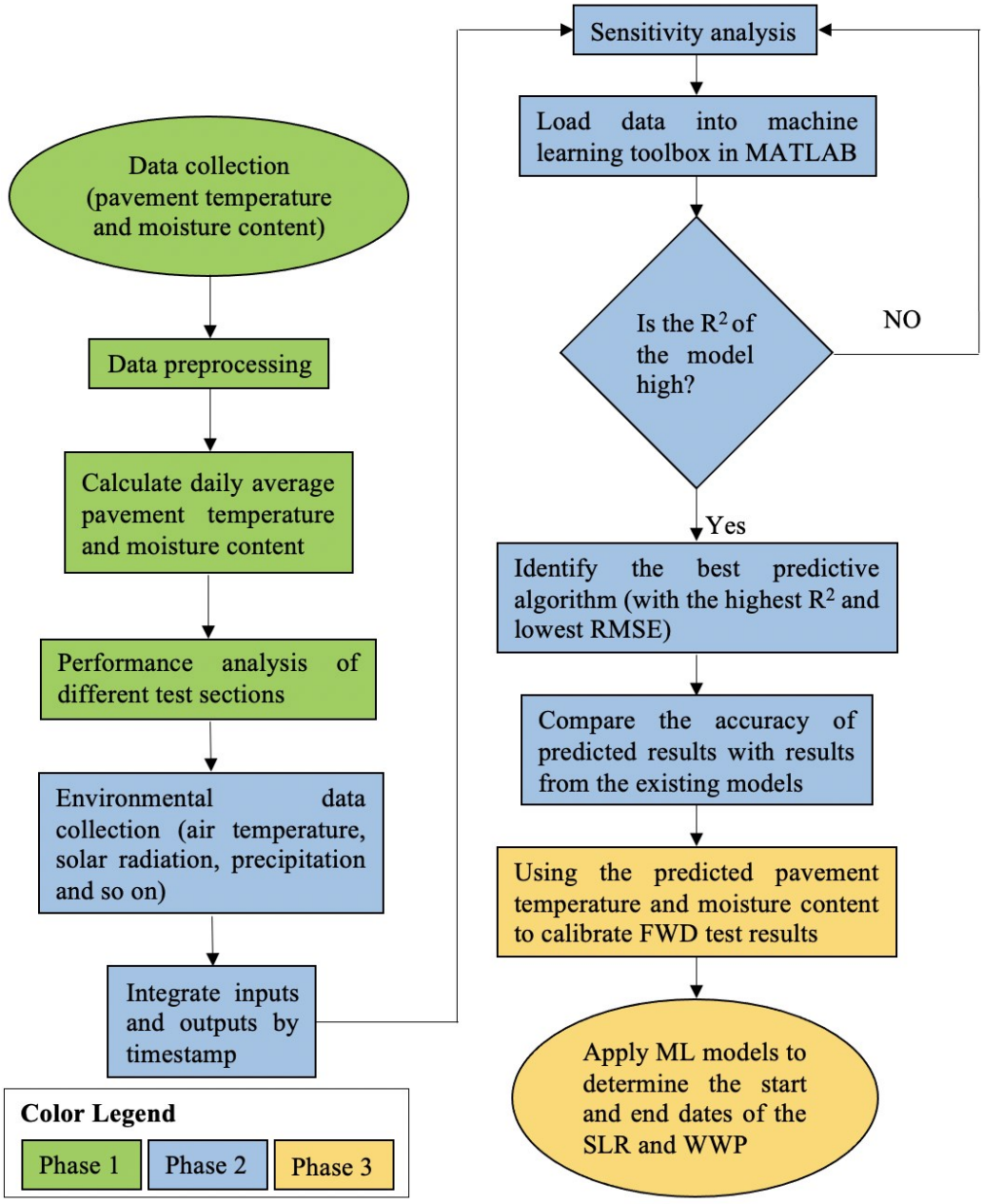

Figure 1-1: The research flowchart

Phase 1 Environmental data, pavement temperature, and moisture content were collected from sensors installed in the IRRF test road. This data underwent preprocessing to eliminate noise and irrelevant values. The years of environmental data were then utilized to assess the performance of various sections within the IRRF test road and to discuss the long-term effects of the bottom ash layer on pavement temperature and moisture content.

Phase 2 Machine Learning Model Development: Figure 1-1 is the flow chart for machine learning model development. In this phase, environmental factors, including air temperature, solar radiation, and precipitation, were gathered from the Oliver AGDM (the Environment Canada weather station located closest to the test road) and integrated with environmental data by timestamp. A sensitivity analysis was conducted to explore the relationships between these inputs and outputs. Subsequently, we harnessed the capabilities of two MATLAB toolboxes: Regression Leaner and Statistics, and Machine Learning Toolbox 11.1, in addition to Neural Net Fitting and Neural Network Toolbox 10.0, to construct machine learning models for the prediction of pavement temperature and moisture content.

The coefficient of determination (R^2) and the root-mean-square error (RMSE) were utilized to assess the performance of the machine learning models. Asefzadeh et al. (2017) previously developed a statistical model to predict daily average pavement temperature within the asphalt layer, achieving an R^2 of 0.849. The rationale for applying machine learning models for pavement temperature prediction was to enhance the accuracy of temperature forecasts, with an anticipated benchmark of 0.849. Teltayev and Suppes (2019) developed a statistical model to predict the unfrozen moisture content in winter, and the R^2 value was greater than 0.92 at a depth above 1.40 m, while the R^2 value was 0.72 at a depth of 1.75 m below the road surface. Thus, the expected threshold for moisture content was 0.92 for depths above 1.40 m.

The training outcomes of the machine learning algorithms being evaluated, including regression trees, support vector machines (SVMs), Gaussian process regression (GPR) models, ensemble trees, and linear regression models, were also subjected to a comparative analysis. In the context of this research, it's crucial to evaluate the strengths and weaknesses of each machine learning (ML) algorithm employed to justify their selection. Linear regression models, for instance, have the limitation of assuming linear relationships between predictors and the target parameter, potentially leading to less accurate predictions compared to other algorithms

(Bonaccorso, 2018). Within the regression learner, four subcategories of linear regression models are available: linear, interaction linear, robust linear, and stepwise linear.

Moving to regression trees, this method involves establishing a series of rules and conditions to split data at various stages. It encompasses roots, branches, and leaves, with predictions extracted from the leaf node at the path's end. The granularity of the resulting tree can be adjusted using parameters like minimum leaf size, allowing for the creation of fine, medium, or coarse trees (Bonaccorso, 2018). It's important to clarify that hyperparameter optimization for overfitting control, beyond the k-fold approach, should be addressed in the methodology section.

Support Vector Machines leverage kernel functions to transform input data into a higher-dimensional space, optimizing the separation between two classes. The choice of kernel type, such as linear, quadratic, or cubic, plays a pivotal role. SVM models also fall into fine, medium, and coarse Gaussian categories based on their kernel scale (Cortes et al., 1995; Zeiada et al., 2020).

Gaussian Process Regression models, characterized by joint Gaussian distributions among random variables, offer non-parametric flexibility. These models, grouped into four categories based on kernel functions, provide superior uncertainty estimations and response reliability compared to kernel-dependent regression models (Bonaccorso, 2018; Swiler et al., 2020; Zeiada et al., 2020).

Lastly, ensemble models involve combining similar or different algorithms to enhance prediction accuracy. Ensemble trees encompass two categories: bagged trees, which create multiple models and merge them into a decision tree, and boosted trees, which improve performance by combining models using specific cost functions (Bonaccorso, 2018; Zeiada et

al., 2020). Further comprehensive information on these algorithms is available in existing literature (Bonaccorso, 2018; Cortes et al., 1995; Swiler et al., 2020; Zeiada et al., 2020).

Cross-validation was employed as a preventive measure against overfitting. In this method, the testing data were initially divided into n groups, with five groups utilized in this particular case. Of these, (n-1) groups were designated for training purposes, while the remaining group was set aside for testing. This process was iterated n times, and the average test error was computed across all n folds, where n was 5 in this research.

Phase 3 Application of Machine Learning Models: Machine learning models were applied to estimate the structural capacities within the IRRF test and determine the start and end dates of spring load restrictions and winter weight premium policies. For the assessment of structural capacities within the IRRF test road sections, we leveraged Falling Weight Deflectometer (FWD) tests, a nondestructive deflection testing method widely used in pavement engineering. FWD tests involve the measurement of pavement surface deflections under a load. These deflections are collected from various sensors strategically placed across the pavement surface. By employing different distances between the sensors and the loading plate during FWD tests, we obtained a dataset of deflection measurements. These measurements were instrumental in our research as they allowed us to perform back-calculations to determine both the subgrade modulus, pavement modulus and effective structural number, critical parameters for assessing the structural integrity of pavements. We utilized the pavement temperature and moisture content data at the test date through machine learning models to calibrate the results obtained from Falling Weight Deflectometer tests. This back-calculation process is in accordance with the guidelines outlined by AASHTO (1993).

Furthermore, in this phase, we extended the utility of machine learning models to predict pavement temperatures at various depths. Subsequently, we calculated frost and thaw depths based on these temperature predictions. These frost and thaw depth measurements served as

critical parameters in our study, enabling us to determine the initiation and conclusion dates of spring load restrictions and winter weight premium policies.

In the final phase of our research, we applied machine learning models to precisely pinpoint the onset and conclusion dates of these seasonal policies. By doing so, we contributed to the advancement of road management practices, enhancing the ability to regulate load limits during the spring thaw period and optimize weight premiums during winter conditions. This comprehensive approach to policy timing, informed by accurate pavement temperature predictions and frost/thaw depth calculations, holds great promise for more effective and efficient road management practices.

1.5. STRUCTURE OF DISSERTATION

This dissertation is structured in an integrated-article format. With the exception of the literature review and conclusions chapters, all other chapters consist of individual journal papers that have been published or are currently under revision.

Chapter 1 provides a general explanation of the study's objectives and the scope of the research.

Chapter 2 offers a quick overview of the impacts of environmental factors on pavement performance, examines existing prediction models, and explores the application of artificial intelligence methods for pavement performance prediction.

Chapter 3 provides an introduction to the background of the IRRF test road and discusses the data availability for this study.

Chapter 4 investigates changes in pavement temperature and moisture content in the test road over multiple years. This chapter also analyzes the influence of external climate and insulation materials on environmental factors, marking the initial phase of our research.

Chapter 5 evaluates the effectiveness of machine learning models for predicting base and subgrade layer temperatures. This chapter utilizes air temperature and day of the year as inputs for pavement temperature prediction.

Chapter 6 incorporates depth as an input parameter and focuses on training powerful machine learning models for predicting average, maximum, and minimum daily pavement temperatures in various layers, including HMA, base, and subgrade.

Chapter 7 explores the application of machine learning models to predict pavement temperature within structures, considering special insulation materials such as bottom ash. This chapter demonstrates the robustness of machine learning models for predicting pavement temperature with these unique insulation materials.

Chapter 8 utilizes machine learning models to predict base and subgrade layer moisture content, using three input parameters: pavement temperature, day of the year, and depth. The focus is on predicting moisture content variations throughout the year.

Chapter 9 focuses on the development of machine learning models to predict pavement temperature and moisture content simultaneously. This chapter includes only three input parameters: air temperature, day of the year, and depth.

Chapter 10 assesses the variation in structural capacity among different test sections after five years of operation. This chapter backcalculates resilient modulus, effective modulus, and effective structural numbers using Falling Weight Deflectometer test results and discuss the influence of environmental factors, embankment materials, and insulation materials.

Chapter 11 explores machine learning models as a novel method to determine the start and end dates of seasonal policies, such as Spring Load Restrictions and Winter Weight Premium. This chapter directly uses frost and thaw depths for policy determination and compare predicted results to measured outcomes.

Chapter 12 provides a summary of the findings and contributions, draws conclusions, and offers recommendations for future studies and practical applications.

1.6. CORRELATION BETWEEN DIFFERENT CHAPTERS

Chapter 1 sets the stage by outlining the study's objectives and scope, providing a foundation for the subsequent chapters. **Chapter 2** serves as a literature review, introducing the impacts of environmental factors and the application of artificial intelligence in pavement performance prediction, setting the context for the research to come. **Chapter 3** introduced the background of the IRRF test road. **Chapter 4** initiates the research process by investigating long-term environmental factors, paving the way for the development of predictive models in later chapters. **Chapters 5** through **9** progressively develop machine learning models for pavement temperature and moisture content prediction, following a progression from simplicity to complexity as illustrated in Table 1-1. **Chapter 5** builds on this foundation by evaluating machine learning models for predicting base and subgrade temperatures, with a focus on inputs like air temperature and day of the year. **Chapter 6** extends the temperature prediction to various pavement layers, incorporating depth as an input parameter, and training models for different temperature scenarios. **Chapter 7** explores the application of machine learning models within pavement structures, particularly focusing on insulation materials like bottom ash and their impact on temperature prediction. **Chapter 8** shifts the focus to moisture content prediction, utilizing machine learning models and inputs like pavement temperature, day of the year, and depth to predict moisture variations throughout the year. **Chapter 9** combines temperature and moisture predictions simultaneously, showcasing the potential of machine learning to provide comprehensive insights into pavement conditions. **Chapter 10** extends the investigation initiated in **Chapter 4**, focusing on the enduring influence of bottom ash insulation on environmental factors. Furthermore, it compares the results of different sections within the IRRF test road, providing insights into the long-term structural capacity effects. To

achieve this, we employed prediction models to determine the actual moisture and temperature conditions at the time of testing. Additionally, we carefully defined material properties, such as modulus, to ensure their accuracy in back calculations and subsequent inputs. This chapter bridges the environmental and structural aspects, shedding light on how bottom ash insulation impacts both. **Chapter 11** explores the practical application of machine learning in determining the timing of seasonal policies, aligning environmental factors with policy decision-making. Machine learning models predict pavement temperatures at various depths, and frost and thaw depths are calculated based on temperature data from different depths. The timing of seasonal policies, specifically SLR and WWP, is directly influenced by the development of frost and thaw depths. In this chapter, we compare the prediction results with measured data to assess the accuracy of the models. Additionally, we validate the timeframes by comparing the moisture content variation in the subgrade layer. **Chapter 12** culminates the study by summarizing findings, drawing conclusions, and providing recommendations for future research and practical applications, thereby closing the research loop.

Table 1-1: Research objectives in chapters 5 to 9.

Chapter	Section	Input				Output	
		Air temperature	Pavement temperature	Day of the year	Depth	Pavement temperature	Moisture content
5	Control section	✔		✔		✔	
6	Control section	✔		✔	✔	✔	
7	Insulation section	✔		✔	✔		
8	Control section		✔	✔	✔		✔
9	Control section	✔		✔	✔	✔	✔

Overall, these chapters form a cohesive narrative that progresses from the introduction of the research goals to the development and application of machine learning models for comprehensive pavement analysis, structural capacity evaluation, and policy decision-making.

CHAPTER 2.LITERATURE REVIEW

In cold regions, pavements face harsh environmental conditions characterized by prolonged periods of extreme cold temperatures and the occurrence of spring freeze-thaw cycles. During winter, as both air and pavement temperatures plummet, ice lenses form within the base and subgrade layers, resulting in differential frost heave on the pavement surface. Notably, when the temperature drops below 0°C (Teltayev and Suppes in 2019), the freezing point of water, a rapid shift in moisture levels takes place. As late winter arrives and temperatures rise, the ice lenses within the pavement begin to melt. However, while the sublayer remains frozen, its permeability remains low, leading to the accumulation of excess water. This accumulation typically leads to an elevated moisture content in the sublayer during the thawing period, resulting in the lowest subgrade modulus throughout the year as shown in Figure 2-1 (Bayat, 2009; Salour, 2015; Haghi, 2019). As a result of these adverse environmental conditions, pavements in cold regions typically experience more extensive damage, exhibit premature deterioration, and suffer from shorter service lives and elevated maintenance costs, among other associated challenges. Prior research has indicated that the root causes of these issues predominantly stem from environmental factors rather than traffic-related factors (Janoo and Shepherd, 2000; Asefzadeh et al., 2016; Haghi et al., 2016). Consequently, addressing these problems requires a distinct approach tailored to the unique conditions of cold region pavements, making solutions applicable to warm region pavements insufficient.

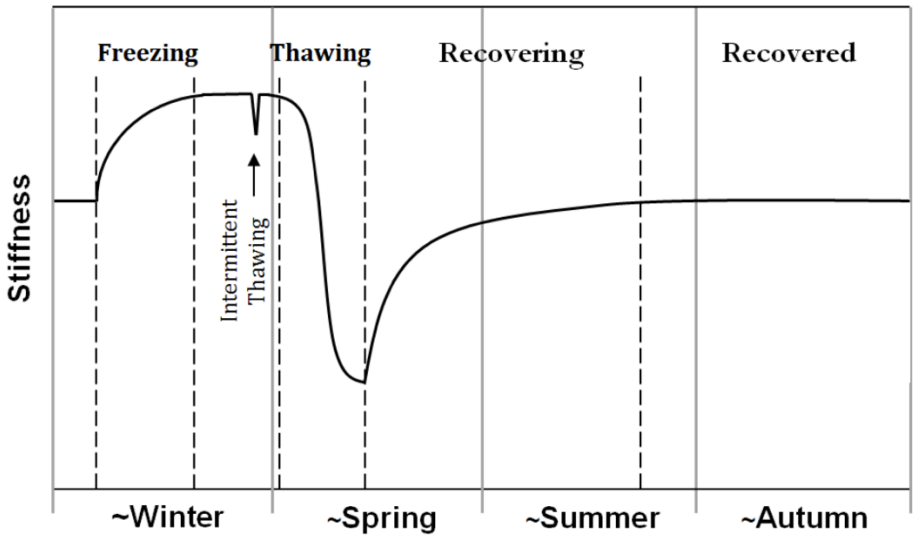

Figure 2-1: Conceptual pavement stiffness variations due to freezing and thawing (Salour, 2015)

2.1. ENVIRONMENTAL FACTORS FOR PAVEMENT PERFORMANCE

2.1.1. Pavement Temperature

The rate and magnitude of deterioration in flexible pavements are intricately linked to the properties of the materials composing various layers. Notably, the strength and stiffness of these pavement materials are profoundly influenced by variations in pavement temperature and moisture content (Birgisson et al., 2000). Pavements situated in cold regions, exposed to prolonged sub-zero temperatures and recurrent freeze-thaw cycles, tend to experience more severe damage compared to their counterparts in warmer regions (Tighe et al., 2006). During the winter season, as the temperature within the hot mix asphalt (HMA) layer plummets, a noteworthy observation is the increase in the modulus of the HMA layer, rising from 1.0×10^8 Pa to 1.4×10^{10} Pa (Aidara et al., 2015). Additionally, extreme temperature fluctuations in cold regions can lead to asphalt hardening and reduced flexibility, increasing the risk of cracking

and rutting, while freeze-thaw cycles can exacerbate damage through thermal cracking and moisture-related distress.

Furthermore, Fredlund et al. (1977) introduced a two-parameter expression for resilient modulus, with matric suction identified as the primary parameter affecting unsaturated soils' behavior. This matric suction is significantly dependent on both temperature and moisture content, as demonstrated by Simonsen et al. (2002). They found that as temperatures drop from 0°C to -20°C, the resilient modulus of soil increases, emphasizing the profound influence of temperature variations.

Moreover, Salour and Erlingsson (2013) conducted modulus back-calculations based on falling weight deflectometer data, revealing a 63% reduction in the resilient modulus of the subgrade and a 48% reduction in the resilient modulus of the granular base layer during the thawing period, compared to values under fully recovered conditions. In a case study by Haghi et al. (2016), it was observed that as temperatures decrease, the modulus of the unbound layer can reach 2.13 times the normal condition (with fall as the reference) (1.4×10^{10} Pa). Simultaneously, the resilient modulus of the unbound layer decreases to 1.3×10^{10} Pa due to the presence of excess water within the unbound layer.

Additionally, the rate of change in the resilient modulus for the subgrade in spring varies among different soil types (Popik et al., 2005). The Mechanistic-Empirical Pavement Design Guide (MEPDG) outlines a method to calculate the temperature of a sublayer, crucial in determining when the unbound material layer will freeze (AASHTO, 2008). This temperature, in turn, impacts the resilient modulus of unbound materials, thus influencing the load-bearing capacity of the pavement.

In essence, while most pavement design methods may not directly account for temperature variations, the material properties and road location may render seasonal temperature

fluctuations a crucial factor affecting unbound layer properties and performance (AASHTO, 2008). For instance, in the case of a weak subgrade soil, freezing can lead to a substantial increase in resilient modulus, while an increase in temperature during the thawing period can result in a significant decrease (AASHTO, 2008). Meanwhile, the pavement temperature was used in the Mechanistic-Empirical Pavement Design Guide (MEPDG) to Determine HMA-Mixture Properties for Load-Related Distresses as indicated in Figure 2-2 (AASHTO, 2008). Consequently, accurate estimation of unbound layer temperature emerges as a critical consideration in pavement engineering.

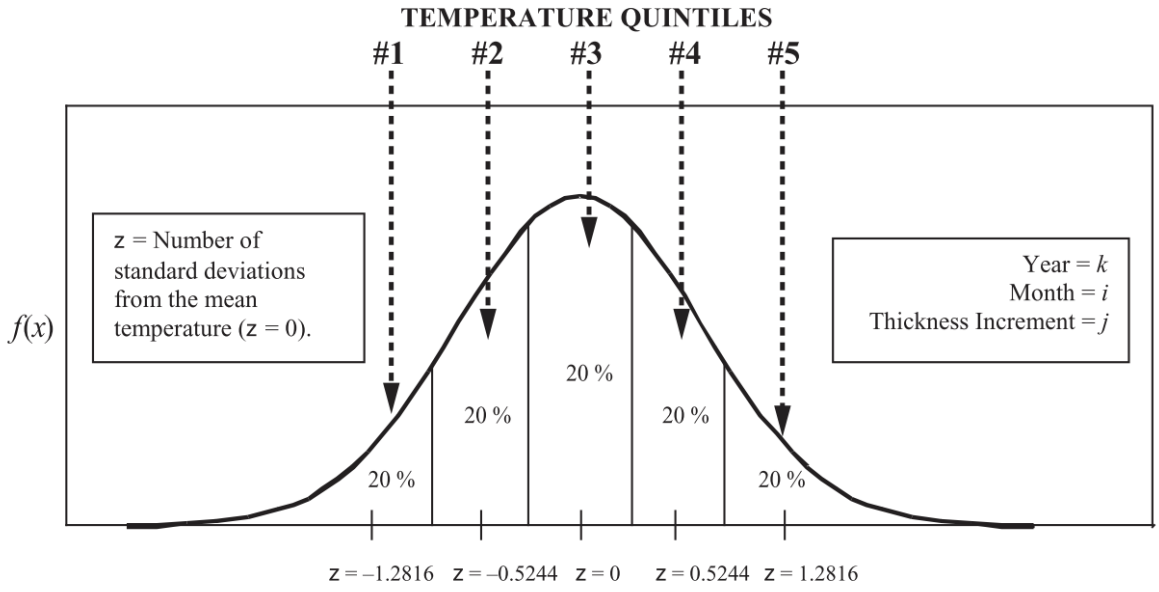

Pavement temperatures within each thickness increment of the HMA layers are calculated for each month via the ICM. The pavement temperatures are then combined into five equal groups, as shown above, assuming a normal distribution. The mean pavement temperature within each group for each month for each HMA thickness increment is determined for calculating the dynamic modulus as a function of time and depth in the pavement.

Figure 2-2: Graphical illustration of the five temperature quintiles used in the MEPDG to determine HMA-mixture properties for load-related distresses (AASHTO, 2008)

2.1.2. Moisture Content

The moisture content of subgrade soils plays a pivotal role in pavement design and performance, primarily due to its influence on subgrade strength. Moisture content is a key environmental parameter, impacting both soil stress states and structural integrity. Notably, it can affect soil

structure through suction or pore water pressure, ultimately shaping subgrade load-bearing capacity. Soils reach their maximum density at an optimum moisture content, with coarse-grained and fine-grained materials experiencing substantial modulus increases when dry, assuming all other conditions remain constant. Additionally, the modulus of cohesive soils is subject to complex clay-water-electrolyte interactions (ARA., 2000; Bohra et al., 1999; Christopher et al., 2006, 2010).

Contrastingly, moisture content may not directly influence bound materials like asphalt, but excessive moisture content can lead to asphalt stripping, causing the separation of the asphalt binder from the aggregate. This issue can have long-term repercussions on the structural integrity of cementitious materials (ARA., 2004; Christopher et al., 2006, 2010). Hence, moisture content exerts a significant impact on pavement performance and subgrade properties (ARA., 2000; Christopher et al., 2006, 2010; Hall and Rao, 1999).

Notably, the variation in moisture content in cold regions such as Edmonton differs significantly from that in warmer regions, where time and precipitation are dominant factors (Hedayati and Hossain, 2015). In cold regions, particularly during winter and spring, moisture content in the pavement layer is influenced by various factors, both environmental and internal (Chuvilin et al. 2020; Haghi et al., 2019; Jin et al., 2020; Patterson and Smith, 1980; Stein and Kane, 1983; Topp et al., 1980). Winter in Edmonton, for instance, witnesses average daily base layer temperatures dropping as low as -15°C (Haghi, 2019). This temperature range falls below the freezing point of bound water closely attached to mineral surfaces in soil, which can vary between -6 to -20°C (Kozlowski, 2007), lower than the freezing point of water at standard atmospheric pressure. Consequently, during winter, a mixture of ice and water coexists within the base and subgrade layers.

Furthermore, previous studies have indicated that capillary action, surface effects, adsorption forces, and the electrical double layer can influence the amount of unfrozen water in soil

(Chuvilin et al. 2020; Hoekstra, 1967; Jin et al., 2020; Stein and Kane, 1983). The soil freezing characteristic curve (Figure 2-3) suggests that even under extremely low soil temperatures, residual water content remains in the soil (Anderson and Tice, 1972; Chuvilin et al. 2020). Consequently, accurately determining the unfrozen moisture content in frozen soil proves challenging. Moreover, the moisture content dynamics in cold regions, such as Edmonton, are heavily influenced by low temperatures. This leads to a moisture content trend that contrasts starkly with that in warmer regions, where moisture content typically varies sinusoidally throughout the year, largely driven by precipitation (Hedayati and Hossain, 2015). However, in Edmonton and similar cold regions, pavement temperature predominantly dictates moisture content, with precipitation playing a limited role (Haghi, 2019).

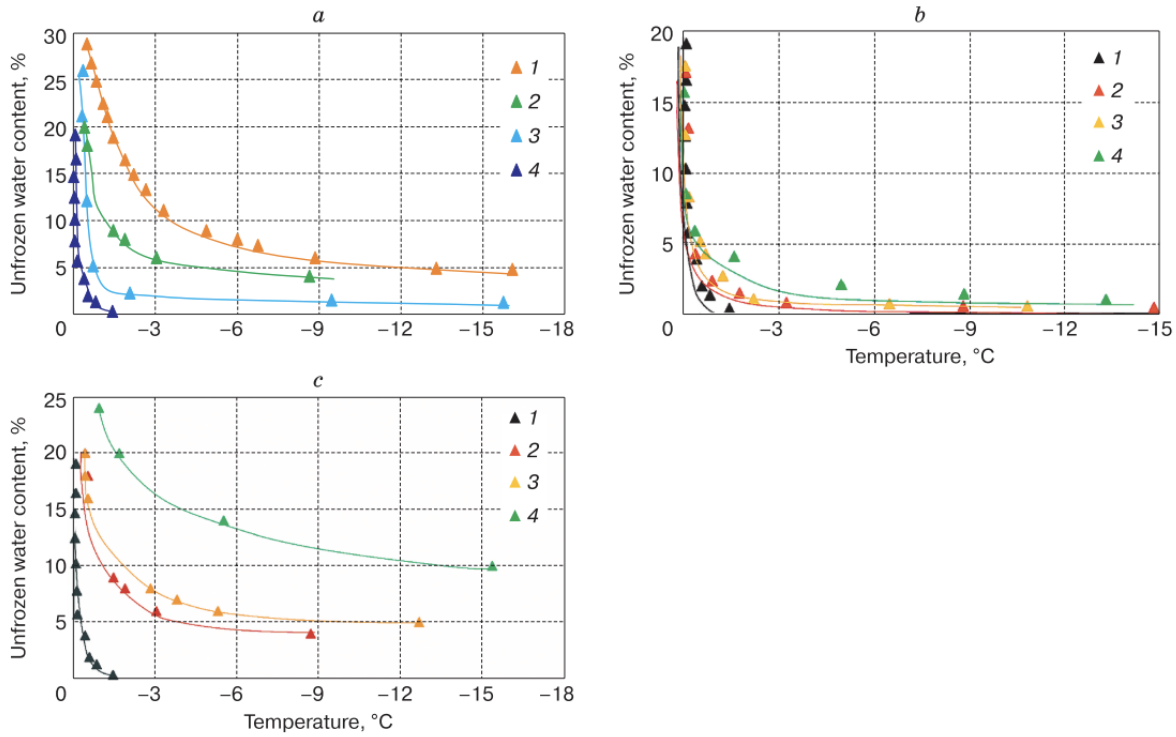

Figure 2-3: Temperature-dependent unfrozen water contents in soils of different grain sizes (a) and in sandy soil with different contents of kaolinite (b) and montmorillonite (c) clay (Chuvilin et al. 2020)

Symbols in panels a-c: *1* = clay silt; *2* = silt-1; *3* = silt-2; *4* = sand (a); *1* = sand; *2* = sand with 15% kaolin; *3* = sand + 25% kaolin; *4* = sand + 40% kaolin (b); *1* = sand; *2* = sand with 15% bentonite; *3* = sand + 25% bentonite; *4* = sand + 40% bentonite (c).

During winter, most of the water in the pavement layers freezes, reducing the unfrozen moisture content. As spring approaches, with rising air and pavement temperatures, solid water (ice) within the unbound layers transforms back into liquid water. The lower layers often remain frozen while thawing progresses from top to bottom. This results in low permeability in the lower layer, leading to the accumulation of excess water above the frozen layer.

Consequently, as the weather warms and pavement temperatures rise, the water content in the subgrade and base layers reaches its highest levels, particularly compared to other times of the year (Haghi, 2019). This moisture accumulation during the thawing period typically leads to a decrease in subgrade bearing capacity, a phenomenon referred to as the freeze-thaw cycle. Cold regions experience multiple freeze-thaw cycles annually, with the number of cycles significantly impacting the resilient modulus of subgrade layers (Haghi et al., 2016; Zhou et al., 2022).

In summary, comprehending the change in moisture content within base and subgrade layers is imperative for improved road design, particularly in cold regions subject to temperature fluctuations. Moisture content dynamics differ significantly in these regions compared to warmer counterparts, making it crucial to account for these variations to enhance pavement performance and subgrade properties.

2.2. BOTTOM ASH

Insulation layers have long been employed as a conventional approach to safeguard pavement structures from extreme cold weather conditions. Polystyrene, depicted as an insulation material in Figure 2-3(a), has been a staple choice for protecting pavements in numerous cold regions since as far back as 1967 (Penner, 1967). Earlier research studies have demonstrated

the effectiveness of a 5-centimeter polystyrene layer in substantially reducing both thaw depth and frost heave. Additionally, case studies examining pavement settlement have consistently revealed that pavement sections incorporating polystyrene insulation layers experienced less settlement compared to those following standard design practices, as evidenced by studies such as those conducted by (Esch, 1973; Hayden and Swanson, 1972; Tatarniuk and Lewycky, 2011).

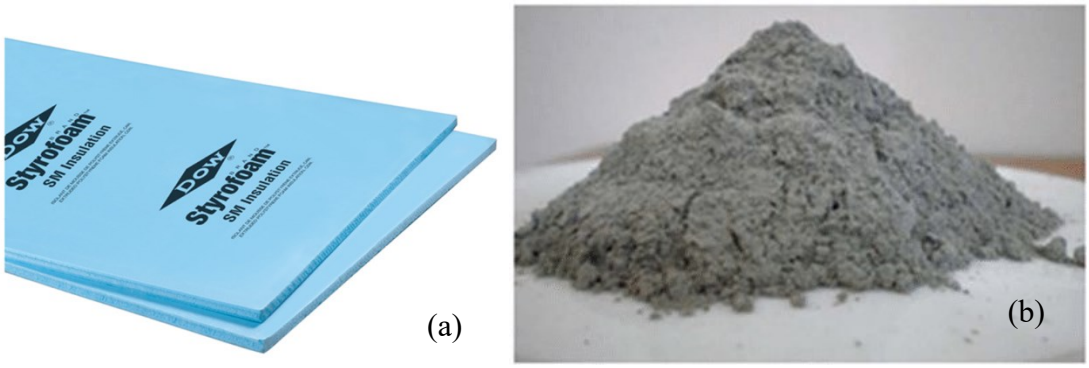

Figure 2-4: Insulated materials used in the IRRF test road (a) polystyrene board and (b) bottom ash

In recent years, there has been a notable shift towards adopting environmentally sustainable practices in pavement construction. This shift has led to the increasing use of bottom ash (BA) (depicted in Figure 2-3(b)), a by-product of coal combustion, as an alternative insulation material. Alberta, for instance, has continued to produce a substantial amount of BA due to its coal-based electricity generation, accounting for 36% of electricity production in 2019 (Provincial and Territorial Energy Profiles – Alberta, 2019). Extensive studies have established BA as a high-quality base material, primarily composed of silica, alumina, and iron, offering excellent insulation properties to safeguard the subgrade against frost heave during harsh winters (Forteza et al., 2004; López et al., 2015; Huang, 1990; Haghi et al., 2014). Research by Haghi et al. (2014, 2016, 2018, 2019) has underscored the effectiveness of both polystyrene and BA in protecting the subgrade layer from frost. However, it's essential to note that the polystyrene layer's use led to increased temperatures in hot mix asphalt and base layers during

summer and lower temperatures during winter (Haghi et al., 2014). Notably, an analysis of falling weight deflectometer (FWD) test results conducted one year after the IRRF test road's construction revealed that the BA-insulated section demonstrated load-carrying capacity similar to the control section (CS, without insulation), while the polystyrene-insulated section experienced a significant reduction in pavement load-bearing capacity (Haghi et al., 2016). Furthermore, the BA-insulated section exhibited similar viscoelastic behavior to the CS; however, the polystyrene-insulated pavement proved more susceptible to damage during summer due to higher HMA temperatures (Haghi et al., 2019).

Despite these promising findings, it's worth noting that research on employing bottom ash as an insulation layer for subgrade frost protection in cold regions commenced only approximately two decades ago, as evidenced by the work of Hashemian and Bayat (2016). While several studies (Haghi et al., 2014, 2016, 2018) have been conducted on the IRRF test road featuring a bottom ash layer after its initial construction, there remains a notable knowledge gap concerning the long-term effects of bottom ash on both moisture content and structural capacity. In Helsinki, Finland, a study revealed that frost depth in bottom ash sections was only 40%–60% of that in conventional sections (Field et al., 2011). Additionally, two separate studies in Edmonton, Alberta (conducted in 2001 and 2014), demonstrated that bottom ash effectively prevented frost penetration into the subgrade, with frost depth contained within the bottom ash layer (Havukanen, 1987; Edgar et al., 2015). Notably, economic investigations conducted at Delhi Technological University explored the use of pond ash, a type of industrial waste subbase material, as a viable replacement for conventional subbase materials in pavement construction. These studies revealed substantial cost savings, with a reduction of 11.5%–12.4% in the total construction cost when the subbase layer consisted solely of pond ash, without any additional materials. Furthermore, incorporating pond ash with fiber and lime was found to yield savings ranging from 5.2% to 13.0% in construction costs (Sarkar and

Dawson, 2015). These collective findings highlight the environmental and economic advantages of utilizing bottom ash and similar materials in pavement construction practices.

2.3. SEASONAL POLICES FOR ROAD MANAGEMENT

Freight transport plays a crucial role in sustaining Canada's economy, but the substantial volume of heavy truck traffic places immense pressure on the country's roadway networks. This pressure leads to premature failure, extensive pavement damage, the need for costly road maintenance, and other related issues. Furthermore, Canada's cold regions present additional challenges for roadways, including frost heave and freeze-thaw cycles. During the thaw weakening period, the temperature of the pavement structure rises, but the moisture content reaches its highest values, leading to a decrease in the structural capacities of the pavement, reaching the lowest values of the year (ARA., 2004; Bohra et al., 1999; Christopher et al., 2006; Haghi et al., 2016; Huang et al., 2021; Janoo and Shepherd, 2000). Consequently, roadways become more vulnerable to the detrimental effects of heavy truck traffic, further exacerbating the strain on the infrastructure (Al-Qadi et al., 2008; Bayat, 2009; Haghi, 2019).

To address these challenges, authorities in North America have implemented seasonal policies like spring load restrictions (SLR) and winter weight premiums (WWP). SLR has traditionally been introduced to protect pavements during the thaw-weakening season, while WWP aims to mitigate the impact of SLR on the trucking industry. SLR involves reducing the maximum axle load of trucks or, in some cases, imposing heavy traffic bans during this period. These measures can have implications for regional economic development and the growth of the trucking sector. Provinces typically enforce restrictions on various aspects of vehicle load weight and dimensions, including vehicle length, axle load, axle spread, and the overall loaded mass of vehicles and combinations. These restrictions often result in substantial reductions, typically ranging from 50% to 90%, on carriers during the Spring Thaw. However, these policies adhere

to fixed dates each year for their implementation as shown in Table 2-1, regardless of the actual structural capacity of the pavement, as highlighted by Asefzadeh et al. (2016). The rigidity of these policy dates can impede the growth of the trucking industry by imposing restrictions on axle loads. Striking a balance between pavement infrastructure preservation and the needs of the industry is crucial.

Table 2-1: Spring load restrictions dates in some Canadian provinces (Canada Cartage Group of Companies, 2021).

Province	Zones/Counties	SLR Dates
Saskatchewan	South	March 15 – June 15
	North	April 1 – June 30
Manitoba	Zone 1A	March 6 – May 29
	Zone 1B	March 8 – May 31
	Zone 2	March 19 – May 31
	Zone 3	March 23 – June 10
Ontario	Schedule 1 Highways	March 1 – April 30
	Schedule 2 Highways	March 1 – May 31
	Schedule 3 Highways	March 1 – June 30
Quebec	Zone 1	March 15 – May 14
	Zone 2	March 15 – May 14
	Zone 3	March 22 – May 21

2.4. EXISTING MODELS FOR PAVEMENT PERFORMANCE PREDICTION AND MANAGEMENT

2.4.1. Pavement Temperature Prediction Models

While environmental factors significantly impact road performance, existing models primarily focus on pavement temperature variations within the asphalt layer (Adwan et al., 2021; Asefzadeh et al., 2017; Milad et al., 2021; Molavi Nojumi et al., 2022). There has been limited research attention on this aspect, resulting in only a few statistical models being developed for pavement temperature prediction. The Strategic Highway Research Program (SHRP) and its Canadian counterpart (C-SHRP) have introduced two models, denoted as Equation 2-1 (SHRP) and Equation 2-2 (C-SHRP), specifically designed for predicting the minimum pavement temperature within the hot mix asphalt (HMA) layer, aiding in the selection of optimal asphalt concrete mixtures (Mohseni, 1998).

$$T_d = T_{air\ (min)} + 0.051d - 0.000063d^2 \quad \text{Equation 2-1}$$

$$T_d = 0.859T_{air\ (min)} + \left(0.002 - 0.0007T_{air\ (min)}\right)d + 0.17 \quad \text{Equation 2-2}$$

In both Equations 2-1 and 2-2, T_d (°C) represents the minimum pavement temperature at depth d (mm) and $T_{air\ (min)}$ (°C) represents the minimum daily air temperature.

Data collected from the Integrated Road Research Facility (IRRF) test road served as the basis for developing statistical models predicting average, minimum and maximum pavement temperature throughout the year. The model for average temperature prediction divides the year into two seasons: a cold season (October to March) and a warm season (April to September), resulting in Equations 2-3 (for the warm season), 2-4 (for the cold season), 2-5, and 2-6.

$$T_{ave} = 3.9832 + 1.1288(T_{air}) + 2.68 \times 10^{-5}(SR) \quad \text{Equation 2-3}$$

$$T_{ave} = -1.7853 + 0.6510(T_{air}) + 3.37 \times 10^{-4}(SR) + 2.0326 \times d \quad \text{Equation 2-4}$$

$$T_{HMA\,(min)} = -2.8704 + 0.89\,T_{air\,(min)} + (1.26 \times 10^{-4})\,SR + 0.1759\left(SR \times T_{air\,(min)}^{2}\right)^{0.25} + 15.2324d \quad \text{Equation 2-5}$$

$$T_{d(\max)} = 2.0237 + 0.8709\,T_{air(max)} + (7.6 \times 10^{-4})\,SR - 16.1886\,d \quad \text{Equation 2-6}$$

where T_{ave} (°C) is the daily average temperature of the HMA layer, T_{air} (°C) is the daily average air temperature, SR is the daily solar radiation (kJ/m^2), d is depth (m), $T_{HMA\,(min)}$ (°C) is the minimum daily HMA temperature, $T_{air\,(min)}$ (°C) is the minimum daily air temperature, $T_{d(max)}$ (°C) represents the maximum daily pavement temperature at depth d (mm), and $T_{air\,(max)}$ is the maximum daily air temperature.

All the models mentioned above are designed exclusively for the HMA layer and did not take temperature variations within the base and subgrade layers into account. In the existing literature, only one model stands out for its applicability to base and subgrade layers. This model, proposed by Heydinger (2003), take into account these base and subgrade layers, and is represented by Equation 2-7:

$$T(t) = A + B\sin\left[\omega(t - \phi)\right] \quad \text{Equation 2-7}$$

where t is time (expressed as the day of the year), A (°C) is the mean temperature, B (°C) is the amplitude, and ω is the normalized frequency ($\omega = 2\pi / 365.25$). To apply this equation, the appropriate values of A and B are estimated based on asphalt and soil temperature measurements. The performance of the model proposed by Heydinger (2003) will be discussed in the subsequent chapters.

2.4.2. Moisture Content Prediction Model

Moisture content is a pivotal environmental factor with a profound impact on pavement system performance. Specifically, the moisture content within the unbound material layer plays a

pivotal role in determining the subgrade's load-bearing capacity, directly influencing stress distribution and structural characteristics of the underlying soil (ARA, 2004). While several models for moisture content prediction exist in the literature (Hedayati et al., 2014; Hedayati and Hossain, 2015), Hedayati and Hossain (2015) developed a parametric model based on field data collected in North Texas. This model, presented in Equations 2-8 and 2-9, effectively captures both seasonal and transient variations in moisture content:

$$\theta_{(z,t)} = \theta_0 + \theta_a \sin(\omega t - 0.2z + C_0) + f(t, rainfall) \quad \text{Equation 2-8}$$

$$\theta_a = 0.053e^{-0.639z} \quad \text{Equation 2-9}$$

where z is the depth (m), t is the time elapsed from an arbitrary starting point (day), $\theta_{(z,t)}$ is the soil moisture content (m^3 H_2O/m^3) at depth z and time t, θ_0 is the average soil moisture (m^3 H_2O/m^3) at depth z over time, θ_a is the moisture content at a given depth over time, ω is the angular frequency (equal to 2π / 365 = 0.0172 day^{-1}), C_0 is the phase correction factor (which can be determined analytically) and f(t, rainfall) is the relationship between the net increase in soil moisture content (m^3 H_2O/m^3) and rainfall. Hedayati and Hossain (2015) calculated θ_0 based on all available field data collected at a depth of z. In Equation 2-8, rainfall was treated as hypothetical noise superimposed on the main signal and was analyzed separately.

However, it is important to note that moisture content in cold regions exhibits distinct and unique trends (Bayat, 2009; Haghi, 2019), and the model designed for moisture content variation in warm regions cannot be directly applied to cold regions. As illustrated in Figures 2-5 and 2-6, moisture content variation in warm and wet regions is primarily influenced by rainfall (Hedayati and Hossain 2015). In contrast, cold regions experience freezing temperatures in winter, causing the water to transform into ice. Consequently, unfrozen moisture content decreases, and a residual moisture content remains. During late winter and early spring, as air temperatures rise, the ice begins to melt, leading to water accumulation in

the soil (Haghi 2019). The extremely low air temperatures experienced in these regions induce significant changes in the moisture status, thereby necessitating specialized models tailored to capture these specific conditions.

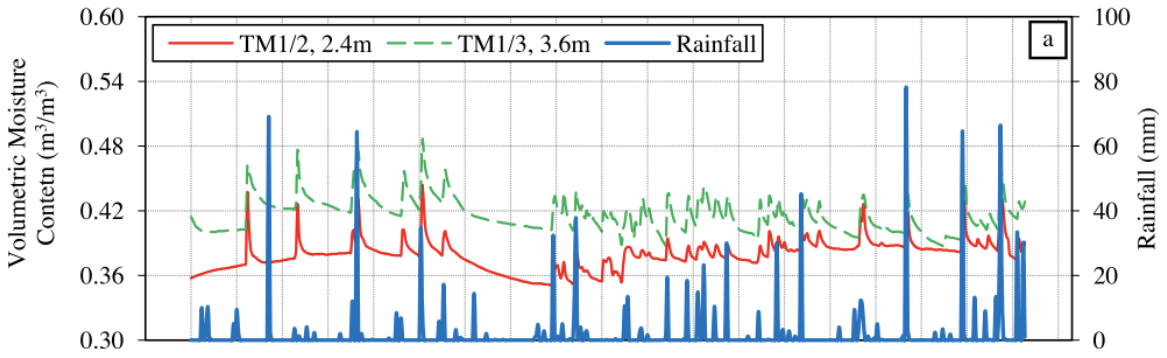

Figure 2-5: Subgrade moisture content and rainfall (Hedayati and Hossain 2015).

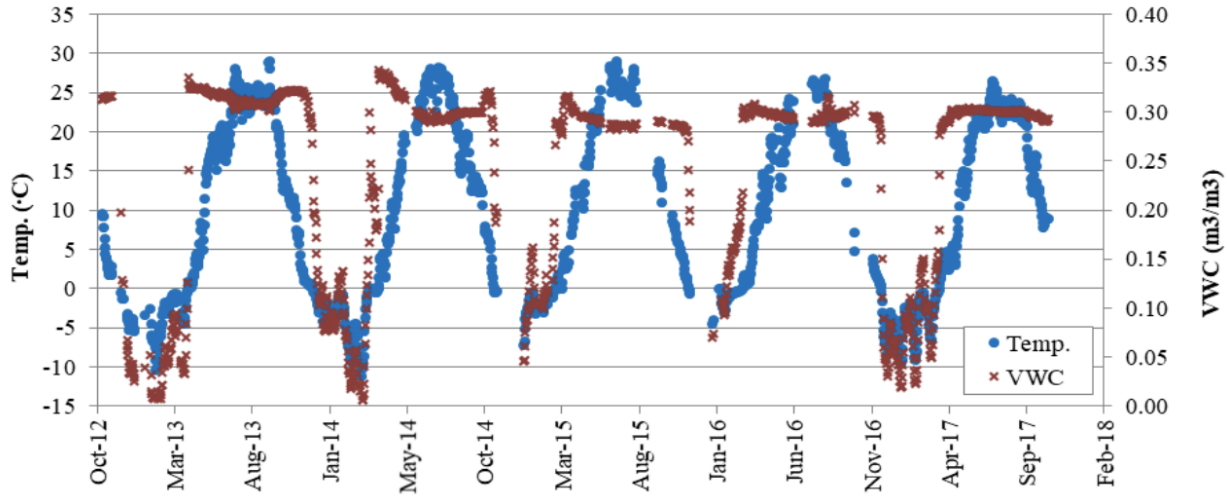

Figure 2-6: Subgrade resilient modulus and soil moisture content (Haghi 2019)

Teltayev and Suppes (2019) developed a semi-logarithmic function to describe unfrozen pavement moisture content in winter, based on negative temperature (i.e. pavement temperature was below 0°C) and initial moisture content (i.e. before the pavement temperature drops below 0°C). The model was based on data collected in the eastern region of Kazakhstan, as represented in Equation 2-10.

$$W_{uf} = 0.911 + 0.634W_0 - 0.552\ln|T| - 0.067W_0\ln|T| \qquad \text{Equation 2-10}$$

Where W_{uf} is the unfrozen soil moisture content (%), W_0 is the initial soil moisture content (%), and T is the temperature (°C), which is always a negative value. This is the only available model in the literature designed for cold regions; however, it still has some limitations. For instance, it only functions for negative temperatures, and initial moisture content data are required. Its performance on the IRRF test road will be assessed in subsequent chapters.

The Enhanced Integrated Climate Model (EICM) (ARA., 2004) is a widely utilized climate prediction model that offers predictions for in situ pavement temperature, moisture content, and stiffness moduli of the pavement layers. However, there are certain limitations associated with this model. Firstly, the accuracy of its predictions heavily relies on the quality and accuracy of the input parameters, such as boundary conditions, climatic conditions, and material properties. Additionally, the EICM assumes that the heat capacity and thermal conductivity of unbound materials remain constant over time. However, this assumption does not hold for unbound materials, such as base course and soil, as their heat capacity and thermal conductivity vary with changing moisture content and frost depth (ARA., 2004). Consequently, the EICM cannot accurately predict the temperature of unbound materials within a pavement structure. Birgisson et al. (2000) found that there was a significant discrepancy between measured temperatures and EICM predictions. In the Minnesota Road Research Project (MN/ROAD), it was observed that the temperature difference between measured values and those predicted by the EICM reached nearly 7°C during summer for densely graded base material. These disparities underscore the limitations of relying solely on the EICM for accurate temperature predictions of unbound materials in a pavement structure.

2.4.3. Spring Load Restrictions and Winter Weight Premiums Dates Prediction Models

To optimize these policies and minimize trade-offs, several models have been proposed to determine the start and end dates of SLR and WWP using cumulative thawing index (CTI) and

cumulative freezing index (CFI). Various methods exist for calculating CTI and CFI. CTI can be calculated using Equation 2-11.

$$CTI = \sum (T_{avg} - T_r) \quad \text{Equation 2-11}$$

where T_{avg} is the average daily temperaturre and T_r is the average air temperature when the asphalt temperture fluctuates around 0°C. T_r should be calibrate by the local data and its value varies with time. CFI is the absolute value of the sum of all days' temperatures falling below 0°C. Mahoney et al. (1987) suggested the calculation of CTI and CFI using a fixed T_r value of -1.67°C. Following the start of thawing period, the recommended CTI values of "should-level" and "must-level" thresholds to implement SLR were 15°C and 28°C, respectively. For thick pavements, Mahoney et al. (1987) proposed Equation 2- 12 to determine SLR lifting.

$$CTI = 0.3\ CFI \quad \text{Equation 2-12}$$

The Manitoba Department of Infrastructure and Transportation recommended that SLR should be applied when the CTI reaches 15°C-days but no earlier than March 11. CTI is expressed as Equation 2-13 (Bradley et al. 2012).

$$CTI = \sum Daily\ TI = \sum T_r + \frac{T_{max} + T_{min}}{2} \quad \text{Equation 2-13}$$

where T_r starts at 1.7 °C on March 1 and increases daily by 0.06 °C until May 31, after which it resets to zero. T_{max} and T_{min} are the maximum and minimum values of daily temperatures, respectively. If $(T_{max} + T_{min})/2 < 0$, then the daily TI will change to $T_r + (T_{max} + T_{min})/4$ to compensate for the period when the ambient air temperature falls temporarily below 0°C. SLR should be removed no later than eight weeks after the application date, when the CTI reaches 350°C-days or 31 May, whichever is sooner. The recommended start date of WWP is when the CFI reaches 150°C-days, corresponding to a frost depth of 75 cm. The recommended removal of WWP is when CTI reaches 1°C-days (Bradley et al. 2012).

The Minnesota Department of Transportation suggested Equation 2-14 to determine the SLR.

$$CTI_n = \sum (Daily\ TI - 0.5 \times Daily\ FI) \qquad \text{Equation 2-14}$$

• When $(T_{max} + T_{min})/2 - T_r < 0°F$ and $CTI_{n-1} \leq 0.5 \times [32°F - (T_{max} + T_{min})/2]$ then daily TI and daily FI should both be assigned 0°F-day.

• When $(T_{max} + T_{min})/2 - T_r > 0°F$ then daily $(T_{max} + T_{min})/2 - T_r$ and daily FI = 0°F-day.

• When $(T_{max} + T_{min})/2 - T_r < 0°F$ and $CTI_{n-1} > 0.5 \times [32°F - (T_{max} + T_{min})/2]$ then daily TI = 0 °F-day and daily FI = 32 °F – $(T_{max} + T_{min})/2$

where CTI_n represents the cumulative thawing index calculated over n days (in °F-days), with CTI resetting to zero on January 1. CTI_{n-1} denotes the cumulative thawing index for the previous day. T_r is the reference air temperature, set at 32 °F for the month of January. T_r decreases by 1.5 °C daily during the first week of February and then by 0.5 °C weekly until the end of thawing season. In this method, the threshold for initiating SLR start is CTI = 15 °C-days, contingent ona continuous forecast of non-freezing weather conditions.

Nonetheless, these investigations often lack a precise delineation of the conclusion date for Spring Load Restrictions, and the computation of CTI and CFI presents considerable difficulties (Asefzadeh et al., 2016). Determining the initial CTI calculation date is challenging due to unforeseen temperature spikes in winter (e.g., during January and February). Furthermore, the CTI and CFI computations necessitate adjustments using a reference temperature specific to each location. The exploration of direct parameters, like freeze and thaw depths, and the exploration of innovative methodologies such as machine learning, can provide valuable insights.

A pioneering method proposed by Baïz et al. (2008) and further refined by Bao et al. (2019, 2021) aims to directly determine the start and end dates of SLR and WWP by taking into

account frost and thaw depths, indicating in Figure 2-7. Leveraging machine learning to determine the initiation and conclusion of these policies based on actual frost and thaw depth in the pavement offers a more dynamic and data-driven approach. This approach can lead to improved pavement performance and reduced industry constraints (Asefzadeh et al., 2016; Bao et al., 2021). While these advanced models hold the potential to enhance road network management, it's worth noting that, as mentioned earlier, moisture content plays a pivotal role in the load capacity of pavements in cold regions. However, these models did not incorporate the variation in moisture content within the subgrade layer.

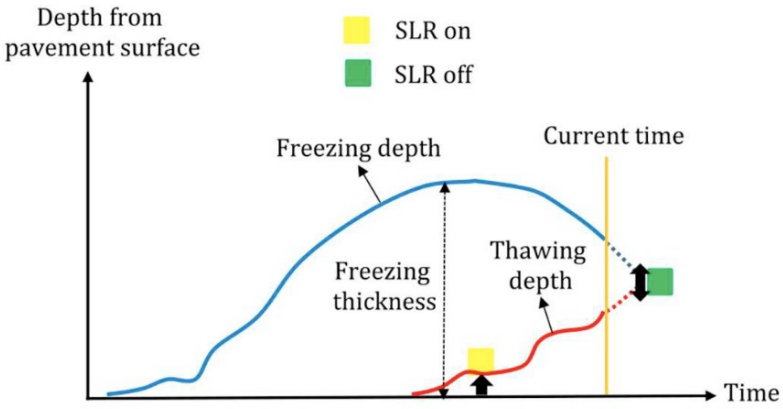

Figure 2-7: Decisions regarding Spring Load Restrictions guided by freezing and thawing depth forecasts (Baïz et al., 2008; Bao et al. 2019, 2021)

2.5. APPLICATION OF ARTIFICIAL INTELLIGENCE FOR PREDICTION PERFORMANCE IN ROAD

In recent years, the application of artificial intelligence (AI) techniques has gained significant momentum in studying and improving road performance, particularly in the field of transportation infrastructure management (Fujita et al., 2017; Inkoom et al., 2019; Marcelino et al., 2019; Nitsche et al., 2014). Traditional methods for predicting pavement conditions and performance have their limitations, prompting researchers to explore AI-driven solutions. This comprehensive literature review aims to provide an overview of the growing body of research on the use of AI, specifically machine learning and deep learning, in predicting two critical factors in pavement performance: pavement temperature and subgrade moisture content.

Machine learning and deep learning, both subsets of AI, offer promising approaches to enhancing our understanding of pavement performance. Compared to conventional methods, these AI techniques have the advantage of automatically identifying patterns within complex datasets and building predictive models without the need for manual intervention (Baştanlar and Özuysal, 2014).

Pavement temperature is a vital parameter affecting the performance and durability of road infrastructure. Several studies have demonstrated the effectiveness of machine learning models in predicting pavement temperature. For instance, Xu et al. (2017) introduced an improved Back Propagation neural network model capable of accurately forecasting pavement temperature for the next three hours. Milad et al. (2021) explored the application of deep learning-based regression models, highlighting the superior performance of Bidirectional Long Short-Term Memory (LSTM) algorithms in predicting asphalt pavement temperature. Similarly, Molavi Nojumi et al. (2022) employed a machine learning model to predict daily average, maximum, and minimum pavement temperatures within the asphalt layer, achieving impressive R^2 values above 0.95. Tabrizi et al. (2021) utilized Convolutional Neural Networks (CNN) to forecast hourly pavement surface temperature with predictions closely aligned with measured values. While these models have shown remarkable accuracy, it's important to note that they predominantly focus on pavement temperature within the asphalt layer.

Subgrade moisture content is a critical factor in determining the load-bearing capacity of the subgrade, influencing stress distribution and structural characteristics (ARA., 2004). Predicting subgrade moisture content is challenging but crucial for pavement performance. Although limited, there have been some attempts to employ AI techniques in this domain. For example, D'Amico et al. (2010) utilized artificial neural networks to estimate unsaturated moisture content within the subgrade by analyzing ground-penetrating radar signals. Similarly, Xing et al. (2017) harnessed remote satellite images to train an artificial neural network for predicting

general surface soil moisture. However, these studies primarily focused on general soil conditions, neglecting the specific influence of pavement layers.

Despite promising advancements in predicting pavement temperature and some limited work on subgrade moisture content, there remains a considerable research gap. Existing models predominantly concentrate on pavement temperature within the asphalt layer, overlooking temperature variations in base and subgrade layers. This limitation hinders a comprehensive understanding of pavement performance since temperature and moisture content in granular layers significantly impact road infrastructure (ARA., 2004; Bayat, 2009; Bohra et al., 1999; Haghi et al., 2016; Hall and Rao, 1999; Olidis and Hein, 2004; Popik et al., 2005; Utilities, 1997).

In conclusion, the application of machine learning and deep learning in predicting pavement performance, specifically pavement temperature and subgrade moisture content, represents a promising avenue for improving transportation infrastructure management. Machine learning models have shown impressive accuracy in temperature prediction, but their application to subgrade moisture content prediction remains relatively unexplored. Addressing these research gaps can lead to more effective pavement design, maintenance, and management strategies, ultimately enhancing the longevity and performance of road infrastructure. As computational capabilities continue to advance, AI-driven approaches hold great potential for revolutionizing the field of pavement engineering.

2.6. FWD TEST

Non-destructive tests, such as Falling Weight Deflectometer (FWD) testing, play a pivotal role in the structural evaluation and determination of pavement layer moduli for both flexible and rigid pavements (Shahin, 2005; Dore and Zubeck, 2008; Haas et al., 2015). FWD testing involves applying an impulsive load to the pavement surface by releasing a specific weight

from a predefined height onto a circular loading plate. Concurrently, surface geophones are strategically positioned at various lateral offsets from the loading plate to record the resulting deflection data induced by this dynamic load (see Figure 2-8). Structural pavement instrumentation, including FWD testing, offers valuable insights into how pavement layers respond to external loading, making it a valuable tool for pavement assessment.

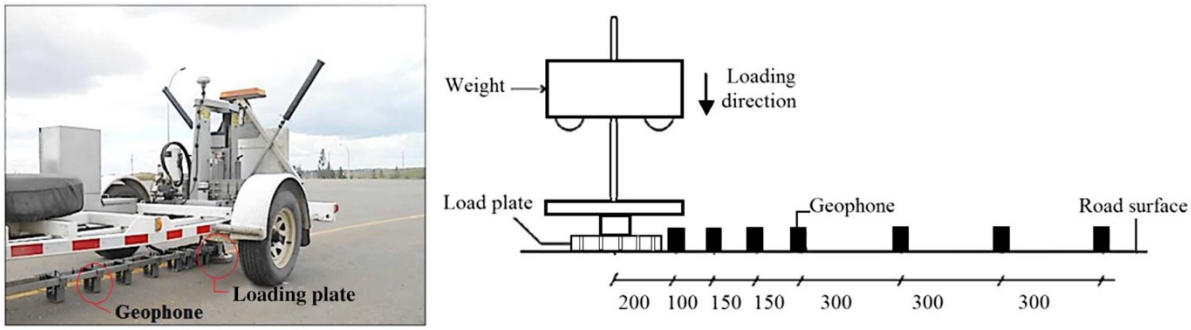

Figure 2-8: Arrangement of FWD equipment and sensor positions during field testing

The IRRF test road has extensively employed FWD testing due to its non-destructive nature. This method emulates dynamic loading similar to that experienced by moving vehicles and captures surface deformations at varying distances from the load plate. A study by Tholen et al. (1985) demonstrated the consistency of FWD testing results with real pavement loading and behavior, underscoring its applicability across a wide range of pavements. One common application of FWD results is the backcalculation of pavement structural bearing capacity, a critical determinant of pavement performance. Pavements with inadequate structural bearing capacities are prone to issues such as crocodile cracks, lateral cracks, and reduced pavement lifespan due to increased bending under traffic loads (Dong and Huang, 2015).

The subgrade modulus, a crucial factor in pavement performance, is significantly influenced by subgrade moisture content. The IRRF test road, located in an area subject to annual freeze-thaw cycles and subgrade weakening during spring thaw, experiences a distinctive moisture pattern. In winter, as temperatures drop, soil moisture freezes. Subsequently, during early spring, pavement temperatures begin to rise from top to bottom, leading to water accumulation

in the subgrade due to limited sublayer permeability. This period witnesses the highest soil moisture content of the year, resulting in a low soil modulus. Past observations at the IRRF test road have revealed that excess subgrade water drains during the summer months (Haghi et al., 2016; Hashemian and Bayat, 2018). To minimize the impact of soil water accumulation on the results, this study intentionally selected FWD test data from the summer season. Monthly FWD testing has been carried out at the IRRF test road, consistently yielding similar results across various test dates. To streamline data presentation and enable meaningful comparisons, this study primarily focuses on one annual test, representative of the overall findings.

CHAPTER 3.THE INTEGRATED ROAD RESEARCH FACILITY TEST ROAD

In response to the distinct challenges faced by pavement in cold regions due to environmental factors, a collaborative initiative involving the University of Alberta, Alberta Transportation, Alberta Recycling, the City of Edmonton, and the Canada Foundation for Innovation led to the establishment of the Integrated Road Research Facility (IRRF) test road in Edmonton, Alberta, in 2012. This endeavor aimed to comprehensively investigate the impact of cold weather on pavement performance, filling a critical research gap. Construction of the IRRF test road spanned from May 2012 to October 2013, and it was opened to public traffic in mid-October 2015, with garbage trucks constituting a notable portion, roughly 10 to 20%, of the total traffic. Situated at the entrance to the Edmonton Waste Management Center (EWMC), the IRRF test road is located approximately 15 km from downtown Edmonton.

The IRRF test road spans a length of approximately 500 meters and comprises two lanes. Figure 3-1 illustrates the structural components of the IRRF test road, with a 0.45-meter granular base layer (GBC) overlying the subgrade layer and a 0.25-meter hot mix asphalt (HMA) layer atop the GBC layer. To gather traffic-related data, a weigh-in-motion (WIM) system was installed, and data collected between 2016 and 2019 revealed an average daily traffic volume of 368 garbage trucks. The IRRF test road is divided into three distinct sections: the insulated section, the control section, and the tire section.

The insulated section serves as a platform to evaluate the performance of bottom ash as an insulation layer. In this section, bottom ash is employed as the insulation material and is placed beneath the base layer and above the subgrade layer, approximately 70 cm below the pavement surface. Within the insulated sections, three variations exist, including a 1-m bottom ash layer (BA), a 0.10-m polystyrene layer (Poly-10), and a 0.05-m polystyrene layer (Poly-5), which

are positioned between the GBC and subgrade layers. Notably, the section with the 5-cm polystyrene layer is left uninstrumented to avoid abrupt temperature transitions between the control and Poly-10 sections, resulting in the absence of data collection.

To assess the suitability of recycled tires as pavement embankment materials, three sections of the test road utilize Tire-Derived Aggregate (TDA) sourced from Passenger Light Truck Tires (PLTT), TDA from Off-the-Road Tires (OTR), and a mixture of TDA from PLTT and soil (as depicted in Figure 3-1). During construction, PLTT and soil were mixed onsite in a 50:50 volume ratio. All TDA backfill materials were enveloped in a nonwoven geotextile to prevent mixing with the surrounding soil. To mitigate internal heating of the TDA, a 0.5-meter layer of native soil was placed between two 3-meter TDA layers. Following three years of monitoring, no internal heating was observed within the tire layers, leading to the subsequent addition of a 1-meter layer of native soil atop the TDA layer.

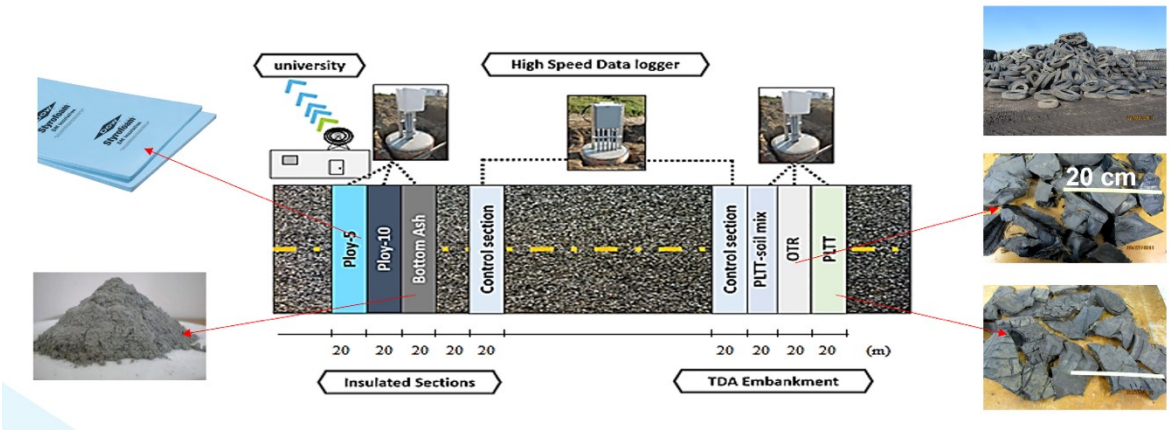

(a)

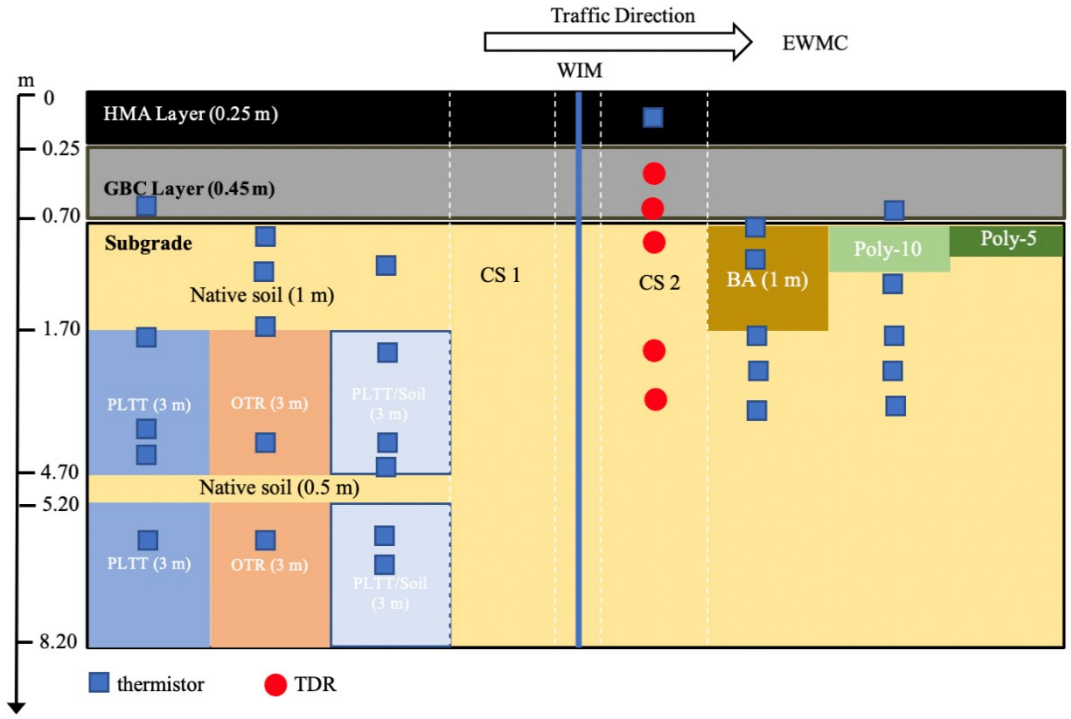

(b)

Figure 3-1: (a) Test and control sections in the IRRF test road and (b) the cross-section of the IRRF test road

The granular base layer (GBC) is characterized as well-graded gravel in accordance with ASTM C 136-06 and the Unified Soil Classification System. In contrast, the subgrade soil exhibits clayey sand properties, as detailed in Figure 3-2. The subgrade has moderate frost susceptibility, with approximately 27% and 21% of the subgrade soil (by weight) passing through 0.075 mm and 0.02 mm sieves, respectively. Notably, the subgrade soil features a liquid limit of 25% and a plastic index of 9%. The insulation layer employs bottom ash with a maximum particle size of about 5 mm and is devoid of significant lumps and impurities. Moreover, based on material weight, the bottom ash contains less than 5% unburned coal particles.

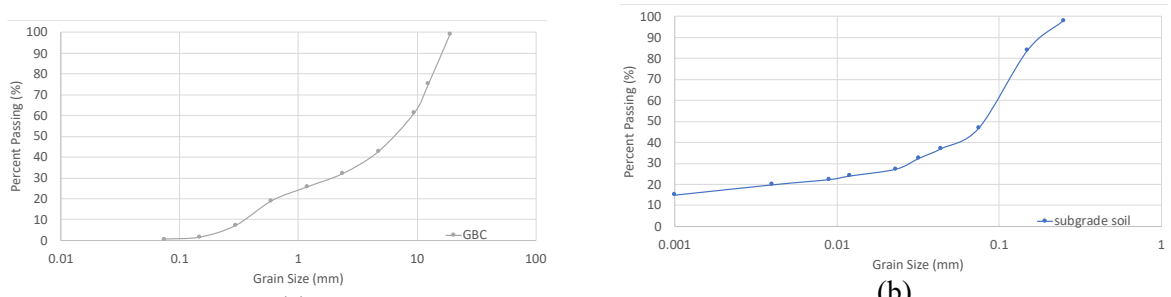

(a) (b)

Figure 3-2: Particle size distribution in (a) granular base course layer and (b) subgrade layer

3.1. INSTRUMENTS

The IRRF test road was equipped with CS650 time domain reflectometers (TDRs) from Campbell Scientific Canada in Edmonton, Alberta, Canada. These TDRs, in conjunction with other sensors, were employed to monitor both pavement temperature and moisture content at various depths. Additionally, Thermistors (specifically Model 109AM-L from Campbell Scientific) were utilized for pavement temperature measurements. Data gathered by the thermistors and TDRs were recorded and stored using a CR1000 datalogger. The datalogger was programmed to collect data from each of the sensors at 15-minute intervals. To facilitate data analysis, information from the IRRF test road sensors was remotely accessed from an on-site computer. Furthermore, an off-site computer located at the University of Alberta was used for in-depth data analysis.

The TDRs employed the Topp equation (Topp et al., 1980) to calculate volumetric water content (VWC) based on the bulk dielectric permittivity of the soil (K_α), as illustrated in Equation 3-1:

$$VWC = -5.3 \times 10^{-2} + 2.92 \times 10^{-2} K_a - 5.5 \times 10^{-4} K_a^2 + 4.3 \times 10^{-6} K_a^3 \qquad \text{Equation 3-1}$$

Here, VWC (m^3/m^3) represents volumetric water content, and K_α denotes the bulk dielectric permittivity of the soil. The speed of electromagnetic wave propagation in the porous medium depends on its dielectric permittivity. As water content increases, the speed of propagation decreases or the time for an electromagnetic wave to traverse from one end to another increases.

This principle underlies the "Time Domain Reflectometer" probe. Laboratory tests were conducted to calibrate the VWC using soil samples collected from the IRRF test road. The permittivity of water is influenced by temperature and water is the main contributor to soil permittivity, so the soil permittivity is temperature dependent.

To eliminate the temperature-dependent nature of the measured results, Equation 3-2 (Haghi, 2019) was applied:

$$VWC_{21} = VWC/(0.0084(T - 21) + 0.9936) \quad \text{Equation 3-2}$$

where 21°C was used as the base point to calibrate the permittivity, VWC_{21} (m^3/m^3) signifies soil permittivity with the temperature effect factored out, and T (°C) represents the temperature of the sample. It is important to note that soil permittivity is also influenced by soil type and soil compaction.

Calibration for the granular base course and subgrade materials was carried out using Equations 3-3 and 3-4 (Haghi, 2019).

$$VWC_{GBC} = 1.338VWC - 0.0901 \quad \text{Equation 3-3}$$

$$VWC_{subgrade} = 1.1619VWC - 25.296 \quad \text{Equation 3-4}$$

where VWC_{GBC} (m^3/m^3) represents volumetric moisture content in the GBC layer, and $VWC_{subgrade}$ (m^3/m^3) signifies volumetric moisture content in the subgrade layer. Notably, the TDRs primarily captured variations in liquid water content during the winter season (Huang et al. 2023a).

3.2. DATA AVAILABILITY

The IRRF test road has served as a focal point for long-term research endeavors, and numerous studies conducted during its early stages have laid a robust foundation for this investigation. Early contributions to the understanding of the IRRF test road include the following key studies:

- Nassiri et al. (2013) conducted a comparative analysis of FWD test results collected in 2012, providing insights into the initial conditions of various sections.
- Meles et al. (2016) examined the influence of different tire embankments on load-bearing capacity using FWD test results obtained on August 28, 2013.
- Hashemian and Bayat (2018) delved into the resilient modulus of pavements constructed with different tire embankment materials, comparing them to the control section.
- Haghi (2019) investigated the impact of bottom ash on pavement temperature variations, utilizing data collected from October 2012 to June 2013. Additionally, seasonal effects on the load-bearing capacity of pavements featuring insulation layers were explored using FWD data collected from July 2014 to July 2015.

Chapter Breakdown and Data Usage:

Chapter 4 leveraged pavement temperature and moisture content data acquired during several time intervals: October 2016 to January 2018, July to September 2018, and April 2019 to April 2020. The focus was on assessing the long-term performance of bottom ash (100 cm) and extruded polystyrene board (10 cm) as insulation layers for HMA pavement.

Chapter 5 harnessed pavement temperature data collected at depths ranging from 0.5 to 2.7 meters below the road surface, spanning from January 2013 to February 2020. These data were instrumental in training and validating machine learning models.

Chapter 6 utilized pavement temperature data gathered from the HMA, GBC, and subgrade layers, covering the period from January 2013 to August 2020. These data were employed for training and validating machine learning models.

Chapter 7 was dedicated to the development of machine learning models for predicting pavement temperature in the presence of insulated layers. Data from January 2017 to April 2020 formed the basis for these models.

Chapter 8 focused on training machine learning models for moisture content prediction at the base and subgrade layers, utilizing moisture content data collected from January 2013 to December 2017.

Chapter 9 harnessed the entirety of available pavement temperature and moisture content data from depths of 0.5 to 2.7 meters below the road surface, spanning from January 2013 to January 2018, for training deep learning models.

Chapter 10 employed FWD test results acquired on August 18, 2015, and August 20, 2020, to compare structural capacity changes across various tire and insulated sections of the test road.

Data Availability and Challenges:

The availability of data crucial to this study is comprehensively detailed in Tables 3-1 and 3-2. The data underwent transformation into daily values. Initially, the data were utilized to assess environmental impacts and the effects of insulation materials on pavement performance. Subsequently, all accessible data were employed in the training and validation of machine learning models.

However, it is worth noting that the harsh winter climate in Edmonton, coupled with traffic loading and technical issues with the data collection system, led to intermittent data recording by several sensors. Additionally, certain time periods experienced data gaps in temperature information. For consistency, all environmental parameters were sourced from the nearest Environment Canada weather station, Oliver ADGM, situated 6 km from the test road location.

Table 3-1: Temperature data availability for different pavement test sections.

Depth (m)	Start Date	End Date	Number of data points
(a) Control section			
0.02	Aug. 2014	Aug. 2016	731
0.09	Aug. 2014	Aug. 2016	731
0.17	Aug. 2014	May. 2020	2084
0.25	Aug. 2014	Dec. 2016	855
0.50	Jan. 2013	Jun. 2020	1849
0.70	Jan. 2013	Jul. 2020	1769
0.80	Jan. 2013	Dec. 2019	1554
1.80	Jan. 2013	Aug. 2020	1904
2.70	Jan. 2013	Dec. 2017	1402
(b) Bottom ash section			
0.72	Jan. 2017	Mar. 2020	765
1.40	Jan. 2017	Feb. 2020	758
1.85	Jan. 2017	Apr. 2020	760
2.83	Jan. 2017	Feb.2020	760
3.36	Jan. 2017	Mar. 2020	784
(c) Polystyrene section			
0.64	Jan. 2017	Feb. 2020	760
0.80	Jan. 2017	Feb. 2020	757
1.80	Jan. 2017	Feb. 2020	760
2.25	Jan. 2017	Jul. 2019	547
3.22	Jan. 2017	Feb. 2020	757

Table 3-2: Availability of moisture content data for the control section.

Depth (m)	Start Date	End Date	Number of Points
0.50	2013.11	2016.03	605
0.70	2013.11	2016.03	448
0.80	2013.01	2015.04	710
1.80	2013.01	2018.01	1023
2.70	2014.01	2017.12	1055

CHAPTER 4.LONG-TERM ANALYSIS OF ENVIRONMENTAL FACTORS VARIATIONS IN THE TEST SECTIONS

This section has been published as Huang, Y., Molavi Nojumi, M., Hashemian, L. and Bayat, A., 2021. Performance evaluation of different insulating materials using field temperature and moisture data. Transportation Research Record, 2675(9), pp.595-607.

4.1. ABSTRACT

Including insulation layers in pavement structures has become a common strategy to minimize frost penetration in cold regions. This study investigated the performance of two different insulation materials, extruded polystyrene board and bottom ash, in a test road in Edmonton, Alberta, Canada, eight years after construction. The two insulation materials were used in a fully instrumented test road, including three insulated sections 20 m in length. The insulated sections are as follows: the first section has 1m of bottom ash (B. Ash), the second section has a 10 cm polystyrene layer (Poly-10), and the third section has a 5 cm polystyrene layer (Poly-5). Both B. Ash and polystyrene layers were placed on top of the subgrade layer, at a depth of 70 cm from the surface. A conventional section next to these three sections was used as the control section. Volumetric water content data and temperature variation were used to analyze the influence of the insulation materials on the subgrade. It was concluded that both B. Ash and Poly-10 layers protected the subgrade from freezing. The Poly-10 section showed the lowest rate of change in subgrade temperature during the monitoring period. B. Ash and Poly-10 reduced the frost depth by 23% and 70% compared with the control section, respectively. It was concluded that Poly-10 protected the subgrade soil from freezing and excessive moisture more effectively than B. Ash; however, the temperature in the layer above the insulation layers (pavement base layer) was significantly lower during winter for the Poly-10 section.

Keywords: volumetric moisture content, temperature, bottom ash, polystyrene, insulation layer, pavement structure

4.2. INTRODUCTION

In cold regions, pavements are subject to harsh conditions, including long periods of extreme cold temperatures, as well as freeze-thaw cycles during spring. In the winter, as both the air and pavement temperatures drop, ice lenses form in the base and subgrade, which can result in differential frost heave on the pavement surface. In particular, a sudden change in moisture occurs when the temperature drops below 0°C (Teltayev and Suppes, 2019), the freezing point of water. As the temperature increases in the late winter, ice lenses in the pavement begin to melt. While the sublayer is still frozen, its permeability remains low, and excess water accumulates, which generally leads to a higher moisture content in the sublayer during the thawing period. Since both unbound pavement materials and thin pavement structures are sensitive to moisture variation, the higher moisture content in the thawing period can potentially lead to lower load capacity (Miller et al., 2012, 2015; Salour, 2015). Thus, pavements in cold regions typically exhibit premature damage, and have shorter service lives and higher maintenance costs, among other issues (Tighe et al., 2006).

The use of insulation layers in pavement structures has been a standard method used to protect pavement structures from extremely cold conditions. Polystyrene has been used as an insulation layer to protect pavement structures in many cold regions since 1967 (Penner, 1967). Previous studies have shown that a 5-cm layer of polystyrene can significantly reduce both thaw depth and frost heave. Moreover, case studies on pavement settlement also showed that, for pavement sections with polystyrene insulation layers, settlement was lower than for pavement sections with a standard design (Esch, 1973; Hayden and Swanson, 1972; Tatarniuk and Lewycky, 2011). Currently, a more environmentally friendly insulation material, bottom ash, has also been used in pavement construction. Bottom ash is a byproduct of electricity

generation by combustion of coal, and is mainly composed of silica, alumina, and iron. However, research on the use of bottom ash as an insulation layer to protect the subgrade from frost heave in cold regions only began two decades ago (Hashemian and Bayat, 2016).

Researchers at the Integrated Road Research Facility (IRRF) designed and constructed a test road located in Edmonton, Alberta, Canada in 2012, with a section of the road used to investigate the long-term performance of bottom ash as an insulation layer. Studies were conducted on the thermal performance of the bottom ash section over a one-year period, the effect of difference insulation materials on the load-bearing capacity of the pavement, pavement strength in different seasons, and damage evaluation of pavement with different insulation layers. The results of this series of studies (Haghi et al., 2014) indicate that insulation layers can block heat exchange between the base layer and subgrade layer and reduce the frost depth compared to the control section. However, it was found that the bottom ash not only protected the subgrade from frost heave in winter, but that the section insulated using bottom ash also had a higher load-bearing capacity in non-freeze/thaw conditions than the section insulated with a polystyrene layer (Haghi et al., 2016, 2018). The pavement section insulated with bottom ash also had a lower risk of fatigue cracking than the control section (Haghi et al., 2019).

Polystyrene board is a traditional insulation material, and much literature has already illustrated its use for various applications. Recently, with economic development and increased environmental awareness, road construction is increasely inclined to adopt more sustainable and environmentally friendly practices and materials. Bottom ash is a recycled material, so it may have less environmental impact than polystyrene. Although researchers have already investigated how bottom ash influences temperature distribution in the pavement structure (Haghi et al., 2014, 2016), only one or two years worth of data from immediately after completion of the IRRF test road construction was available and no traffic loading data

available at that time. The IRRF test road has now been open to public traffic for over eight years, with detailed information about traffic patterns available from the time that it was opened. In previous studies on the insulated test sections, moisture content variation that has a significantly influence on pavement load capacity also was rarely involved. The primary purpose of this study is to investigate the long-term thermal performance of each of the test road sections (containing either bottom ash or polystyrene as an insulation layer) under field conditions and thus determine how the insulation material influences the moisture content in the subgrade.

Studies by other researchers have indicated that slippery conditions formed on a surface with an insulation layer, while an adjacent conventional surface remained dry (Côté and Konrad, 2005, 2006). A test road in Québec City was used to measure the rate of surface cooling of the pavement. In this case, the pavement had one layer of a granular material as a base course on top of a clayed silt subgrade soil. For the uninsulated section, a 7-cm layer of hot mix asphalt (HMA) was placed on a 48.5-cm layer of granular material (base course). In the insulated section, the thickness of the HMA layer and the base course were the same as for the uninsulated section, but a 5-cm polystyrene layer was placed at a depth of 21 cm. Compared to the adjacent uninsulated pavement, the surface cooling rate of the pavement with a 5-cm polystyrene layer was drastically increased when a freezing front reached and stayed in the polystyrene layer. The surface cooling rate was 0.20 to 0.37 °C/hr for the uninsulated pavement, whereas the surface cooling rate reached 0.46 to 0.59 °C/hr in the insulated pavement (Côté and Konrad, 2002). In the case of the IRRF test road, no sensors were installed in the HMA layer of the polystyrene section and the bottom ash section, so similar data regarding cooling rates of insulated and non-insulated test sections is not available.

4.3. BACKGROUND

The IRRF test road is an access road to the Edmonton Waste Management Center (EWMC) and is located 15 km from downtown Edmonton. The test road consists of two lanes and is about 500 meters long, with a pavement width of 14.1 m and a pavement slope of 4:1. Construction of the test road took place in two stages (as shown in Figure 4-1). The first stage took place from May 2012 to August 2012, when a 16-cm layer of HMA was completed. The second stage took place in October 2013, with the existing HMA layer topped with another 9 cm of HMA. The test road has been open to public traffic since 2015 (mid-October), with garbage trucks accounting for 10 to 20% of all traffic. Weigh-in-motion (WIM) systems installed on the test road have been collecting data since June 2015. Based on WIM data, the average daily traffic was 745 in 2015, 2312 in 2016, and 2548 in 2019. Average daily traffic increased by 10% from 2016 to 2019.

As shown in Figure 4-1, there are three insulation sections and one control section in the test road. Each of the sections is 20 m long, and all sections are composed of 25 cm of HMA on top of a 45 cm granular base course (GBC) layer. The required pavement thickness was calculated based on traffic loading. Bottom ash was used as an insulation layer in one section of the test road. Closed-cell Styrofoam Highload 100 extruded polystyrene boards, provided by Dow Chemical Company, were used in the polystyrene test sections. Insulation layers were intended to protect the subgrade layer from freezing; thus, the insulation layer was placed under the base layer and on top of the subgrade layer (at a depth of 70 cm from the pavement surface).

Figure 4-1 shows the first section, from Station 130 + 240 to 130 + 260, which is the control section. The control section, which has no insulation layer, is used for comparing the variation in temperature and moisture content. In the three insulated sections, a 100-cm bottom ash layer

(B. Ash), a 10 cm polystyrene layer (Poly-10), and a 5 cm polystyrene layer (Poly-5) are located between the GBC and subgrade layers. The purpose of the section containing the 5 cm polystyrene layer is to avoid a sudden temperature change between the control section and the Poly-10 section and thus this section is not instrumented (i.e., no data is collected).

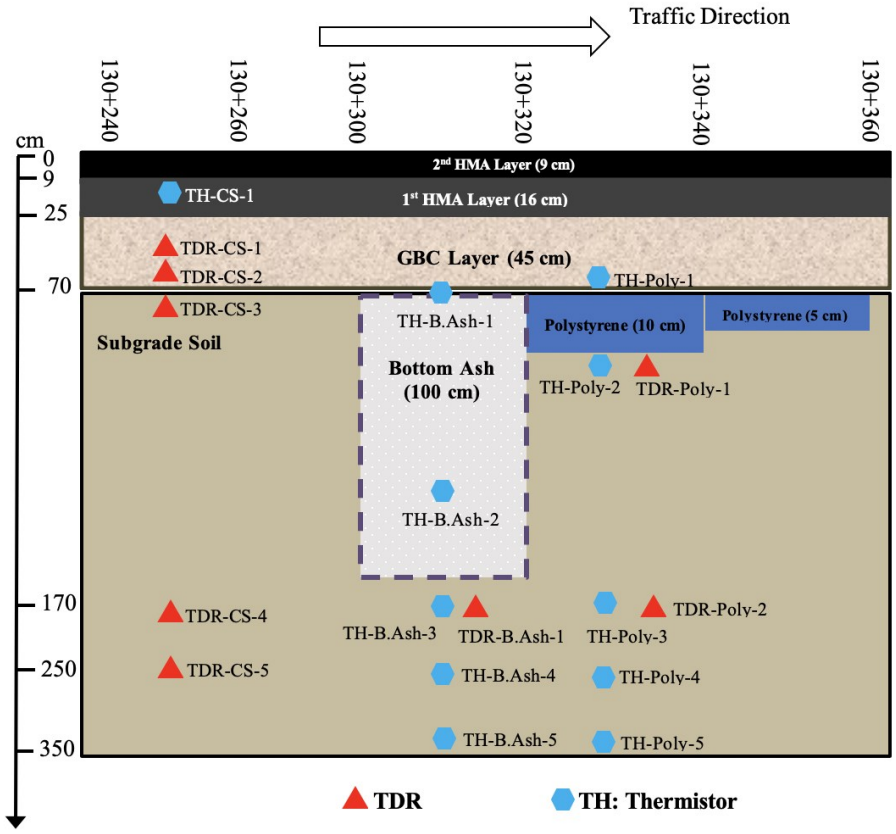

Figure 4-1: Cross section of pavement layers and as-built depth of thermistors and moisture probes

Note: HMA = hot mix asphalt; GBC = granular base course; TDR = time domain reflectometer.

Based on ASTM C 136-06 and the Unified Soil Classification System, the GBC layer is well-graded gravel, and the subgrade soil is clayey sand. The subgrade is moderately frost-susceptible. Approximately 27% and 21% of subgrade soil (by weight) passed through a 0.075 mm sieve and a 0.02 mm sieve, respectively. The liquid limit of the subgrade soil is 25%, and the plastic index is 9%. The bottom ash used for the insulation layer had a maximum particle size of about 5 mm, and did not contain large lumps and impurities. According to the weight of the material, the amount of unburned coal particles in the bottom ash was less than 5%.

The thermal resistivity, *R*, of the insulation materials is defined by Equation 4-1:

$$R\text{-value} = D / k \qquad \text{Equation 4-1}$$

where *D* is the layer thickness, and *k* is the thermal conductivity. *R* is generally used to compare the resistance of a material with conducting heat (i.e., a material with higher *R* value shows that a material is more effective as insulation). For bottom ash, *R* is equal to 1.43 $m^2 \cdot °C/W$, while for the 10 cm polystyrene board, the *R* is 16.67 $m^2 \cdot °C/W$ (Klein et al., 2003), as in Table 4-1.

Table 4-1: Properties of materials used in integrated road research facility test road construction.

Material	**C_p (kJ/kg·°C)**	***k* (W/m·°C)**	***R* value ($m^2 \cdot °C/W$)**	**Density (ton/m^3)**	**Reference**
Hot mix asphalt	0.92	1.21	0.13	2.35	Thompson et al. (1987)
Granular base course	0.71	0.90	0.50	2.10	Thompson et al. (1987)
Subgrade soil	0.71	0.60	n/a	1.85	Thompson et al. (1987)
Bottom ash	0.80	0.70	1.43	0.34	Klein et al. (2003)
Polystyrene	1.25	0.006	16.67	n/a	Haghi et al. (2014)

Note: C_p = specific heat at constant pressure*; k* = thermal conductivity*; n/a* = not applicable.

During construction of the IRRF test road, 109AM-L thermistors and CS650 time domain reflectometers (TDRs) were installed to monitor variation in temperature and moisture content. The thermistors only capture the temperature, whereas the TDRs record both temperature and volumetric water content (VWC) (i.e., water that is not frozen). As shown in Figure 4-1, one thermistor was placed at a depth of 0.18 m in the middle of the HMA layer in the control section, while no sensors was installed in the HMA layer in both B. Ash and Poly-10 sections. Two TDRs were installed in the GBC layer, and three TDRs were installed in the subgrade layer at

a depth of 2.65 m from the top of the subgrade. In the B. Ash section, there are five thermistors, one in the GBC layer, one in the bottom ash layer, and three in the subgrade layer. There is a TDR installed in the B. Ash section at a depth of 1.85 m from the pavement surface. There are also five thermistors in the Poly-10 section: one at the bottom of the GBC layer, and four others in the subgrade layer, along with two TDRs. One TDR is located at a depth of 0.75 m from the pavement surface and just below the 10 cm polystyrene, and the other one was installed 1 m below this. All VWC data collected was adjusted using a formula determined by calibration of the TDRs in the laboratory. The temperature and VWC data collected by the thermistors and TDRs was stored using a CR1000 datalogger, which was programmed to collect data from each of the sensors at 15 min intervals. Data is retrieved from the IRRF test road sensors by remote access from an on-site computer, with an off-site computer at the University of Alberta used for analysis of the data.

Precipitation is one of the most critical factors influencing moisture content variation in warm wet regions, with its effect decreasing with increasing depth (Hedayati and Hossain, 2015). However, in cold dry regions (such as Edmonton), the moisture content variation is dominated by temperature instead of precipitation. For example, in Figure 4-2, the moisture content variation (as measured using a TDR-CS-1 at a depth of 0.48 m, in the GBC layer) is shown for 2015, as well as precipitation. The observed trend is that moisture content dropped in fall, remained at a low level through winter, and increased in spring. Through summer, the moisture content was high.

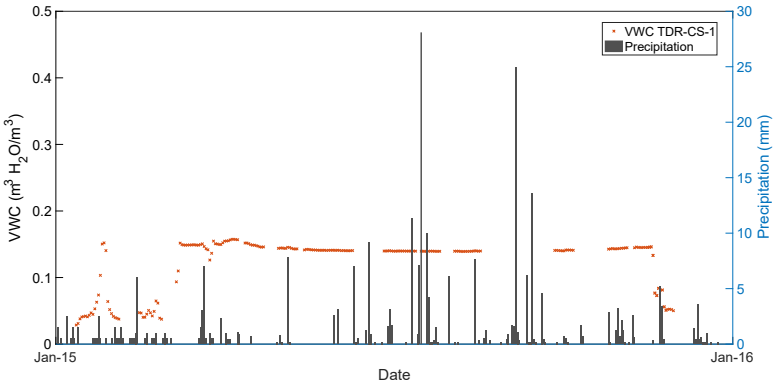

Figure 4-2: Moisture content variation at a depth of 0.48 m (in granular base course layer) and precipitation over time (2015 data)

Note: VWC = volumetric water content.

4.4. DATA COLLECTION AND ANALYSIS

4.4.1. Control Section

Ambient temperature data were collected from the Oliver AGDM weather station, which is the weather station that is closest to the Edmonton Waste Management Centre (there is a distance of about 6 km between the IRRF test road and the weather station, as determined using Google maps). From 2012 to 2020, the average air freezing index was 1177 °C·day, and the air average thawing index was 662 °C·day, based on air temperature recordings collected at Oliver AGDM over this time period. The daily ambient temperature over 42 months, along with the temperature measured in the base and subgrade layers, are shown in Figure 4-2. From October 2016 to April 2020, the maximum average daily ambient temperature (24 h average) was 23°C and the minimum average daily ambient temperature (24 h average) was -38°C (January 14, 2020).

Figure 4-3 illustrates the temperatures of the base and subgrade layers of the control section from October 2016 to April 2020. As a result of technical issues, temperature data for February 2018 to June 2018 and September 2018 to March 2020 are missing for all sections. The temperature data for the base layer and the subgrade layer were collected using a TDR-CS-2

and a TDR-CS-4. The as-built depths for the TDR-CS-2 and TDR-CS-4 sensors are 0.67 m and 1.79 m from the pavement surface, respectively. Temperature data, which was collected from the sensors every 15 minutes, were used to calculate the average daily temperature. The temperature in the base layer was observed to change synchronously with ambient temperature, but the change in subgrade temperature lagged behind. The lowest temperature recorded in the base layer was -14°C (January 18, 2020). The temperature of base layer was below 0°C from November to April, however, the subgrade temperature remained between -1°C and 0°C from January to April.

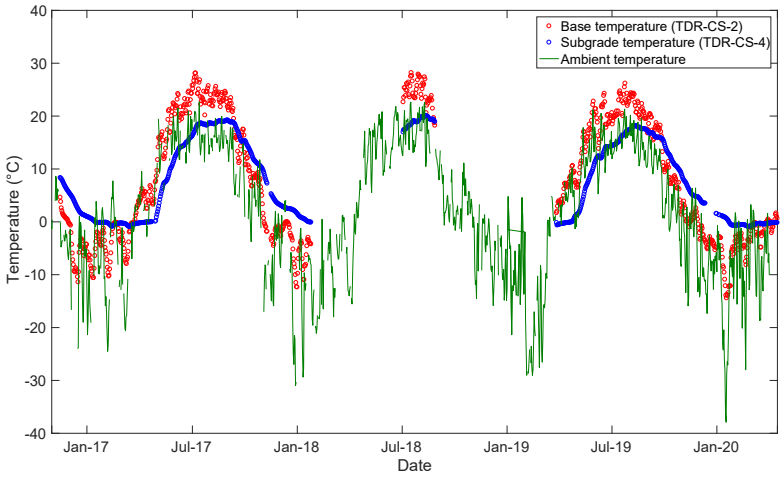

Figure 4-3: Daily ambient temperature and average daily temperature from sensors installed in the base layer and the subgrade layer (control section)

Figure 4-4 indicates the variation in temperature with depth from February 2017 to January 2018 for the control section. As seen in Figure 4-4, the range in temperature values decreases with increasing depth. The temperature in the HMA layer (at a depth of 0.18 m) varies from -23°C to 32°C, whereas the temperature variation at a depth of 2.70 m is between 1°C and 16°C. The base layer stays frozen from November to March, while the subgrade layer is frozen from January to March. As seen in Figure 4-4, freezing can be observed in the subgrade in colder months (as early as October and as late as April). Although the range of temperature variation

decreases with increasing depth, temperatures below 0°C are observed in the subgrade until a depth of 2.1 m is reached.

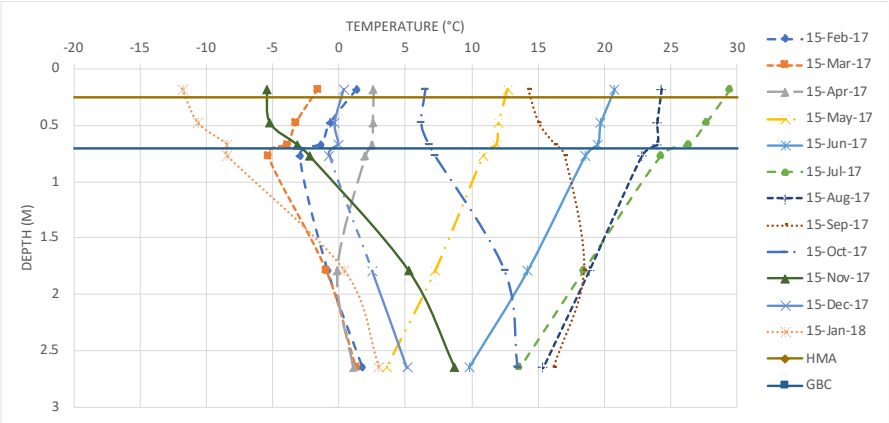

Figure 4-4: Temperature variation with depth in the control section of the Integrated Road Research Facility test road

VWC in the various layers was determined using TDRs (excluding frozen water) and subgrade temperature. Once the temperature drops below 0°C, the form of water changes from liquid to solid, so when the subgrade temperature goes below 0°C in the winter, VWC decreases (Teltayev and Suppes, 2019). Later, when the subgrade temperature increases above 0°C, VWC spikes, and, due to inadequate drainage of the lower frozen soil in spring, the moisture content reaches the highest value of the year. As the accumulated water slowly drains and evaporates, VWC falls to a more stable value.

Figure 4-5 (a) shows the daily pavement temperature and VWC for the control section at a depth of 0.80 m (the as-built depth of the sensor TDR-CS-3 is 0.83 m). The subgrade temperature varied from -10°C to 28°C, and VWC ranged from 0.03 m^3 H_2O/m^3 to 0.39 m^3 H_2O/m^3. At the top of the subgrade layer, VWC started to drop in December, reached its minimum in about February and increased to its highest value in March.

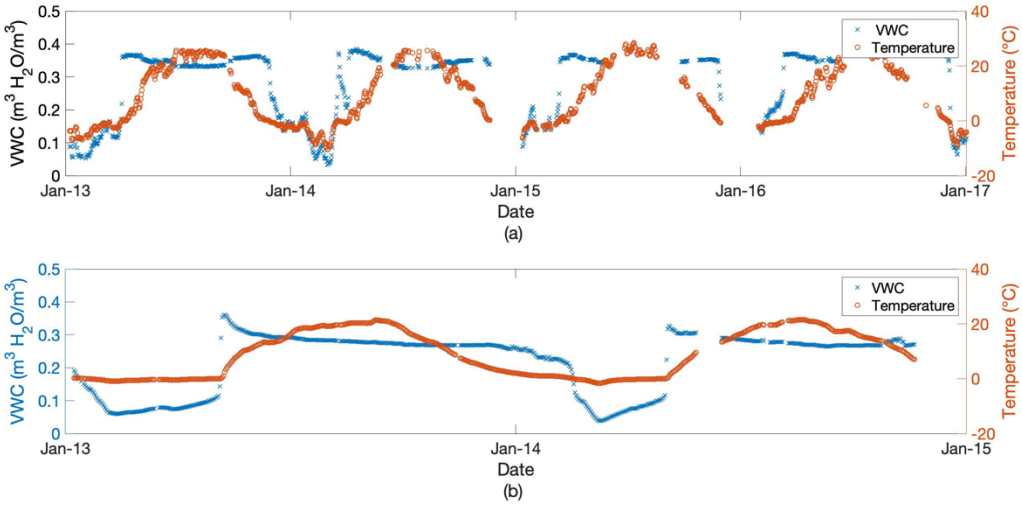

Figure 4-5: Volumetric water content (VWC) and temperature in the control section: (a) depth of 0.8 m and (b) depth of 1.8 m

Figure 4-5 (b) shows the daily pavement temperature as well as VWC for the control section recorded by TDR-CS-4, which is installed 1 meter below TDR-CS-3 in the subgrade layer (the as-built depth for TDR-CS-4 is 1.82 m). From 2014 to 2015, the temperature of the pavement varied between -2°C and 22°C and VWC ranged from 0.06 m^3 H_2O/m^3 to 0.36 m^3 H_2O/m^3. At a depth of 1.8 m from the pavement surface in the control section, VWC was observed to decrease in February, reach its minimum in February 2014 and March 2015, and reach its maximum in May 2014 and 2015.

4.4.2. Bottom Ash Section

Figure 4-6 shows the average daily temperature for the base and subgrade layers in the section of the IRRF test road insulated using bottom ash (for October 2016 to April 2020). The recordings were recorded by the sensors TH-B. Ash-1 and TH-B. Ash-3 (see Figure 4-1), with as-built depths of 0.72 m and 1.80 m. The maximum base temperature observed was 28°C in July, and the minimum base temperature was -17°C on January 17, 2020. Over the same time period, the temperature in the subgrade layer varied from 2°C to 15°C, never dropping below 0°C.

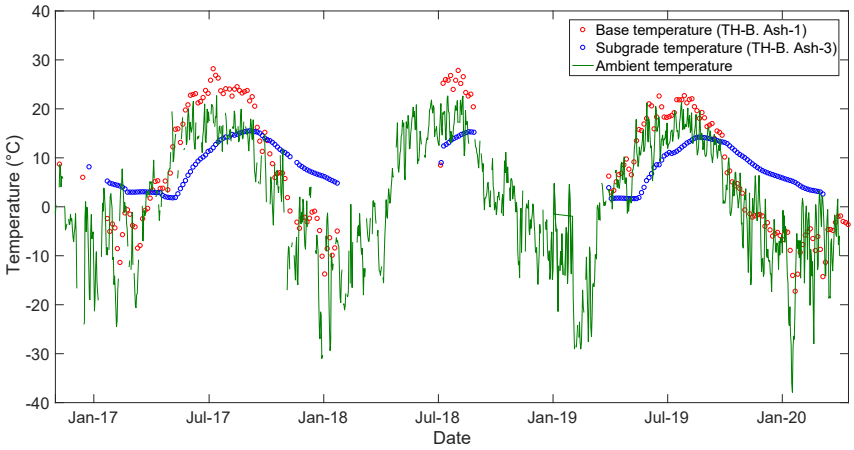

Figure 4-6: Daily ambient temperature and average temperature recorded at sensors installed in base layer (depth 0.72 m) and subgrade layer (depth 1.80 m) in Integrated Road Research Facility test road section insulated with bottom ash

Figure 4-7 shows the temperature distribution in the test section insulated using 100 cm of bottom ash. Although the range of the temperature change also decreases with increasing depth, the subgrade temperature below the insulating bottom ash layer stays in a more stable range, because of the presence of the bottom ash layer. The temperature at the bottom of the GBC layer (at a depth of 0.60 m) varies from -10°C to 27°C (a range of 37°C), the temperature at a depth of 1.80 m varies from 2°C to 15°C (a range of 13°C), and the temperature at a depth of 3.2 m varies from 3°C to 13°C (a range of 10°C). The GBC layer remains frozen from November to March. At the same time, the maximum frost depth of the B. Ash section was 1.60 m and the temperature of the subgrade remained above 0°C all year.

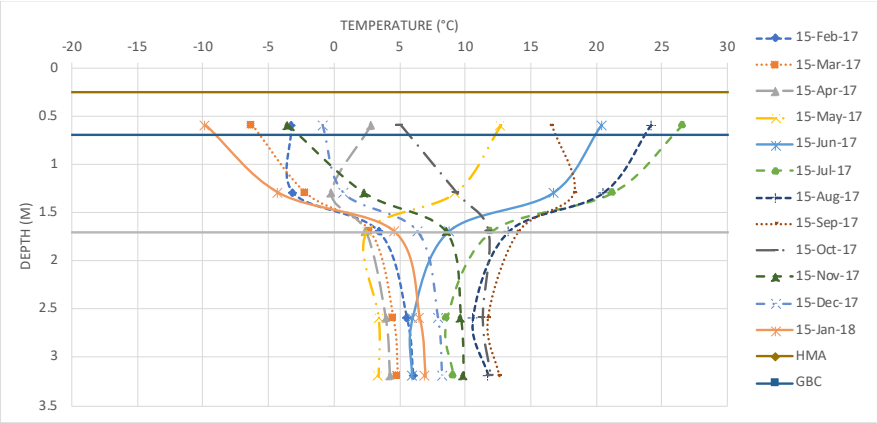

Figure 4-7: Temperature variation along depth across pavement structure in the bottom ash section

Figure 4-8 presents VWC and daily average temperature recorded in the section of the test road insulated with bottom ash. The data was collected using the sensor TDR-B. Ash-1 (see Figure 4-1) which is located at a depth of 1.85 m. VWC varied from 0.21 m^3 H_2O/m^3 to 0.31 m^3 H_2O/m^3. The temperature of the subgrade below the bottom ash layer never dropped below 0°C, so water in this layer does not freeze. This may be the reason that VWC did not show a drop as observed for VWC in the control section at the same depth. However, VWC showed a small decline from January 2013 to February 2013 and December 2013 to May 2014. In Hoekstra's laboratory measurements of moisture content in unconsolidated undrained soil (Hoekstra, 1967), it was shown that moisture content migrates from thawed to frozen areas of soil when there is a moisture content gradient. According to Hazen's equation, the coefficient of permeability can be expressed as in Equation 4-2:

$$k = C(D_{10})^2 \qquad \text{Equation 4-2}$$

where k is the coefficient of permeability (cm/s), C is a constant ranging from 0.4 to 1.2 (typically assumed to be 1.0), and D_{10} is the grain size corresponding to 10% by weight passing, also referred to as the effective size (mm) (Hazen, 1892). In this work, C is assumed to be 1.0. The grain size corresponding to 10% by weight passing is 0.18 mm for the subgrade soil and 3.79 mm for bottom ash. Therefore, for the subgrade soil, k is 0.03 cm/s, and for bottom ash, k is 14.36 cm/s. Thus, the coefficient of permeability of the subgrade soil is much lower than the bottom ash, thus it is possible for water to migrate from the subgrade to the bottom ash. In winter, the decline in moisture content observed at a depth of 1.8 m indicates that water migrated upwards to the bottom ash in the winter due to water suction.

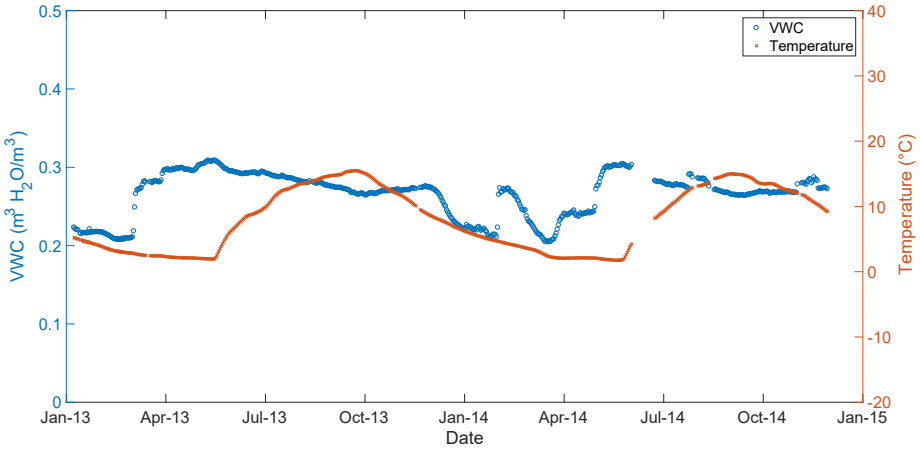

Figure 4-8: Volumetric water content (VWC) and temperature in the bottom ash test section measured at a depth of 1.8 m

4.4.3. Polystyrene Section

Figure 4-9 shows the base temperature and subgrade temperature in the IRRF test section insulated with 10 cm of polystyrene board from October 2016 to April 2020. The as-built depths of the sensors, as shown in Figure 4-1, were 0.64 m (GBC layer), 0.75 m (subgrade layer), and 1.75 m (subgrade layer). The temperature observed at these three depths varied from -26°C to 31°C, 1°C to 13°C, and 3°C to 11°C, respectively. Below the Poly-10 layer, the subgrade temperature remained above freezing. The lowest base temperature, -26°C, was measured on January 16, 2020, and the highest temperature values were measured in July, August, and September for the base layer, the top of the subgrade, and one meter below the top of the subgrade, respectively. The hysteresis between ambient temperature and the temperature within the pavement structure increases with depth.

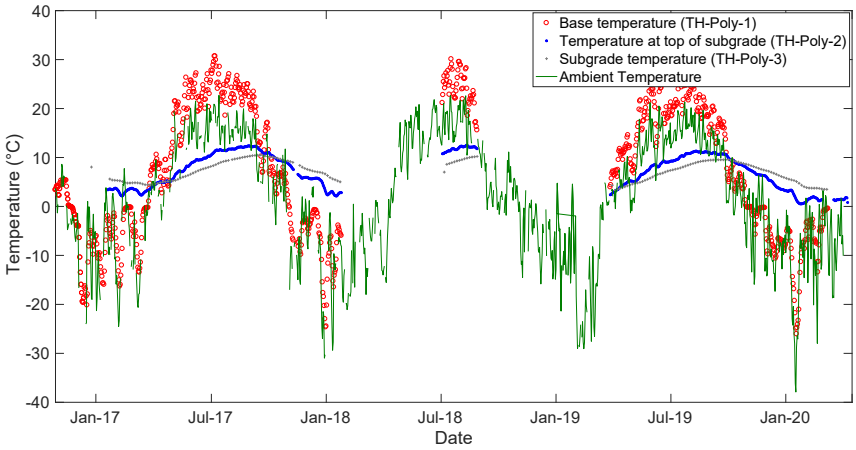

Figure 4-9: Variation in daily ambient temperature and average temperature over time at various depths in the 10 cm polystyrene test section

Figure 4-10 presents the variation in pavement temperature with depth in the test section containing 10 cm polystyrene from February 2017 to January 2018. The temperature was recorded by five thermistors (as in Figure 4-1): sensor TH-Poly-1 is located in the GBC layer, with an as-built depth of 0.64 m, and sensor TH-Poly-2 is just below the polystyrene layer, with an as-built depth of 0.75 m. The temperature measured within the GBC layer indicates that it is frozen from November to March. The temperature variation measured by the thermistor TH-Poly-1 (GBC layer) ranges from -14°C to 26°C, a difference of 40°C. In contrast, the temperature measured just below the polystyrene layer (by TH-Poly-2) ranges from 1°C to 12°C, a difference of 11°C. The 10 cm polystyrene layer blocks heat exchange between the GBC layer and the subgrade layer, which leads the temperature to decrease rapidly with depth over a short distance (0.11 m). The yearly variation in temperature measured at depths from 2.25 m to 3.25 m in the Poly-10 test section is less than 5°C, as shown in Figure 4-10.

Figure 4-11 shows the temperature and VWC measured just below the polystyrene layer (using TDR-Poly-1, which has an as-built depth of 0.75 m; see in Figure 4-1) from January 2013 to January 2017. The same data is shown for a depth 1 m below (measured using TDR-Poly-2, located at an as-built depth of 1.72 m) from January 2013 to January 2015.

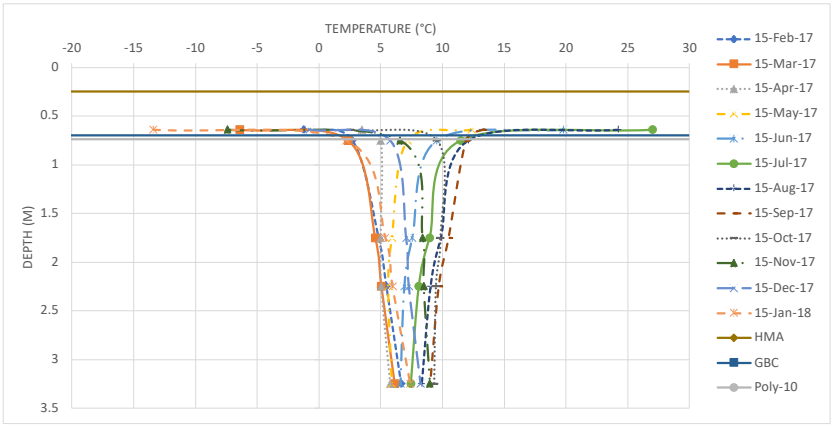

Figure 4-10: Temperature variation along depth across pavement structure in the 10 cm polystyrene section

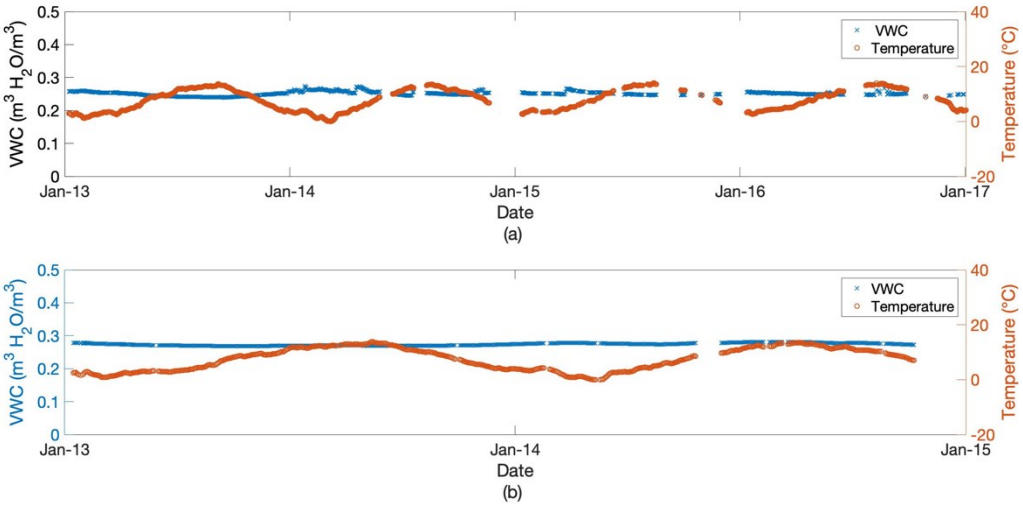

Figure 4-11: Change of Volumetric water content (VWC) and temperature in the 10 cm polystyrene section at depths of (a) 0.8 m and (b) 1.8 m

As discussed previously, due to the phase change of water from liquid to solid at 0°C, the VWC of the subgrade layer will drop in winter. Figure 4-5 (a) shows the change in VWC in the control section at the same depth, however, the subgrade in the test section is insulated by the 10 cm polystyrene layer. For the Poly-10 section, the subgrade temperature remains above freezing all year, and there is no significant drop in VWC observed during the winter. Also, the temperature of the GBC (above the polystyrene layer) changed from -14°C to 26°C, so the GBC layer in the Poly-10 section will have frost in winter. Unlike VWC measured at a depth of 1.80 m in the B. Ash section, VWC measured at a depth of 0.8 m in the Poly-10 section only varies between 0.24 m^3 H_2O/m^3 and 0.27 m^3 H_2O/m^3, a difference of 0.03 m^3 water/m^3. This

means that no water suction occurs, and moisture does not migrate from the subgrade (where there is no freezing) to the frozen GBC layer. The deepest sensor in the Poly-10 section (TDR-Poly-2) is at 1.72 m, and VWC varies from 0.27 m^3 H_2O/m^3 to 0.29 m^3 H_2O/m^3 at a depth of 1.80 m, a difference of only 0.02 m^3 H_2O/m^3. Thus, the VWC of the subgrade does not change as much in the test section insulated with 10 cm polystyrene.

4.5. DISCUSSION

Insulation materials block heat exchange between the base layer and the subgrade layer of the pavement structure, resulting in different base temperatures. The thermal characteristics of the three test sections are presented in Table 4-2. From February 2017 to January 2018, the maximum base temperature in the control section and the B. Ash section was 28°C, whereas the maximum base temperature in the Poly-10 section was 31°C, 3°C higher than the control section. From April 2019 to April 2020, the maximum base temperature in the control section was 26°C, 3°C higher than the B. Ash section and 2°C lower than the Poly-10 section. In the summer, the maximum base temperature difference observed between the control and B. Ash sections was 3°C. However, in the winter, the maximum base temperature difference observed between the control and Poly-10 sections was 12°C. Furthermore, in winter, the maximum base temperature difference between the control section and the B. Ash section was 3°C. The pavement structure containing the 10 cm polystyrene layer results in a much lower base temperature in winter, which negatively influences the pavement performance. Lower pavement temperatures in winter make the pavement more prone to low-temperature cracking. This is in contrast to the B. Ash section, which performs closer to the control section; thus, the bottom ash layer prevents low-temperature pavement damage more effectively.

Table 4-2: Thermal characteristics of integrated road research facility test road.

Duration	**February 2017 to January 2018**			**April 2019 to April 2020**		
Test section	**CS**	**B. Ash**	**Poly-10**	**CS**	**B. Ash**	**Poly-10**
Base temperature (°C)	-12 to 28	-14 to 28	-24 to 31	-14 to 26	-17 to 23	-26 to 28
Subgrade temperature (°C)	-1 to 19	2 to 15	4 to 11	-1 to 18	2 to 4	3 to 10
Temperature gradient (°C/m)	-5.7 to 6.1	-2.6 to 1.4	-1.7 to 2.1	na	-2.2 to 1.2	-1.3 to 2.2
Rate of base temperature change (°C/day)	0.23	0.24	0.32	0.23	0.23	0.23
Rate of subgrade temperature change (°C/day)	0.12	0.12	0.03	0.10	0.31	0.31
Rate of temperature change at deepest sensor (°C/day)	0.07	0.04	0.03	n/a	0.12	0.12

Note: CS = control section; B. Ash = bottom ash section; Poly-10 = 10 cm polystyrene section; na = not applicable.

R was used to justify how insulation materials influence the temperature trend. *R* for the bottom ash layer is 1.43m^2°C/W, while *R* for the polystyrene layer is 16.67m^2°C/W, ten times that of the bottom ash layer. The polystyrene layer, with a higher *R*, blocks heat exchange and results in a much lower base temperature in winter. However, when used in road construction, the polystyrene layer is 10 cm thick, while the bottom ash layer is 100 cm thick. Thus, the temperature in the section insulated with a 10 cm polystyrene layer changed more rapidly. Because of the presence of insulation materials in the test sections, the sensors in the subgrade (depth 1.80 m) showed less temperature variation compared with the control section. During the monitoring period, the maximum difference observed in subgrade temperature was 20°C, 13°C, and 7°C for the control section, B. Ash section and Poly-10 section, respectively. In the

same period, the bottom ash and 10 cm polystyrene layers had a lower difference in subgrade temperature, and in both cases the temperature of the subgrade remained above 0°C all year round.

To compare the bottom ash layer and 10 cm polystyrene layer as insulation materials, the temperature gradient and temperature change rate were calculated, with the results summarized in Tables 4-2 and 4-3. The temperature gradient was calculated using Equation 4-3,

$$Temperature\ gradient = \frac{\Delta T_1}{\Delta D} \quad \text{Equation 4-3}$$

where ΔT_1 is the difference in temperature (as measured by the shallowest and deepest sensors in the subgrade), and ΔD is the distance between the sensors.

The rate of temperature change is calculated as in Equation 4-4,

$$Rate\ of\ temperature\ change = \frac{\Delta T_2}{\Delta t_1} \quad \text{Equation 4-4}$$

where ΔT_2 is the temperature difference between the maximum and minimum temperatures over the time period, and Δt_1 is the change in time. A lower value of temperature gradient or rate of temperature change in the subgrade layer demonstrates that the material works more effectively as an insulation layer. The comparison ratio—that is, the ratio of difference in rate of temperature change between the test section and the control section to the rate of temperature change for the control section—is defined as in Equation 4-5.

$$Comparison\ ratio = \frac{Temperature\ change\ rate\ of\ (other\ section - control\ section)}{Temperature\ change\ rate\ of\ control\ section} \quad \text{Equation 4-5}$$

Since there are no data available from sensor TDR-CS-5 between April 2019 and April 2020, as a result of technical difficulties, the temperature gradient for the control section and rate of

temperature change at a depth of 2.65 m for the control section are not available for that period. The temperature gradient for the control section is -5.7 to 6.1°C/m, while the same value ranges from -2.6 to 1.41°C/m and -1.7 to 2.1°C/m for the B. Ash and Poly-10 sections, respectively. For the next year when data are available (April 2019 to April 2020), the Poly-10 section has a lower temperature gradient than the B. Ash section.

Table 4-3: Comparison of rates of temperature change of test sections with control section for different layers.

	February 2017 to January 2018		**April 2019 to April 2020**		**Average**	
	B. Ash (%)	**Poly-10 (%)**	**B. Ash (%)**	**Poly-10 (%)**	**B. Ash (%)**	**Poly-10 (%)**
Rate of temperature change in base	-4	-39	0	-35	-2	-37
Rate of temperature change in subgrade	0	75	-20	70	-10	73
Rate of temperature change at deepest sensor (subgrade)	43	57	na	na	43	57

Note: B. Ash = bottom ash section; Poly-10 = 10 cm polystyrene section; na: not applicable.

The annual average rate of temperature change in the base layer was 0.23°C/day, 0.24°C/day, and 0.32°C/day, for the control section, B. Ash section, and Poly-10 section, respectively, from February 2017 to January 2018. The results for April 2019 to April 2020 did not change significantly, so the test section insulated with bottom ash performed similarly to the control section and better than the test section with the 10 cm layer of polystyrene. In the subgrade layer, the rate of temperature change in the control section was 0.12°C/day from February 2017 to January 2018 and 0.10°C/day from April 2019 to April 2020. For the test section containing bottom ash, similar rates of temperature change were observed in the subgrade and the control sections. However, the rate of temperature change calculated for the polystyrene section was 0.03°C/day, 73% less than for the control section. Thus, the test section insulated with a 10 cm polystyrene layer resulted in relatively more stable temperatures within the subgrade layer.

Considering the data recorded at the deepest sensor, although the rate of temperature change rate in the control section declined to 0.07°C/day, the rate of temperature change was still the lowest in the Poly-10 test section. The rate of temperature change at the deepest sensor was similar for the B. Ash and Poly-10 sections. Therefore, the results for the test section with the 10 cm polystyrene layer had both the highest rate of temperature change in the base layer and lowest rate of subgrade temperature change. This indicates that the use of a 10 cm polystyrene layer as insulation within the road structure is beneficial for the subgrade but worse for the top layer. In contrast, the test section insulated with bottom ash not only resulted in protection of the subgrade layer, but also did not lead to lower temperatures in the top layers during winter. Overall, the bottom ash layer performed better as an insulation material than the 10 cm polystyrene layer.

Maximum frost depths were obtained based on temperature data collected from February 2017 to January 2018, as shown in Figure 4-12. The maximum frost depths were found to be 2.10 m, 1.60 m, and 0.71 m for the control section, B. Ash section, and Poly-10 section, respectively. Thus, both bottom ash and polystyrene layers decreased the maximum frost depth and protected the subgrade layer below this depth from freezing. The bottom ash layer reduced the frost depth by 23%, and the polystyrene layer decreased the frost depth by 70%, indicating that the polystyrene layer performed best at protecting the subgrade.

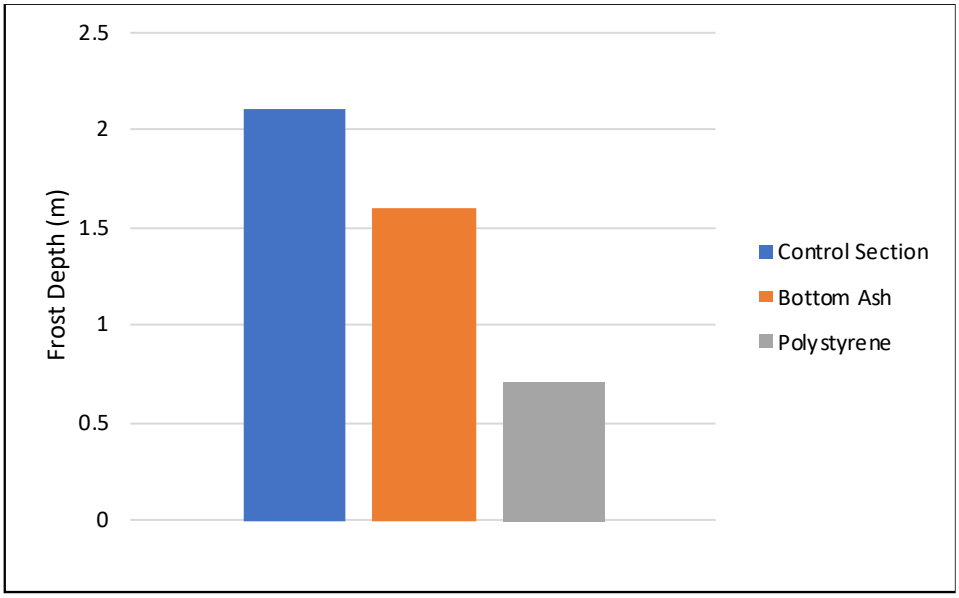

Figure 4-12: Maximum frost depths for test sections from February 2017 to January 2018

The moisture content and moisture content change ratios at a depth of 1.80m in the subgrade layer for the control, B. Ash, and Poly-10 sections are shown in Figure 4-13 and Table 4-4. Based on the temperature and VWC in the subgrade, the year can be divided into times in which the ground is frozen (frozen period), thawing (thawing period), and with no freezing or thawing (non-freeze–thaw period) (Haghi et al., 2018). Late summer, when the ground is drained and recovered, belongs to the non-freeze–thaw period. It is clear that only the control section freezes at a depth of 1.80 m from the pavement surface in the subgrade during winter, and both solid and liquid water was present in the subgrade layer.

$$Change\ ratio = \frac{Highest\ VWC - Lowest\ VWC}{Lowest\ VWC} \qquad \text{Equation 4-6}$$

During the two monitoring periods, VWC is the most stable in the Poly-10 section, with the lowest change ratio, between 0% and 7%, while VWC in the B. Ash section shows the most significant change in moisture content, with a change ratio of 48% and 50%. The maximum values of VWC observed for the control section were $0.36m^3$ H_2O/m^3 in 2013 and $0.33m^3$ H_2O/m^3 in 2014, which was higher than the maximum VWC observed in the B. Ash and Poly-10 sections in May. Salem (2004) and Bayat (2009) have reported that there is an inverse

correlation between resilient modulus and soil moisture content. In Alberta, the lowest subgrade resilient modulus typically is observed in April and May (Utilities, 1997). Thus, the higher subgrade VWC in May leads to a lower load capacity for the control section. The bottom ash and polystyrene layers did protect the subgrade and avoid the lower load capacities in May. VWC was more stable and had a lower value in the Poly-10 section, so, with respect to load capacity, the polystyrene layer functioned better as an insulation layer than the bottom ash layer.

Although extruded polystyrene board works effectively as an insulation material and is time saving for construction, previous studies have shown that it is not a cost-effective solution as an insulation material (Edgar et al., 2015; Haghi et al., 2016; Uzarowski et al., 2013). However, as a waste material, bottom ash may be an economical alternative as an insulation material for road construction, particularly in regions such as Alberta, where a large amount of bottom ash is produced as a byproduct of power generation. A previous study compared cost effectiveness and sustainability for a bottom ash layer and a 5 cm polystyrene layer in the IRRF test road. It was concluded that for frost depths between 1.7 and 3.5 m in the control section, using bottom ash would be more cost effective than polystyrene. Since the maximum frost depth in the IRRF test road was determined to be 2.10 m in that study, bottom ash was considered to be the more cost-effective material (Haghi et al., 2014, 2019).

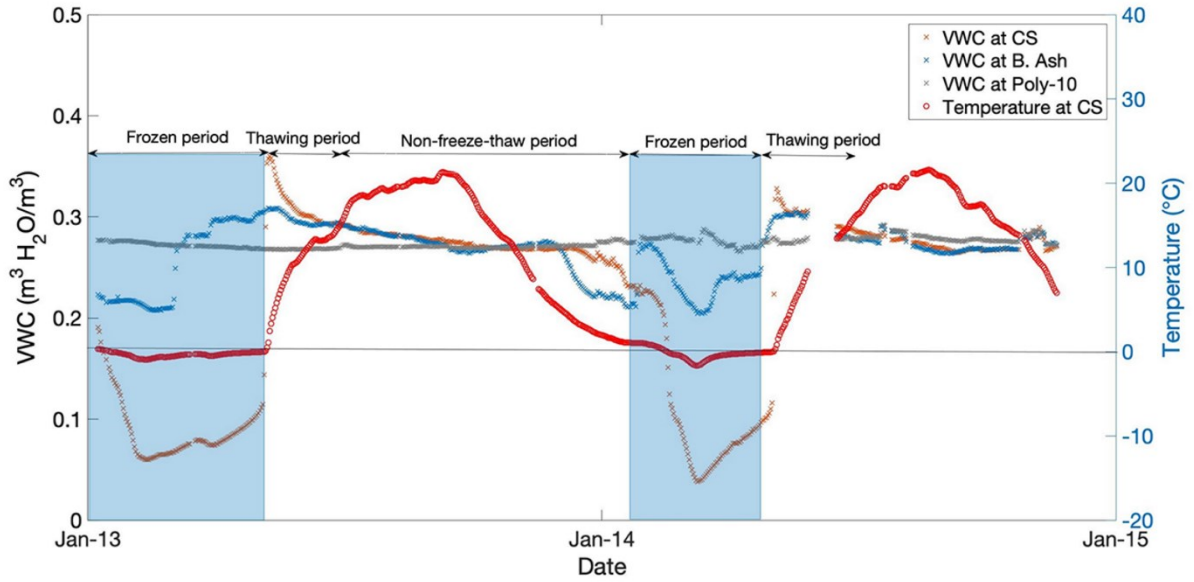

Figure 4-13: Temperature and volumetric water content (VWC) at a depth of 1.8m (subgrade) for control section, bottom ash test section, and polystyrene test section

Table 4-4: Moisture content and change ratio.

Year	Volumetric water content (m^3 H_2O/m^3)			Change ratio (%)		
	CS	B. Ash	Poly-10	CS	B. Ash	Poly-10
2013	0.26 to 0.36	0.21 to 0.31	0.27	38	48	0
2014	0.25 to 0.33	0.20 to 0.30	0.27 to 0.29	32	50	7

Note: CS = control section; B. Ash = bottom ash section; Poly-10 = 10 cm polystyrene section.

When choosing material for an insulation layer within pavement, there are also other factors to be considered, such as pavement load-bearing capacity. Various reports in the literature (Haghi et al., 2016, 2018, 2019) discuss how bottom ash and polystyrene board influence structural capacity and pavement life. The use of 10 cm polystyrene board as an insulation layer in the IRRF test section could potentially result in a loss of 34% of the load-bearing capacity of the pavement structure compared with the control section, whereas the 100 cm bottom ash layer does not have a negative impact on the load-bearing capacity (Haghi et al., 2016).

Since the IRRF test road was opened to traffic in 2015 (over five years ago), no visible pavement deflection has been observed for either the control section or the insulation sections.

Long-term monitoring of the IRRF continues, including visual inspections. While surface frost heaving and differential icing are other important considerations in the appropriate selection of insulation material, this would require regular on-site observations during winter and is beyond the scope of the project.

4.6. CONCLUSIONS

The ambient temperature collected from the Oliver AGDM weather station and temperature data recorded using sensors embedded in the IRRF test road in Edmonton, Alberta, from October 2016 to January 2018, July to September 2018, and April 2019 to April 2020, were used to investigate the long-term performance of bottom ash (100 cm) and extruded polystyrene board (10 cm) as insulation layers for HMA pavement. The bottom ash and polystyrene insulation layers are 70 cm from the pavement surface (on top of the subgrade). VWC data from sensors installed in the test road sections was used to determine the impact of the bottom ash layer and 10 cm polystyrene layer on the moisture content in the subgrade. The following conclusions were made, based on a detailed analysis of temperature and VWC data for the different IRRF test sections.

1. Both insulation layers (10 cm extruded polystyrene board and 100 cm bottom ash) block heat exchange between the base layer and the subgrade layer. The Poly-10 test section, with a higher R (16.7 m^2°C/W), resulted in a larger temperature variation in the base layer than the B. Ash section, which has an R of 1.4 m^2°C/W. Furthermore, the difference in base temperature between the control section and the Poly-10 section in winter is 12°C, which is four times the temperature difference of 3°C observed in summer.
2. During the two monitoring periods, from October 2016 to January 2018 and April 2019 to April 2020, the rate of base temperature change is highest in the Poly-10 section. The base temperature change rates for the control section and the B. Ash section are the same,

0.23°C/day, while the temperature change rate of the base for the Poly-10 section is 0.31°C/day, which is much higher than the rate observed for the control section. This indicates that the pavement insulated with the 10 cm polystyrene layer is prone to low-temperature cracking in winter.

3. Although the rate of change of temperature for the control and B. Ash sections is similar for the subgrade, the temperature change ratio at the deepest monitoring location of the Poly-10 section and the B. Ash section are lower than for the control section. Thus, both the polystyrene and the bottom ash did protect the subgrade layer from freezing when used as insulation layers. However, the rate of temperature change for the test section insulated with a 10 cm polystyrene layer is lower than the section with bottom ash, so the subgrade temperature in the Poly-10 section is the most stable among these three sections.
4. The maximum frost depths observed are 2.10 m, 1.60 m, and 0.75 m for the control, B. Ash, and Poly-10 sections, respectively. Compared with the control section, the test sections insulated with bottom ash and polystyrene showed a reduction in frost depth of 23% and 70%, respectively.
5. Pavement temperature data indicated that subgrade temperature of the B. Ash section never dropped below 0°C and VWC data showed that the bottom ash layer protected the subgrade below it from freezing, however, the bottom ash layer itself was frozen. Although the subgrade under the bottom ash layer did not freeze, the effect of water suction from the frozen bottom ash layer caused VWC in the subgrade layer to decrease in winter. At the same time, the VWC of the subgrade in the Poly-10 section did not show any variation at a depth of 0.80m.
6. The VWC change ratio (in the subgrade) for the Poly-10 section was found to be 0% and 7% for 2013 and 2014, respectively, while the B. Ash section has a VWC change ratio of 48% and 50% for 2013 and 2014. This indicates that the value of VWC is the most stable

in the Poly-10 section. In spring, the control section, which has the highest VWC in the subgrade, will have a lower load capacity compared with the insulated sections, since there is an inverse correlation between resilient modulus and soil moisture content.

Based on the observations listed above, it can be concluded that both bottom ash and polystyrene protect the subgrade below from frost when used as insulation layers. In both cases, no frozen water was observed in the subgrade. However, the two insulation materials (bottom ash and polystyrene) show some differences. The temperature gradient and rate of temperature change for the B. Ash section is close to that of the control section, so the IRRF test section with bottom ash performed similarly to the control section. Although the test section insulated with a 10 cm polystyrene layer decreased the frost depth by 70% and resulted in the lowest variation in moisture content in the subgrade layer (depth 1.80 m), it also had a lower base temperature in winter, indicating the pavement would be more prone to low-temperature cracking. Thus, while the 10 cm polystyrene insulation layer protected the subgrade from freezing, it made the top layers more prone to low-temperature cracking in winter, compared with the control section and B. Ash section.

4.7. RECOMMENDATIONS FOR FUTURE WORK

As this study primarily focuses on the comparison of pavement temperature and moisture content in different pavement sections with insulation materials, there are several areas for future research that can build upon the findings presented in this chapter:

- While Chapter 3 offers insights into the performance of insulation materials, future work can explore the integration of machine learning models, as demonstrated in subsequent chapters, to provide a more comprehensive understanding of how these materials impact pavement behavior over time.

- Address the comment provided regarding the comparison of measured data with conventionally available models for temperature gradient prediction. Including this analysis could enhance the robustness of the research by providing a benchmark for evaluating the performance of insulation materials.

By addressing these recommendations in future research endeavors, we can enhance our understanding of insulation materials' impact on pavement performance in cold regions and further strengthen the robustness of our investigations.

4.8. ACKNOWLEDGMENTS

The authors would like to thank Alberta Transportation, the Edmonton Waste Management Centre, the City of Edmonton and Alberta Recycling for their financial and in-kind support of the IRRF test road. The authors would also like to thank to Lana Gutwin for her assistance in the preparation of this paper. Funding from NSERC is gratefully acknowledged.

CHAPTER 5.APPLICATION OF MACHINE LEARNING MODEL IN TEMPERATURE PREDICTION OF UNBONDED MATERIAL LAYERS

This section has been published as Huang, Y., Molavi Nojumi, M., Hashemian, L. and Bayat, A., 2023. Evaluation of a Machine Learning Approach for Temperature Prediction in Pavement Base and Subgrade Layers in Alberta, Canada. Journal of Transportation Engineering, Part B: Pavements, 149(1), p.04022076.

5.1. ABSTARCT

The performance of flexible pavement is influenced by pavement material properties and the strength or the stiffness of the pavement layers. Pavement temperature significantly impacts the material properties of flexible pavements. However, to date there has not been much research that investigates the prediction of the pavement temperature in unbound material (base and subgrade layers). The goal of this research is to apply a new approach, machine learning, to predict pavement temperature in unbound material. Pavement temperature recordings collected at the Integrated Road Research Facility (IRRF) test road in Alberta from January 2013 to February 2020 were used to train and validate machine learning models. Finally, high performance machine learning models with two parameters (air temperature and day of the year) were developed to predict the average daily pavement temperature at 0.5–2.7 m below the road surface. The accuracy of the temperature in the base and subgrade layers predicted using the machine learning models was found to be higher than for an existing model.

Keywords: base layer temperature, subgrade layer temperature, machine learning, time domain reflectometer (TDR) data, temperature prediction models

5.2. INTRODUCTION

The rate and magnitude of deterioration in flexible pavements are significantly influenced by the properties of the materials that comprise the various layers, and the strength or stiffness of the pavement materials is mainly dominated by pavement temperature and moisture content variation (Birgisson et al., 2000). Pavements in cold regions—which are subject to low temperatures and multiple freeze–thaw cycles—tend to be more severely damaged than pavement in warm regions (Tighe et al., 2006). In winter, as the temperature in the hot mix asphalt (HMA) layer dropped, the modulus of the HMA layer was observed to increase from 1.0×10^8 Pa to 1.4×10^{10} Pa (Aidara et al., 2015). Fredlund et al. (1977) proposed a two-parameter expression for resilient modulus and found that matric suction was the primary parameter affecting the behavior of unsaturated soils. Meanwhile, matric suction was highly dependent on temperature and moisture content. Simonsen et al. (2002) found that the change in soil resilient modulus was dependent on temperature change, and the resilient modulus of soil increased as the temperature decreased from 0°C to −20°C. Salour and Erlingsson (2013) back-calculated the modulus based on falling weight deflectometer data, and demonstrated a 63% reduction in the resilient modulus of the subgrade and a 48% reduction in the resilient modulus of the granular base layer during the thawing period compared with the resilient modulus under fully recovered conditions. In a case study by Haghi et al. (2016), it was found that as the temperature drops, the modulus of the unbound layer can reach 2.13 times the normal condition (with fall used as the reference) (1.4×10^{10} Pa). Simultaneously, the resilient modulus of the unbound layer also decreases to 1.3×10^{10} Pa due to the presence of excess water in the unbound layer.

The rate of change in the resilient modulus for the subgrade in spring is also different for different soil types (Popik et al., 2005). The method outlined in the Mechanistic-Empirical Pavement Design Guide (MEPDG) can be used to calculate the temperature of a sublayer and

thus determine when the unbound material layer will freeze (AASHTO, 2008). The temperature affects the resilient modulus of unbound materials, which impacts the load-bearing capacity of the pavement. Most pavement design methods do not directly consider the effect of temperature variation because the soil does not directly influence the thickness in the design. However, depending on the material properties and the road location, seasonal temperature variation could affect the properties and performance of the unbound layer (AASHTO, 2008). For example, for a weak subgrade soil, freezing could result in a significant increase in resilient modulus, and an increase in temperature of the unbound layers during the thawing period leads to a significant decrease in resilient modulus (AASHTO, 2008). Thus, accurate estimation of the temperature of the unbound layers is important.

Although real-time temperature measurements can be obtained using a sensor (such as a thermistor) installed in a road, there are some limitations to this approach. The installation cost for a buried sensor is high, and it is difficult to apply the same data measurement and collection system to all roadways. Furthermore, maintenance is not simple, particularly when sensors are located below the road surface. Sensors can be located 2 m (or even more) below the road surface. If a sensor stops working, there are costs associated with removal and reinstallation. Because of these considerations, an accurate temperature prediction model is often more practical.

Although the temperature of the base and subgrade layers has a significant influence on the performance of the road surface, many temperature prediction models primarily focus on analyzing temperature changes at the road surface and in asphalt layers. However, existing models generally do not take into account the base and subgrade temperature (Arellano, 2007; Asefzadeh et al., 2017; Hall and Rao, 1999). The enhanced integrated climate model (EICM) (ARA., 2004), which is the most widely used climate prediction model, can be used to predict in situ pavement temperature, moisture content, and stiffness moduli of pavement layers. Still,

this model is not accessible to all researchers, and the accuracy of the results is highly dependent on the inputs, including boundary conditions, climatic conditions, and material properties. Furthermore, for EICM the assumption is that the heat capacity and thermal conductivity of the unbound materials do not change over time. However, heat capacity and thermal conductivity are not constant, especially for unbound materials (e.g., base course and soil) because the moisture content and frost depth change with time (ARA., 2004). Therefore, EICM cannot be used to accurately predict the temperature of unbound materials within a pavement structure. For example, in the Minnesota Road Research Project (MN/ROAD) (Birgisson et al., 2000), the difference in the measured temperature and temperature predicted using EICM was found to be nearly 7°C in summer for dense-graded base material.

Most existing literature models for the prediction of pavement temperature are specific to the asphalt layer. Only one model, a sinusoidal function proposed by Heydinger (2003), is applicable to predicting temperature in the base and subgrade layers. This model, which is a sinusoidal function of time, was developed to analyze the daily average air temperature and pavement temperature in the base and subgrade layers, with mean temperature, amplitude, and time shift included as variables. Because this is the only available model for temperature prediction in unbound layers and it was found to have high accuracy, the sinusoidal function (Heydinger, 2003) will be used for comparison with the machine learning models proposed in the current work. The lack of available literature models for temperature prediction in the base and subgrade layers also underscores the importance of expanding available methods for modeling the temperature in the unbound layers of road structures.

Environmental factors (such as ambient temperature, solar radiation, and precipitation) and external factors (such as pavement structure and pavement materials) may influence the pavement temperature distribution, either directly or indirectly; thus, it is a very complicated problem to predict pavement temperature at different depths (Birgisson et al., 2000).

Conventional methods, including numerical models (Alavi et al., 2014; Hermansson, 2004; Minhoto et al., 2005), analytical models (Dumais and Doré, 2016), and regression models (Asefzadeh et al., 2017; Islam et al., 2015), have all been used to predict the pavement temperature in the asphalt layer, but difficulties arise with the prediction of irregular changes (such as discontinuous changes in the base temperature in winter and discontinuities in material properties between layers). Inclusion of insulation material could change the temperature variation in the base and subgrade layers (Haghi et al., 2016; Huang et al., 2021). Moreover, some of the parameters used as model inputs (e.g., heat convection and heat diffusion) are hard to determine.

Both machine learning and deep learning are branches of artificial intelligence. Compared with the conventional methods discussed previously (e.g., numerical models and analytical models), machine learning is more powerful because it can be used to detect patterns in data and automatically build an analysis model without manual intervention. Even with very large data sets, machine learning can be used to make successful predictions in reasonable times (Baştanlar and Özuysal, 2014).

Recently, machine learning methods used to investigate road parameters and performance have been reported in the literature. Machine learning models have been applied to predict cracking condition rating [i.e., the difference between the deducted value of the confined wheel paths and the deducted value of the outside of the wheel paths (Inkoom et al., 2019)], detect cracks (Fujita et al., 2017), evaluate pavement roughness (Nitsche et al., 2014), predict international roughness index (Marcelino et al., 2019), and predict the alligator deterioration index (Fathi et al., 2019). All the machine learning models reported in the literature show high accuracy and outperform traditional methods.

Despite promising recent papers related to the use of machine learning models to predict pavement performance, there has been very little work on the prediction of the pavement

temperature of the base and subgrade layers using machine learning models. Previous studies have instead focused on prediction of pavement surface temperature or temperature of the asphalt layer. For instance, to precisely predict road surface temperature, a back-propagation (BP) neural network model was introduced. Through improved algorithms, new dynamic and static prediction methods were proposed using pavement temperature collected in real time to predict the road temperature for the subsequent 3 h (Xu et al., 2017). A machine learning algorithm that utilized gradient boosting to assemble a rectified linear unit (ReLU)/Softplus extreme learning machine (ELM) was proposed to predict road surface temperature. The model was applied to an airport express route, with a root-mean-square error (RMSE) within 3°C and accuracy of 81.8% (Liu et al., 2018). As part of a University of California Pavement Research Center study, a four-layer artificial neural network model was designed to predict pavement temperature in the HMA layer, with a model accuracy of 99.7% (Nivedya and Mallick, 2020). Machine learning algorithms based on three parameters (air temperature, solar radiation, and day of the year) were also used to predict the average, minimum, and maximum daily pavement temperatures in the HMA layer. The accuracy of the machine learning algorithms was found to be higher than the accuracy of existing analytical and statistical models (Nojumi et al., 2021).

The main objective of this paper is to compare various machine learning algorithms' ability of predicting pavement temperature in different layers. The machine learning algorithms investigated in this work were compared with an existing literature model for base and subgrade temperature prediction (Heydinger, 2003) to assess their performance. The training results of the machine learning algorithms under consideration, namely, regression trees, support vector machines (SVMs), Gaussian process regression (GPR) models, ensembles of trees, and linear regression models, were also compared. Machine learning tool-boxes in MATLAB version R2017a were employed to develop the models. Field measurements of

pavement temperature conducted at the Integrated Road Research Facility (IRRF) test road between January 2013 and February 2020 were used to train and test the models.

5.3. DESCRIPTION OF THE IRRF TEST ROAD FACILITY

The IRRF test road is an access road to the Edmonton Waste Management Centre, located 15 km from downtown Edmonton, Canada. Construction of the IRRF test road started in May 2012 and was complete by October 2013. The IRRF test road has been open to public traffic since October 2015. The entire test road is about 500 m long and consists of two lanes, and was designed with several sections to study different embankment backfill materials and pavement structures, as described elsewhere (Nassiri et al., 2013). In this paper, the focus is on data collected in the control section, located from 130 + 240 m to 130 + 260 m, as shown in Figure 5-1.The pavement structure consists of a 25-cm layer of HMA (a 9-cm wearing course and 16-cm binder course) on top of a well-graded, 45-cm granular base course (GBC). The HMA mixes for the wear and binder courses were based on City of Edmonton Transportation, Canada (2012) design and construction standards.

The IRRF test road was instrumented with CS650 time domain reflectometers (TDRs) (Campbell Scientific Canada, Edmonton, Alberta, Canada) to monitor pavement temperature at different depths (along with other sensors). Pavement temperature data were collected and analyzed for the GBC and subgrade and used to develop a data set for training the machine learning models presented in this work. Figure 5-1 includes a cross section of the test road and indicates the locations of the TDRs. There are 15 TDRs in the GBC and subgrade layers, located at depths of 0.5, 0.7, 0.8, 1.8, and 2.7 m below the pavement surface. To avoid unreliable data due to sensor failure or damage during installation or operation, three TDR devices were installed at the same depth in the road during construction. The temperature data

from the TDRs were collected using a CR1000 data logger (Campbell Scientific Canada, Edmonton, Alberta, Canada), which was programmed to collect data from each of the sensors at 15-min intervals. Data were retrieved from an on-site computer using remote access, and an off-site computer was used for data analysis.

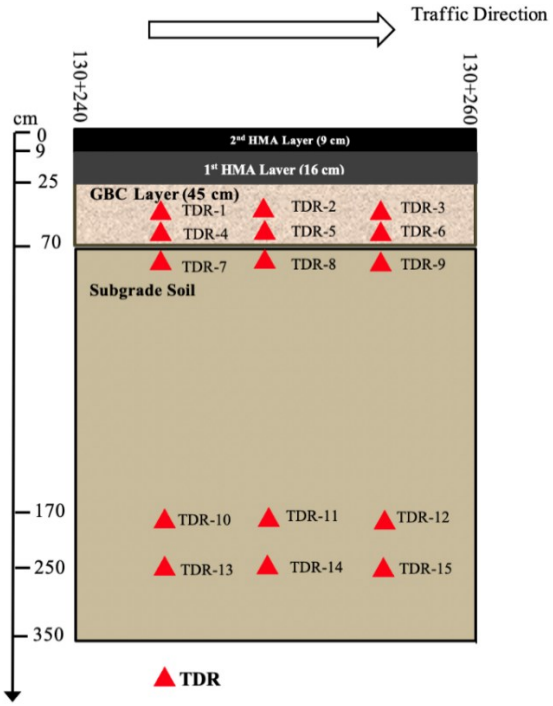

Figure 5-1: IRRF test road pavement structure, showing the location of TDRs embedded in the GBC and subgrade layers

Figure 5-2 shows the grain size distribution in the GBC and subgrade layers. Based on the Unified Soil Classification System (USCS), the subgrade soil is clayey sand and the GBC is well-graded gravel. The gravel used in the GBC layer had a maximum particle size of 19 mm. For the subgrade soil, the liquid limit was 25%, the plastic index was 9%, and the maximum particle size was 0.5 mm.

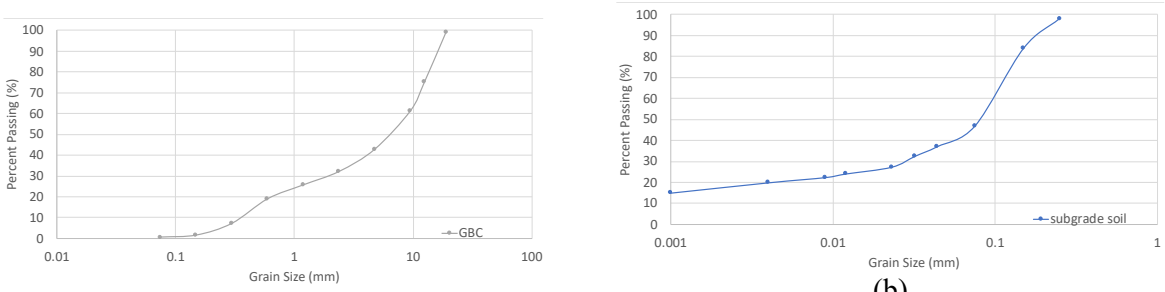

(a) (b)

Figure 5-2: Particle size distribution in (a) GBC layer and (b) subgrade layer

5.4. PROCEDURE FOR MODEL DEVELOPMENT

Figure 5-3 shows the procedure used to implement predictive machine learning models. First, the temperature data collected at 15-min intervals were preprocessed. Irrelevant and noisy data were removed from the data set. Then a time window was defined, and raw temperature data within that time window were compared with data collected from the two other temperature sensors located at the same depth. If the data from the three sensors were not consistent, the time window for the analysis was adjusted so that all temperature recordings within the window were consistent. Next, the reliable raw data were used to calculate the average daily temperature at depths of 0.5, 0.7, 0.8, 1.8, and 2.7 m below the pavement surface. Climatic data (including air temperature, solar radiation, and precipitation) collected from Oliver AGDM (the Environment Canada weather station located closest to the test road) were integrated with the daily average temperature data using time stamps. All data were then loaded into the MATLAB machine learning toolbox. To study the correlation between climatic parameters and pavement temperature, a sensitivity analysis was performed, and the most effective parameters were determined. Each of the machine learning models (listed in Table 5-2) was trained and validated, and the most accurate algorithm for temperature prediction was identified. The parameters used to evaluate model performance included the coefficient of determination (R^2), RMSE, and mean absolute error (MAE). Higher R^2 values, lower RMSE values, and lower MAE values indicated better model performance, with predicted results closer to measured

values. The most effective input parameters were determined for each depth. Then only the most accurate algorithms (i.e., those with the highest R^2, lowest RMSE, and lowest MAE) were carried forward. Finally, the accuracy of the predicted results was compared with the only conventional model for temperature prediction in the base and subgrade layers identified in the literature (Heydinger, 2003).

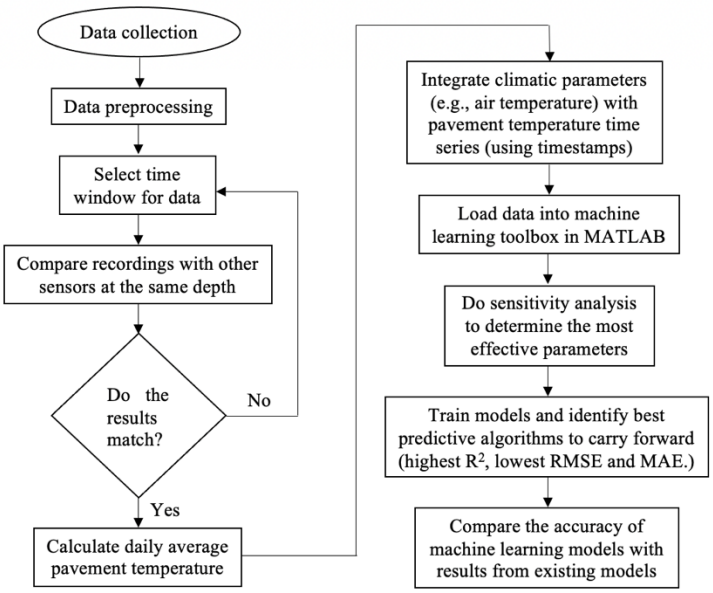

Figure 5-3: Procedure for developing machine learning predictive models

5.4.1. Data Availability

Due to the harsh winter weather conditions in Edmonton, traffic loading, and technical problems with the data collection system, several of the TDRs recorded data intermittently, and for some time periods temperature data were missing. Table 5-1 summarizes the data available from the TDRs at different depths. Any results that did not match the data recorded at other TDRs (located at the same depth) were removed from the data set. Data that covered more than 15 days of the same month were considered to cover a full month.

Table 5-1: Data availability for machine learning analysis.

Thermistor Depth (m)	Start Data	End Date	Duration
0.50	Jan. 2013	Feb. 2020	Six years, two months
0.70	Jan. 2013	Feb. 2020	Four years, ten months
0.80	Jan. 2013	Feb. 2020	Four years, ten months
1.80	Jan. 2013	Feb. 2020	Five years, three months
2.70	Jan. 2013	Dec. 2017	Four years, three months

5.4.2. Machine Learning Algorithms

The regression learner included in MATLAB includes five different machine learning algorithms and 19 subcategories, as shown in Table 5-2. To predict pavement temperature, each of these algorithms was applied (using the available historic temperature data for training), and the performance of the various algorithms was compared. The algorithm types are discussed in detail elsewhere in the literature (Zeiada et al., 2020); however, an in-depth analysis of each of these algorithms and their subcategories is beyond the scope of this research.

5.4.3. Sensitivity Analysis

Generally, environmental parameters—such as air temperature, solar radiation, and precipitation—are taken into consideration in the prediction of the temperature of the HMA layer using conventional models, and the impact of different parameters varies in different locations and weather conditions (Asefzadeh et al., 2017; Nivedya and Mallick, 2020). The temperature of the base and subgrade layers is related to the temperature of the HMA layer; thus, it is important to also investigate the influence of these three environmental parameters (air temperature, solar radiation, and precipitation) on the temperature of the base and subgrade layers. Previous studies indicate that material thermal properties and the thickness of each layer influence the pavement temperature profile (Haghi et al., 2016). If the material thermal

properties and thickness of each layer are used as input parameters, the models would need to be trained on data collected from different pavement structures. However, data are limited—only measurements from the IRRF test road are available and inclusion of the material thermal properties or layer thickness did not improve the model. Thus, these parameters were not included in the model in this paper.

Table 5-2: Machine learning algorithms used for temperature prediction.

Algorithm	**Subcategory**
Linear regression models	Linear
	Interaction linear
	Robust linear
	Stepwise linear
Regression trees	Complex tree
	Medium tree
	Simple tree
Support vector machines (SVM)	Linear SVM
	Quadratic SVM
	Cubic SVM
	Fine Gaussian
	Medium Gaussian
	Coarse Gaussian
Gaussian process regression	Rotational Quadratic
	Squared exponential
	Matern 5/2
	Exponential GPR
Ensembles of trees	Boosted trees
	Bagged trees

An important time-based parameter is the day of the year (Heydinger, 2003), which is represented by a number ranging from 1 to 365 (with 1 assigned to January 1). By observing the change in the temperature of the base and subgrade layers, it was found that the temperature declines in fall and increases in spring, in an annual cycle change (Huang et al., 2021). Both

the base and subgrade temperature are time dependent. The time-based parameter day of the year is easy to obtain and has been used previously to express the relationship between temperature and time (Heydinger, 2003; Nojumi et al., 2021). Therefore, day of the year was also included in the model training.

A correlation coefficient (*r*) was calculated and compared for each input parameter and the pavement temperature. This procedure was repeated for temperature data collected from the TDRs at each depth, and similar results were observed. A representative example is presented in Figure 5-4, where the relationship between each input parameter and pavement temperature at a depth of 0.5 m is plotted. The corresponding correlation coefficients (*r*) are listed in Table 5-3. The correlation coefficients for air temperature (with pavement temperature) and day of the year (with pavement temperature) were observed to be much higher than the correlation coefficients for the other parameters (with pavement temperature), so these were determined to be the most important input parameters for the pavement temperature prediction models.

Table 5-3: Correlation coefficients for climatic and time-dependent parameters.

Parameter		**Correlation with pavement temperature (*r*)**
Air temperature (°C)		0.93
Solar radiation (W/m^2)		0.75
Precipitation (mm)		0.16
Day of the year	First part of the year (DOY = 1 - 181)	0.93
	Second part of the year (DOY = 182 - 365)	-0.96

To examine the correlation between other parameters and day of the year, the year was divided into two equal parts (January 1 to June 30 and July 1 to December 31). The correlation coefficients for day of the year were found to be 0.93 and −0.96 for the first and second half of the year, respectively. The same trend is also evident in Figure 5-4 (d): for the first half of the year, the pavement temperature increases as the day of the year increases. In the second half of

the year, the pavement temperature reaches its peak value when the day of the year is approximately 200. From this point, the pavement temperature decreases as the day of the year increases. Although there is a high correlation between pavement temperature and day of the year, the correlation coefficient for solar radiation is low (r = 0.75). For precipitation, the correlation coefficient is only 0.16, indicating very poor correlation. Overall, air temperature and day of the year were determined to be the most significant input parameters for pavement temperature prediction within the GBC and subgrade layers.

To study the influence of input parameters on the performance of the prediction models, different combinations of input parameters were used to train the models. The whole procedure was also repeated for TDR data at all depths, with similar results observed. Table 5-4 summarizes the performance of each combination of input parameters for a depth of 0.5 m from the road surface. When air temperature was used as the only input parameter, the best performance was observed for matern 5/2 GPR. According to the results summarized in Table 5-4, air temperature and day of the year were identified as the most robust input parameters, while including solar radiation and precipitation as inputs did not significantly improve model results (R^2 did not change, and the improvement in RMSE and MAE was less than 1%). The R2 value reached an impressive 0.97, and no additional input parameters were included to enhance the model's performance. Thus, air temperature and day of the year were used to train the models, and other parameters were removed from the model.

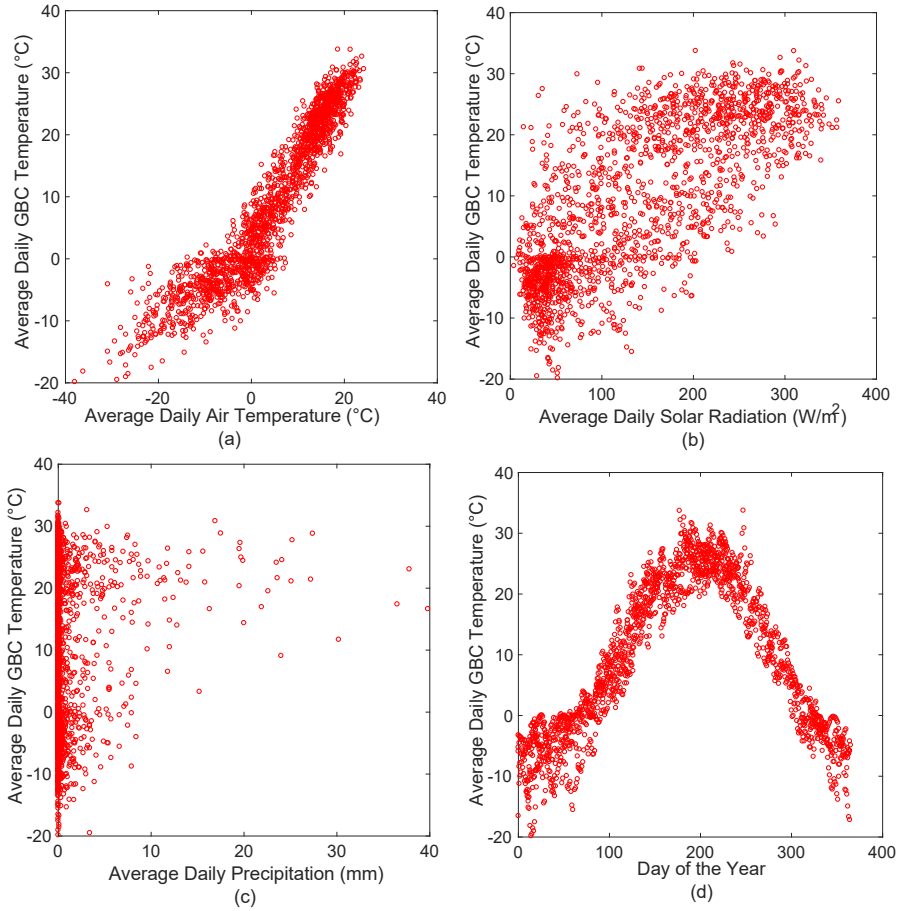

Figure 5-4: GBC temperature versus (a) air temperature; (b) solar radiation; (c) precipitation; and (d) day of the year

5.4.4. Training Data and Model Validation

After determination of the input parameters, the algorithms were trained and validated. For validation of machine learning models, there are two possible methods in MATLAB, holdout validation and cross-validation. Holdout validation is generally recommended for large data sets, but because of the limited data used in this paper, cross-validation was applied. For the cross-validation method, the available testing data were randomly divided into n groups (in this case five), with (n-1) groups used for training, and the remaining group used for testing. This process was repeated n times, and the average test error was calculated over all n folds.

Table 5-4: Impact of contributing parameters on the model performance.

Best Predictive Model	Environmental Parameters			Time-related Parameter	Performance Indices		
	Air temperature (°C)	Solar radiation (W/m^2)	Precipitation (mm)	Day of the year (DOY)	Coefficient of determination (R^2)	Root mean square error (RMSE)	Mean absolute error (MAE)
Matern 5/2 GPR	✔				0.93	3.45	2.69
	✔	✔			0.93	3.31	2.56
	✔			✔	0.97	2.14	1.65
	✔	✔		✔	0.97	2.13	1.64
	✔	✔	✔	✔	0.97	2.16	1.66
Exponential GPR	✔	✔	✔		0.94	3.20	2.49

Table 5-5 gives the performance of the various models for the prediction of daily average pavement temperature at a depth of 0.5 m. Most of the machine learning algorithms performed well, as indicated by 74% of the models having R^2 values higher than 0.95. The model with the best performance was matern 5/2 GPR, with R^2 of 0.97, RMSE of 2.14 (the lowest of any model), and MAE of 1.65 (for temperatures recorded at a depth of 0.50 m). This process of model validation was repeated for the temperature data sets collected at different depths, and the five machine learning algorithms that showed the best performance were identified. The performance obtained using these algorithms is given in Table 5-6, compared with the results of a conventional literature model.

Table 5-5: Performance of different machine learning algorithms for temperature prediction in GBC and subgrade layers.

Algorithm	Subcategory	Performance measures		
		R^2	RMSE	MAE
Linear regression models	Linear	0.88	4.46	3.54
	Interaction linear	0.88	4.40	3.47
	Robust linear	0.88	4.47	3.51
	Stepwise linear	0.88	4.40	3.47
Regression trees	Complex tree	0.96	2.46	1.88
	Medium tree	0.96	2.44	1.88
	Simple tree	0.95	2.79	2.14
Support vector machines (SVM)	Linear SVM	0.87	4.49	3.50
	Quadratic SVM	0.95	2.75	2.15
	Cubic SVM	0.97	2.26	1.76
	Fine Gaussian SVM	0.97	2.23	1.73
	Medium Gaussian SVM	0.97	2.16	1.67
	Coarse Gaussian SVM	0.96	2.67	2.11
Gaussian process regression	Rotational Quadratic	0.97	2.15	1.66
	Squared exponential	0.97	2.15	1.66
	Matern 5/2	**0.97**	**2.14**	**1.65**
	Exponential GPR	0.97	2.15	1.66
Ensembles of trees	Boosted trees	0.96	2.39	1.87
	Bagged trees	0.97	2.17	1.69

Note: Bold represents the best performed model.

5.5. COMPARISON OF MACHINE LEARNING MODELS WITH CONVENTIONAL MODEL

To ensure optimal performance of the prediction models, the procedures used to train the machine learning models described previously were repeated for the temperature data sets collected at different depths. The best input parameters for average daily pavement temperature prediction were found to be air temperature and day of the year. The performance of the

machine learning models was then compared with the performance of a conventional predictive model from the literature, which is briefly described in the following.

Based on temperature recordings taken at the Ohio Strategic Highway Research Program (SHRP) test road, a general expression describing the temperature within the pavement structure—Equation 5-1 (Heydinger, 2003)—was developed

$$T(t) = A + Bsin[\omega(t - \phi)] \quad \text{Equation 5-1}$$

where t = day of the year; $\omega = 2\pi/365.25$ is the normalized frequency; A = mean temperature; B = amplitude; and ϕ = time shift. The values for A, B, and ϕ were determined using temperature measurements (Heydinger, 2003). Equation 5-2 was applied to the temperature measurements taken at the IRRF test road, and the results were compared with the machine learning models developed in this work. The results of this comparison are included in Figure 5-5. Any gaps in the data in Figure 5-5 correspond to periods when the temperature data from the IRRF test road were not available (e.g., due to malfunctioning sensors). From Figure 5-5, the temperature difference between maximum and minimum temperature was 54°C, 49°C, 41°C, 24°C, and 17°C for depths of 0.50, 0.70, 0.80, 1.80, and 2.70 m, respectively. It is evident that the measured pavement temperature range varies significantly at shallower depths. At the same time, the magnitude of the measured temperature change at greater depths is smaller, and the variation in temperature data over time is more gradual. The machine learning predictions are close to the measured temperatures for all depths. However, there is a large difference between the temperature measurements from the IRRF test road and the results predicted using Equation 5-1 for both winter and summer. Although there is less difference between the measured temperature data and calculated values in summer (at depths of 1.8 and 2.7 m), the temperatures calculated using Equation 5-1 are consistently lower than the measured temperature for winter. Because Equation 5-1 is a sinusoidal function of time (which only accounts for mean

temperature and amplitude), the shape of the curve changes periodically, and thus Equation 5-3 does not reflect any irregular changes in temperature within the pavement structure. However, machine learning models do not have the same constraint because the predicted results are based on historical temperature measurements and reflect the actual variation in climatic parameters, giving a better prediction of the actual variation of pavement temperature with time (based on the input parameters). Thus, the application of machine learning results in a more flexible, reasonable, and accurate prediction model.

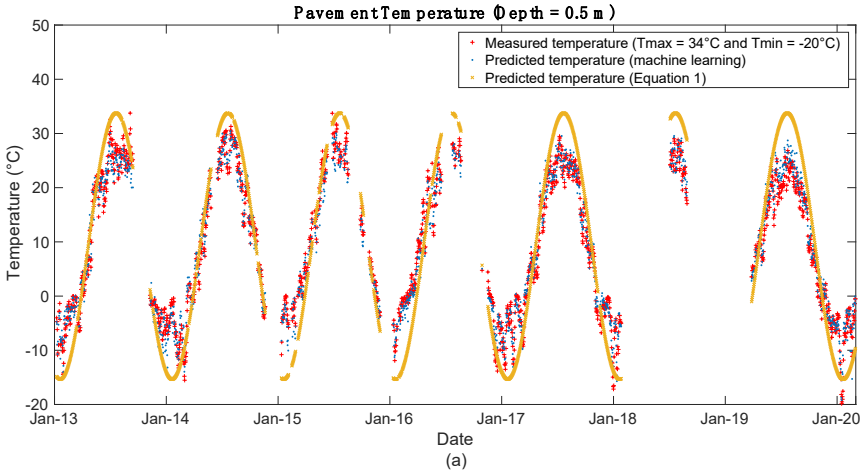

(a)

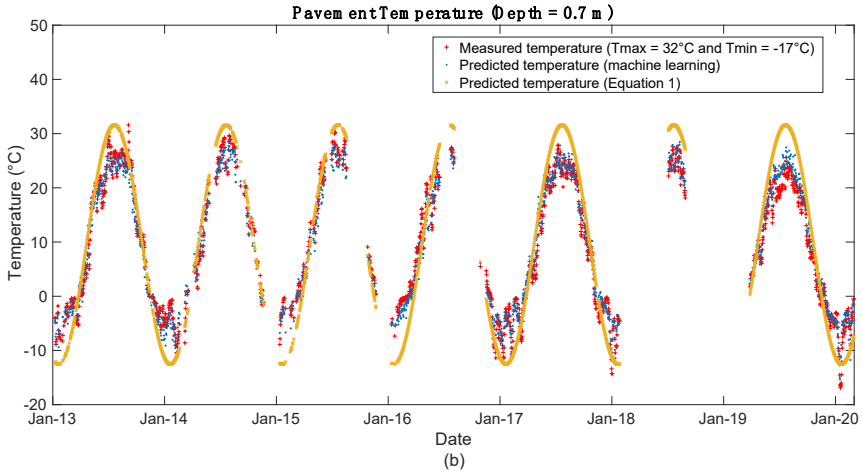

(b)

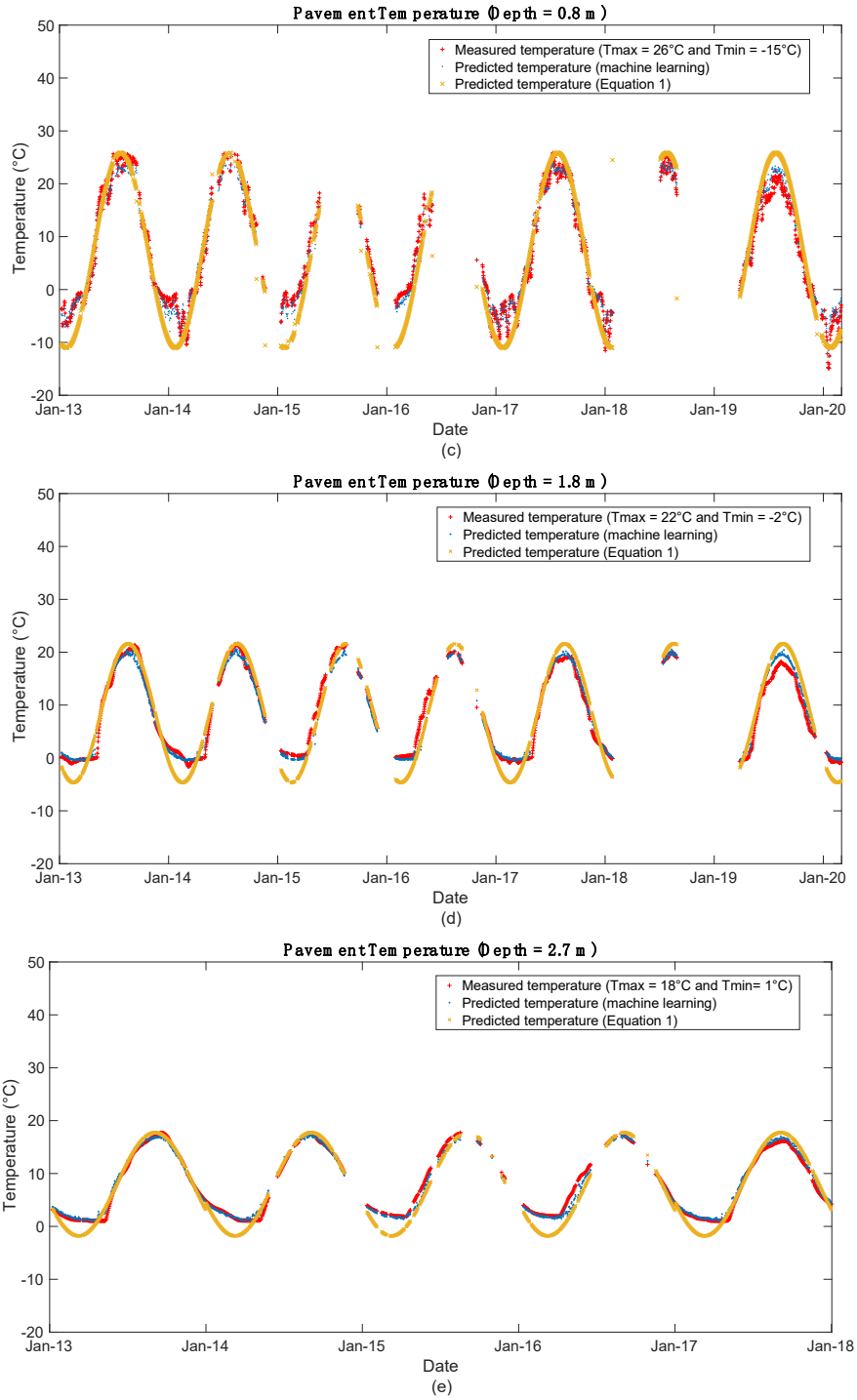

Figure 5-5: Comparison between measured and predicted pavement temperatures at depths of (a) 0.5 m; (b) 0.7 m; (c) 0.8 m; (d) 1.8 m; and (e) 2.7 m

The machine learning model predictions were compared with the temperature values calculated using Equation 5-1, with the results presented in Table 5-6. From these data, it is evident that the machine learning models resulted in a higher level of accuracy for temperature prediction. For the machine learning model, the R^2 values are above 0.96, while the RMSE and MAE range

from 0.98 to 2.19 and 0.72 to 1.70 (for various depths). The results show that the performance of Equation 5-1 improves as the depth increases, as indicated by the increase in R^2 values and decrease in RMSE and MAE. The difference in performance between the machine learning model and Equation 5-1 decreased with increasing depth. At a depth of 0.5 m, the value of R^2 for the machine learning results was 5% higher than for Equation 5-1; however, this difference decreased to 1% at a depth of 2.7 m.

Table 5-6: Comparison of the performance of machine learning and literature model from Heydinger (2003).

Depth (m)	Machine learning models				$T(t) = A + Bsin[\omega(t-\phi)]$ (Heydinger, 2003)					
	Best predictive model	R^2	RMSE	MAE	R^2	RMSE	MAE	Mean Temperature (°C)	Amplitude (°C)	Time Shift (day)
0.50	Matern 5/2 GPR	0.97	2.14	1.65	0.92	3.48	5.65	9.21	24.54	110
0.70	Squared exponential	0.97	2.19	1.70	0.94	2.94	4.53	9.53	22.06	110
0.80	Exponential GPR	0.96	2.15	1.69	0.93	2.78	3.23	7.43	18.42	115
1.80	Exponential GPR	0.97	1.38	1.01	0.95	1.78	2.18	8.48	13.11	138
2.70	Matern 5/2 GPR	0.97	0.98	0.72	0.96	1.15	1.48	7.97	9.77	157

Table 5-7 compares the performance of Equation 5-1 and the machine learning model in terms of the accuracy of temperature prediction in winter. The accuracy of Equation 5-1 dropped significantly in winter, especially at shallower depths (i.e., closer to the road surface). The R^2 value for results obtained using the machine learning model was 47% higher than for results obtained using Equation 5-1 (at a depth of 0.50 m). In addition, RMSE and MAE for the machine learning results were consistently lower than the corresponding RMSE and MAE obtained from Equation 5-1 for the temperature data in winter. Thus, machine learning can be used to predict the temperature in base and subgrade layers more accurately than Equation 5-1.

Figure 5-6 shows the performance of the two methods machine learning and Equation 5-1 at a depth of 0.50 m, with predicted temperature versus measured temperature plotted for both methods. From these results, it is clear the predicted temperature from the machine learning model was closer to the measured temperature values. At the same time, there is a large difference between the temperatures predicted using Equation 5-1 and measured temperatures, especially for temperatures in the high and low range (e.g., from −20°C to 0°C and 20°C to 30°C). The results shown in Figure 5-6 demonstrate that the temperatures predicted by machine learning for different locations within the pavement structure are closer to the actual temperatures, whereas Equation 5-1 results have lower accuracy. This is especially the case at shallow depths: for example, the RMSE of Equation 5-1 is 1.63 times higher than the RMSE for machine learning (matern 5/2 GPR) at a depth of 0.50 m.

Table 5-7: Comparison of accuracy of temperature prediction in winter for machine learning model and conventional predictive model (Heydinger, 2003) given in Equation 5-1.

Depth (m)	**Machine Learning**			$T(t) = A + Bsin[\omega(t - \phi)]$ **(Heydinger, 2003)**			**Ratio of performance indices (Equation 5-4 index/Machine Learning index)**		
	R^2	**RMSE**	**MAE**	**R^2**	**RMSE**	**MAE**	**R^2**	**RMSE**	**MAE**
0.50	0.81	1.99	1.45	0.35	3.69	6.56	0.43	1.85	4.52
0.70	0.68	2.14	1.64	0.39	2.97	5.06	0.57	1.39	3.09
0.80	0.73	1.68	1.17	0.34	2.62	4.40	0.47	1.55	3.76
1.80	0.76	0.67	0.51	0.58	0.88	2.78	0.76	1.31	5.45
2.70	0.86	0.48	0.33	0.65	0.77	2.21	0.76	1.60	6.70

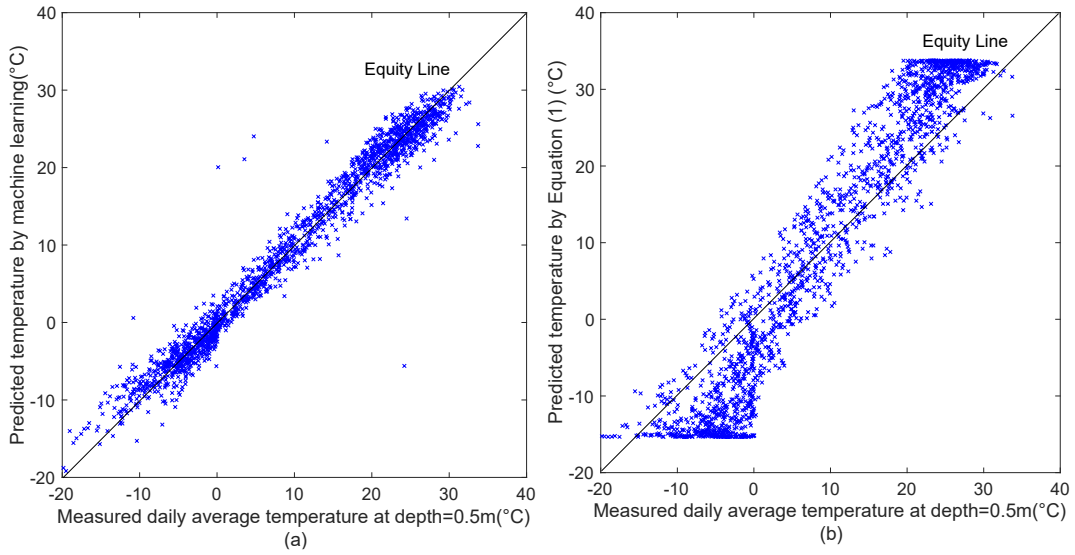

Figure 5-6: Comparison of temperature predictions using (a) machine learning; and (b) Equation 5-5 temperature data at a depth of 0.50 m

Machine learning models can provide an accurate estimate of temperature prediction for a specific pavement structure provided temperature data for the pavement structure are available. For a new pavement or rehabilitation design, MEPDG first involves proposing a trial design. Then the trial design is evaluated for a given set of site conditions and using certain failure criteria at a specified level of reliability. If any criteria are not met in the initial design, the materials used, layer thickness, or other design features are altered. The analysis of the trial design is based on the accumulation of damage as a function of time and truck traffic. The resilient modulus values of the pavement layers present in the pavement structure are adjusted over time based on temperature and moisture conditions. At the same time, the temperature within each unbound sublayer is used to determine the months for which any particular sublayer is frozen. For frozen sublayers, the resilient modulus increases during the time when the layer is frozen and decreases during the thaw period (resulting in a relatively weaker layer as the temperature increases). Thus, for pavement, temperature at various depths plays an important role in the design process. Meanwhile, if a field investigation identifies frost-susceptible soil, the designer will need to take steps to prevent frost heave. In this case, the

temperature distribution in the unbound layer determines the maximum frost depth and influences the decision of the designer (AASHTO, 2008).

Previously, the resilient modulus of the subgrade layer of the IRRF test road was backcalculated based on falling weight deflectometer data, and the ratio of the back-calculated resilient modulus for each season to the resilient modulus of the test road in fall was calculated. When the temperature increased during the spring, the maximum measured volumetric water content was observed (the measurement captures only liquid water, not any frozen water) and the resilient modulus dropped to its lowest value, with a backcalculated ratio of spring resilient modulus ratio to fall resilient modulus of 0.89. Then a gradual decline in moisture content was observed from April to July, with the minimum moisture content occurring in September. With the decreasing volumetric water content, the resilient modulus increased, and the ratio of resilient modulus in summer to resilient modulus in fall was 0.93. In winter, the subgrade soil is frozen; the ratio of the resilient modulus in winter to the resilient modulus in fall is 2.02 (Haghi et al., 2016).

The machine learning models presented in this work are based on temperature data recorded at one location, the IRRF test road. To validate the temperature profiles of other roads with different material and structures, temperature data from other roads—or an expansive database including many road structures (with the inclusion of thermal material properties and thickness of layers as inputs)—in different conditions is necessary. Moreover, the environmental inputs that give the most accurate temperature predictions for a machine learning model may vary, depending on the pavement structure, the climate where the road is located, and the soil type of the base and subgrade layers.

The generality of the proposed temperature models in this paper is restrictive in that these models are only applicable to the IRRF test road. To develop a similar model for other pavement, a data set including temperature measurements from the pavement structure would

be necessary. Including more input parameters (such as material properties and layer thickness) could increase the generality of the model. However, all machine learning models are trained using data, and such an expansive data set is not currently available. Thus, currently the generality of the model cannot be improved.

However, the development of machine learning models—even if limited in terms of their generality—is meaningful. First, because the temperature variation in the base and subgrade layers is influenced by many factors, including internal and external factors, the prediction of the variation is very difficult. So far, other than the equation developed by Heydinger (2003), no feasible method has been reported in the literature. Meanwhile, a case study previously conducted at the IRRF test road has shown that the presence of an insulating layer (e.g., 10-cm polystyrene board) can dramatically change the temperature variation in the base and subgrade layers. Therefore, it is difficult to predict the temperature variation of different structures or in different climates by a simple model with only two input parameters. Even the equation developed by Heydinger (2013) requires the calculation of average temperature and amplitude based on recorded temperature. Finally, the life span of the sensors installed to collect data is limited. With the development of the machine learning model, it may be possible to predict the future temperature of the base and subgrade layers based on historical measured data.

5.6. CONCLUSIONS AND RECOMMENDATIONS

This study involved application of several machine learning models to predict daily pavement temperature in the unbound materials (i.e., GBC and subgrade layers) within a pavement structure. The machine learning models were developed based on temperature data collected at the IRRF test road located in Edmonton, Alberta, Canada. Pavement temperature data from January 2013 to February 2020 were used to train and validate the machine learning models. Environmental parameters collected from the nearest weather station—including air

temperature, solar radiation, and precipitation—were examined as parameters for the prediction of the temperature within the road structure at various depths. A sensitivity analysis was conducted, and the results indicate that machine learning models including two parameters—air temperature and day of the year—could be used to predict the temperature at depths ranging from 0.5 to 2.7 m below the road surface with reasonably high accuracy.

The temperature values predicted using the machine learning models were compared with the values from an existing literature model for temperature prediction within pavement. Although the performance of both models increased with increasing depth, the machine learning algorithm outperformed the literature model for all depths. The lowest R^2 for the machine learning algorithms was 0.96 (at a depth of 0.80 m), which was 3% higher than the R^2 for the existing model. For depths of 0.5 to 2.7 m, respectively, RMSE for the five machine learning models decreased from 2.14 to 0.98 and MAE decreased from 1.65 to 0.72.

The literature model involves a sinusoidal function of time, and only the mean pavement temperature, amplitude, and day of the year are included in the equation. Thus, the shape of the equation proposed in the literature model (Heydinger, 2003) is fixed, and the predicted temperature is not a function of air temperature or other climatic parameters. However, in winter the temperature variations in the base and subgrade layers are irregular. For low-temperature conditions, the accuracy of the existing literature model decreased significantly, especially at locations closer to the road surface, and R^2 declined to 0.35 at a depth of 0.50 m. However, R^2 for the machine learning model was 47% higher than for the existing model at the same depth. In all cases, the R^2 values for the results obtained using the machine learning models were higher than for the existing model, while all RMSE and MAE values for the machine learning models were less than for the existing model.

Based on the results of this research, machine learning algorithms could be a flexible, reasonable, and accurate approach for predicting the pavement temperature in the base and

subgrade layers. Unlike EICM, machine learning algorithms do not require boundary conditions or material properties (heat capacity and thermal conductivity) as inputs. This study indicates that machine learning models can predict temperature within unbound pavement layers with very high accuracy using only two parameters, one environmental parameter (air temperature) and one time-related parameter (day of the year). Although the accuracy of the existing conventional literature model was found to increase with depth, machine learning models maintained a high accuracy for pavement temperature prediction at depths ranging from 0.50 to 2.70 m. The temperature variation within the base and subgrade layers is irregular in winter, and it was noted that the accuracy of the conventional model decreased significantly at low temperatures. However, the five machine learning models provided reasonable temperature predictions, even with irregular temperature fluctuations. Provided that historical temperature data are available, it is possible to apply machine learning models to accurately predict future pavement temperatures year-round (at depths of up to 2.70 m below the road surface), with just two readily available input parameters, air temperature and day of the year. Temperature changes in the base and subgrade layers influence moisture variation and resilient modulus of the base and subgrade layers. In future work, the impact of moisture variation on resilient modulus could be investigated using machine learning models that incorporate falling weight deflectometer data.

CHAPTER 6.MULTI-DEPTH TEMPERATURE PREDICTION

This section has been submitted to Journal of Applied Remote Sensing on May 2023 as Huang, Y., Molavi Nojumi, M., Ansari, S., Hashemian, L. and Bayat, A. Multi-Depth Temperature Prediction using Machine Learning for Pavement Sections.

6.1. ABSTRACT

The temperature of hot mix asphalt (HMA), base, and subgrade layers plays a significant role in pavement performance, because temperature influences the strength of the materials. Therefore, a model to predict temperature throughout the entire pavement structure is desirable. However, most existing models only focus on predicting the temperature of the road surface or the HMA layer, and these models usually need some information related to boundary conditions or material properties that is difficult to obtain. This research aims to demonstrate that machine learning (ML) model can be a powerful generalized approach to predict the temperature within a pavement structure at multiple depths. Data from the Integrated Road Research Facility test road in Edmonton, Alberta, Canada, were used to train ML models. Sensitivity analysis was performed to analyze the influence of several input parameters on asphalt and soil temperature. ML models with three input parameters—average daily air temperature, day of the year, and depth—resulted in better performance compared to ML models based on other combinations of parameters. Three ML models were established to predict the average daily temperature, minimum daily temperature, and maximum daily temperature of the pavement structure. To validate model performance, the three ML models were compared with four existing models, and of these the ML models showed the highest accuracy with the coefficient of determination values above than 0.97 and root mean square error values below than 2.21. These results demonstrate that ML models can be used to give

accurate predictions of road temperature at multiple depths with only one environmental predictive parameter, average daily air temperature.

Keywords: temperature prediction, machine learning, HMA layer temperature, base layer temperature, subgrade layer temperature

6.2. INTRODUCTION

The performance of flexible pavements is greatly affected by the material properties of the hot mix asphalt (HMA), base and subgrade layers, and their strength is decided by temperature (AASHTO, 2008). HMA mixture is a material with viscoelastic behavior, and its strength and load capacity are dependent on temperature (Elseifi et al., 2006). Temperature variation in the HMA layer can lead to different types of pavement damage. For example, high pavement temperatures in summer make the HMA layer prone to rutting, while low pavement temperature in winter leads to low-temperature cracking of the HMA layer (El-Maaty, 2017; Y. Huang et al., 2021). The temperatures of the base and subgrade layers also influence pavement performance. For example, in cold regions such as Alberta, pavements are weakened by thawing during spring freeze-thaw cycles (Smith, 2006). Freeze-thaw cycles mean that water inside the base and subgrade layers freezes and turns into ice lenses in winter. Later, ice lenses melte and turn into liquid water again in spring. But, because the pavement temperature rises (from the top to the bottom of the pavement structure), the ice lenses in the upper layer begin to melt, while the sublayer remains frozen with low permability. This typically results in a higher moisture content and lower pavement load capacity in late winter or early spring than under normal conditions (Haghi et al., 2019). Thus, accurate estimation of the temperature in the HMA, base, and subgrade layers is necessary for such applications as determination of seasonal load capacity.

The prediction of temperature in the HMA, base, and subgrade layers is complex, since many factors influence asphalt and soil temperature (AASHTO, 2008; Adwan et al., 2021; Chen et al., 2019; Molavi Nojumi et al., 2022). Previous studies have indicated that environmental factors such as air temperature, solar radiation, wind speed, and relative humidity affect the temperature of a pavement structure, and the impact of these parameters on temperature distribution may vary depending on the climate type (Adwan et al., 2021; Chen et al., 2019; Molavi Nojumi et al., 2022). Other parameters related to the road materials, such as thermal conductivity, specific heat capacity, and density, also affect asphalt and soil temperature (Adwan et al., 2021) and should to be considered in analytical and numerical models. For analytical and numerical models, boundary conditions are also necessary (Chen et al., 2019; Hermansson, 2000). Although models based on the material properties of the materials can be used to predict asphalt and soil temperature, some parameters may not be available for specific road structures. In addition, the accuracy of the model accuracy may be negatively impacted due to the inaccuracy of one or more parameters (Chen et al., 2019).

Conventional approaches—including analytical methods (Barber, 1957; Qin, 2016; Solaimanian and Kennedy, 1993), numerical methods (Hermansson, 2004; Mrawira and Luca, 2002), and empirical methods (Asefzadeh et al., 2017; Heydinger, 2003a, 2003b; Li et al., 2018), have been used to predict the temperature in HMA, base, and subgrade layers. In 1957, Barber (1957) developed a solution to predict pavement temperature based on wind, precipitation, air temperature, and solar radiation. The thermal properties of the pavement (i.e., density, specific heat, conductivity, and so on) and weather conditions are also necessary. Qin (2016) established an analytical model to predict the maximum and minimum surface temperature of pavement, as well as the amplitude of the variation in temperature with time based on the pavement surface absorptivity, the daily-zenith incident solar irradiation, and the reciprocal thermal inertia. Mrawira and Luca (2002) calculated pavement temperature using a

numerical method based on the estimated thermal conductivity and measured thermal diffusivity. Hermansson (2004) used solar radiation, long-wave radiation, wind speed, and convection to establish a finite difference model for predicting surface pavement temperature. Li et al. (2018) developed a statistical model to predict pavement temperature based on air temperature and solar radiation; however, this model is restricted to cases when the asphalt layer thickness exceeds 30 cm. The Strategic Highway Research Program (SHRP) and Canadian (C)-SHARP also resulted in two statistical models to predict the minimum temperature of HMA layers (Mohseni, 1998). Heydinger (2003a, 2003b) developed an equation to predict the temperature within the Ohio/SHRP test road. The empirical equation was based on daily mean temperature, amplitude of the temperature variation, and day of the year. This sinusoidal equation was the only model found in the literature to allow prediction of the temperature of the base and subgrade layers within the pavement, so the equation developed by Heydinger was used for comparison in this work. Asefzadah et al. (2017) were established to predict daily average pavement temperature, maximum pavement temperature, and minimum pavement temperature based on data collected at the IRRF test road in Edmonton, Alberta.

The models mentioned above show high accuracy; however, they each have limitations. For example, although the consideration of temperature within the base and subgrade layers is essential for pavement design, most of the existing literature models can only be applied to predict the temperature at the pavement surface or in the HMA layer, with the exception of the empirical model developed by Heydinger (2003b). Other models, such as the default sinusoidal temperature model developed by Lei et al. (2011), can be used to predict soil temperature at various depths (e.g., 2.5 cm, 4.5 cm, 9.5 cm, and 18.5 cm). However, the model by Lei et al. (2011) does not take into account the impact of the HMA layer on the pavement structure, and can not be applied for temperature prediction of the pavement. The lack of models that can be

used to predict the temperature of the various pavement layers within the pavement structure—e.g., the HMA, base, and subgrade layers—also emphasizes the importance of extending the methods available for determining temperature throughout the pavement structure.

In recent years, with the rapid improvement in computing capacity, computing methods based on artificial intelligence, including machine learning (ML), have received increasing attention for various applications, such as predicting the temperature within pavement structures. Gungor and Al-Qadi (2018) applied ML to calculate the temperature of an HMA layer using a model that included air temperature, direction and speed of the wind, dew point temperature, station pressure, and cloud ceiling. Qiu et al. (2020) used a type of algorithm known as a gradient boosting decision tree to predict the surface temperature of pavement during winter.

The thermal properties of materials are very important for conventional methods but it is difficult to obtain accurate data (like the thermal conductivity of a material is influenced by its status, such as whether the material is frozen or not), and once the temperature recordings are available, the ML models could be developed to predict the temperature for specific roads without the thermal properties of materials. The ML models (Gungor and Al-Qadi, 2018; Molavi Nojumi et al., 2022; Qiu et al., 2020) summarized above show high accuracy in predicting the pavement structure's temperature, and parameters related to the road materials—i.e., thermal conductivity, specific heat capacity, and so on—are not necessary. This indicates that ML models have potential for improving the temperature prediction at various depths within pavement structures. Although temperature of the soil layer also influence the pavement’s performance (Haghi et al., 2019; Smith, 2006), previous work (Gungor and Al-Qadi, 2018; Molavi Nojumi et al., 2022; Qiu et al., 2020) focused on the temperature of the HMA layer and surface temperature. Thus, it is necessary to extend the application of ML models to different sub-layers.

The primary purpose of this paper is to apply ML algorithms for temperature prediction of the entire pavement structure at multiple depths. Temperature measurements from January 2013 to August 2020 within both asphalt and soil layers at the IRRF test road in Edmonton, Alberta were used to train and test several ML models. The machine learning toolbox and regression learner in MATLAB were used to develop the models. Depth was used as an input parameter to train the ML models. Different algorithms, including linear regression, regression trees, support vector machine (SVM), gaussian process regression (GPR), and ensembles of trees, were examined. To evaluate the performance of the ML models developed in this work, the algorithm that gave the most accurate results was compared against literature models (SHRP (Mohseni, 1998), (C)-SHARP (Mohseni, 1998), a parametric model (Heydinger, 2003b) and statistical models).

6.3. DATA COLLECTION

The IRRF test road is situated on an access road to the Waste Management Centre in Edmonton, Alberta, Canada , where the minimum air temperature in winter can reach -38°C (Y. Huang et al., 2021). The test road comprises two lanes with a length of approximately 500 m. The pavement consists of a 0.25 m layer of HMA (0.09 m wearing course and 0.16 m binder course) on top of a well-graded granular base course (GBC) 0.45 m thick. Construction of the test road was completed in August 2013, with the road open to traffic in November 2015. Based on the data collected using the embedded weigh-in-motion system, an average of 368 garbage trucks drive on the test road every day. More details about the test road and its construction can be found in previous work (Haghi et al., 2019; Huang et al., 2021; Molavi Nojumi et al., 2022).

Thermistors and CS650 time domain reflectometers (TDRs, Campbell Scientific) were installed in the HMA, GBC, and subgrade layer to collect asphalt and soil temperature at various depths. Figure 6-1 shows the cross-section of the test road, along with the location of

thermistors and TDRs, at depths of 0.02, 0.09, 0.17, 0.25, 0.50, 0.70, 0.80, 1.80, and 2.70 m. Identical sensors were installed at three locations for each depth to provide redundancy in the case of damage during installation or malfunctioning during operation. Temperature measurements are collected at each thermistor every 5 minutes. For the TDRs, temperature data is collected every 15 minutes. The data are transferred to the University of Alberta for analysis via a remote connection. All environmental parameters are based on data from the nearest Environment Canada weather station (Oliver ADGM), which is located 6 km from the test road location.

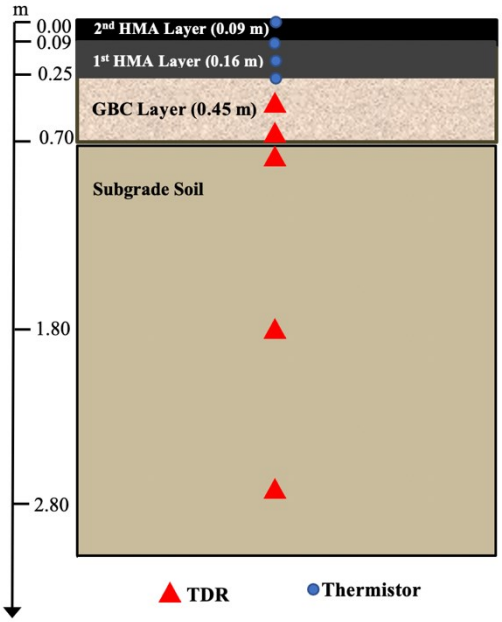

Figure 6-1: Cross-section of the test road indicating the location of TDRs and thermistors

6.4. MODEL DEVELOPMENT

Environmental factors such as air temperature, solar radiation, relative humidity, and wind speed significantly influence asphalt and soil temperature (Adwan et al., 2021). The influence of environmental parameters may vary depending on location, depth, and pavement structure (Adwan et al., 2021; Chen et al., 2019; Molavi Nojumi et al., 2022). Hence, the impact of environmental parameters on the temperature of the HMA, base, and subgrade layers is

discussed in the following sections. Asphalt and soil temperature vary with seasonal changes (Huang et al., 2021). A time-related parameter, DOY, has been shown to affect the temperature of the HMA layer (Molavi Nojumi et al., 2022). Thus, DOY is also included as a parameter. DOY ranges from 1 to 365, and with DOY = 1 corresponding to January 1. Molavi Nojumi et al. (2022) developed ML models that outperformed traditional methods and showed higher R^2 value and lower RMSE values in predicting temperature within the HMA layer, but were restricted to a specific depth. The temperature measured by three sensors installed at the same depth showed the same results, thus in this work, the position in the horizontal direction is not considered and the depth is included as an input parameter, and the ML models have been trained using asphalt and soil temperature measurements recorded at multiple depths.

Figure 6-2 outlines the procedure used to develop ML models. First, asphalt and soil temperature measurements were preprocessed, with irrelevant and noisy data removed from the dataset. Sometimes, the collected numbers are 7999 or NAN, which is considered noisy and removed from the dataset. Next, the time window for data analysis was selected. Temperature data from the three sensors located at the same depth should be the same, so data within the time window were compared for each time point. The analysis time window was adjusted to ensure that all asphalt and soil temperature measurements within the time window were consistent. When this was achieved, the raw data were used to calculate the average, minimum, and maximum daily temperature. Other input parameters—four environmental parameters, one time-related parameter, and depth—were integrated with the dataset using timestamps. Three data sets were prepared: one each for the average, minimum, and maximum daily temperature prediction, respectively. Each set of data included asphalt and soil temperature measurements at depths of 0.02 m to 2.7 m from the surface.

For model development, data were loaded into the machine learning toolbox in MATLAB. A sensitivity analysis was conducted in which the correlation coefficient (R) was used to examine

the influence of each parameter on the prediction of asphalt and soil temperature. The coefficient of determination (R^2) and root mean square error (RMSE) were used to evaluate model performance. Five different algorithms—linear regression models, regression trees, SVM, GPR, and ensembles of trees—were applied. More details on the benefits of the different ML algorithms can be found in the literature (Baştanlar and Özuysal, 2014; Wei-Lun, 2011). Only the ML model using the algorithm that gave with the highest R^2 and the lowest RMSE was carried forward and compared with other existing models from the literature. If the accuracy of a model was low, another sensitivity analysis was conducted to determine whether different combinations of input parameters would result in increased accuracy. The processes mentioned above were repeated three times, resulting in three ML models—one each to predict the average daily temperature, minimum daily temperature, and maximum daily temperature, respectively.

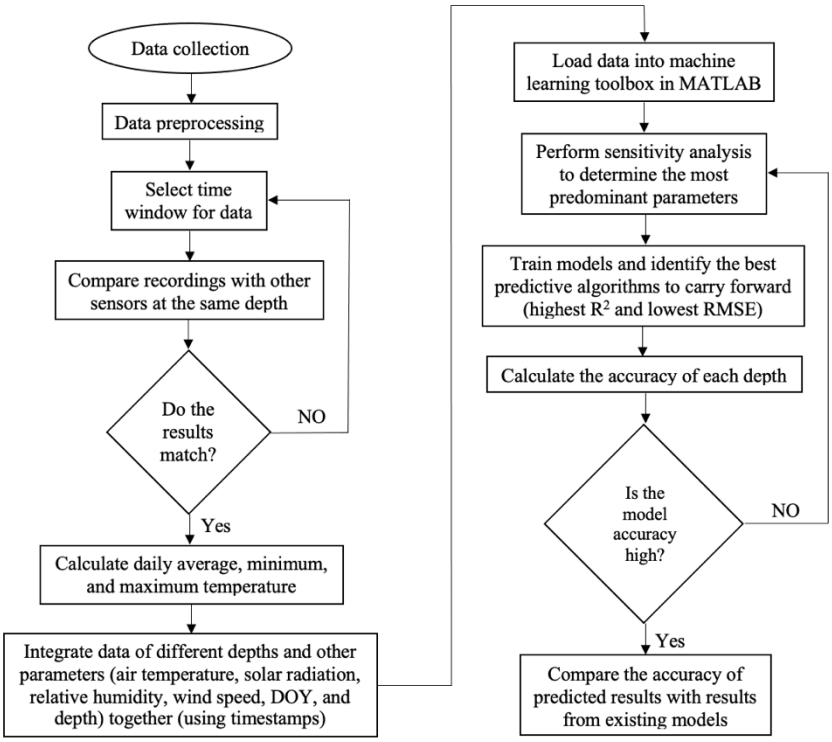

Figure 6-2: Model building flow chart

6.4.1. Data Availability

Table 6-1 shows the available datasets for the development of ML models. Due to technical issues, sensors at depths of 0.02 m, 0.09 m, and 0.50 m malfunctioned in 2016, and sensors at a depth of 2.70 m stopped working in 2017. As discussed previously, data were pre-processed to remove noise and irrelevant data, so that only valid data were used in model development. The number of temperature measurements available was highest for a depth of 0.17 m.

Table 6-1: Data availability for development of ML models.

Thermistor Depth (m)	Start Date	End Date	Number of Daily Average Temperatures (Processed)
0.02	Aug. 2014	Aug. 2016	731
0.09	Aug. 2014	Aug. 2016	731
0.17	Aug. 2014	May. 2020	2084
0.25	Aug. 2014	Dec. 2016	855
0.50	Jan. 2013	Jun. 2020	1849
0.70	Jan. 2013	Jul. 2020	1769
0.80	Jan. 2013	Dec. 2019	1554
1.80	Jan. 2013	Aug. 2020	1904
2.70	Jan. 2013	Dec. 2017	1402

6.4.2. Sensitivity Analysis

Table 6-2 shows the correlation between the input parameters and the average daily temperature of the subgrade layer at a depth of 0.70 m. These calculations were repeated for each depth, with similar results. Figure 6-3 shows the relationship between the input parameters and the subgrade temperature at a depth of 0.70 m.

The correlation coefficient between the subgrade temperature and the air temperature was the highest (R = 0.91) for the four environmental input parameters, indicating that air temperature is the main input parameters for subgrade temperature prediction. The correlation coefficient between subgrade temperature and solar radiation was 0.72, indicating that solar radiation also

affected subgrade temperature, but its effect was not as strong as air temperature. The influence of wind speed on the temperature distribution of IRRF test road was previously found to show obvious seasonal differences (Asefzadeh et al., 2017b; Molavi Nojumi et al., 2022). Therefore, to analyze the influence of wind speed, the year was divided into a cold season (October to March) and a warm season (April to September). The correlation of subgrade temperature with relative humidity is weak, as is the correlation between subgrade temperature and wind speed. As shown in Figure 6-3 (e), for the first part of the year, the subgrade temperature increased with as DOY increased. For the second part of the year, the subgrade temperature decreased as DOY increased. Therefore, to analyze the correlation between the subgrade temperature and DOY, the data were divided into two parts ($1 \leq \text{DOY} \geq 181$ and $182 \leq \text{DOY} \geq 365$). The correlation coefficient for DOY and subgrade temperature was even higher than the correlation coefficient for air temperature and subgrade temperature. Based on the sensitivity analysis, DOY and air temperature are expected to be the most robust input parameters.

Table 6-2: Correlation coefficients of air temperature, solar radiation, relative humidity, wind speed, and day of the year with subgrade temperature.

Parameter		**Correlation with subgrade temperature (*R*)**
Air temperature (°C)		0.91
Solar radiation (W/m^2)		0.72
Relative humidity (%)		0.19
Wind speed (km/h)	Warm season	0.24
	Cold season	0.09
Day of the year	First part of the year (DOY = 1 to 181)	0.94
	Second part of the year (DOY = 182 to 365)	-0.96

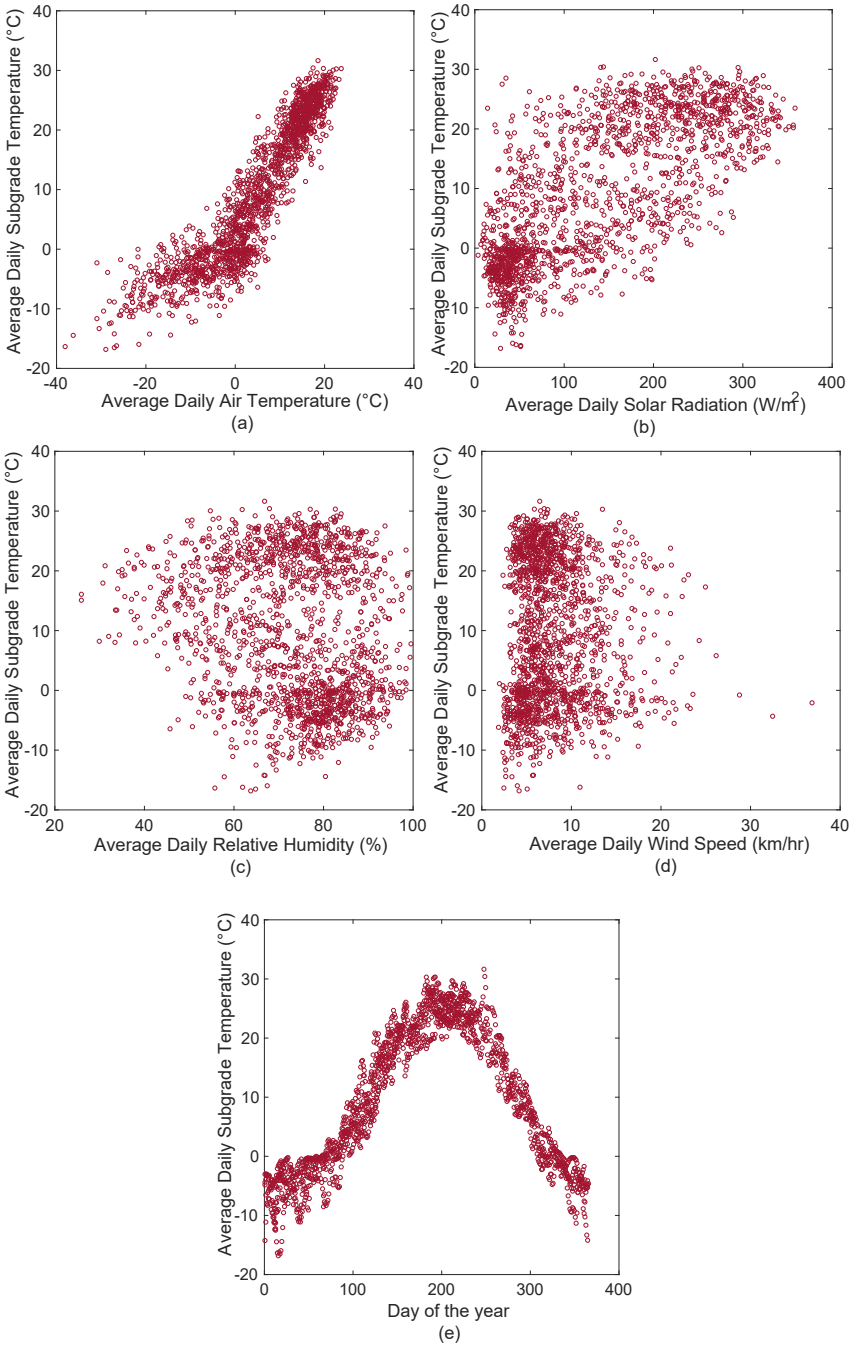

Figure 6-3: Relationship between average daily subgrade temperature (°C) and (a) average daily air temperature (°C), (b) average daily solar radiation (W/m^2), (c) average daily relative humidity (%), (d) average daily wind speed (km/hr), and (e) day of the year

Table 6-3 shows the results of training machine learning models for average daily temperature using different combinations of input parameters. Similar results were obtained for prediction of daily minimum temperature and daily maximum temperature. To predict pavement temperature at multiple depths, depth was indispensable as an input parameter. The ML model with depth and DOY as input parameters resulted in accuracy (R^2 = 0.93 and RMSE = 2.86).

Adding air temperature as an input parameter significantly improved the accuracy of the model (R^2 = 0.97 and RMSE = 1.80). Although solar radiation was an important parameter in many conventional models, the effect of solar radiation and relative humidity on the final results of the machine learning models developed in this work is not significant (R^2 decreased from 0.97 to 0.98, RMSE decreased from 1.80 to 1.58), including more input parameters would make the model more complex. Thus, solar radiation and relative humidity was not used as an input parameter for the final machine learning model. DOY, average daily air temperature, and depth, were used as input parameters in models to predict average daily asphalt and soil temperature, minimum daily asphalt and soil temperature, and maximum daily asphalt and soil temperature.

Table 6-3: Results of Machine learning model for different combinations of input parameters.

Best Predictive Model	**Input Parameters**						**Performance Parameters**	
	Depth (m)	**Day of the Year (DOY)**	**Air Temperature (°C)**	**Solar Radiation (W/m²)**	**Relative Humidity (%)**	**Wind Speed (km/h)**	**R^2**	**RMSE**
Exponential GPR	✔	✔					0.93	2.86
Exponential GPR	✔	✔	✔				0.97	1.80
Bagged Trees	✔	✔	✔	✔			0.98	1.58
Exponential GPR	✔	✔	✔	✔	✔		0.98	1.50
Exponential GPR	✔	✔	✔	✔	✔	✔	0.99	1.24

There are five algorithms and nineteen subcategories in the regression learner. Linear regression models are limited by their requirement for linear relationships between predictors and the target parameter. As a result, they may not provide the same level of accuracy in predictions as other algorithms (Bonaccorso, 2018). In regression learner, there exist four different subcategories of linear regression models, which are linear, interaction linear, robust

linear, and stepwise linear. The regression trees method involves defining a series of rules and conditions at multiple stages to split data. This algorithm includes roots, branches, and leaves, and captures results at the leaves upon completion. The outcome of the tree's prediction is obtained by extracting it from the leaf node located at the path's termination. Essentially, the process of partitioning the data relies on diminishing the deviation from the average of the output characteristics. The degree of granularity in the resulting tree can be adjusted by varying the minimum leaf size, resulting in fine, medium, or coarse trees (Bonaccorso, 2018). The SVM approach employs kernel functions to convert the input data into a higher-dimensional space, which facilitates the largest possible separation between the two classes. Greater separation directly correlates with superior SVM performance. The choice of the kernel for SVM can include linear, quadratic, or cubic options. Additionally, SVM methods are grouped into fine, medium, and coarse Gaussian categories according to their kernel scale (Cortes et al., 1995; Zeiada et al., 2020). A Gaussian process comprises a group of random variables that exhibit joint Gaussian distributions, consistently across any finite number of variables. GPR models are non-parametric and offer flexibility in modelling. In comparison to other regression models that are dependent on kernel functions, GPR models provide better uncertainty estimations and response reliability. GPR models can be grouped into four categories based on the kernel functions utilized: rotational quadratic, squared exponential, matern 5/2 and exponential GPR (Bonaccorso, 2018; Swiler et al., 2020; Zeiada et al., 2020). Apart from the models discussed earlier, ensemble models involve using a combination of similar or different algorithms to produce more precise predictions. Ensemble trees fall into two categories: bagged trees and boosted trees. Bagged trees create several models within the ensemble and merge them into a decision tree. On the other hand, boosted trees use subsets of the original data to create models and improve performance by combining them using a particular cost function (Bonaccorso,

2018; Zeiada et al., 2020). More detailed information about these algorithms is available in the literature (Bonaccorso, 2018; Cortes et al., 1995; Swiler et al., 2020; Zeiada et al., 2020).

All nineteen subcategories were used to train the models and the exponential GPR algorithm was found to give the best performance in all cases (maximum, minimum and daily temperature). Based on the results from Figure 3, the relationships between the pavement temperature and these input parameters are not linear, thus the performances of the linear regression models are not the highest. Exponential GPR models can capture smooth variations in data, making them well-suited for modelling problems where the underlying relationship between variables is continuous and smooth. This is particularly useful in modelling natural phenomena, such as weather patterns or biological processes. In addition, GPR offers more dependable responses compared to other regression models that rely on kernels. Additional information regarding GPR models can be found elsewhere (Bonaccorso, 2018; Swiler et al., 2020; Zeiada et al., 2020). The results of these ML models were compared with existing literature models.

6.4.3. Model Validation

Two measures were employed to avoid overfitting the ML model and ensure optimal performance in processing new data. First, five-fold cross-validation was used for model training. All data were randomly divided into five groups. For each of the five training cycles, four sets of data were used for training, with the remaining set used for verification. This process was repeated for each of the datasets (e.g., maximum, minimum and average daily temperature). Finally, the accuracy of each model was evaluated by taking the average of the R^2 and RMSE for the five training cycles. MATLAB was used throughout this validation process.

Data from one day per month in 2015 (day 108 was randomly selected in each case) was excluded from training and retained for model validation at nine separate depths, and this process was repeated for three datasets (e.g., maximum, minimum and average daily temperature). Figure 6-4 indicates the result of this model verification process. All three models (average daily temperature, minimum daily temperature, and maximum daily temperature) showed high accuracy for the different depths. For the ML models for average, minimum, and maximum daily temperature, R^2 was determined to be 0.99, 0.98, and 0.99, respectively. Similarly, the RMSE was 1.45, 1.60, and 1.89 for the ML models for average, minimum, and maximum daily temperature, respectively. This indicates that the three ML models maintained a high accuracy rate when processing new data.

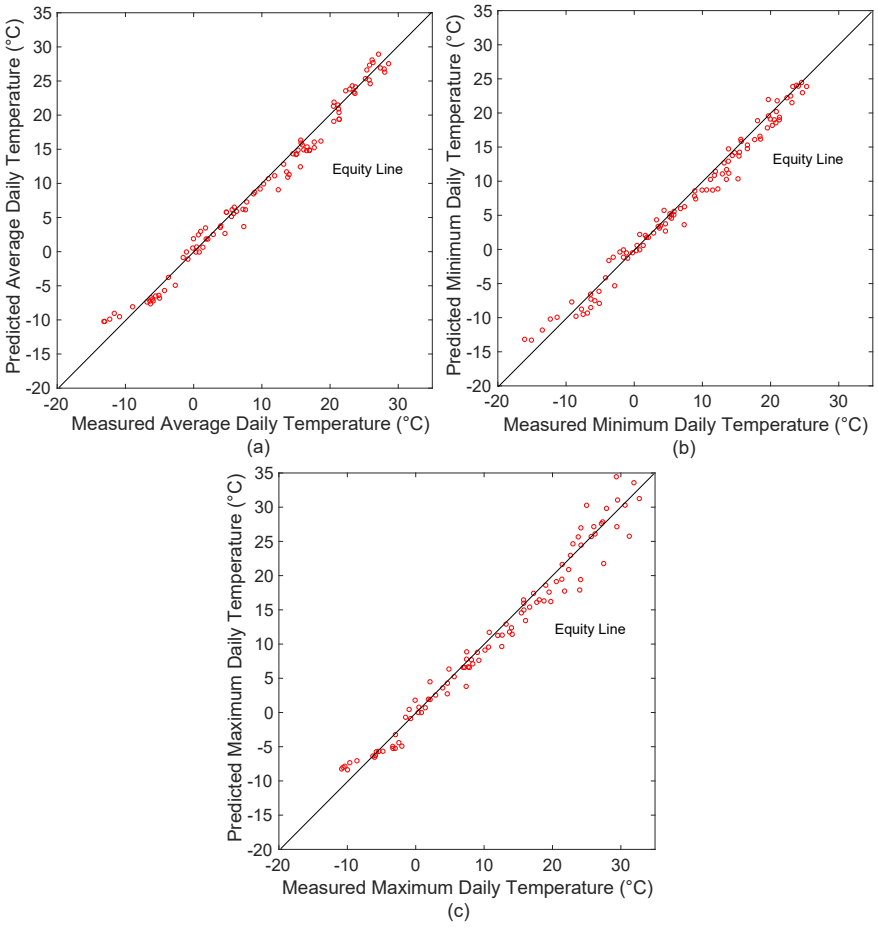

Figure 6-4: Model validation for (a) average daily temperature, (b) minimum daily temperature, and (c) maximum daily temperature

6.5. COMPARISON OF PERFORMANCE BETWEEN ML MODELS AND EXISTING MODELS

Three ML models were established through the sensitivity analysis and model validation steps to predict the average, minimum, and maximum daily temperature. Three input parameters—namely average daily air temperature, DOY, and depth—were included in these models. The ML models employing the exponential GPR algorithm showed the highest accuracy. In this section, the ML models developed in this work for prediction of average daily temperature, minimum daily temperature and maximum daily temperature in the asphalt and soil layers at various depths are compared with existing models in the literature.

6.5.1. Average Daily Temperature

Figure 6-5 compares the temperature from the ML model and measured temperature at different depths. The ML model developed in this work showed high accuracy, its R^2 values were higher than 0.98 and RMSE values were less than 1.80, as shown in Table 6-4.

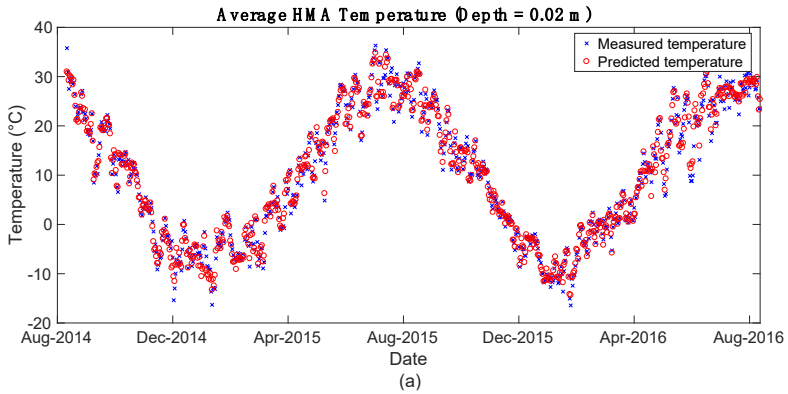

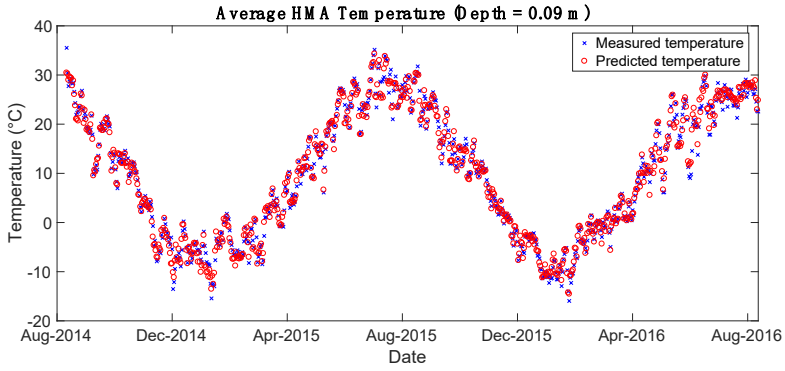
Average HMA Temperature (Depth = 0.09 m)
Measured temperature
Predicted temperature
Temperature (°C)
40
30
20
10
0
-10
-20
Aug-2014
Dec-2014
Apr-2015
Aug-2015
Dec-2015
Apr-2016
Aug-2016
Date

(b)

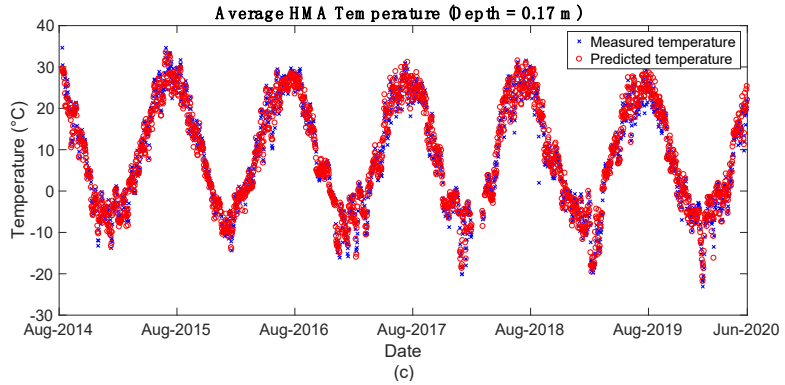
Average HMA Temperature (Depth = 0.17 m)
Measured temperature
Predicted temperature
Temperature (°C)
40
30
20
10
0
-10
-20
-30
Aug-2014
Aug-2015
Aug-2016
Aug-2017
Aug-2018
Aug-2019
Jun-2020
Date

(c)

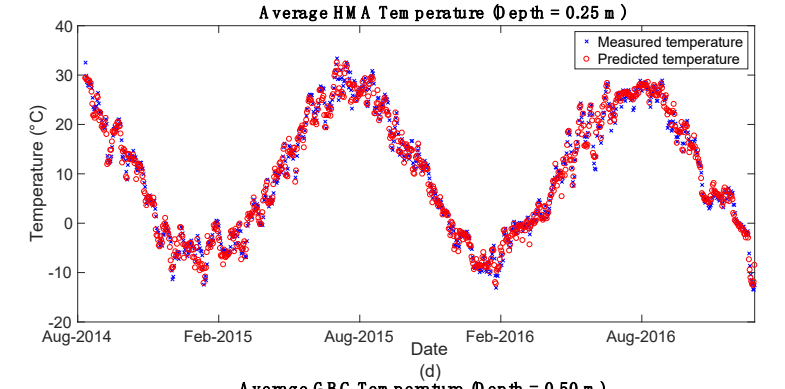
Average HMA Temperature (Depth = 0.25 m)
Measured temperature
Predicted temperature
Temperature (°C)
40
30
20
10
0
-10
-20
Aug-2014
Feb-2015
Aug-2015
Feb-2016
Aug-2016
Date

(d)

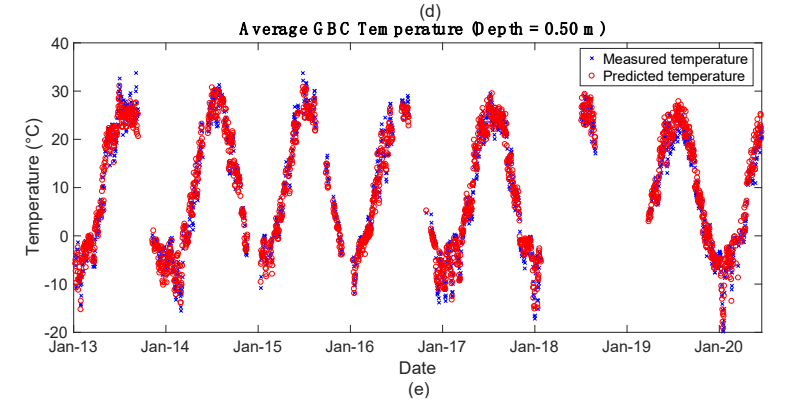
Average GBC Temperature (Depth = 0.50 m)
Measured temperature
Predicted temperature
Temperature (°C)
40
30
20
10
0
-10
-20
Jan-13
Jan-14
Jan-15
Jan-16
Jan-17
Jan-18
Jan-19
Jan-20
Date

(e)

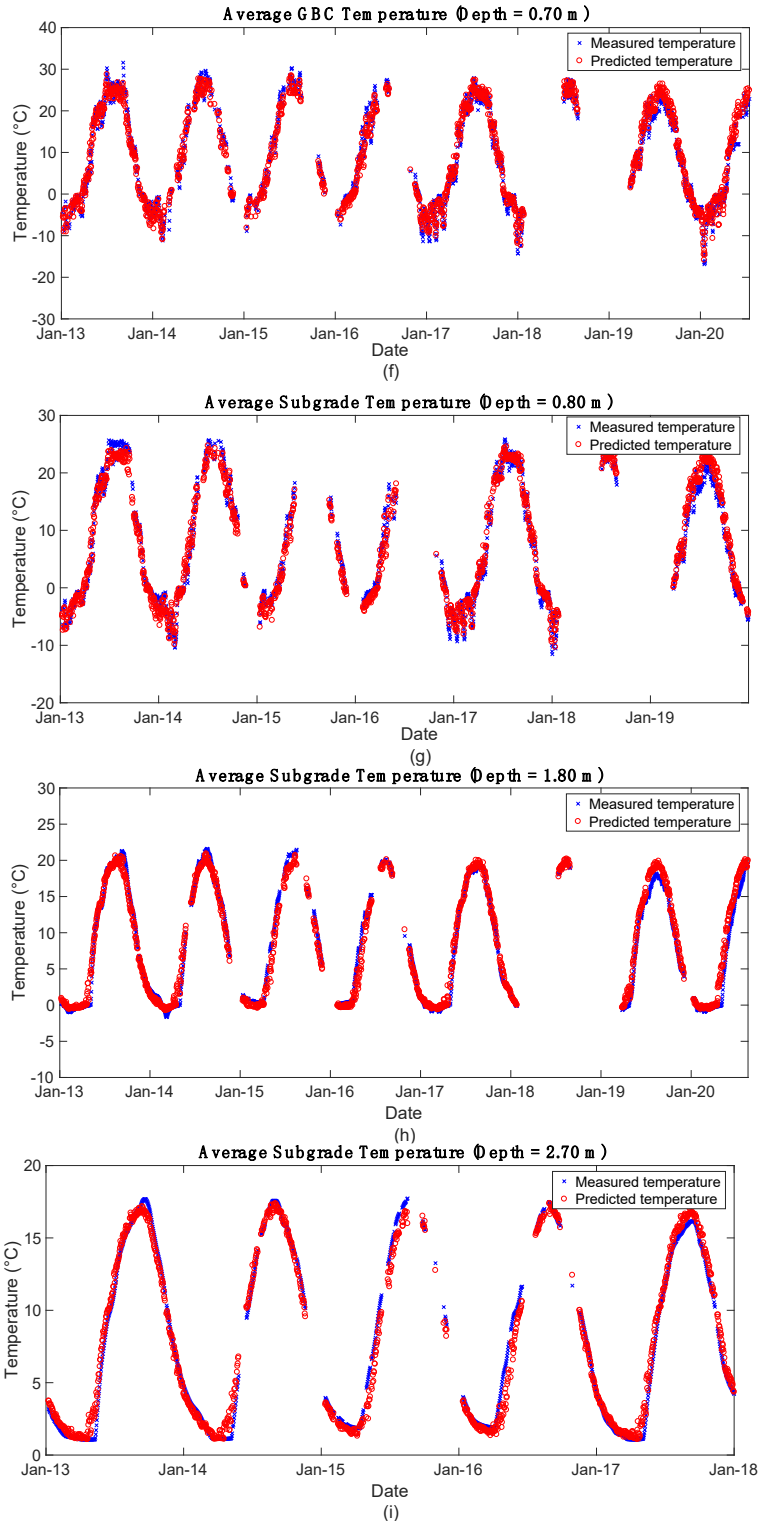

Figure 6-5: Comparison of the measured and predicated values (using ML model) of average daily road temperature at depths of (a) 0.02 m, (b) 0.09 m, (c) 0.17 m, (d) 0.25 m, (e) 0.50 m, (f) 0.70 m, (g) 0.80 m, (h) 1.80 m, and (i) 2.70 m

Table 6-4: Comparison of performance between ML models and literature models for prediction of average daily asphalt and soil temperature (Asefzadeh et al., 2017; Heydinger, 2003b).

Depth (m)	Exponential GPR Model		Parametric Model		Statistical Model			
					Cold Season		Warm Season	
	R^2	RMSE	R^2	RMSE	R^2	RMSE	R^2	RMSE
0.02	0.99	1.24	0.92	7.12	0.85	3.44	0.89	3.19
0.09	0.99	1.48	0.93	6.82	0.81	2.95	0.88	3.26
0.17	0.99	1.50	0.90	8.92	0.81	2.87	0.88	3.2
0.25	0.99	1.20	0.94	5.20	0.73	3.2	0.83	3.93
0.50	0.98	1.70	0.92	8.06				
0.70	0.98	1.80	0.94	6.72				
0.80	0.98	1.62	0.93	5.02				
1.80	0.98	1.20	0.95	1.96				
2.70	0.98	0.76	0.96	1.40				

Heydinger (2003b) used a parametric model, to predict the average daily temperature of asphalt and soil, resulting in the sinusoidal expression shown in Equation 6-1:

$$T(t) = A + B\sin\left[\omega(t - \phi)\right] \quad \text{Equation 6-1}$$

where t is time (expressed as the day of the year), A (°C) is the mean temperature, B (°C) is the amplitude, and ω is the normalized frequency ($\omega = 2\pi / 365.25$). To apply this equation, the appropriate values of A and B are estimated based on asphalt and soil temperature measurements. A statistical model in literature was developed to predict HMA layer temperature based on data collected from the IRRF test road (Asefzadeh et al., 2017). The model involved division of the whole year into two parts, a cold season (October to March) and a warm season (April to September). The equations are as in Equation 6-2 (for the warm season) and Equation 6-3 (for the cold season).

$$T_{ave} = 3.9832 + 1.1288(T_{air}) + 2.68 \times 10^{-5}(SR) \quad \text{Equation 6-2}$$

$$T_{ave} = -1.7853 + 0.6510(T_{air}) + 3.37 \times 10^{-4}(SR) + 2.0326 \times d \quad \text{Equation 6-3}$$

where T_{ave} (°C) is the daily average temperature of the HMA layer, T_{air} (°C) is the daily average air temperature, SR is the daily solar radiation (kJ/m^2), and d is depth (m).

Table 6-4 compares the performance of the ML model with two existing literature models, with the results shown in Figure 6-6. The measured temperature changed sinusoidally with time as shown in Figure 6-5. However, when the measured temperature was higher than 20°C or lower than 0°C, there was a deviation between the measured and predicted temperatures by the parametric model and it was observed to decrease as the depth increased. The parametric model was based on a sinusoidal expression based on mean temperature, amplitude, and day of the year (Heydinger, 2003b). In this case, air temperature and other factors were not taken into account; thus, the temperature followed the sinusoidal function completely and has a fixed shape (Heydinger, 2003b). The result of the temperature predictions using parametric model were consistent with the actual measurements, as indicated by the R^2 value, which was very high. However, when the temperature was greater than 20°C or less than 0°C, the predicted values differed significantly from the measured values, as shown in Figure 6-6 (a). Then, the temperature predicted using the parametric equation showed higher RMSE than values gave by the ML models, especially for shallow depths. The statistical model included air temperature, solar radiation, and depth as inputs (Asefzadeh et al., 2017). As results showed in Figure 6-5, temperature varies at different depths. However, in the statistical model, depth only works in the cold season and the statistical model assumes the HMA layer temperature is the same in warm season. The accuracy of the statistical model was low, with an R^2 value less than 0.89. As indicated in Figure 6-6 (b), the temperatures calculated using the statistical model were more scattered than the results obtained using the ML model. On average, the R^2 values of the ML models were 6% and 19% higher, respectively than the parametric model and statistical

model used to predict the average daily temperature of the IRRF test road. Likewise, the RMSE values were 69% and 58% lower. In this case, the machine learning model developed with average daily air temperature, day of the year and depth as input parameters gives a robust method to determine the average daily temperature of the HMA, base and subgrade layers.

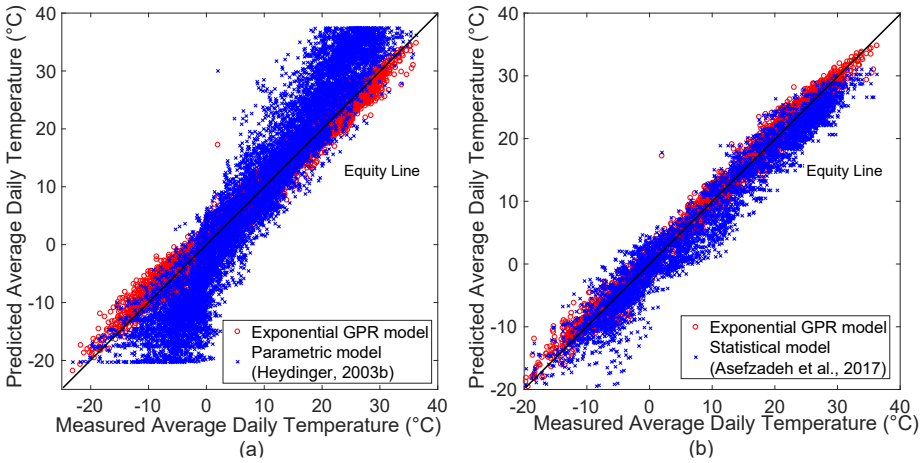

Figure 6-6: Comparison of predicted and measured average daily temperature for the (a) parametric model (Heydinger, 2003b) and (b) statistical model (Asefzadeh et al., 2017) with the Exponential GPR model

6.5.2. Minimum Daily Temperature

The minimum daily temperatures obtained using the ML model were also compared with the values determined using available literature models, as shown in Figure 6-7 and 6-8. The performance of the ML model and the other available literature models were summarized in Table 6-5. The ML model gives a high accuracy for predicting minimum daily temperature, with a R^2 was greater than 0.97, and RMSE was less than 1.87.

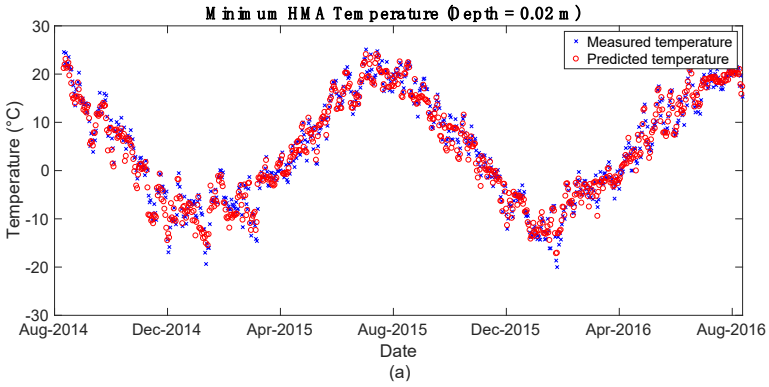

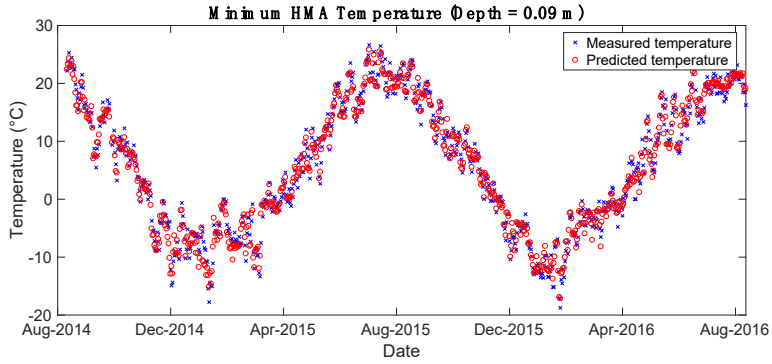
Minimum HMA Temperature (Depth = 0.09 m)
Measured temperature
Predicted temperature
Temperature (°C)
30
20
10
0
-10
-20
Aug-2014
Dec-2014
Apr-2015
Aug-2015
Dec-2015
Apr-2016
Aug-2016
Date

(b)

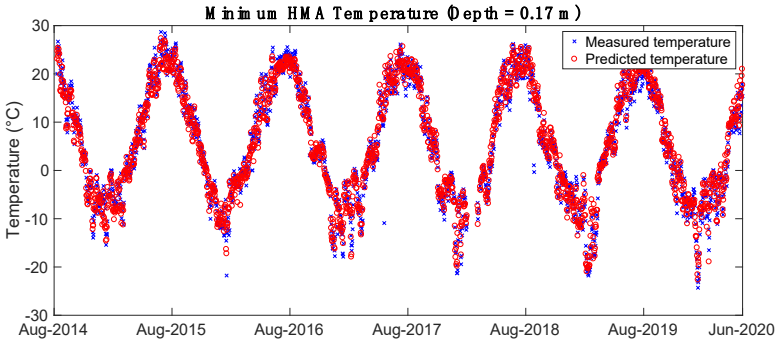
Minimum HMA Temperature (Depth = 0.17 m)
Measured temperature
Predicted temperature
Temperature (°C)
30
20
10
0
-10
-20
-30
Aug-2014
Aug-2015
Aug-2016
Aug-2017
Aug-2018
Aug-2019
Jun-2020
Date

(c)

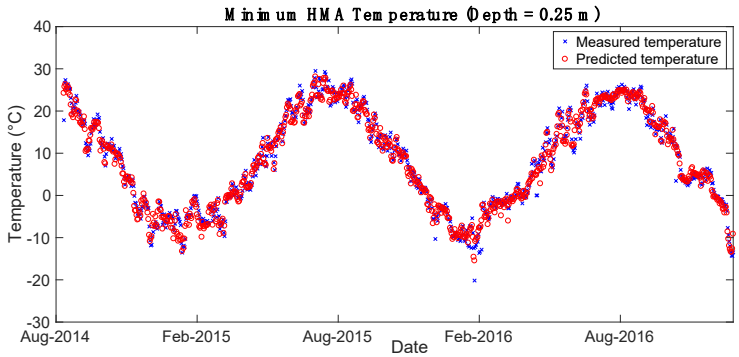
Minimum HMA Temperature (Depth = 0.25 m)
Measured temperature
Predicted temperature
Temperature (°C)
40
30
20
10
0
-10
-20
-30
Aug-2014
Feb-2015
Aug-2015
Feb-2016
Aug-2016
Date

(d)

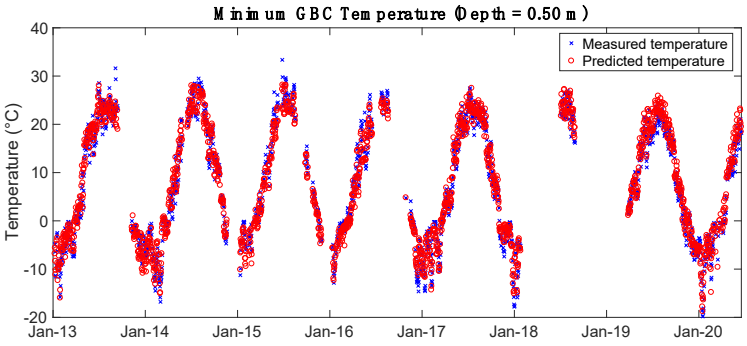
Minimum GBC Temperature (Depth = 0.50 m)
Measured temperature
Predicted temperature
Temperature (°C)
40
30
20
10
0
-10
-20
Jan-13
Jan-14
Jan-15
Jan-16
Jan-17
Jan-18
Jan-19
Jan-20
Date

(e)

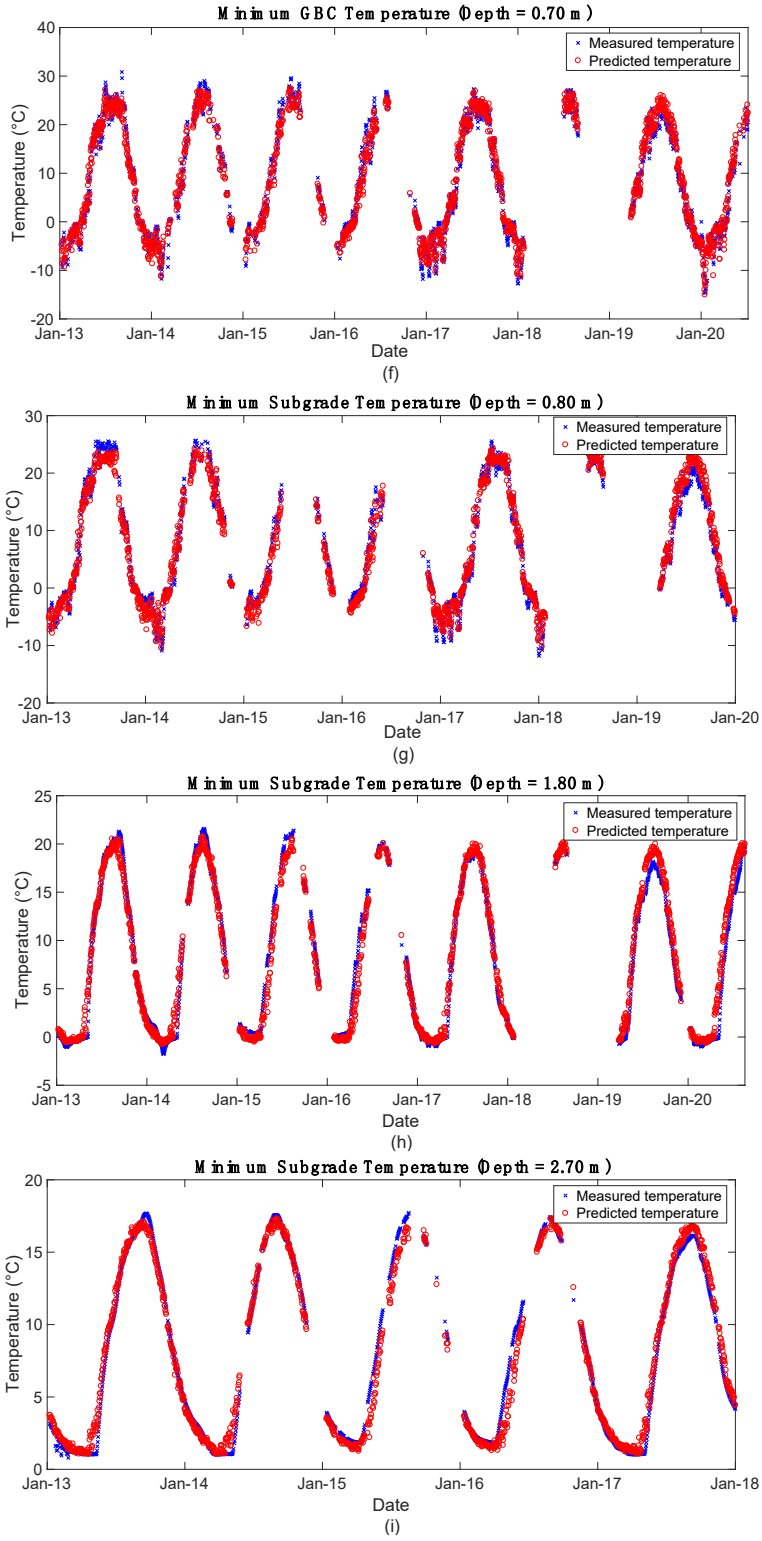

Figure 6-7: Comparison of the measured and predicted minimum daily temperature at depths of (a) 0.02 m, (b) 0.09 m, (c) 0.17 m, (d) 0.25 m, (e) 0.50 m, (f) 0.70 m, (g) 0.80 m, (h) 1.80 m, and (i) 2.70 m

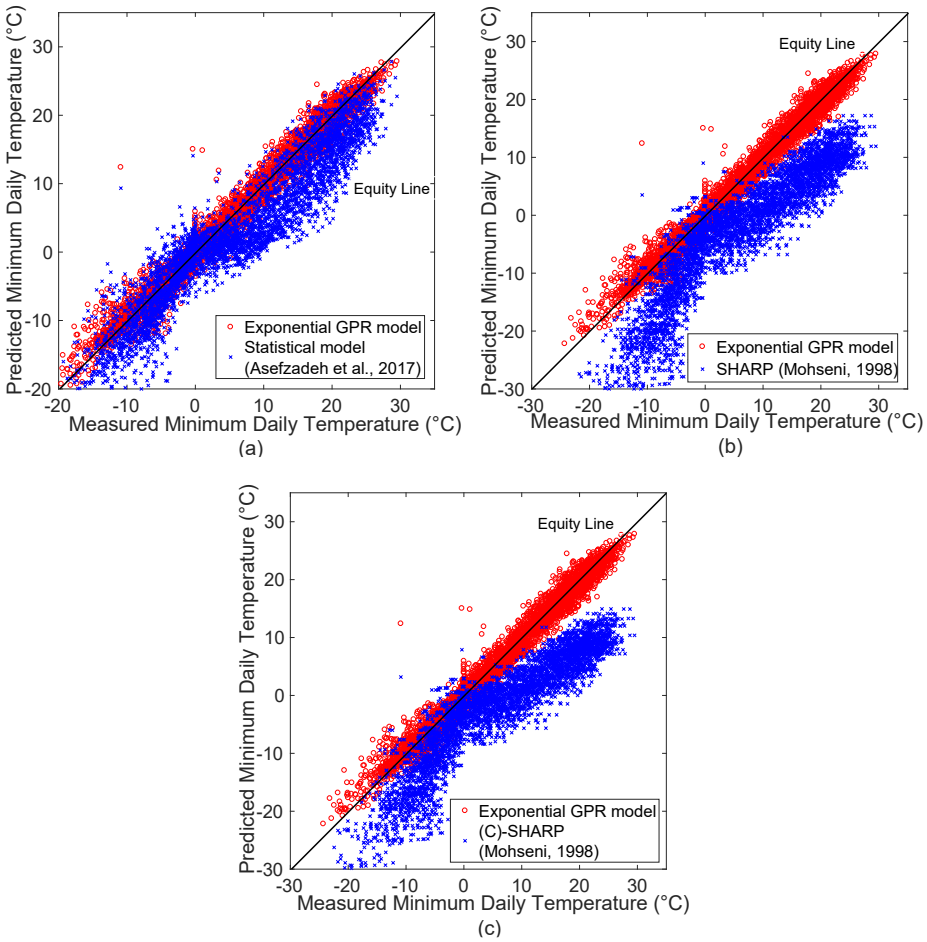

Figure 6-8: Comparison of the predicted minimum daily temperatures and measured minimum daily temperature for (a) statistical model(Asefzadeh et al., 2017b), (b) SHRP (Mohseni, 1998), and (c) C-SHRP (Mohseni, 1998)

In literature, a statistical model (Asefzadeh et al., 2017) was developed to predict minimum daily pavement temperature in the HMA layer at various depths, as in Equation 6-4.

$$T_{HMA\,(min)} = -2.8704 + 0.89\,T_{air\,(min)} + (1.26 \times 10^{-4})\,SR + 0.1759\left(SR \times T_{air\,(min)}^{2}\right)^{0.25} + 15.2324d \qquad \text{Equation 6-4}$$

where $T_{HMA\,(min)}$ (°C) is the minimum daily HMA temperature, $T_{air\,(min)}$ (°C) is the minimum daily air temperature, SR is the daily solar radiation (kJ/m^2), and d is the depth (m).

Table 6-5: Comparison of performance between ML models and existing models for prediction of minimum daily asphalt and soil temperature (Asefzadeh et al., 2017; Mohseni, 1998).

Depth (m)	Exponential GPR model		Statistical model		SHARP		(C)-SHARP	
	R^2	RMSE	R^2	RMSE	R^2	RMSE	R^2	RMSE

0.02	0.98	1.40	0.90	4.95	0.85	7.40	0.85	7.84
0.09	0.98	1.37	0.89	5.03	0.84	5.98	0.84	8.68
0.17	0.98	1.81	0.90	4.63	0.85	5.03	0.85	9.09
0.25	0.98	1.52	0.86	5.41	0.79	5.32	0.79	10.74
0.50	0.98	1.87						
0.70	0.98	1.75						
0.80	0.97	1.75						
1.80	0.98	1.26						

The Strategic Highway Research Program (SHRP) and Canadian ((C)-SHRP) developed two models to predict minimum pavement temperature within the HMA layer to inform the choice of optimum asphalt concrete mixtures (Mohseni, 1998). These two models are presented as Equation 6-5 (SHRP) and 6-6 ((C)-SHRP).

$$T_d = T_{air\ (min)} + 0.051d - 0.000063d^2 \quad \text{Equation 6-5}$$

$$T_d = 0.859T_{air\ (min)} + \left(0.002 - 0.0007T_{air\ (min)}\right)d + 0.17 \quad \text{Equation 6-6}$$

In both Equation 6-5 and 6-6, T_d (°C) is the minimum pavement temperature at depth d (mm) and $T_{air\ (min)}$ (°C) is the minimum daily air temperature.

The existing models only works within the HMA layer, and Table 6-5 summarizes the performance of the performance when applied in the IRRF test road. On average, the R^2 values for the ML model developed in this work were 10%, 18%, and 18% higher than the statistical model (Asefzadeh et al., 2017), SHRP model (Mohseni, 1998), and (C)-SHRP model (Mohseni, 1998), respectively. The RMSE values for the ML model were found to be 69%, 73%, and 83% lower. As shown in Figure 6-8, both the SHRP and (C)-SHRP models underestimate the pavement temperature. Compared with the three statistical methods in the literature, the ML models showed higher accuracy in predicting the minimum daily pavement temperature. Furthermore, the ML model developed in this work also showed high accuracy when applied

to prediction of the minimum daily temperature within the base and subgrade layers. Thus, given enough temperature measurements within the pavement structure and average daily air temperature, ML models can provide a robust method to predict the minimum temperature at various depths within the pavement structure.

6.5.3. Maximum Daily Temperature

Table 6-6 and Figure 6-9 indicate the performance of the ML model in predicting the maximum temperature of the HMA layer and the unbound material layers. The R^2 value obtained by the ML model was higher than 0.98, and the RMSE value was lower than 2.21, indicating that the maximum daily pavement temperatures predicted using the ML model were very close to the measured values.

Table 6-6: Comparison of performance between ML models and existing models for prediction of maximum daily asphalt and soil temperature (Asefzadeh et al., 2017).

Depth (m)	Exponential GPR model		Statistical Model	
	R^2	RMSE	R^2	RMSE
0.02	0.98	2.21	0.96	4.12
0.09	0.99	1.66	0.94	5.11
0.17	0.98	1.67	0.92	6.23
0.25	0.99	1.19	0.88	6.25
0.50	0.98	1.70		
0.70	0.98	1.58		
0.80	0.98	1.20		
1.80	0.98	1.17		
2.70	0.98	0.94		

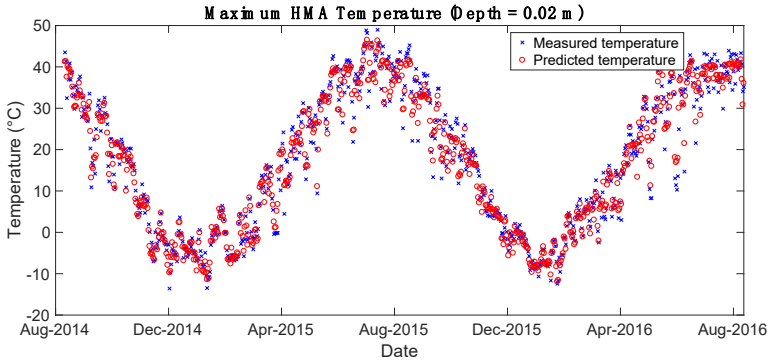
Maximum HMA Temperature (Depth = 0.02 m)
Measured temperature
Predicted temperature
Temperature (°C)
50
40
30
20
10
0
-10
-20
Aug-2014
Dec-2014
Apr-2015
Aug-2015
Dec-2015
Apr-2016
Aug-2016
Date

(a)

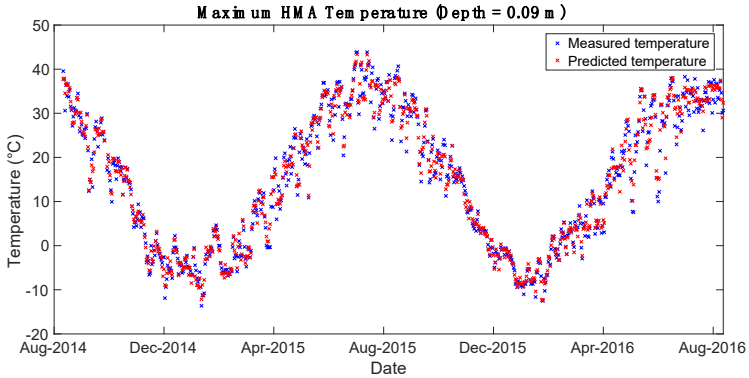
Maximum HMA Temperature (Depth = 0.09 m)
Measured temperature
Predicted temperature
Temperature (°C)
50
40
30
20
10
0
-10
-20
Aug-2014
Dec-2014
Apr-2015
Aug-2015
Dec-2015
Apr-2016
Aug-2016
Date

(b)

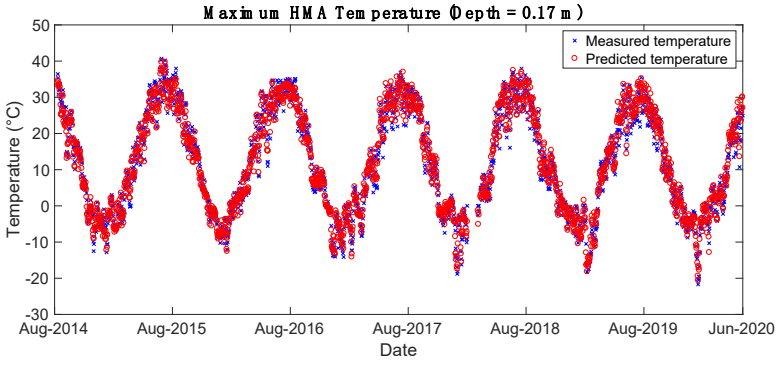
Maximum HMA Temperature (Depth = 0.17 m)
Measured temperature
Predicted temperature
Temperature (°C)
50
40
30
20
10
0
-10
-20
-30
Aug-2014
Aug-2015
Aug-2016
Aug-2017
Aug-2018
Aug-2019
Jun-2020
Date

(c)

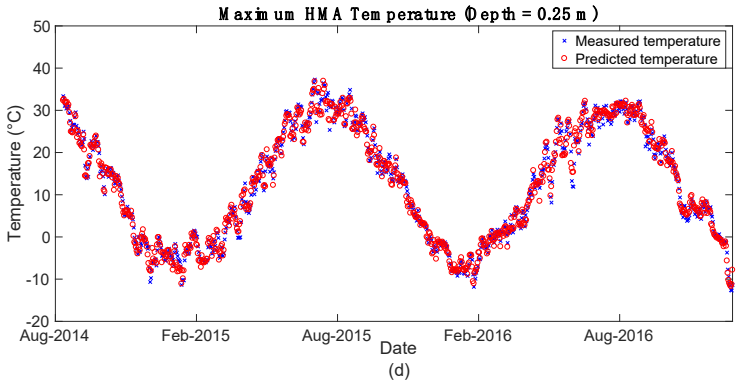
Maximum HMA Temperature (Depth = 0.25 m)
Measured temperature
Predicted temperature
Temperature (°C)
50
40
30
20
10
0
-10
-20
Aug-2014
Feb-2015
Aug-2015
Feb-2016
Aug-2016
Date

(d)

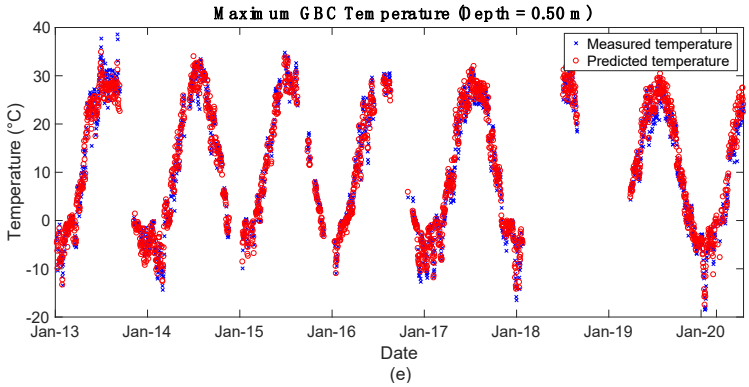
Maximum GBC Temperature (Depth = 0.50 m)
Measured temperature
Predicted temperature
Temperature (°C)
Date
Jan-13
Jan-14
Jan-15
Jan-16
Jan-17
Jan-18
Jan-19
Jan-20

(e)

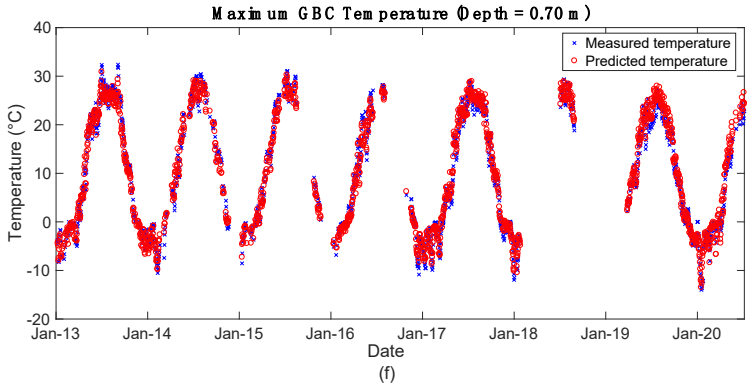
Maximum GBC Temperature (Depth = 0.70 m)
Measured temperature
Predicted temperature
Temperature (°C)
Date
Jan-13
Jan-14
Jan-15
Jan-16
Jan-17
Jan-18
Jan-19
Jan-20

(f)

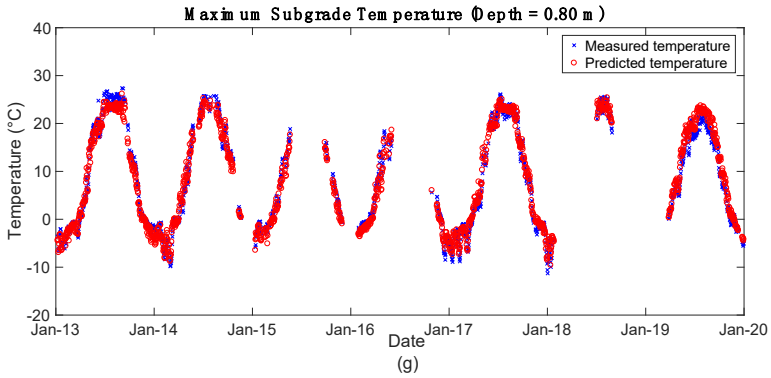
Maximum Subgrade Temperature (Depth = 0.80 m)
Measured temperature
Predicted temperature
Temperature (°C)
Date
Jan-13
Jan-14
Jan-15
Jan-16
Jan-17
Jan-18
Jan-19
Jan-20

(g)

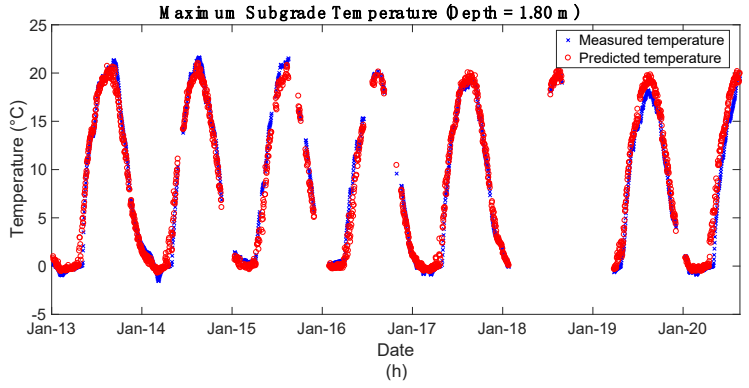
Maximum Subgrade Temperature (Depth = 1.80 m)
Measured temperature
Predicted temperature
Temperature (°C)
Date
Jan-13
Jan-14
Jan-15
Jan-16
Jan-17
Jan-18
Jan-19
Jan-20

(h)

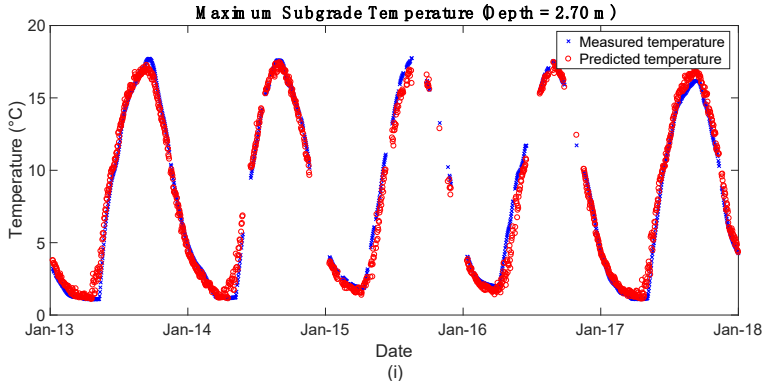

Figure 6-9: Comparison of the measured and predicted maximum daily road temperature at a depth of (a) 0.02 m, (b) 0.09 m, (c) 0.17 m, (d) 0.25 m, (e) 0.50 m, (f) 0.70 m, (g) 0.80 m, (h) 1.80 m, and (i) 2.70 m

The statistical model in literature (Asefzadeh et al., 2017) was developed for maximum daily pavement temperature, is included in Equation 6-7.

$$T_{d(\max)} = 2.0237 + 0.8709\,T_{air(max)} + (7.6 \times 10^{-4})\,SR - 16.1886\,d \qquad \text{Equation 6-7}$$

where $T_{d(max)}$ (°C) represents the maximum daily pavement temperature at depth d (mm), $T_{air\,(max)}$ is the maximum daily air temperature, and SR (kJ/m^2) represents the solar radiation.

Table 6-6 compares the performance of the statistical model in predicting the maximum daily temperature of the HMA layer with the performance of the ML model developed in this work. R^2 for the results obtained using the ML model was 7% higher than the statistical model. Furthermore, the RMSE for the ML model was 67% lower than the statistical model. Figure 6-10 includes a comparison of the predicted and measured maximum daily temperatures obtained using both the ML model and the statistical model. From Figure 6-10, it can be seen that the statistical model overestimated pavement temperature when the maximum pavement is above 0°C. Even the ML model based on only one environmental parameter (i.e., air temperature) also maintained high accuracy, with R^2 values greater than 0.98 and RMSE values less than 2.21. Therefore, once pavement temperature measurement and air temperature are available, ML could be a powerful tool for predicting the maximum daily temperature of pavement structures.

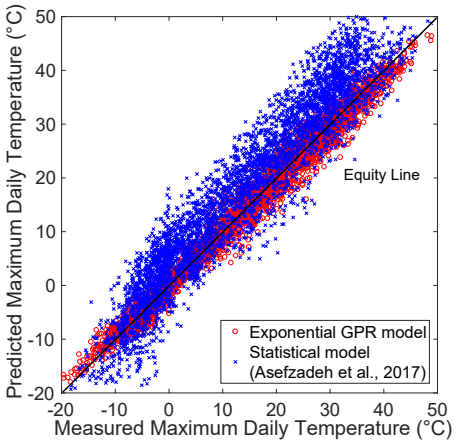

Figure 6-10: Comparison of predicted and measured maximum daily temperature for ML model and statistical model (Asefzadeh et al., 2017)

6.6. CONCLUSIONS

In this work, temperature measurements for the HMA, base, and subgrade layers collected from the IRRF test road were used to train three ML models to predict the average, minimum, and maximum daily temperature within the pavement structure. A sensitivity analysis was done to determine the influence of average daily air temperature, solar radiation, relative humidity, wind speed, and DOY on the average, minimum and maximum daily temperature. Based on this, the average daily air temperature and DOY were determined to be the most robust input parameters. ML models were developed using five different algorithms (linear regression models, regression trees, SVM, GPR, and ensembles of trees), and the ML model based on the exponential GPR algorithm outperformed the other ML models. To predict temperature at various depths, depth was also included in the three ML models. The ML models based on average daily air temperature, DOY and depth, were then used to determine the temparature at various depths and compared with four existing models in the literature.

For the prediction of average daily temperature, the R^2 of the ML model was 6% and 19% higher than the parametric and statistical models, respectively. The RMSE was 69% and 58% lower. It was found that for predicting the minimum temperature of the HMA layer, the ML model resulted in R^2 values 10% higher than the statistical model, and 18% higher than the

SHRP and (C)-SHRP models. Furthermore, RMSE values for the ML model (again when predicting the minimum temperatuer of the HMA layer)were 69%, 73%, and 83% lower than the statistical model, SHRP and (C)-SHRP models, respectively. Moreover, the ML model developed in this work resulted in improved accuracy for prediction of the maximum daily temperature of the HMA layer, with R^2 increasing by 7% and RMSE decreasing by 67% compared to the statistical model. The higher R^2 values and the lower RMSE lower indicated that ML models with one environmental parameter, average daily air temperature, could be a powerful tool to predict the temperature of the HMA layer.

Only one model, a parametric model, was found that could be applied to predict the average daily temperature within the asphalt and soil layers of the pavement. In contrast, the three ML models developed in this work showed a high accuracy when used to predict the average, minimum, and maximum daily temperature in the base and subgrade layers (with $R^2 > 0.97$ and RMSE < 1.85). Compared with the existing literature models, the three ML models developed in this work used only average daily air temperature, DOY, depth, and measurements of temperature within the asphalt and soil temperature layer. Other boundary conditions, which must be defined, and material parameters (such as thermal conductivity, ratio, heat capacity, density, etc. which can be difficult to obtain) were not required for the three ML models. Therefore, the use of ML models can be a practical method for predicting the temperature within pavement structures at multiple depths.

Although ML models outperform other conventional methods, a dataset of temperature measurements is necessary. Furthermore, the accuracy of the ML model applied to other road structures is not clear and will be addressed in future work.

CHAPTER 7.TEMPERATURE PREDICTION AT THE PRESENCE OF INSULATING MATERIALS

This section has been published as Huang, Y., Molavi Nojumi, M., Ansari, S., Hashemian, L. and Bayat, A., 2023. Evaluation of machine learning approach for base and subgrade layer temperature prediction at various depths in the presence of insulation layers. Journal of Pavement Engineering, Part B: Pavements, 24(1), 2180640.

7.1. ABSTRACT

To protect pavement in cold regions, insulation layers have been used in pavement construction. The insulation layer blocks the heat exchange, resulting in different pavement temperature distributions at different layers. Pavements in cold regions are subject to frost heave, thaw weakening, and freeze–thaw cycling, and the moisture content of unbound materials is affected by the temperature of the pavement. Therefore, the base and subgrade temperature can affect the pavement performance, and the insulation layer influences the performance of the pavement. This work aims to demonstrate the capability of the machine learning method to predict the pavement temperature of the base and subgrade layers in the presence of insulation layers. Pavement temperature measured from sensors embedded in the pavement at the IRRF test road and environmental factors collected from a weather station were used to train machine learning models. The results obtained from machine learning models indicated that the air temperature and day of the year were the most robust input prediction parameters at each depth. Machine learning models outperformed the existing model and proved that it could be a method to improve pavement temperature prediction with insulation layers, especially when the base layer temperature is below 0°C.

Keywords: insulation layer, base layer temperature, subgrade layer temperature, machine learning, thermistor data, temperature prediction models

7.2. INTRODUCTION

Freezing weather negatively influences pavement performance, and pavements in cold regions are prone to cracking, rutting, and moisture damage due to frost heave, thaw weakening, and freeze–thaw cycling (Smith, 2006). Water in the base and subgrade layers freezes in winter, and the pavement temperature increases in the spring, with temperatures highest at the road surface and lowest in the subgrade. At the same time, the underlying soil remains frozen, and its drainage capacity is insufficient to drain away excess water. Excess water thus starts to accumulate in the upper layer, leading to an increase in moisture content in the base and subgrade layers, and a decrease in modulus and load capacity (Miller et al., 2012; Haghi et al., 2016). In Canada, 75% of the degradation of a flexible road surface has been shown to be caused by climatic factors (Doré et al., 2005). Pavements in cold areas generally exhibit premature distress, lower load capacity, and higher maintenance costs (among other issues) compared to pavements in warm regions (Tighe et al., 2006).

Insulation layers have been used in pavement construction to protect the pavement from damage caused by cold weather (Penner, 1967; Hayden and Swanson, 1972; Haghi et al., 2014; Huang et al., 2021). Polystyrene board was first reported as an insulation layer for pavement in 1967 (Penner, 1967). Successive studies have proved that it can protect the subgrade layer from frost (Penner, 1967; Hayden and Swanson, 1972; Haghi et al., 2014). Bottom ash, which is a by-product of coal combustion burned for electric power plants and is considered to be a recycled material (Nassiri et al., 2013), has also been used as an insulation material. It is a more environmentally friendly alternative to styrofoam. Bottom ash has been used as a component in cold-mix asphalt, in the construction of embankments, and as a base course (Mohammed and Karim, 2017). At the Integrated Road Research Facility test road in Edmonton, AB, a one-meter layer of bottom ash was used as an insulation layer in a test section, with extruded

polystyrene board used in another test section. It has been shown that the presence of an insulation layer affects temperature distribution in the base and subgrade layers and influences pavement performance (Haghi et al., 2014; Huang et al., 2021). Bottom ash and extruded polystyrene board were found to limit frost and protect the subgrade layer from weakening during freeze–thaw cycles (Haghi et al., 2014). In winter, a more significant temperature variation was observed in the base layer for the Integrated Road Research Facility (IRRF) test section insulated with a polystyrene layer than in the control section without an insulation layer, which makes the pavement with a polystyrene layer more susceptible to low-temperature damage. In contrast, the observed base temperature range in the bottom ash section was similar to the control section (Huang et al., 2021).

Birgisson et al. (2000) demonstrated that subsurface conditions of the pavement layers, including pavement temperature, moisture content, and state of moisture, determine the strength and stiffness of the materials. Moisture content and state of moisture are affected by pavement temperature, thus the temperature in the base and subgrade layers dominates the load capacity of pavements (Fredlund et al., 1977; Birgisson et al., 2000; Simonsen et al., 2002; AASHTO, 2008). To improve pavement performance, it is necessary to understand the temperature variation in the base and subgrade layers of pavements with insulation layers. Fredlund et al. (1977) showed that matric suction, which is dependent on temperature and moisture content, determined the behaviour of unsaturated soils, such as those used in subgrade layers. Simonsen et al. (2002) found a significant increase in the soil resilient modulus as the temperature decreased from 0°C to −20°C. The Mechanistic-Empirical Pavement Design Guide (MEPDG) (AASHTO, 2008) also indicates that the resilient modulus of a frozen pavement layer rises in winter but falls with increasing temperature during spring when thawing occurs.

Different methods, including analytical (Birgisson et al., 2000; Dumais and Doré, 2016), numerical (Hermansson, 2004; Minhoto et al., 2005; Alavi et al., 2014), and statistical (Heydinger, 2003; Asefzadeh et al., 2017) methods, have previously been utilised to predict pavement temperature. However, most of these methods focus on predicting the temperature of the road surface or hot mix asphalt (HMA) layer. Heydinger (2003) proposed a sinusoidal function to predict the temperature of the entire pavement structure based on mean temperature, amplitude, and time shift. However, this function was developed based on a conventional pavement structure, i.e. without any insulation layer with high thermal conductivity. The applicability of this method on pavements with insulation layers is unknown; however, it will be applied to pavement sections with insulation layers in the following sections. The lack of available models for temperature prediction of pavement with insulation layers also emphasises the importance of extending available methods for determining temperature for these pavements.

With the development of computer computing capacity and artificial intelligence theory, artificial intelligence techniques have received significant attention. Machine learning, a branch of artificial intelligence, has been used to investigate road surface temperature (Li et al., 2018; Qiu et al., 2020) and temperature variation within the asphalt layer (Molavi Nojumi et al., 2022). Liu et al. (2018) utilised gradient extreme learning machine boosting to predict road surface temperature at an airport expressway with 81.8% accuracy (i.e. a difference of less than 3°C between measured and predicted temperature values). Qiu et al. (2020) applied machine learning to predict the surface temperature of asphalt pavement; in this case, a gradient boosting decision tree showed the highest accuracy among the different algorithms investigated. Molavi Nojumi et al. (2022) used machine learning to predict the average, minimum, and maximum daily pavement temperature in an HMA layer. In this work, it was found that the developed machine learning models outperformed other existing models. In general, machine learning

models have shown higher accuracy for temperature prediction in pavement compared to traditional methods. However, based on the existing literature, machine learning methods have not been applied to predict the temperature for base and subgrade layers in pavements with an insulation layer.

The primary purpose of this study is to utilise machine learning models to predict temperatures at multiple depths in the base and subgrade layers of pavement structures with insulation materials. The regression learner in MATLAB was used to develop machine learning models. Five machine learning algorithms were trained, including regression trees, support vector machines (SVM), Gaussian process regression (GPR) models, ensembles of trees, and linear regression. The coefficient of determination (R^2) and root-mean-square error (RMSE) were used to evaluate the performance of the machine learning models. The best-performing machine learning model (i.e. the machine learning model that attains the highest value of R^2 and lowest value of RMSE) was compared with the sinusoidal function for temperature prediction in pavement developed by Heydinger (2003).

7.3. PROCEDURE FOR MODEL DEVELOPMENT

Environmental factors, including air temperature, solar radiation, precipitation, wind speed, and relative humidity, can influence the annual range of temperature measured in the pavement structure, and their effect may vary depending on pavement conditions (Chen et al., 2019, Adwan et al., 2021). However, pavement temperature in this study is collected at depths of at least 0.64 m from the road surface, far from the road surface, so the influence of wind speed and relative humidity on the pavement temperature at these depths is limited. Thus, these two factors have not been included in this study. Previous studies indicate that pavement temperature changes seasonally, and the inclusion of a time-related input parameter significantly improves the accuracy of pavement temperature prediction (Heydinger, 2003;

Molavi Nojumi et al., 2022). Thus, a time-related parameter, day of the year (DOY), is included in this study, with 1 corresponding to January 1st. Machine learning algorithms for predicting temperature variation in the base and subgrade layer were developed using available data for temperature prediction at different depths for pavement insulated with bottom ash and polystyrene layer. The depth of each sensor has been used as an input parameter.

Figure 7-1 illustrates the procedure for developing a machine learning model. Initially, the raw temperature measurements collected by thermistors are preprocessed. Any irrelevant data (such as NAN and 7999) are deleted. The reliability of the records is checked by comparing the raw data with previous records and environmental data. For example, if the pavement temperature has been changing with the air temperature, but suddenly the air temperature keeps rising for a certain period, and the pavement temperature remains the same. Then the data are treated as unreliable records and excluded from the analysis. The next step involves the calculation of the average daily temperature from the temperature measurements (which are collected hourly). Data for environmental factors (e.g. air temperature and precipitation, and the list will be updated, if the performance of the models is low) are obtained from the Environment Canada weather station nearest to the IRRF test road (Oliver AGDM). These data are integrated with the average daily pavement temperature data using timestamps. The complete dataset, including air temperature, solar radiation, day of the year, depth, and pavement temperature measured at different depths, is then loaded into a MATLAB R2017a regression learner toolbox. Next, the most important predictive parameters are determined, among air temperature, solar radiation, and day of the year, by performing sensitivity analysis. Data are divided into two parts, one for training and one for validation. All the five machine learning algorithms, including regression trees, support vector machines, gaussian process regression models, ensembles of trees, and linear regression were used to train models, and the best-performing algorithm is carried forward. Cross-validation in MATLAB was applied to avoid overfitting in

the training process. Data were randomly divided into five folds, and for each training cycle, four folds were used to train the model, while one data fold was used to test its performance. The whole process was repeated five times, with each fold used for testing in turn. The final test errors, R^2 and RMSE, were calculated considering data from all five folds and were used for the statistical comparison of different models. R^2 and RMSE can be calculated by Equations 7-1 and 7-2.

$$R^2 = 1 - \frac{\sum_i (x_i - f_i)^2}{\sum_i (x_i - \bar{x})^2} \quad \text{Equation 7-1}$$

$$RMSE = \sqrt{\frac{\sum_{i=1}^{N} (x_i - f_i)^2}{N}} \quad \text{Equation 7-2}$$

where x_i is the actual value, f_i is the predicted value, $\bar{x}$ is the mean value of the dataset, and N is the number of data points.

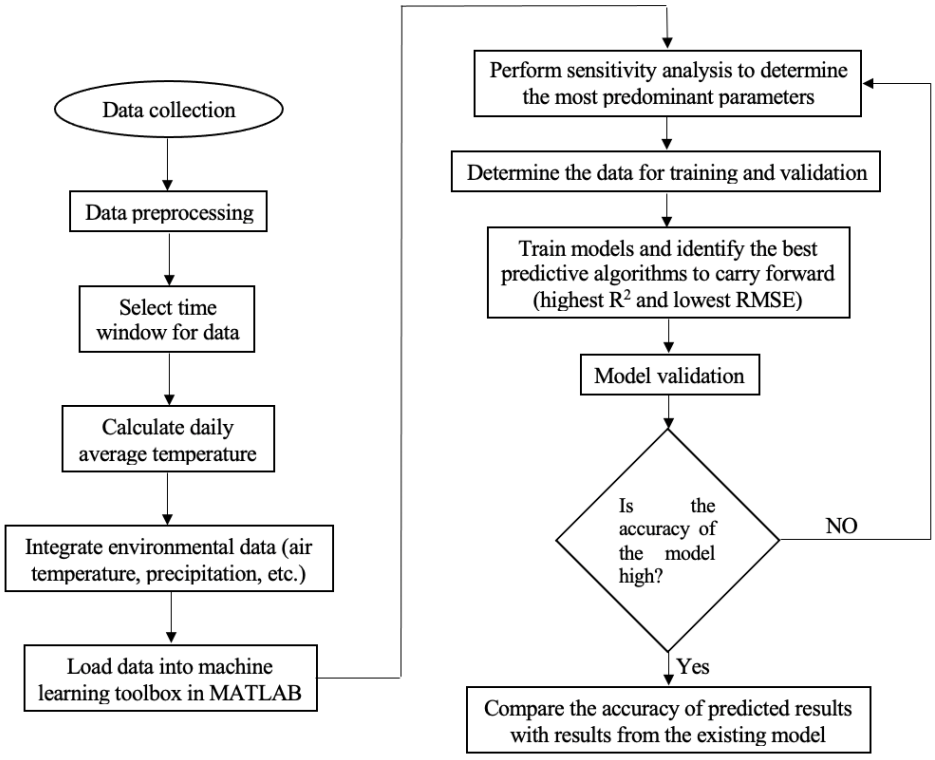

Figure 7-1: Procedure for developing machine learning predictive models

Then, the model is validated using the portion of the dataset set aside for model validation. If the machine learning models show high accuracy in both training and validation processes, and the predicted temperature values are in good agreement with temperature measurements for all the depths discussed in this work, the final model is determined. Finally, the performance of each machine learning model is compared with the existing model. But, if the accuracy of a model accuracy drops during model validation, sensitivity analysis will be carried out again, and different input parameters will be included.

7.3.1. Data Availability

The Integrated Road Research Facility (IRRF) test road is located in northeast Edmonton, Alberta, Canada, and is an access road to the Edmonton Waste Management Center. Construction of the IRRF test road was completed in October 2013, and the road was opened to public traffic in 2015. According to data from a weigh in motion (WIM) system installed on the test road, the average daily traffic was 2312 in 2016 and 2548 in 2019 (an increase of 10%). Garbage trucks account for 10–20% of all traffic on this test road.

The test road consists of two lanes, with a total length of about 500 m. The road width is 14.1 m. There are several test sections and a control section. Figure 7-2 shows a cross-section of two 20 m long test sections containing different insulation layers. One insulated test section has a one-meter layer of bottom ash (BA) and another test section has a layer of 0.10 m polystyrene board (PS). The insulation layers (both BA and PS) were placed between the subgrade and the granular base course (GBC) layers (the GBC layer is 0.45 m thick). An HMA layer (0.25 m) is on top of the GBC layer. More detailed information about the IRRF test road is available in the literature (Nassiri et al., 2013; Hashemian and Bayat, 2016; Huang et al., 2021).

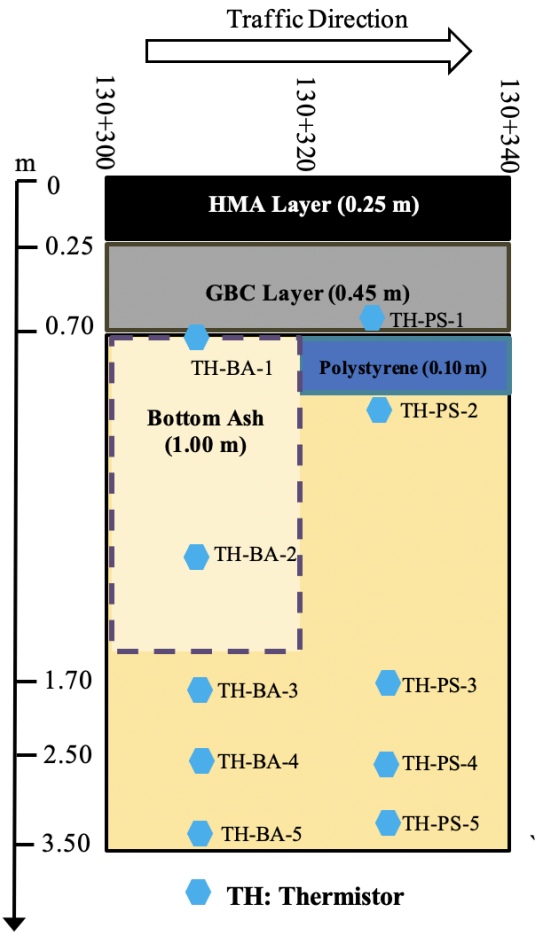

Figure 7-2: Schematic illustration of the pavement cross-section at the IRRF test road for test sections containing BA and PS insulation layers

Thermistors (109AM-L, Campbell Scientific) were used to monitor pavement temperature in the IRRF test road. Five thermistors are located in the test section with bottom ash, the first two at depths of 0.72 m (top of the bottom ash layer), and 1.40 m (in the middle of the bottom ash layer) relative to the pavement surface. The remaining three thermistors are located at depths of 1.85, 2.83, and 3.36 m (all in the subgrade layer). In the PS section, two sensors are located at depths of 0.64 and 0.80 m (at the top and bottom of the polystyrene layer, respectively). Another three sensors are located in the subgrade, at depths of 1.80, 2.25, and 3.25 m from the pavement surface. The system was programmed to collect and record temperature data hourly. It should be noted that from 2012 to 2020, the lowest average daily air temperature in Edmonton was −38°C (Huang et al., 2021).

Table 7-1 shows the properties of the materials used in the test sections insulated with BA and PS layers. The thermal conductivity (k) of a material measures its ability to conduct heat, and is influenced by whether the material is frozen or not; in Table 7-1, the minimum value of k is included, for a period in which the material is not frozen (Côté and Konrad, 2005; Bai et al., 2015). According to available literature (Klein et al., 2003; Côté and Konrad, 2005; Haghi et al., 2014; Bai et al., 2015), of the materials considered, k is the lowest for polystyrene board. Thermal resistance represents the resistance of materials to the conduction of heat; and is calculated by the thickness of a material divided by its thermal conductivity. A higher thermal resistance value indicates a better-performing insulation layer. The thermal resistance of the bottom ash layer is 1.43 $m^2 \cdot °C/W$, while the thermal resistance value of the 0.10 m polystyrene board is much higher (16.67 $m^2 \cdot °C/W$). The thermal resistance of the insulation layers is higher than that of the GBC and subgrade layers. Therefore, the insulation layers protect the subgrade from frost and influence the range of pavement temperatures in the subgrade. Also, the higher thermal resistance of the 10-cm polystyrene layer blocks heat exchange and results in more significant temperature variation in the base layer (above the polystyrene layer) (Huang et al., 2021).

Table 7-1: Properties of materials used in insulation sections.

Material	**k (W/m·°C)**	**Layer thickness (m)**	**Thermal Resistance ($m^2 \cdot °C/W$)**	**Reference**
HMA	1.87	0.25	0.13	(Bai et al., 2015)
GBC	2.60	0.45	0.17	(Côté and Konrad, 2005)
Bottom ash	0.70	1.00	1.43	(Klein et al., 2003)
Polystyrene	0.006	0.10	16.67	(Negar et al., 2014)

Since the installation of sensors in 2012, several thermistors have ceased working due to technical issues with the data collection system; thus, the data availability for each sensor is different. Table 7-2 summarises the data available for the thermistors at different depths.

Table 7-2: Temperature data availability for the pavement test sections (BA and PS).

Depth (m)	Sensor ID	Start Date	End Date	Number of data points
(a) Bottom ash section				
0.72	TH-BA-1	Jan. 2017	Mar. 2020	765
1.40	TH-BA-2	Jan. 2017	Feb. 2020	758
1.85	TH-BA-3	Jan. 2017	Apr. 2020	760
2.83	TH-BA-4	Jan. 2017	Feb.2020	760
3.36	TH-BA-5	Jan. 2017	Mar. 2020	784
(b) Polystyrene section				
0.64	TH-PS-1	Jan. 2017	Feb. 2020	760
0.80	TH-PS-2	Jan. 2017	Feb. 2020	757
1.80	TH-PS-3	Jan. 2017	Feb. 2020	760
2.25	TH-PS-4	Jan. 2017	Jul. 2019	547
3.22	TH-PS-5	Jan. 2017	Feb. 2020	757

7.3.2. Statistical Analysis of Pavement Temperature

A statistical analysis has been done to show how the pavement temperature changes with depth and insulation material. Table 7-3 summarises the statistical analysis results of pavement temperature collected from the bottom ash and polystyrene sections. Mean ($\bar{x}$), median ($\tilde{x}$), minimum (*min*), maximum (*max*), and standard deviation (*SD*) of the pavement temperature for each year and also for the entire data have been included in Table 7-3. *SD* can be represented in Equation 7-3.

$$SD = \sqrt{\frac{\sum(x_i - \bar{x})^2}{N}}$$ Equation 7-3

It was observed that depth influenced the pavement temperature variation, at shallower depths the *SD* values were much larger than that at deeper locations. Meanwhile, pavement temperature at the same location was not the same for a different year. For example, at a depth of 0.64 m in the polystyrene section, the minimum pavement temperature was −24°C in 2018, but the minimum pavement temperature was −11°C in 2019. Due to the higher thermal resistance of the polystyrene board, the pavement temperature changed significantly around the polystyrene board. The maximum pavement temperature was 31°C and the minimum pavement temperature was −26°C at a depth of 0.64 relatives to the road surface, while the maximum pavement temperature was 13°C and the minimum pavement temperature was 1°C at a depth of 0.80 m below the road surface. At the same time, the *SD* values were smaller in the subgrade layer of the polystyrene section than that in the bottom ash section, indicating that the subgrade temperature below the polystyrene board was more stable than in the bottom ash section.

It was observed that depth influenced the pavement temperature variation, at shallower depths the *SD* values were much larger than that at deeper locations. Meanwhile, pavement temperature at the same location was not the same for a different year. For example, at a depth of 0.64 m in the polystyrene section, the minimum pavement temperature was −24°C in 2018, but the minimum pavement temperature was −11°C in 2019. Due to the higher thermal resistance of the polystyrene board, the pavement temperature changed significantly around the polystyrene board. The maximum pavement temperature was 31°C and the minimum pavement temperature was −26°C at a depth of 0.64 relatives to the road surface, while the maximum pavement temperature was 13°C and the minimum pavement temperature was 1°C at a depth of 0.80 m below the road surface. At the same time, the *SD* values were smaller in

Table 7-3: Statistical analysis results were collected from two insulation sections.

Depth (m)	2017(°C)					2018 (°C)					2019 (°C)					2020 (°C)					Total (°C)				
	$\bar{x}$	$\tilde{x}$	*max*	*min*	*SD*	$\bar{x}$	$\tilde{x}$	*max*	*min*	*SD*	$\bar{x}$	$\tilde{x}$	*max*	*min*	*SD*	$\bar{x}$	$\tilde{x}$	*max*	*min*	*SD*	$\bar{x}$	$\tilde{x}$	*max*	*min*	*SD*
(a) Bottom ash section																									
0.72	9	7	29	-14	12	14	23	28	-15	15	10	12	25	-7	9	-9	-8	-4	-18	4	9	7	29	-18	12
1.40	8	7	22	-5	9	14	20	23	-4	11	10	10	20	-1	7	-4	-3	-1	-8	2	8	8	23	-8	9
1.85	8	8	15	2	5	11	13	15	5	4	9	9	14	2	4	4	4	6	3	1	8	8	15	2	5
2.83	8	8	14	2	4	10	11	14	6	3	8	9	13	2	4	5	5	6	4	1	8	8	14	2	4
3.36	8	8	13	3	3	9	9	12	7	2	8	8	11	3	3	5	4	7	4	1	8	8	13	3	3
(b) Polystyrene section																									
0.64	9	8	31	-25	13	14	22	30	-24	17	11	14	28	-11	11	-9	-7	-1	-26	7	9	9	31	-26	13
0.80	8	8	12	2	3	9	12	13	2	4	8	8	11	2	3	2	2	3	1	1	7	8	13	1	4
1.80	7	7	11	4	2	8	9	10	5	2	7	8	10	3	2	4	4	6	3	1	7	7	11	3	2
2.25	7	7	10	5	2	8	8	9	6	1	5	5	7	3	1	-	-	-	-	-	7	7	10	3	2
3.22	7	7	9	6	1	8	8	9	7	1	7	8	9	5	1	7	7	7	6	1	7	7	9	5	1

the subgrade layer of the polystyrene section than that in the bottom ash section, indicating that the subgrade temperature below the polystyrene board was more stable than in the bottom ash section.

7.3.3. Machine Learning Algorithms

The regression learner in MATLAB is a general tool and has been employed to predict the average, minimum, and maximum daily pavement temperature within an HMA layer. All these five built-in machine learning algorithms showed high accuracy (R^2 was higher than 0.91 and RMSE was lower than 4.02) (Molavi Nojumi et al., 2022). Thus, in this work, the regression learner in MATLAB has been applied to predict the temperature for the base and subgrade layers in pavements with an insulation layer and all five built-in algorithms were taken into account. More details information about machine learning algorithms is available in the literature (Bonaccorso, 2018).

A linear regression model assumes that there is a linear relationship between a dependent variable and independent variables. A linear regression model can be represented in Equation 7-4:

$$\widetilde{y_k} = \alpha_0 + \sum_{i=1}^{m} \alpha_i \bar{x}_k^{(i)} + \eta_k, where\ \alpha_i \in \mathbb{R}\ and\ \eta_i \sim N(0, \Sigma) \qquad \text{Equation 7-4}$$

that is, the linear regression method cannot be applied to solve a non-linear problem, due to it is based on flat structures. There are four subcategories of linear regression models in MATLAB, namely linear, interaction linear, robust linear and stepwise linear (Bonaccorso, 2018).

Decision Tree is a commonly supervised learning algorithm used in machine learning. Tree models in which the target variable can take on a set of discrete values are called classification trees; in these tree structures, the leaves represent class labels and the branches represent

combinations of features that lead to those class labels. Decision trees where the target variable can take on continuous values (usually real numbers) are called regression trees. Based on the minimum leaf size, there are three subcategories in MATLAB, Fine tree, medium tree and coarse tree (Bonaccorso, 2018).

Support Vector Machines are a system to train supervised learning machines for classification and regression analysis. In support vector machine methods, kernel functions are used to transform the input data into a high-dimensional space that represents the maximum separation between two classes. If this degree of separation is greater, the performance of SVM will be better. Kernels used in SVMs can be linear, quadratic, or cubic. Based on the kernel scale, SVM can be divided into six subcategories, linear SVM, quadratic SVM, cubic SVM, fine Gaussian, medium Gaussian, and coarse Gaussian (Cristianini and Shawe-Taylor, 2000; Bonaccorso, 2018).

Gaussian process regression implements Gaussian processes for regression and is a nonparametric Bayesian method. Gaussian process regression computes the probability over all acceptable functions that fit the data. To do this, a prior for the Gaussian process needs to be specified. The prior mean is assumed to be constant and zero or the mean of the training data. The prior covariance is specified by passing a kernel object. The hyperparameters of the kernel are optimized during fitting a Gaussian process regressor by maximizing the log-marginal likelihood with a pass-based optimiser. The first run always starts with the kernel's initial hyperparameter values; subsequent runs are based on hyperparameter values randomly selected from the range of allowed values. GPR has four subcategories, rotational quadratic GPR, squared exponential GPR, matern 5/2 GPR, and exponential GPR (Bonaccorso, 2018; Schulz et al., 2018).

Ensembles of trees combines several weak decision trees to produce better predictive performance than using a single decision tree. MATLAB uses two subcategories, bagged trees

and boosted trees. Bagged trees are creating several subsets of data from randomly selected training samples and replacing them. Now, each subset data set is used to train its decision tree. As a result, we end up with an ensemble of different models. Use the average of all predictions from different trees, which is more robust than a single decision tree. Boosted trees are another ensemble technique for creating sets of predictors. In this technique, learners learn sequentially, with early learners fitting simple models to the data and then analysing the data for errors (Bonaccorso, 2018; Zeiada et al., 2020).

7.3.4. Sensitivity Analysis

Figure 7-3 visualises the relationship between the pavement temperature in the bottom ash section at a depth of 1.40 m and air temperature, solar radiation, precipitation, and day of the year. Similar results were found for all depths, only results for a depth of 1.40 m are displayed. Correlation coefficients (R) were used to evaluate the strength of the relationship between the pavement temperature and input parameters. The R was expressed as Equation 7-5:

$$R = \frac{Cov(X,Y)}{\sqrt{S_X^2 S_Y^2}} \qquad \text{Equation 7-5}$$

where Cov(X, Y) is the covariance, and S^2_X and S^2_Y are the sample variance for X and Y. As shown in Figure 7-3 (a), the pavement temperature increases with air temperature. A significant correlation coefficient value (R = 0.81) is observed, confirming that air temperature should be a robust input parameter. As indicated in Figures 7-3 (b, c), the correlation of pavement temperature with both solar radiation and precipitation is weak, and the correlation coefficients are low (R = 0.59 for solar radiation and R = 0.18 for precipitation). There is a clear trend between the pavement temperature and the day of the year; however, the slope of the graph of pavement temperature versus day of the year for the first and second halves of the year are different, so the correlation coefficient values were calculated separately. The correlation coefficient for the first half of the year (i.e. DOY = 1–181) is 0.88, and the correlation

coefficient value for the second half of the year (i.e. DOY = 182–365) is −0.95. Since air temperature and day of the year gave the best correlations (as measured by the correlation coefficient), it was assumed that they are the most robust input parameters for the ML models.

Machine learning models for the bottom ash section were trained using different combinations of input parameters, and the algorithms giving the best results are summarised in Table 7-4. Depth was used as an input parameter, so the pooled data collected at sensors located at five different depths in the bottom ash section was used to train the machine learning models. Table 7-4 shows the final results for the various models developed based on the pooled data (at five depths). As seen in Table 7-4, the inclusion of time-related parameters improves the performance of machine learning models for pavement temperature prediction (i.e. R^2 increases from 0.75–0.97, and RMSE decreases from 3.73–1.34). In contrast, the improvement observed when adding solar radiation and precipitation is limited. R^2, for the models adding solar radiation and precipitation, does not change and RMSE even increases from 1.34 to 1.37. Thus, the exponential GPR model with three parameters of depth, air temperature, and day of the year was determined as the best performing model in the bottom ash section, and its accuracy at each depth was calculated separately, as shown in Table 7-5 (a). Its R^2 was higher than 0.98 and RMSE was lower than 1.62. Therefore, the exponential GPR model was chosen and these three parameters, depth, air temperature, and day of the year were used as the input parameters for the temperature prediction in the BA section.

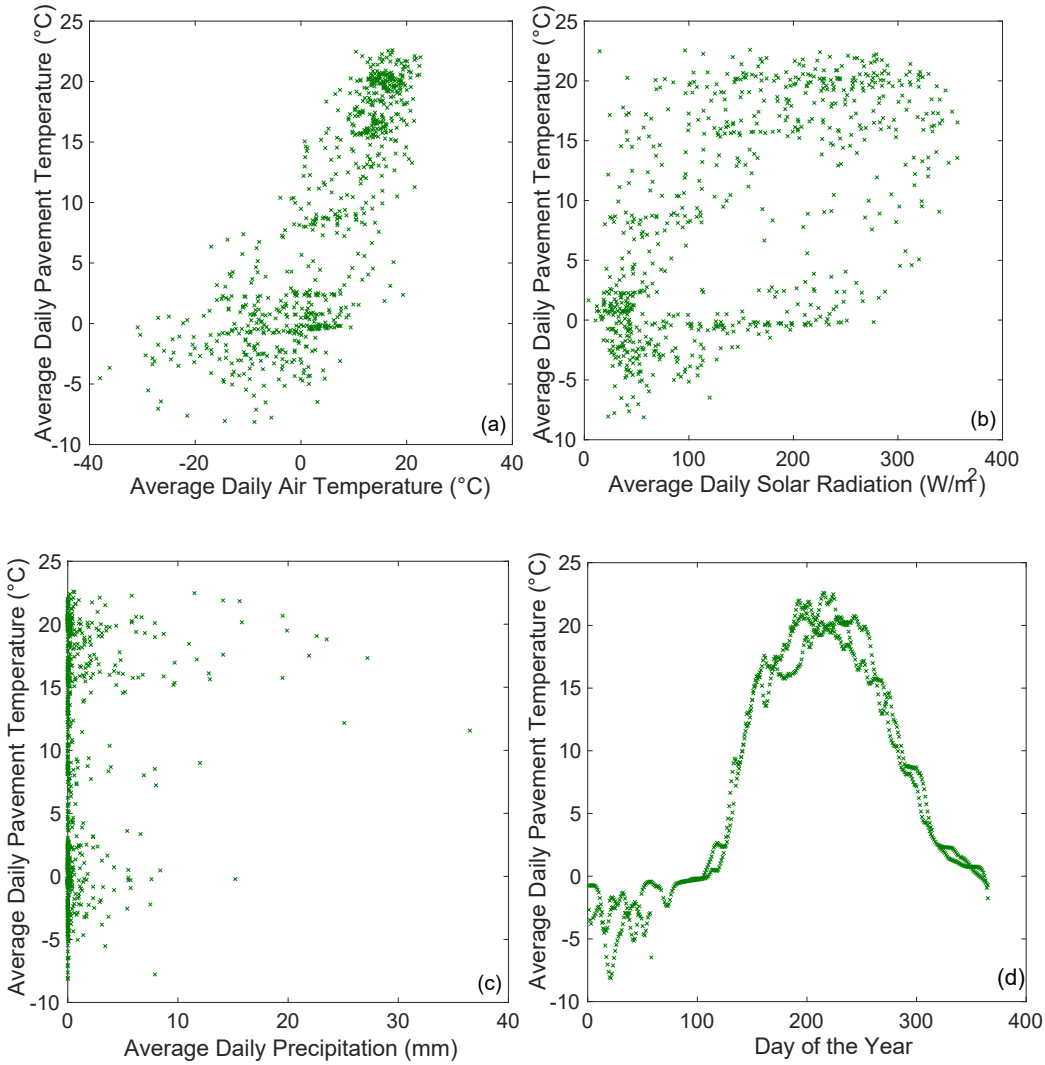

Figure 7-3: Pavement temperature at a depth of 1.4 m versus (a) air temperature, (b) solar radiation, (c) precipitation, and (d) day of the year

The same procedure was repeated for the models developed based on data from the polystyrene section, and similar results were obtained. The algorithm that gave the best results for the PS test section was the squared exponential GPR, with air temperature, day of the year, and depth as input parameters. The correlation coefficient, R^2, for this model was 0.95, and RMSE was 1.47. Table 7-5 (b) illustrates the results obtained for the model and three parameters that resulted in the highest accuracy for temperature predictions at each depth. Therefore, the combination of air temperature, day of the year, and depth also has been chosen to predict the pavement temperature of the base and subgrade layers with an insulation layer.

Table 7-4: The influence of parameter inclusion on model performance.

Best predicting algorithm	Input parameters					Performance parameters	
	Depth (m)	Air temperature (°C)	Solar radiation (W/m^2)	Precipitation (mm)	DOY	R^2	RMSE
Rational Quadratic GPR	✔	✔				0.75	3.73
Matern 5/2 GPR	✔	✔	✔			0.79	3.42
Bagged Trees	✔	✔	✔	✔		0.82	3.15
Exponential GPR	✔	✔			✔	***0.97***	***1.34***
Matern 5/2 GPR	✔	✔	✔		✔	0.97	1.34
Rational Quadratic GPR	✔	✔	✔	✔	✔	0.97	1.37

Values in bold indicate this is the final model used in this study.

Three primary input variables affect pavement temperature: day of the year, air temperature, and depth. When predicting pavement temperature, it is important to consider the correlation between these variables to ensure that multicollinearity does not exist. Multicollinearity is a statistical phenomenon that occurs when two or more predictor variables are highly correlated with each other. This can lead to problems when estimating regression models because the coefficients of the correlated predictors will be unstable and difficult to interpret. Depth is constant, so it could not have a high correlation with other inputs. The correlation between air temperature and day of the year is 0.18, indicating a low correlation. Thus, no high correlation was found between these three inputs.

7.3.5. Validation of the Model

As mentioned earlier, data were divided into two groups, one for training and one for validation. For model validation, a random day was selected from each month, so in total there is 12 days' worth of data (for each depth) excluded for later validation of the model. The best-performing

models developed in the last section (i.e. exponential GPR model for the BA section and squared exponential GPR model for the PS section) were validated using the validation data (which were excluded from the training dataset). Table 7-5 shows the results of model validation. Compared with model training results, the machine learning model maintained high accuracy in model validation. R^2 value for model validation decreased by less than 0.01 and RMSE value increased by 0.20. Thus, machine learning models maintain their high accuracy during model validation as they did during model training.

Table 7-5: Machine learning training and testing results.

Depth (m)	**Training**		**Validation**	
	R^2	**RMSE**	R^2	**RMSE**
(a) Bottom ash section				
0.72	0.98	1.62	0.98	1.78
1.40	0.99	0.78	0.99	0.93
1.85	0.99	0.35	0.99	0.41
2.83	0.99	0.33	0.99	0.49
3.36	0.99	0.33	0.99	0.41
(b) Polystyrene section				
0.64	0.95	2.87	0.96	2.67
0.80	0.96	0.68	0.96	0.79
1.80	0.96	0.44	0.95	0.61
2.25	0.93	0.46	0.98	0.47
3.25	0.97	0.23	0.99	0.21

7.4. COMPARISON OF THE MACHINE LEARNING RESULTS WITH A STATISTICAL MODEL

The two machine learning models developed in this study show high accuracy in training and verification, and their results were compared with a high-performance statistical model for evaluating its performance. Heydinger (2003) developed a statistical model to describe the pavement temperature of the Ohio Strategic Highway Research Program (SHRP) Test Road. Three parameters were included in the statistical model, which is expressed as in Equation 7-6:

$$T(t) = A + Bsin[\omega(t - \phi)] \quad \text{Equation 7-6}$$

where A is the mean pavement temperature, B is the amplitude, $\omega = 2\pi/365.25$ is the normalised frequency, t is the day of the year, and ϕ is a time shift. A, B, and ϕ are determined based on temperature measurements (Heydinger, 2003). Although this statistical model was not developed for pavements with insulation layers, it is the only existing statistical model found in the literature that applies to the subgrade layer. Moreover, this model has previously shown good accuracy when applied to the conventional pavement at the IRRF test road (Huang et al., 2022), and its performance on the sections with insulated layers is unknown. Therefore, this model was used to compare the performance of conventional models and machine learning models.

The results of the comparisons between measurements and predicted values using the machine learning models and the statistical model are depicted in Figures 7-4 and 7-5. In a previous study on the IRRF test road, it has been shown that the temperature range of the base layer is larger due to the presence of the insulation layers, and the base temperature changes irregularly, while the temperature is more stable in the subgrade layer for pavements with insulation compared to the conventional pavement (with no insulation layer) (Huang et al., 2021). Both BA and PS have higher thermal resistance than the base layers, blocking heat exchange

between the base and subgrade layers. However, since the thermal resistance of the polystyrene board is 10 times that of the bottom ash, the influence of the polystyrene board on the temperature variation is more significant than the bottom ash. From February 2017 to January 2018, the temperature measured in the base layer (i.e. data measured by the thermistor located in the GBC layer at a depth of 0.48 m below the road surface) of the conventional section ranges from −12 to 28°C. In the test sections insulated using bottom ash and polystyrene, the temperatures range from −14 to 28°C and −24 to 31°C, respectively. The annual average rate of temperature change is the temperature difference between the maximum and minimum temperatures over the period divided by their change in time, and the values in the base layer are 0.23°C/day, 0.24°C/day, and 0.32°C/day, for the conventional, bottom ash, and polystyrene sections, respectively. In the subgrade layer, the annual average rate of temperature change is 0.12°C/day, 0.12°C/day, and 0.03°C/day, for the conventional, bottom ash, and polystyrene sections, respectively (Huang et al., 2021).

The pavement temperature predicted using the statistical model (Heydinger, 2003) varies sinusoidally, and the results using this model are consistent with measurements. However, due to the presence of BA and PS layers, the base layer is colder in winter, and the statistical model overestimates the temperature of the base in summer and underestimates the base temperature in winter. Prediction pavement temperatures that are high during summer could lead to lower load capacities being allowed than necessary (and a corresponding loss in capacity for transportation of goods in the trucking industry). Meanwhile, the lower prediction pavement temperatures in winter may make designers overestimate the traffic load of the pavements. Thus, accurate pavement temperature estimation is necessary.

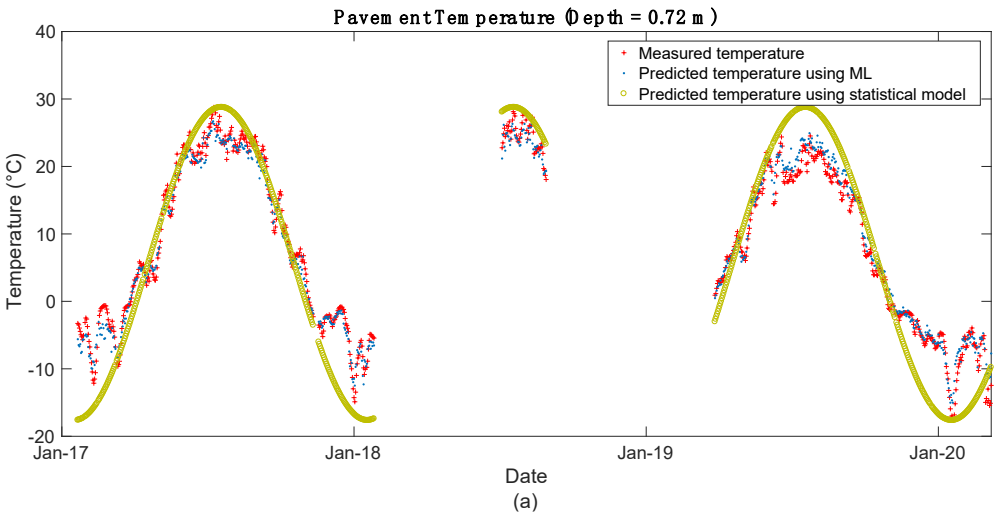
Pavement Temperature (Depth = 0.72 m)
Measured temperature
Predicted temperature using ML
Predicted temperature using statistical model
Temperature (°C)
40
30
20
10
0
-10
-20
Jan-17
Jan-18
Jan-19
Jan-20
Date

(a)

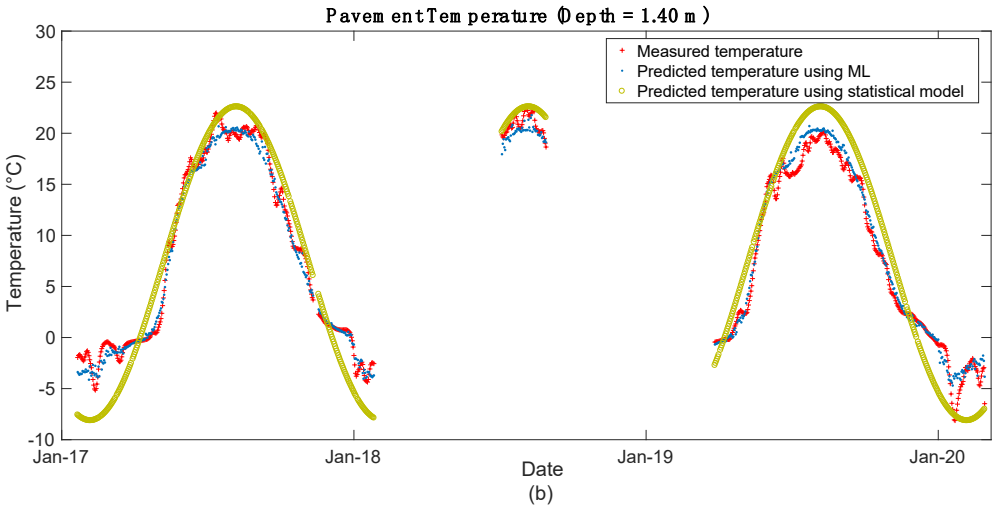
Pavement Temperature (Depth = 1.40 m)
Measured temperature
Predicted temperature using ML
Predicted temperature using statistical model
Temperature (°C)
30
25
20
15
10
5
0
-5
-10
Jan-17
Jan-18
Jan-19
Jan-20
Date

(b)

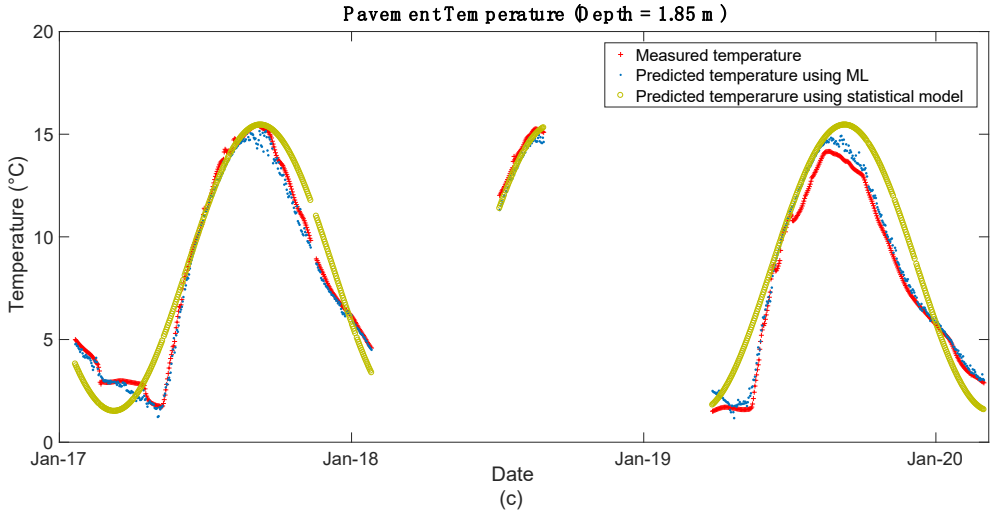
Pavement Temperature (Depth = 1.85 m)
Measured temperature
Predicted temperature using ML
Predicted temperarure using statistical model
Temperature (°C)
20
15
10
5
0
Jan-17
Jan-18
Jan-19
Jan-20
Date

(c)

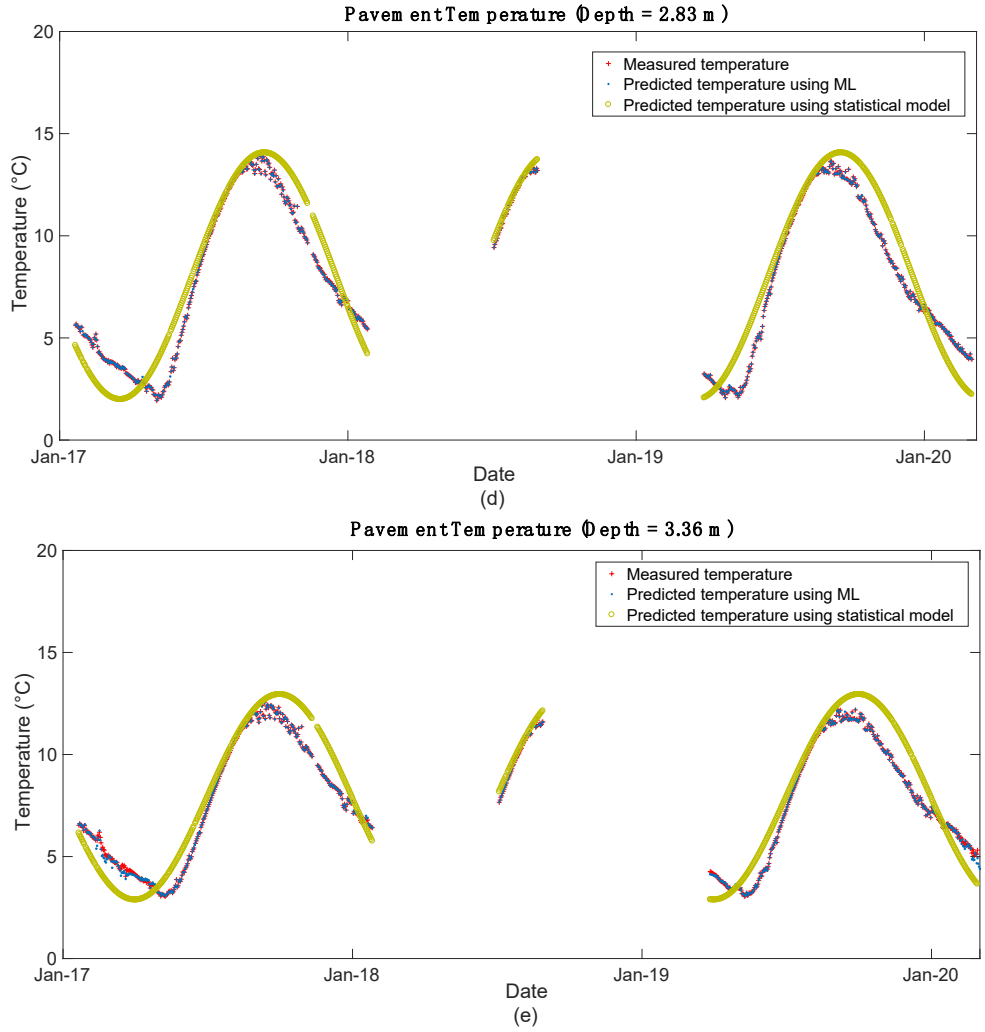

Figure 7-4: Comparison of measured and predicted temperature in the bottom ash section for depths of (a) 0.72 m, (b) 1.40 m, (c) 1.85 m, (d) 2.83 m, and (e) 3.36 m

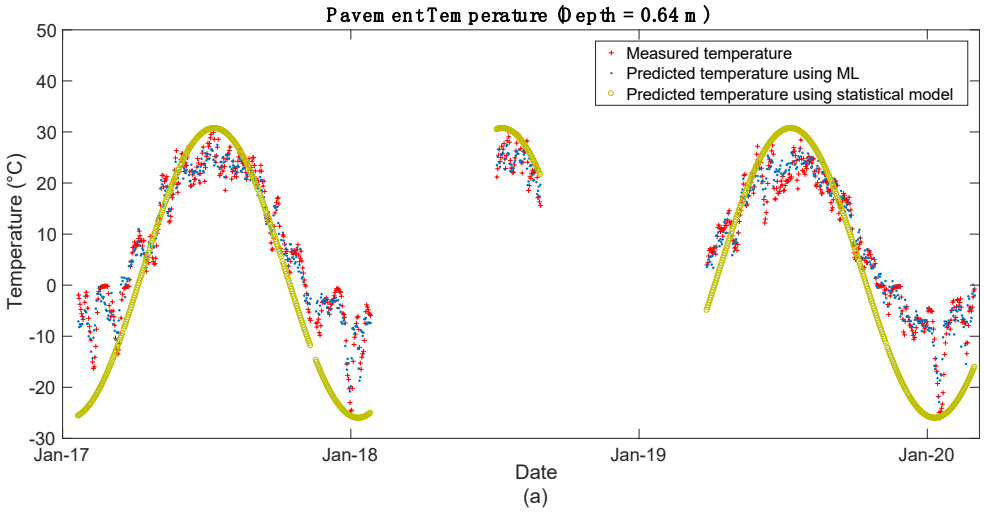

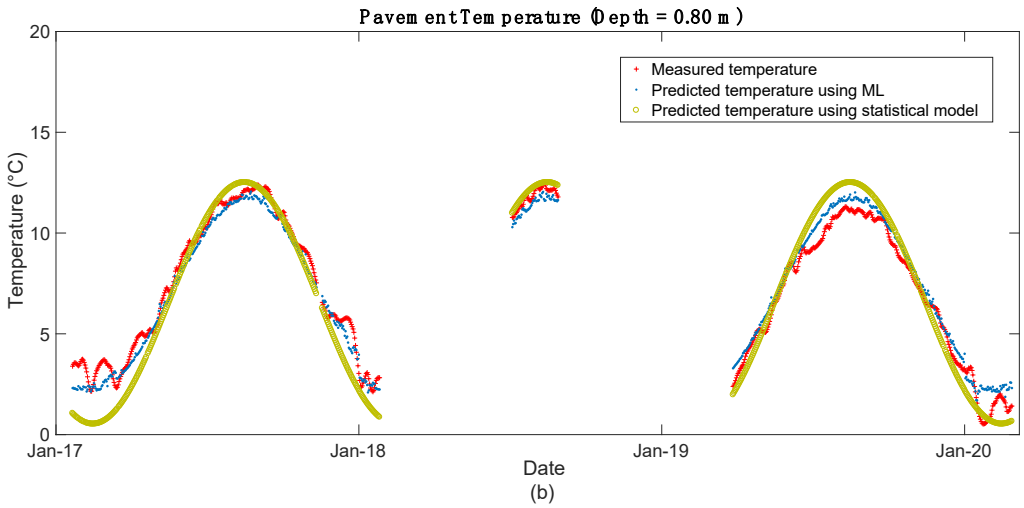
Pavement Temperature (Depth = 0.80 m)
Measured temperature
Predicted temperature using ML
Predicted temperature using statistical model
Temperature (°C)
0
5
10
15
20
Jan-17
Jan-18
Jan-19
Jan-20
Date

(b)

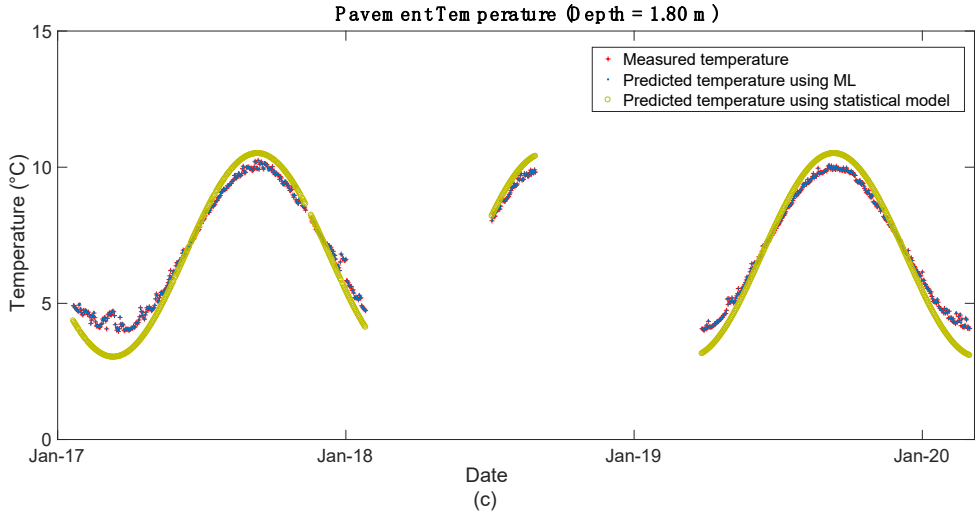
Pavement Temperature (Depth = 1.80 m)
Measured temperature
Predicted temperature using ML
Predicted temperature using statistical model
Temperature (°C)
0
5
10
15
Jan-17
Jan-18
Jan-19
Jan-20
Date

(c)

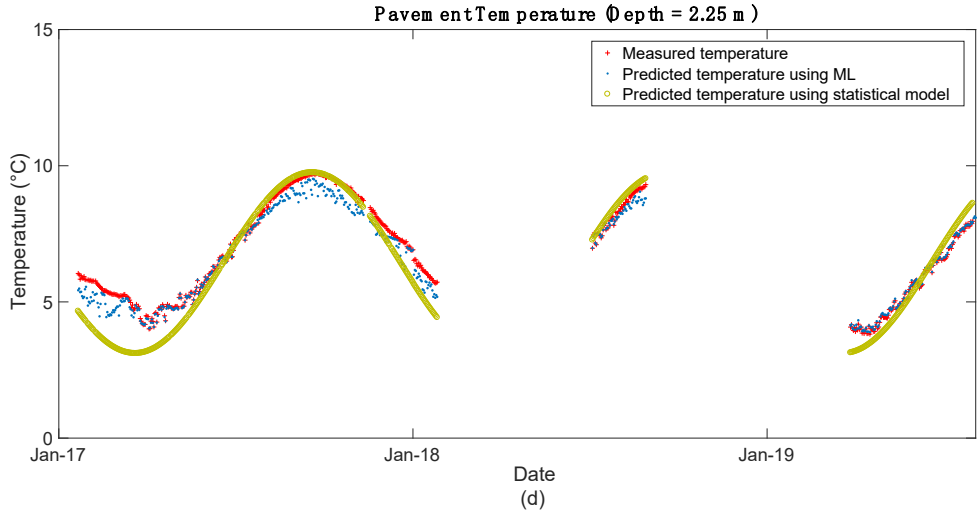
Pavement Temperature (Depth = 2.25 m)
Measured temperature
Predicted temperature using ML
Predicted temperature using statistical model
Temperature (°C)
0
5
10
15
Jan-17
Jan-18
Jan-19
Date

(d)

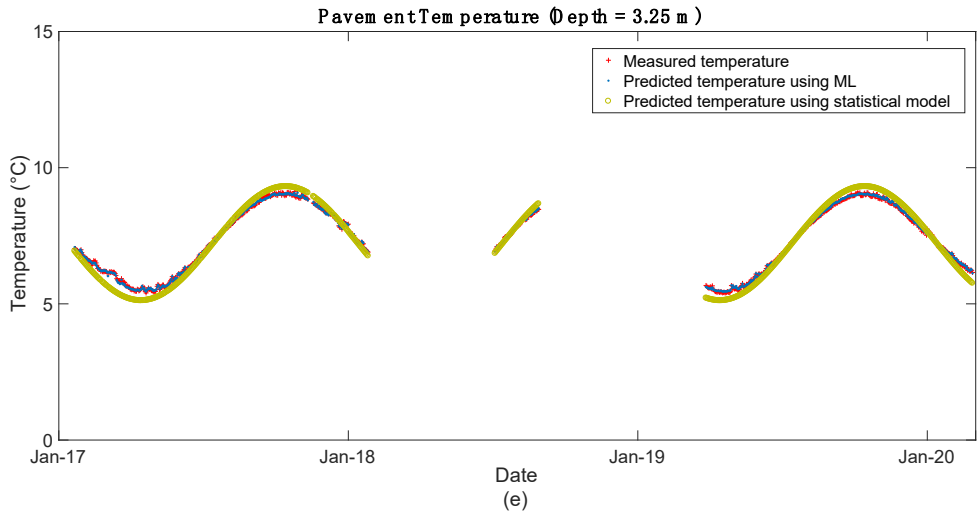

Figure 7-5: Measurements and predicted temperature in the polystyrene section for depths of (a) 0.64 m, (b) 0.80 m, (c) 1.80 m, (d) 2.25 m, and (e) 3.25 m.

Table 7-6 summarises the performance of the statistical model applied to temperature data for the IRRF test road. Although the overall pavement temperature varies sinusoidally and is influenced by mean temperature and time as expressed by the statistical model, the pavement temperature rises and falls repeatedly from November to March that does not conform to the sinusoidal change as shown in Figures 7-4 (a) and 7-5 (a). R^2 represents the proportion of the variance in the response variable of a model that the predictor variables can explain (Zach, 2021). High R^2 values were observed for the machine learning models and the statistical model when pavement temperature was above 0°C. However, as seen in Figure 7-6, the statistical model did not give accurate estimations of pavement temperature in winter, when temperatures were below 0°C. The RMSE is an indication of how far apart the predicted values and observed values are in a dataset (Zach, 2021). Temperature range of the base layer is larger than that of the subgrade layer, and the difference between the measured values and prediction is bigger, as shown in Figures 7-4 and 7-5. For both machine learning models and the statistical models, higher RMSE values were observed for the results of the base layers than for the subgrade layer. The RMSE values of the statistical model were higher than the results given by the machine learning models. At the same time, R^2 and RMSE values of the machine learning model and the statistical model observed in the subgrade of the test section with polystyrene insulation

were similar, confirming that the statistical model of the subgrade was more accurate when used for more minor temperature changes. The use of PS between the base and subgrade resulted in more temperature variation in the base and less temperature variation in the subgrade compared to the control and BA sections according to the statistical model, as expected due to the high thermal resistance of PS (Huang et al., 2021). Although the statistical model can be used to accurately estimate the temperature variation in the subgrade (e.g. below the PS insulation layer), the accuracy of this model drops when applied to the base layer. However, this high degree of variability in the measured temperature (-26 to 31°C) above the insulation layer in the PS section was observed and was not captured by the statistical model. Overall, the RMSE values of the machine learning models for the BA and PS sections are much lower than that of the statistical model. Compared with the statistical model, the machine learning models developed in this work give a more accurate prediction of pavement temperature in the base and subgrade layers.

The pavement temperature in cold regions can easily vary from −20°C to 0°C, and the resilient modulus of the base and subgrade layers changes significantly within this temperature range (Simonsen et al., 2002). The MEPDG developed by AASHTO (2008) demonstrates that temperature affects the material properties and the resilient modulus of the base and subgrade layers. Therefore, accurate estimations of the temperature of the base and subgrade layers are necessary, particularly in winter. As shown in Figures 7-4 (a) and 7-5 (a), the presence of PS and BA results in a more drastic temperature change in the base layer in winter (i.e. pavement temperature ranges between −26 and 0°C). The difference between measured and predicted temperatures is more significant for the statistical model compared to machine learning models, as shown in Figure 7-6. For base pavement temperature prediction for the test section with the bottom ash layer from November through March, R^2 of the machine learning model was 0.82 and RMSE was 1.77, whereas for the statistical model, R^2 was 0.28, and RMSE was 8.34. For

temperature prediction in the base layer of the polystyrene test section during winter, R^2 for the machine learning model was 0.63, and RMSE was 3.47, while R^2 for the statistical model was 0.22, and RMSE was 14.86. When the base pavement temperature is below 0°C, the R^2 values for the machine learning model are 193% and 186% higher for the bottom ash and polystyrene test sections, respectively, compared to temperature values calculated using the statistical model. Also, for the machine learning results, the RMSE values are 79% and 77% lower than the statistical model for the test sections insulated using bottom ash and polystyrene, respectively. Although the insulation layers resulted in more irregular temperature changes in the base layer during winter as shown in Figure 7-5 (a), the accuracy of the machine learning models (as measured by RMSE) was much higher than the statistical model. At the same time, a study discussed the base and subgrade layers' temperature predicted by different models by Huang et al. (2022) indicated that even for the pavement without insulation layers, the same statistical model used in this work showed lower accuracy when applied to shallows depths and low temperatures (e.g. in the range of −20°C to 0°C). Thus, the application of machine learning models could improve temperature prediction in the base and subgrade, even with insulation layers present. Measured base and subgrade temperatures are necessary to develop machine learning models.

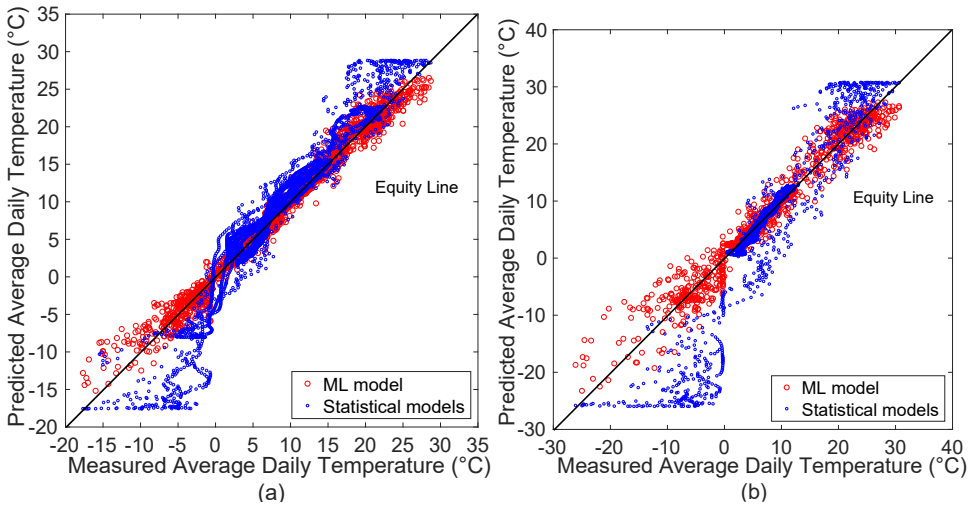

Figure 7-6: Pavement temperature predicted using the machine learning model and statistical model in the (a) BA and (b) PS sections

Table 7-6: Comparison of the performance of machine learning and statistical model models.

Depth (m)	Pavement temperature (°C)	The exponential GPR model		$T(t) = A + B\sin[\omega(t-\phi)]$ (Heydinger, 2003)				
		R^2	RMSE	R^2	RMSE	A (°C)	B (°C)	ϕ (day)
(a) Bottom ash section								
0.72	< 0	0.82	1.77	0.28	8.34	5.57	23.2	108
	> 0	0.96	1.54	0.89	4.07			
1.40	< 0	0.78	0.90	0.39	4.10	7.24	15.36	127
	> 0	0.99	0.74	0.94	2.56			
1.85	> 0	0.99	0.35	0.92	1.47	8.48	6.97	159
2.83	> 0	0.99	0.33	0.91	1.30	8.03	6.04	168
3.36	> 0	0.99	0.33	0.91	1.24	7.61	5.33	182
(b) Polystyrene section								
0.64	< 0	0.63	3.47	0.22	14.86	2.33	28.37	101
	> 0	0.90	2.49	0.82	5.76			
0.80	> 0	0.96	0.68	0.97	1.12	6.52	5.99	136
1.80	> 0	0.96	0.44	0.96	0.71	6.77	3.74	162
2.25	> 0	0.93	0.46	0.89	0.91	6.43	3.32	170

7.5. DISCUSSION

Although the temperature determines the material properties and stiffness of the base and subgrade layers within a pavement structure, the prediction of temperature at some depth within a pavement structure is not simple. Furthermore, not many models are available in the literature for temperature prediction within pavement. The inclusion of an insulating layer further complicates the problem of the temperature profile within the pavement structure with depth. Machine learning algorithms could be an effective way to accurately estimate the temperature within base and subgrade layers for pavements with insulation layers. However, measured pavement temperature data over time at various depths and other related input parameters are necessary to develop machine learning models. Furthermore, previous studies also show that

the thermal properties of a material (e.g. specific heat and thermal resistance) and layer thickness affect temperature distribution (Haghi et al., 2016; Huang et al., 2021) and including these parameters can expand the applicability of the model. To develop a model that accounts for the material properties of various layers (e.g. base and subgrade and insulation layers), a database of temperature data measured at various depths over time would be necessary for different road structures (e.g. pavement thicknesses and materials) in various locations. Currently, such an expansive database collected from different pavement structures and containing so many input factors (such as material thermal properties and layer thickness) is not available, so the machine learning models developed in this study do not include more inputs. Machine learning models need to be trained individually using datasets obtained from different pavement structures. Even for statistical models for temperature prediction such as the one developed by Heydinger (2003), recorded data are necessary.

7.6. CONCLUSIONS

Pavement temperature data recorded at the IRRF test road in Edmonton, Alberta, along with environmental data from the Environment Canada Oliver AGDM weather station from January 2017 to April 2020 were used to develop machine learning models for the prediction of average daily temperature in the base and subgrade layer of pavement insulated using bottom ash or polystyrene layers. A sensitivity analysis was done to identify the most robust input parameters for the machine learning models, and air temperature and day of the year were identified as the most robust input parameters. Separate machine learning models were established for each of the two test sections (insulated using polystyrene and insulated using bottom ash), and five machine learning algorithms were examined for each of the test sections. Only the best-performing algorithm (i.e. the machine learning algorithms that had the highest R^2 and lowest RMSE) was carried forward. All the machine learning models developed in this work showed high accuracy (with R^2 values above 0.93, and RMSE values below 2.87). Some data were

excluded from the dataset used to develop the machine learning models for use as validation. All machine learning models performed well during validation.

To evaluate the performance of the machine learning models, temperature predictions obtained using machine learning were compared with a statistical model for temperature prediction developed based on data collected from the SHRP test road (Heydinger, 2003). For the test section at the IRRF test road insulated using PS, the temperature variation is more in the base and less in the subgrade than that of the control and BA sections, and these results are explained by the higher thermal resistance of the polystyrene board (Huang et al., 2021). The measured temperature of the subgrade layer in the polystyrene section varies regularly and sinusoidally; thus, the statistical model showed higher accuracy for this layer than in the base. However, the statistical model over-estimated the base pavement temperature in summer and underestimated the base pavement temperature in winter for all the situations of the IRRF test road. The statistical model also had higher RMSE values for predicted and measured temperatures compared to the machine learning models. Overall, the RMSE values of the machine learning models are considerably lower in the bottom ash and polystyrene sections than that in the statistical model.

The performance of the statistical model dropped significantly when it was used to predict the temperature of the base layer for insulated pavement in winter (R^2 of 0.28 and 0.22 and RMSE of 8.34 and 14.86 for BA and PS, respectively). The machine learning models had higher accuracy for temperature prediction in the base and subgrade layers (R^2 of 0.82 and 0.63 and RMSE of 1.77 and 3.47 for BA and PS, respectively) compared to the statistical model. The R^2 values obtained from the machine learning model are 193% and 186% higher compared to those obtained using the statistical model for the BA and PS test sections, respectively. The RMSE values for the temperature predictions generated using the machine learning models are 79% and 77% lower than those obtained using the statistical model for BA and PS test sections,

respectively. Therefore, provided that pavement temperature measurements and air temperature are available, the application of machine learning models can improve pavement temperature prediction with insulation layers.

CHAPTER 8.EVALUATING THE USE OF MACHINE LEARNING FOR MOISTURE CONTENT PREDICTION IN BASE AND SUBGRADE LAYERS

This section has been published as Huang, Y., Molavi Nojumi, M., Ansari, S., Hashemian, L. and Bayat, A., 2023. Evaluating the use of machine learning for moisture content prediction in base and subgrade layers. Road Materials and Pavement Design, 1-19.

8.1. ABSTRACT

Subgrade moisture content significantly influences soil strength and pavement bearing capacity. Pavement moisture content varies greatly throughout the year, especially in cold regions. Thus, having a better understanding of seasonal variation in moisture content in the pavement is needed to be developed. This research aims to apply machine learning models to predict the moisture content of unbound materials in the pavement. Unfrozen volumetric moisture content measurements recorded at the Integrated Road Research Facility test road in Edmonton, Alberta were used to train machine learning models to predict moisture content at depths within 2.7 m of the road surface. Machine learning models were implemented based on three parameters of pavement temperature, day of the year and depth. The results from the machine learning model were compared with a statistical model and showed higher accuracy than the existing model, indicating that machine learning models could enhance moisture content prediction in the pavement.

Keywords: moisture content, moisture content prediction models, machine learning, unfrozen water, unbound materials

8.2. INTRODUCTION

Subgrade strength is a major factor that needs to be considered in pavement design and it depends on moisture content. Moisture content is an important environmental parameter since it affects both the stress state of soil and the soil structure by suction or pore water pressure, and, ultimately, the load-bearing capacity of the subgrade. Soil reaches its maximum density at an optimum moisture content, and (assuming that all other conditions are the same) coarse-grained and fine-grained materials can increase the modulus by more than five times when dry. The modulus of cohesive soil is influenced by complex clay-water-electrolyte interactions (ARA., 2000; Bohra et al., 1999; Christopher et al., 2006, 2010). In contrast, while moisture content does not directly influence bound materials, such as asphalt, excessive moisture content can cause the separation of the asphalt binder from the aggregate (asphalt stripping) and have long-term effects on the structural integrity of the cementitious material (ARA., 2004; Christopher et al., 2006, 2010). Therefore, moisture content can have a significant effect on pavement performance and subgrade properties (ARA., 2000; Christopher et al., 2006, 2010; Hall and Rao, 1999).

Different from the variation of moisture content in warm regions, which is dominated by time and precipitation (Hedayati and Hossain, 2015), the variation in moisture content of pavement temperature in cold regions such as Edmonton is influenced by many factors (environmental and internal), especially in winter and spring (Haghi et al., 2019; Huang et al., 2021; Jin et al., 2020; Patterson and Smith, 1980; Stein and Kane, 1983; Topp et al., 1980). In winter, the average daily base layer temperature could be as low as −15°C in Edmonton (Huang et al., 2021). The freezing point of bound water closely attached to the mineral surface in the soil varies between −6 to −20°C (Kozlowski, 2007), which is lower than the freezing point of water at standard atmospheric pressure. Thus, in winter, there is a mixture of ice and water in the base and subgrade layers. Previous studies proved that capillary action, surface effects,

adsorption forces, and the electrical double layer could also influence the amount of unfrozen water in soil (Hoekstra, 1967; Jin et al., 2020; Stein and Kane, 1983). Based on the soil freezing characteristic curve, even in the case of extremely low soil temperature, there is residual water content in the soil (Anderson and Tice, 1972). Thus, it is hard to determine the accurate content of unfrozen moisture in the frozen soil.

The moisture content of cold regions such as Edmonton is affected by low temperatures, thus it shows a completely different trend than warm regions and shows a very high correlation with the resilient modulus of the subgrade (ARA., 2000; Huang et al., 2021). Moisture content in warm regions normally varies sinusoidally throughout the year and is influenced by precipitation (Hedayati and Hossain, 2015). However, the moisture content of the subgrade layer in Edmonton is dominated by pavement temperature, and the effect of precipitation on the moisture content is limited (Huang et al., 2021). Most of the water freezes in winter, and the unfrozen moisture content in the base and road bases is greatly reduced. The subgrade layers in winter normally show a higher resilient modulus than in normal conditions. In spring, when the air temperature increases, the pavement temperature increases, and solid water (ice) is transformed into liquid water again in the unbound layers. The lower layer remains frozen as the thawing occurs from top to bottom, and its permeability is low, causing excess water to accumulate above the frozen layer. As a result, when the weather is warm and the temperature rises within the pavement, the water content within the subgrade and base layers reaches the highest level (compared to other times in the year) (Huang et al., 2021). This accumulation of moisture in the subgrade layer and base layer generally leads to a low subgrade bearing capacity during spring. The change of moisture state in the subgrade layer is also called the freeze–thaw cycle. Subgrades in cold regions experience more than one freeze–thaw cycle per year, and the number of freeze–thaw cycles experienced by a subgrade layer has been shown to have a significant impact on the resilient modulus of the subgrade layer (Haghi et al., 2016; Zhou et

al., 2022). A better understanding of moisture content change in the base and subgrade layers can thus help to improve road design.

Considerable research, including theoretical and empirical approaches, has been done to predict moisture content in the subgrade and base layers (Anderson and Tice, 1972; Croney and Coleman, 1948; Haghi et al., 2014; Hedayati and Hossain, 2015; Jin et al., 2020; Teltayev and Suppes, 2019; Zhang et al., 2019; Zheng and Zhang, 2013). However, each of the reported approaches has certain limitations. In 1948, a theoretical approach using principles of thermodynamics was adopted to estimate the moisture distribution beneath a road pavement, and it includes an assumption that the temperature of the soil remains constant (Croney and Coleman, 1948). However, the assumption is not valid in many cases. For example, there are large variations in temperature in the subgrade layer in cold regions – in Alberta, a maximum temperature difference of approximately 20°C has been measured within the pavement subgrade over a single year (Haghi et al., 2014). Another study has used a Hydrus-2D model to predict moisture distribution in soil, but this approach gives a rough estimation and also requires additional laboratory data and field tests to validate the simulation results (Zhang et al., 2019). A two-dimensional subgrade-atmosphere interaction model has been developed to study the moisture content variation of the subgrade layer at the Longlin-Baise Expressway in Guangxi. This model does not show seasonal variations in moisture content, as is observed in cold regions (Zheng and Zhang, 2013). The Mechanistic-Empirical Pavement Design Guide recommends using the Enhanced Integrated Climatic Model to predict the moisture content of the pavement and unbound materials. However, its performance was not so satisfactory. In winter and thawing seasons, the predicted value was much lower than the measured value (Bulut et al., 2013; Zapata and Houston, 2008). A statistical model which takes into account the influence of depth and precipitation has been used to predict moisture variation with 95% accuracy in North Texas; but in this model, pavement temperature variation was not included

(Hedayati and Hossain, 2015). Teltayev and Suppes (2019) also proposed a statistical model for the prediction of moisture content (for temperatures below freezing) in cold areas. This model is only applicable for moisture content prediction in winter when the temperature within the road structure is below freezing (Teltayev and Suppes, 2019), and its performance is compared with the new model established in this work.

Due to the limitations of the available conventional methods and improvements in computing capabilities, there is a growing interest in applying artificial intelligence techniques – such as machine learning and deep learning – in predicting pavement performance and conditions. Some comprehensive literature reviews on the application of machine learning models to predict or estimate the performance of pavement materials and structures have been completed. Machine learning algorithms can find natural patterns in large amounts of data, and make informed decisions based on better predictions, thus machine learning models can speed up the decision-making process and improve the efficiency of pavement maintenance (Hou et al., 2021; Justo-Silva et al., 2021). Machine learning models have been used to estimate the pavement temperature of the asphalt, base and subgrade layers in cold regions (Huang et al., 2023; Molavi Nojumi et al., 2022).

Although these examples and others demonstrate that machine learning has attracted increasing interest in predicting and analysing pavement parameters and performance, to date, there have only been a few attempts to apply machine learning techniques to predict subgrade moisture content. For instance, D'Amico et al. (2010) applied artificial neural networks to indicate the unsaturated moisture content of the subgrade by exploring the frequency spectrum of a reflected ground-penetrating radar signal. Xing et al. (2017) used remote satellite images to train an artificial neural network for prediction of general surface soil moisture.

The current study involves application of machine learning algorithms (and their variations) to predict moisture content in base and subgrade layers in cold regions for the whole year. Data

(i.e. volumetric moisture content (VWC) and base and subgrade temperature data from January 2013 to January 2018) collected from sensors embedded at different depths in the Integrated Road Research Facility (IRRF) test road (located in Edmonton, Alberta) were used as a basis for the machine learning models. To verify the performance of machine learning models for moisture content prediction, the coefficient of determination (R^2) and root mean square error (RMSE) were analysed. The results obtained using the machine learning model for moisture content prediction were compared with an existing model.

8.3. DESCRIPTION OF THE IRRF TEST ROAD FACILITY

The IRRF test road is a two-lane, 500 m access road to the Edmonton Waste Management Center, located 15 km from downtown Edmonton. Construction of the IRRF test road started in May 2012 and was completed in October 2013, and the road opened to public traffic in October 2015.

Figure 8-1 shows the schematic of the layers of the pavement structure in the IRRF test road. Five time-domain reflectometers (TDRs) installed in the base and subgrade layers of the IRRF test road were used to collect data on temperature and moisture content – Figure 8-1. TDR is a method to indirectly measure the soil moisture content by calculating the dielectric constant based on the Topp equation (Topp et al., 1980). In warm seasons, TDR detects all the moisture content in the soil, while in cold seasons, there is a mixture of ice and water and its dielectric constantly changes. Previous studies have proved that the Topp equation can be applied to calculate the unfrozen moisture content of ice and water mixture, and TDR can detect unfrozen water in frozen soil using the Topp equation (Kahimba and Ranjan, 2007; Patterson and Smith, 1980; Stein and Kane, 1983). The dielectric constant is influenced by temperature, water content, and soil type (Watanabe and Wake, 2009). Therefore, TDRs were calibrated according to the soil samples collected from the test road, moisture content, and temperature in the

laboratory of the University of Alberta (Haghi et al., 2019). These sensors were installed at different locations in the test road, respectively at depths of 0.5, 0.7, 0.8, 1.8, and 2.7m below the road surface. Moisture content data from the sensors were recorded at 15-minute intervals and collected using a CR-1000 data logger (Campbell Scientific Canada). All data were transferred to a computer located at the University of Alberta using a remote connection.

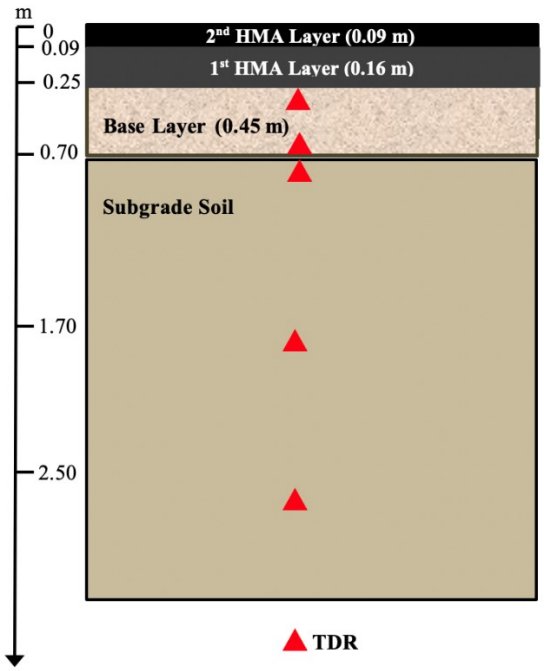

Figure 8-1: Pavement structure and location of time-domain reflectometers installed in the base and subgrade of the IRRF test road

Figure 8-2 shows the grain size distribution for the base and subgrade soils. Using the Unified Soil Classification System, the base was classified as well-graded gravel, and the subgrade soil was classified as clayey sand. The maximum particle size of the base layer was 19 mm, and its density was 2.10 ton/m^3. For the subgrade, nearly 27 and 21wt% passed through sieves of 0.075 and 0.02 mm, respectively, and the maximum particle size was 0.5 mm. The subgrade density was 1.85 ton/m^3. The liquid limit of the subgrade soil was 25%, and the plastic index was 9%. The segregation potential of the subgrade was more than 200×10^{-5} mm^2/s°C (Haghi et al., 2016). According to Saarelainen's categorisation, the subgrade was considered to be moderately frost-susceptible (Saarelainen, 1996).

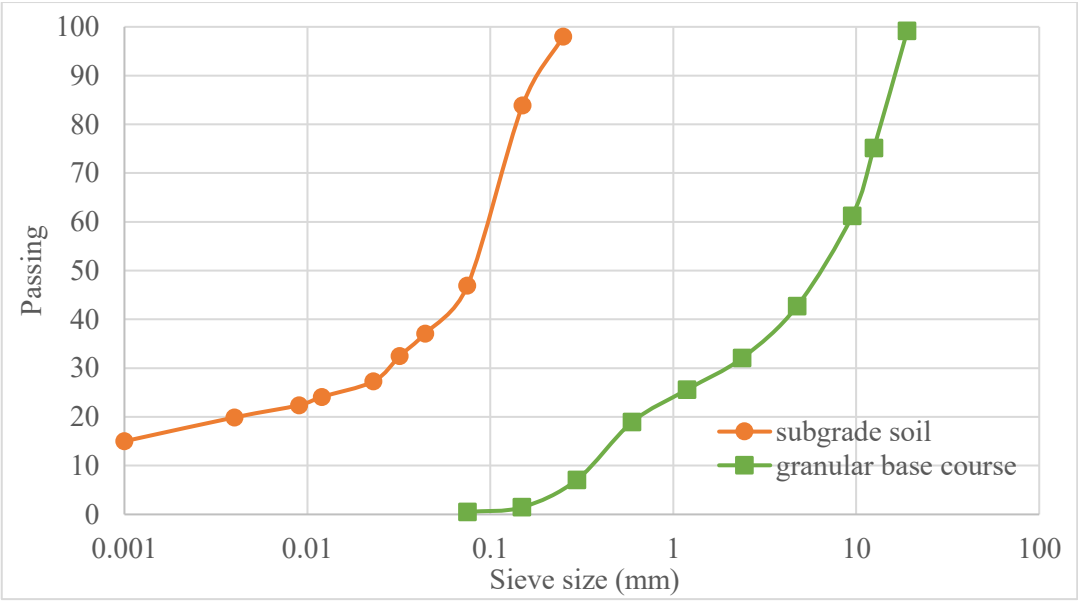

Figure 8-2: Grain size distribution of the granular base course and subgrade soil used in the construction of the IRRF test road

8.4. MODEL DEVELOPMENT

The study by Huang et al. (2021) showed that the variation of moisture content in the base and subgrade layers was affected by temperature. The constant moisture content for the same days at different years suggested that in addition to the temperature, the day of the year has a significant effect on the moisture content in the base and subgrade layers. Thus, a time-related parameter known as day of the year (DOY) – a number which ranges from 1 to 365, where January 1st corresponds to DOY = 1 – was used to describe the relationship between moisture content and time. The inclusion of precipitation data (collected from Environment Canada and data reported from Oliver ADGM, a weather station located 6 km from the IRRF test road) was also investigated to improve model performance, since Hedayati and Hossain (2015) previously determined that precipitation dominated the variation in moisture content. Depth was used to locate the position of the sensors.

Figure 8-3 shows the procedure used to implement the machine learning models for moisture content prediction. Measured moisture content, base temperature, and subgrade temperature data collected from sensors embedded at different depths at the IRRF test road were used for

the model development. Before building the models, moisture content and temperature data were preprocessed. Any irrelevant data or outliers were removed from the data set. Then, the time window of data for analysis was determined. In the preprocessing procedure, the base layer moisture content before October 2013 was excluded. This is due to the different time of the installation of the HMA layer (October 2013) which results in a difference in the moisture content variation of the base layer compared to the following year. Next, raw data were used to calculate the daily average moisture content and daily average temperature. Other model input parameters (e.g. precipitation, day of the year and depth) were integrated with the daily average moisture content and temperature data set using timestamps.

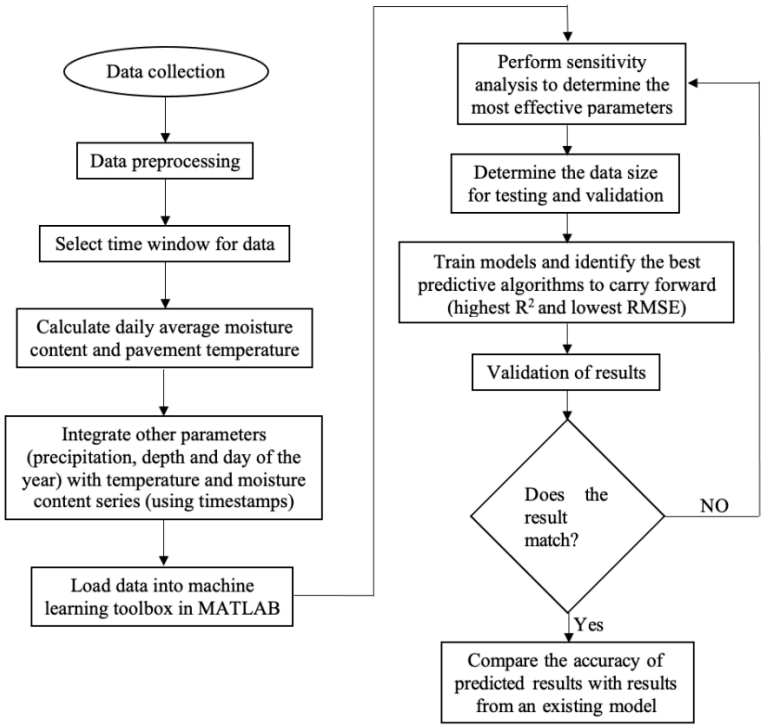

Figure 8-3: Procedure for implementing predictive machine learning models

After processing, the data set was uploaded to the MATLAB machine learning toolbox. To study the correlation between the input parameters (temperature, precipitation, and day of the year) and moisture content, a sensitivity analysis was performed for the different models. A small amount of data was randomly selected, not used for training but reserved for verification. Each machine learning model was trained using MATLAB, and the most accurate algorithm

for moisture content prediction was identified. Two parameters (R^2 and RMSE) were used to evaluate model performance. RMSE is a measure of model accuracy, as it shows the average difference between the predicted value and the actual value. R^2, on the other hand, is a measure of model precision, as it shows how closely the predicted values match the actual values. While R^2 is a common measure of precision, the standard deviation of error can also be used as an alternative measure. Then, the most effective input parameters were determined. Five machine learning algorithms (Baştanlar and Özuysal, 2014; Bonaccorso, 2018), regression trees, support vector machines, Gaussian process regression (GPR) models, ensembles of trees, and linear regression, and nineteen subcategories, were trained and validated using the pavement moisture content dataset, and the performance of the various models was compared. A set of rules and conditions are defined in the regression trees approach at multiple stages to split the data. A regression tree algorithm consists of a root, branches, and leaves, and the final result is created at the end of the process (Bonaccorso, 2018). According to the complexity of the model, the regression tree models can be divided into three subcategories, fine, medium, and coarse trees. For the support vector machine approach, a kernel function is used to transform the input data into a high-dimensional space that represents the maximum separation between two classes. The greater the degree of separation, the better the performance of the SVM (Bonaccorso, 2018). The Kernel functions used in support vector machine can be linear, quadratic, or cubic. Furthermore, support vector machine methods can be categorised as fine, medium and coarse Gaussian. Gaussian process regression is a nonparametric Bayesian method and it implements Gaussian processes for regression. Gaussian process regression calculates the probability of all acceptable functions that fitting to the data. Nonparametric means that once enough data is available, Gaussian process regression can model arbitrarily complex systems calibrated to the data. Bayesian methods offer a principled approach to dealing with uncertainty, which produces a credible interval containing upper and lower probability bounds.

It is critical for making informed decisions (Zeng et al., 2020). Based on the Kernel functions used, Gaussian process regression models have four subcategories, namely rotational quadratic, squared exponential, matern 5/2 and exponential. Ensemble of trees is a method that combines similar (or different) algorithms to achieve more accurate predictions (Baştanlar and Özuysal, 2014). There are two types of ensemble trees, bagged trees and boosted trees. The linear regression model is one of the most common machine learning algorithms, and it assumes there is a linear relationship between the predictor variable and the target parameter. Therefore, when it is applied to non-linear relationships, it can lead to less accurate predictions compared to other algorithms. Liner regression models can be categorised into linear, interaction linear, robust linear and step-wise linear (Bonaccorso, 2018). A detailed discussion of the above algorithms and their subcategories is beyond the scope of this study. However, machine learning models have been proven as a powerful approach to estimate pavement performance (Hou et al., 2021; Justo-Silva et al., 2021).

Then, only the most accurate algorithms (with the highest R^2 and lowest RMSE) were carried forward and validated. Predicted values have been validated using cross-validation and data reserved for validation. If the model's accuracy was low, a different combination of parameters was used, and a sensitivity analysis was performed with the new parameters. Finally, the accuracy of the predicted moisture content results was compared with an existing prediction model.

8.4.1. Data Availability

Due to the harsh winter weather conditions in Edmonton, heavy traffic loading (on average, 368 garbage trucks travelled on the test road per day), and some technical issues with the data collection system, data was not available for some of the embedded TDR sensors during certain time intervals. Table 8-1 summarises the available TDR data for the sensors installed at different depths.

Table 8-1: Availability of VWC data for training and validation datasets to use in development of machine learning models.

Depth (m)	Start Date	End Date	Number of Points
0.50	2013.11	2016.03	605
0.70	2013.11	2016.03	448
0.80	2013.01	2015.04	710
1.80	2013.01	2018.01	1023
2.70	2014.01	2017.12	1055

8.4.2. Sensitivity Analysis

Although pavement temperature, day of the year, and precipitation affect the moisture content in the base and subgrade layers, the influence of each of these parameters on the variation in moisture content varies at different locations (Hedayati and Hossain, 2015; Huang et al., 2021). Correlation coefficient (*R*) was used to examine the effect of each parameter on the prediction of moisture content using each model. Since similar results were obtained for different depths, only a representative result for one sensor is discussed below. The TDR located at depth of 0.7 m from the road surface was selected as the representative.

The *R* for pavement temperature and moisture content was 0.68. A clear relation was also observed between the pavement temperature and moisture content, as shown in Figure 8-4 (a). When the pavement temperature was below 0°C, the moisture content significantly dropped below 0.14 m^3/m^3.This condition could be due to the water phase change from liquid to solid and unfrozen moisture content detected by TDR drops significantly (Huang et al., 2021; Watanabe and Wake, 2009). When the pavement temperature was above the water freezing point (0°C), the moisture content ranged between 0.17 and 0.24 m^3/m^3. In spring, when the pavement temperature increases to above 0°C, the melting of ice in the soil and insufficient drainage capacity of the sublayer usually lead to an increase in water content. As the road

temperature stabilises, the accumulated water is discharged, and the moisture content gradually decreases and stabilises.

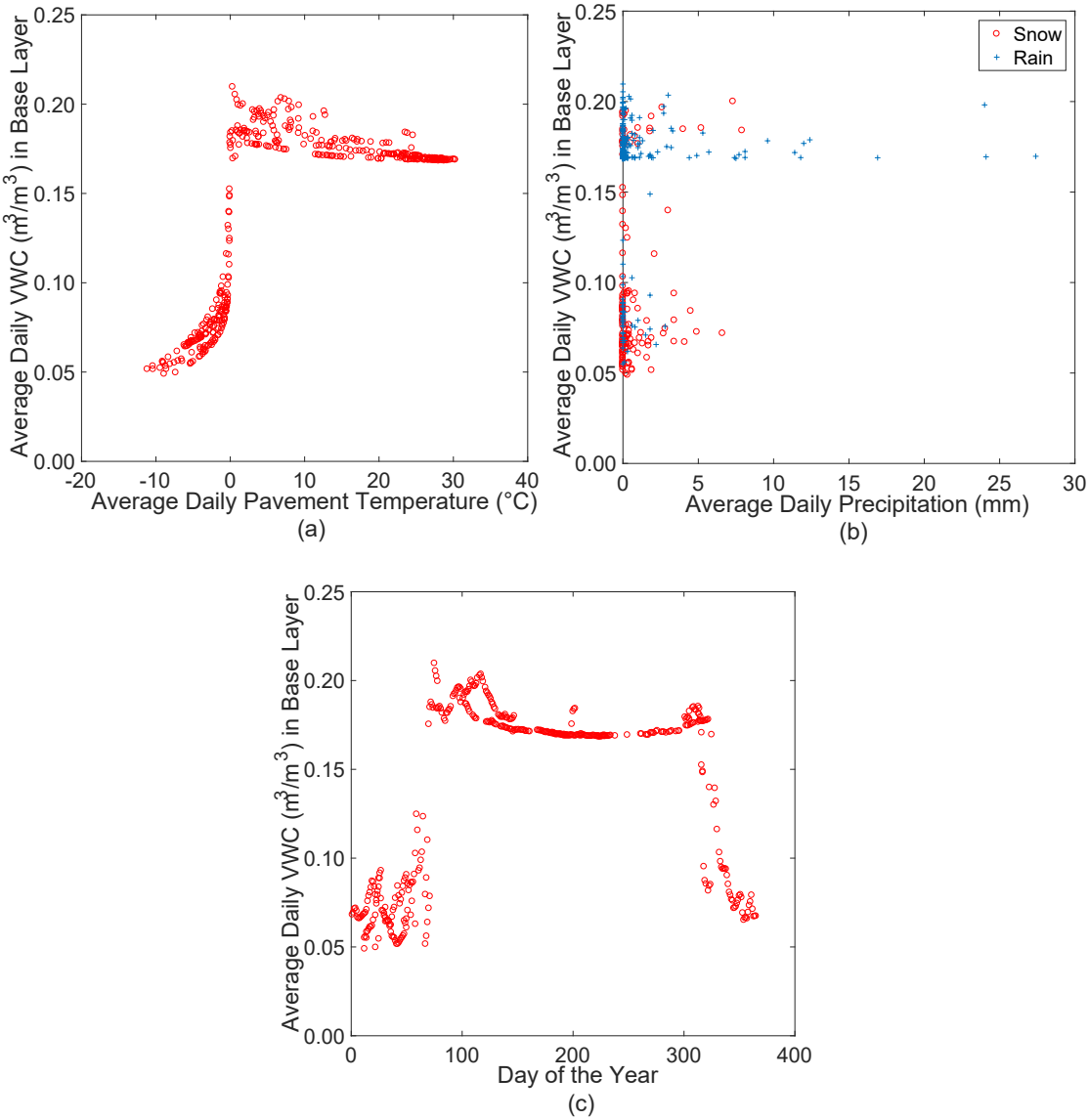

Figure 8-4: Visualisation of moisture content data (depth 0.7 m) correlations with (a) pavement temperature, (b) precipitation, and (c) day of the year

The permeability time of snow and rain is different, thus, the whole dataset was divided into two groups (one group is when the air temperature was above 0°C and the precipitation was in the form of rain, and another group is when the air temperature was below 0°C and the precipitation was in the form of snow) to discuss the correlation between precipitation and moisture content, as shown in Figure 8-4 (b). *R* was 0.07 between the rain and moisture content,

while *R* was 0.18 between the snow and moisture content (measured at a depth of 0.7 m in the base layer). Unlike the strong correlation between pavement temperature and moisture content, the correlation between precipitation and moisture content was weak. Precipitation is one of the most important factors that affect the moisture content variation in warm regions (Hedayati and Hossain, 2015), however as explained by Huang et al. (2021), in cold dry regions (like Edmonton), the influence of precipitation on moisture content is limited.

The relationship between the moisture content and day of the year is depicted in Figure 8-4 (c). Comparing the moisture at different days of the year showed that the moisture content was low at the beginning of the year, increased for the period corresponding to spring (when temperatures started to increase), and decreased again (when temperatures began to decline). Thus, the data was divided into three sets corresponding to the first part of the year, January 1 to April 10 (DOY = 1–100), the second part of the year, April 11 to October 27 (DOY = 101–300), and the third part of the year, October 28 to December 31 (DOY = 301–365), and the correlation coefficient was calculated separately for each set. For the first and third parts of the year, the base and subgrade layers were frozen, so the resilient modulus of the subgrade layer was higher. However, at the beginning of the second part of the year, due to the changes in the pavement temperature and the moisture content accumulation in the subgrade layer, the resilient modulus of the subgrade layer decreased a lot during this period (Haghi et al., 2016). If the structure is not designed with weakened subgrade support in mind, excess water can cause premature failure of the pavement structure (ARA., 2004). Data in each group showed a strong correlation with moisture content (R = 0.80 for DOY = 1–100, R = −0.68 for DOY = 101–300, and R = −0.89 for DOY = 301–365). Although there was a strong relation between precipitation and day of the year in some warm and wet regions, the R between precipitation and day of the year was 0.05 based on data collected from the nearest weather station, thus the correlation between precipitation and day of the year for the IRRF test road was weak. Day of

the year is also related to the angle of sunshine, air temperature change, wind speed and so on, so day of the year and precipitation should be used as two independent parameters. Therefore, pavement temperature and day of the year were determined to be the most robust parameters for predicting moisture content.

Table 8-2 indicates the performance of the three best models (with different input parameters) in predicting the moisture content. While various algorithms were trained, only the best-performing models with the highest R^2 and lowest RMSE were listed. It was found that Gaussian process regression outperformed other machine learning algorithms. Gaussian process regression is a non-parametric Bayesian approach that offers many other unique advantages, such as it has shown great advantages in learning kernel and regularisation parameters, integrating feature selection, and generating fully probabilistic predictions (Zeng et al., 2020). Although linear regression is one of the most popular used algorithms, the moisture content variation in this study is not truly linear and it showed complex correlations between pavement temperature, precipitation, and day of the year. Thus, a non-linear algorithm that can model complex systems is required.

Table 8-2: Impact of parameters on model performance.

Best Predictive Model	**Time-related Input Parameter**	**Input Parameters**			**Performance Parameters**	
	Day of the Year (DOY)	**Pavement Temperature (°C)**	**Precipitation (mm)**	**Depth (m)**	**Coefficient of Determination (R^2)**	**Root Mean Square Error (RMSE)**
Rational Quadratic GPR	✔			✔	0.95	0.025
Rational Quadratic GPR	✔	✔		✔	0.99	0.009
Matern 5/2 GPR	✔	✔	✔	✔	0.97	0.008

It was observed that the model accuracy was lowest when only the DOY and depth were used. The inclusion of pavement temperature improved the model performance, while including precipitation improved its accuracy slightly. Although RMSE decreased from 0.009 to 0.008, R^2 decreased from 0.99 to 0.97. The decrease in R^2 value indicated that the precipitation could not explain the moisture content variation and using precipitation as an input parameter makes the model more complicated than before, thus precipitation did not be used as an input parameter in this study. Thus, the Rational Quadratic GPR model with three input parameters, pavement temperature, day of the year and depth, was used to train the models at multiple depths.

Machine learning models in this study only have been trained by data collected from the IRRF test road, so only one kind of climate (cold dry region) has been considered. While including the precipitation did not improve the performance of the machine learning models, if machine learning models were trained by data collected from other climatic regions, the effects of precipitation could vary and precipitation may become one of the most effective input parameters.

8.4.3. Model Validation

There are two methods available in MATLAB to validate machine learning models: holdout validation and cross-validation. Holdout validation is generally recommended for large data sets. Due to the limited size of the available dataset, cross-validation was used to validate the machine learning models in this research. The cross-validation method is used to protect against overfitting and to estimate the model performance. Using five-fold cross-validation, the input data were randomly divided into five folds. Four folds of data were used for training, and the remaining was used for validation. This process was repeated five times, and the average test error was calculated for all five data folds. In this way, MATLAB was used to automatically train and validate model performance.

All the above training processes were repeated for each model development. All the algorithms and their subcategories have been examined, and only keep the algorithms with the best performance. The performance of the rational quadratic GPR model was established for moisture content prediction at each depth, as shown in Table 8-3 and Figure 8-5. The machine learning model showed high accuracy in the training process (i.e. R^2 was above 0.98 and RMSE was lower than 0.013). As expected, a high correlation between moisture content and temperature was observed. Moisture content is influenced by soil type and depths, so moisture content shows a different trend at five different depths – Figure 8-5. At a depth between 0.50m to 1.80 m, the pavement temperature drops below 0°C in winter, so the water turns into ice in winter, and unfrozen moisture content detected by TDR decreases (Kahimba and Ranjan, 2007; Kozlowski, 2007; Patterson and Smith, 1980; Stein and Kane, 1983). But, at the depth of 2.70 m, the temperature remained above 0°C, this moisture content change at this depth can be explained by considering the moisture migration, that is water migrates from an unfrozen area to a frozen area (Hoekstra, 1967).

Table 8-3: Summary of machine learning model training and test comparison results.

Depth (m)	Training Results		Validation Results	
	Coefficient of Determination (R^2)	Root Mean Square Error (RMSE)	Coefficient of Determination (R^2)	Root Mean Square Error (RMSE)
0.50	0.99	0.005	0.98	0.008
0.70	0.99	0.005	0.99	0.006
0.80	0.99	0.013	0.97	0.012
1.80	0.99	0.012	0.99	0.012
2.70	0.98	0.004	0.98	0.005

In addition to the cross-validation method, results were validated by comparing moisture measurements that were not used during the training of the model. For this purpose, 12 daily measurements were randomly selected (one record for each month of the year). Table 8-3

summarises all the training and validation results. During model validation, models maintained the same high accuracy as the model training (i.e. R^2 was higher than 0.97 and RMSE was lower than 0.012). Figure 8-6 shows the comparison of predicted moisture content and measured moisture content. Whether the moisture content was high or low, the predicted value was in good agreement with the actual measured value. Thus, machine learning models could be a powerful method for moisture content prediction.

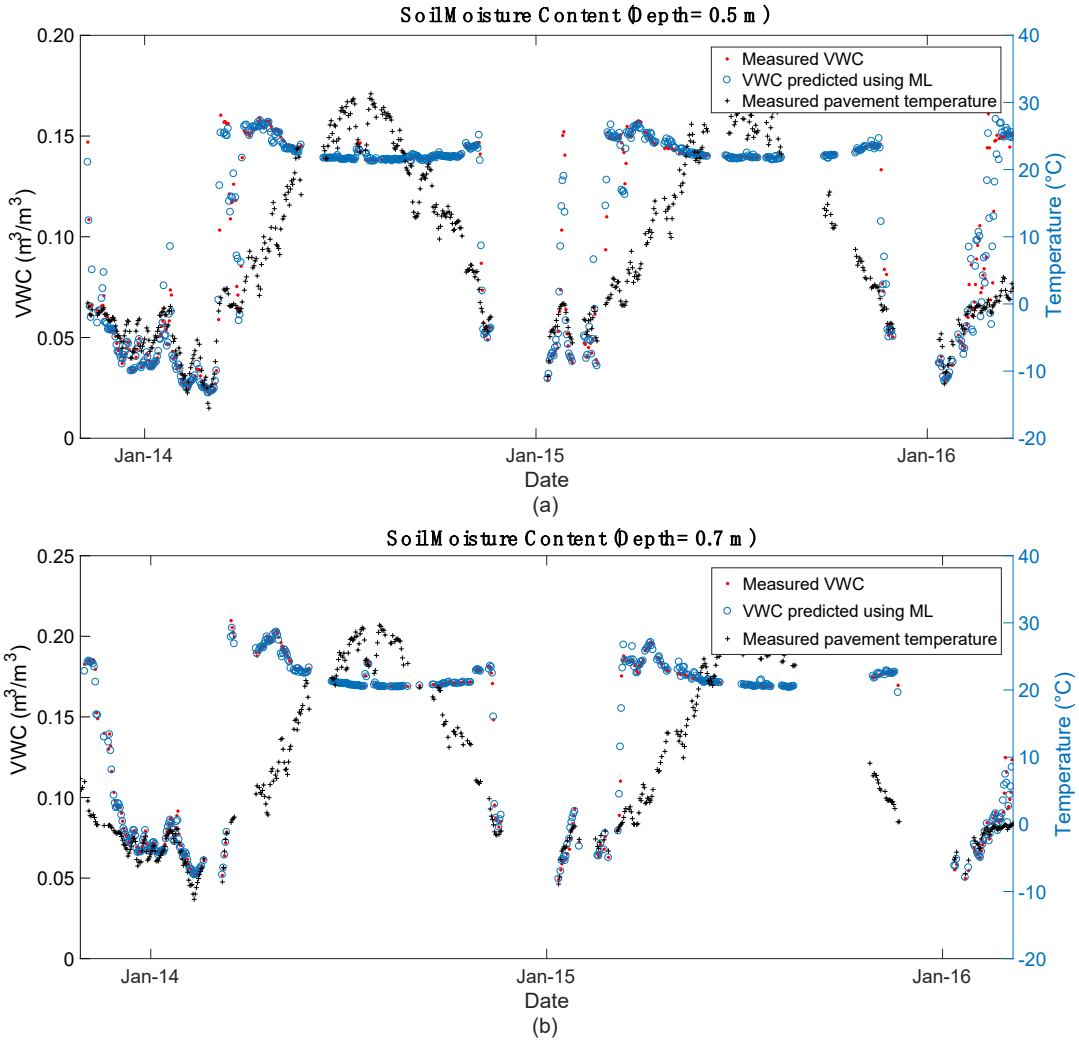

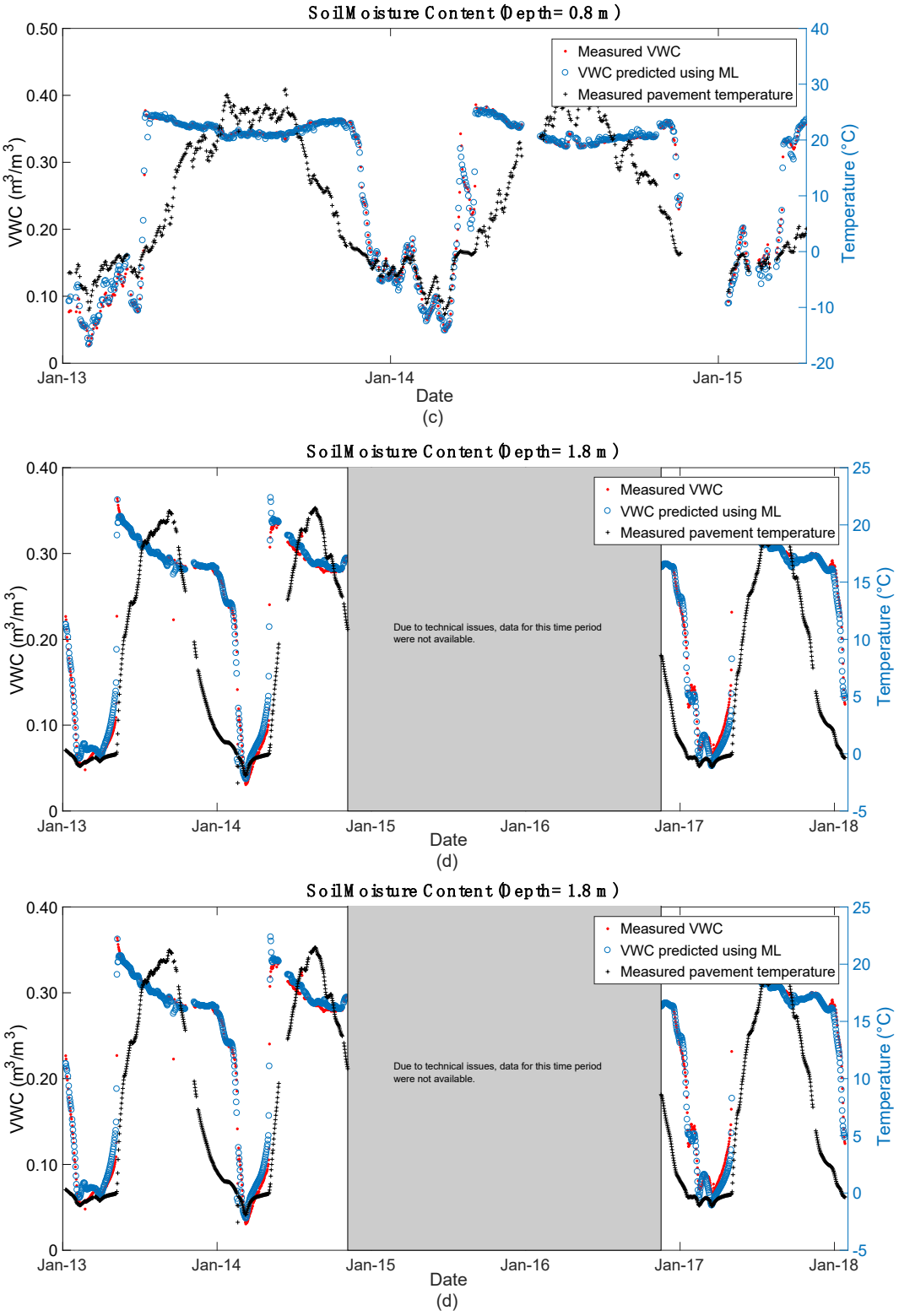

Figure 8-5: Average daily soil moisture content predicted results comparison at (a) 0.5 m, (b) 0.7 m, (c) 0.8 m, (d) 1.8 m, and (e) 2.7 m

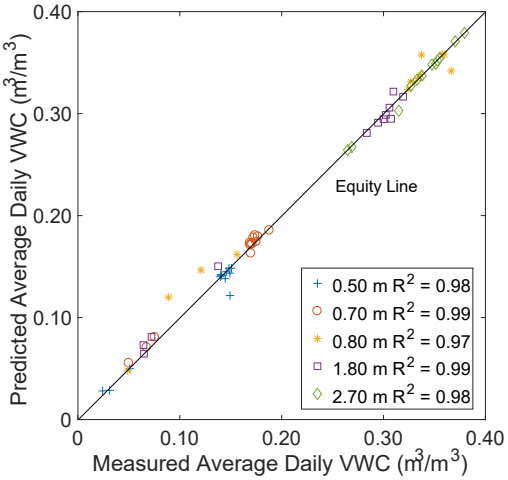

Figure 8-6: Predicted versus measured moisture content in five different depths.

8.5. COMPARISON OF MACHINE LEARNING RESULTS WITH AN EXISTING MODEL

All machine learning models show high accuracy of moisture content prediction. To evaluate their performance, compare them with an existing model. Teltayev and Suppes (2019) developed a semi-logarithmic function to describe unfrozen pavement moisture content in winter, based on negative temperature (i.e. pavement temperature was below 0°C) and initial moisture content (i.e. before the pavement temperature drops below 0°C). The model was based on data collected in the eastern region of Kazakhstan, as represented in Equation 8-1.

$$W_{uf} = 0.911 + 0.634W_0 - 0.552\ln|T| - 0.067W_0\ln|T| \qquad \text{Equation 8-1}$$

Where W_{uf} is the unfrozen soil moisture content (%), W_0 is the initial soil moisture content (%), and T is the temperature (°C), which is always a negative value. As mentioned above, when the pavement temperature drops below 0°C in winter, part of the water becomes solid, while part of the water remains unfrozen (Watanabe and Wake, 2009). TDR can only detect liquid water, so, when the pavement temperature is negative, TDR and the machine learning model reflects the change in the unfrozen water content in the soil (Stein and Kane, 1983; Topp et al., 1980). The moisture content calculated based on Equation 8-1 is given as a weight percentage,

while the soil moisture content calculated using the machine learning model is the volumetric moisture content (m^3/m^3), so the results obtained using Equation 8-1 were converted to volumetric moisture content using Equation 8-2:

$$\theta = W_{uf} \times \rho_{water} / \rho_{soil} \quad \text{Equation 8-2}$$

where θ is the volumetric moisture content (m^3/m^3), ρ_{water} is the density of water (kg/m^3), and ρ_{soil} is the soil density (kg/m^3). Since the semi-logarithmic function (Equation 8-1) is only valid for temperatures below 0°C and the temperature at a depth of 2.7 m below the IRRF road surface always remains above 0°C, the semi-logarithmic function was only used to predict moisture content in winter when the corresponding pavement temperature was below 0°C (at depths of 0.5 m to 1.8 m below the road surface).

There were some models for predicting changes in water content throughout the year. For example, Hedayati and Hossain (2015) also developed a conventional model for predicting daily average moisture content for the whole year. However, it was developed for warm regions where the temperature did not drop below 0°C, and the moisture content was predicted to change sinusoidally. It did not consider the water phase change in winter and the accumulation of water during spring. Thus, it could not be applied in cold regions.

Table 8-4 includes a comparison of the machine learning model results with results obtained using the semi-logarithmic function. The accuracy of the machine learning model was high, as indicated by the values of R^2 for the machine learning model being higher than 0.94 (except for a TDR, at a depth of 1.8 m). In addition, for the machine learning model, RMSE did not exceed 0.018. However, the accuracy of the semi-logarithmic function varied for different depths. When the semi-logarithmic function was used to predict moisture content at a depth of 0.8 m, its accuracy was high (with R^2 values of 0.92). However, when the semi-logarithmic function was applied to predict moisture content at different depths the accuracy dropped

significantly. The R^2 for the depths of 0.5 and 0.7 m was less than 0.92, and the value of R^2 was 0.48 for moisture content prediction at a depth of .8 m. Equation 8-1 was based on all the data observed at different depths, and it showed a low accuracy at a depth of 1.75 m in the literature, and it also showed lower accuracy at a depth of 1.8 m in this work, confirming that it can't be applied at deeper locations. The R^2 values obtained by the machine learning models were 12%, 17%, 4%, and 65% higher than the results calculated based on the semi-logarithmic function developed by Teltayev for depths of 0.5, 0.7, 0.8, and 1.8 m. The RMSE values of the results obtained using the machine learning model were 82%, 92%, 74%, and 76% lower than those calculated using the semi-logarithmic function developed by Teltayev and Suppes (2019) for depths of 0.5, 0.7, 0.8, and 1.8 m.

Table 8-4: Performance comparison at different depths.

Depth (m)	**Machine Learning Model**		**Semi-logarithmic Function** (Teltayev & Suppes, 2019b)	
	R^2	**RMSE**	**R^2**	**RMSE**
0.5	0.94	0.007	0.84	0.039
0.7	0.95	0.003	0.81	0.036
0.8	0.96	0.014	0.92	0.054
1.8	0.79	0.018	0.48	0.076

Figure 8-7 depicts moisture content measured by the sensors installed in the IRRF test road, machine learning predictions, and the results obtained using the semi-logarithmic function. As discussed in previous literature, the unfrozen moisture content existed in the frozen soil, even when the temperature dropped to −10°C (Hoekstra, 1967; Jin et al., 2020; Stein and Kane, 1983). As expected, based on the high accuracy of the machine learning model, the moisture content values predicted using the machine learning model were in very good agreement with the measured moisture content values. In contrast, the accuracy of the results obtained using the semi-logarithmic function (including initial moisture content and negative temperature)

was lower than that of the results based on the machine learning model, and the statistical model overestimated the unfrozen moisture content. This difference between the measured and the semi-logarithmic predicted values in Figure 8-7 could be explained as the pavement structure and soil type play an essential role in unfrozen moisture content (Anderson and Tice, 1972; Jin et al., 2020), while they are different on these two test roads.

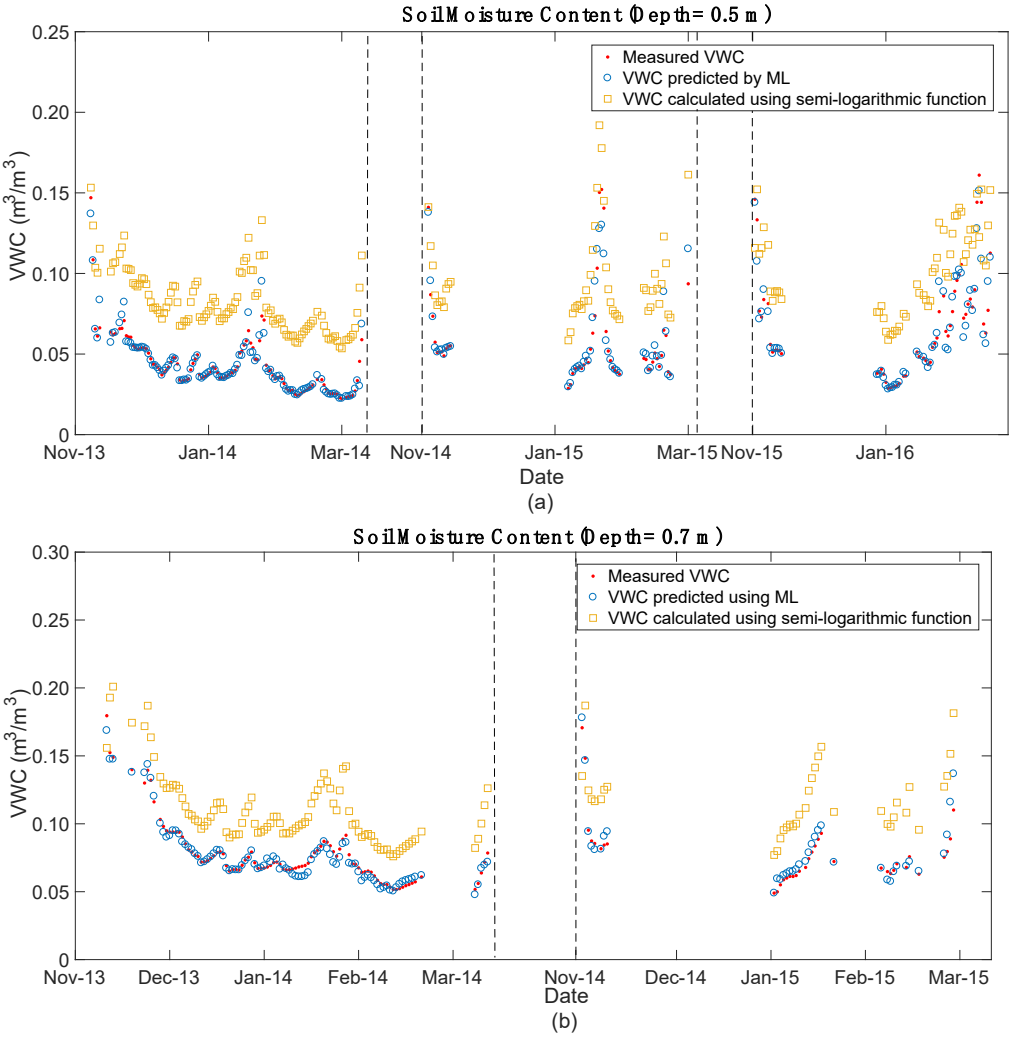

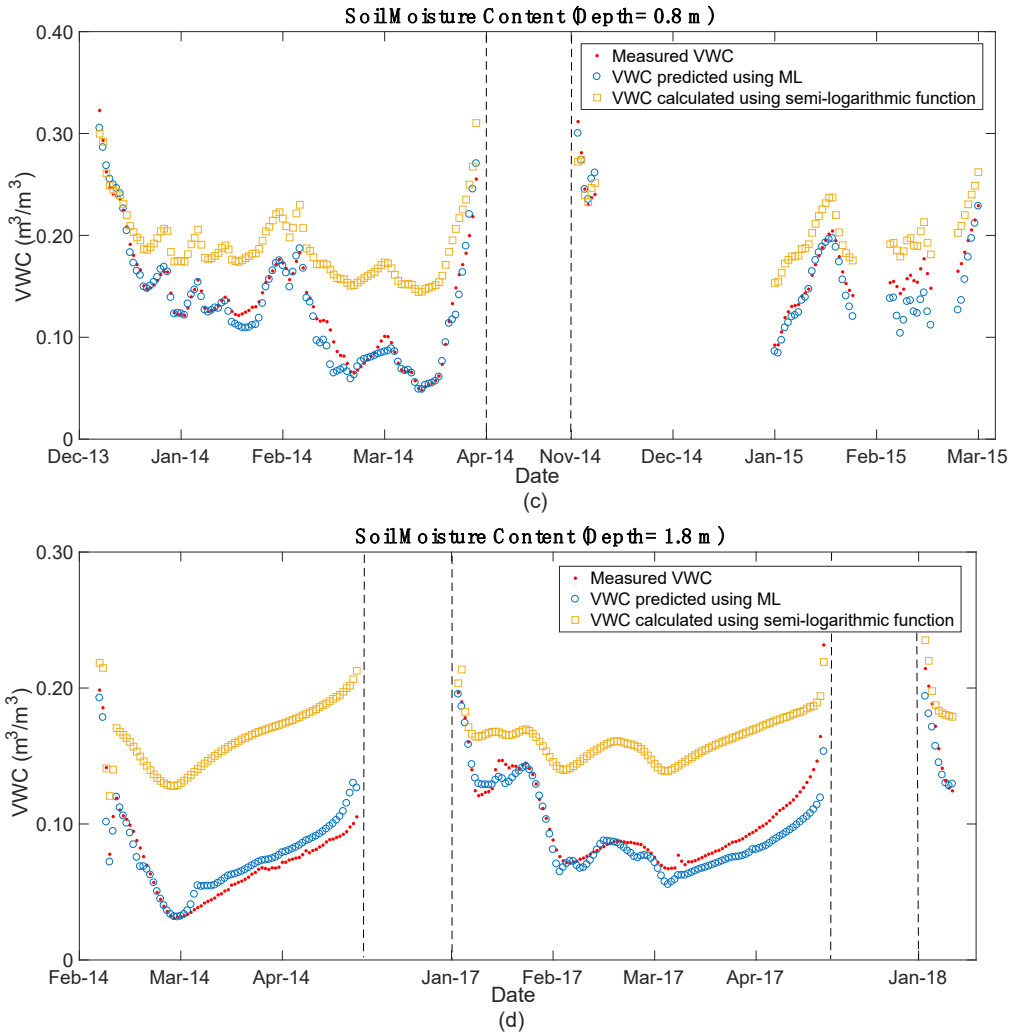

Figure 8-7: Comparison of measured average daily volumetric moisture content and VWC results based on the machine learning model and a literature model (semi-logarithmic function developed by Teltayev and Suppes (2019) based on initial moisture content and temperature) at depths of (a) 0.5 m, (b) 0.7 m, (c) 0.8 m, and (d) 1.8 m.

Although the model developed by Teltayev and Suppes (2019) (Equation 8-1) does involve pavement temperature as an input parameter and shows a similar trend as the measurements, it overestimates the moisture content in winter. This could be explained by the difference in pavement structure and soil type, and this model may need calibration. This model also does not take the influence of depth into account. However, depth was found to affect moisture content variation, as shown in Figures 8-5 and 8-7. This model (Teltayev and Suppes, 2019) has the limitation that it can only be used to predict moisture content in winter (when the temperature is below 0°C). However, the machine learning model investigated in this work can be trained based on data for different depths (provided that such data is available) and the

validity of the machine learning model is not restricted to a certain time of year. The machine learning model generally showed higher accuracy in the prediction of the moisture content variation for all locations within the test road structure. Thus, if measured data is available, machine learning models can improve moisture content prediction.

8.6. LIMITATIONS OF THE PROPOSED MODEL

Unlike conventional models, the machine learning model were implemented based on three readily available parameters (pavement temperature, day of the year and depth), without the need for input parameters related to the road surface, the water table, and so on. The machine learning model can successfully be used to predict moisture content in unbound materials, even with significant seasonal variations in conditions. Meanwhile, all the results showed high accuracy for the five depths, even at a depth of 2.7 m below the road surface. After training the machine learning algorithms based on field measurements of moisture content and pavement temperature, the models can be used to accurately predict the daily average moisture content in pavements (at different depths within the pavement structure), regardless of the time of the year.

TDR can only detect unfrozen moisture content (liquid water) in winter, thus, the amount of solid moisture content (ice) has not been taken into account in this study. However, the amount of unfrozen moisture content shows a high correlation with the resilient modulus of the subgrade layer (ARA., 2000; Christopher et al., 2006, 2010; Haghi et al., 2016, 2019). Thus, even though the TDR only detects liquid water, a better understanding of unfrozen moisture content change in the base and subgrade layers for the whole year can help to improve road design. In the future, more sensors will be used to detect frozen water in winter.

The machine learning model demonstrated high accuracy in predicting moisture content at different depths, indicating that the machine learning model is a robust method for predicting

moisture content in base and subgrade layers. However, the machine learning models developed in this study were only trained by data collected from the IRRF test, thus only data collected from one pavement structure and two unbound materials were used to train the models. The proposed model only works for the IRRF test road and the generality of this model is restrictive. Machine learning is a data-driven approach, thus if the models could be trained by a data set that includes data collected from different pavement structures with different pavement materials and different climatic regions. More input parameters, such as material properties, number of layers, thickness of the layer and so on, could be included to improve the generality of the machine learning models. However, such an expansive data set is not currently available. If measured data are available, machine learning models could be trained to estimate moisture content for other specific pavements. Input parameters may change based on the pavement structure, materials properties and the climatic regions. Future work will involve the implementation of machine learning models that can predict moisture content over different pavement structures.

The generality of the proposed machine learning model is limited, however, the building of the machine learning model is meaningful. There are no existing models in the literature that could estimate the year-round moisture content in cold regions, and measurements from a specific site are necessary for the existing models. Even for the semi-logarithmic function developed by Teltayev and Suppes (2019), which could only estimate the moisture content in winter, the initial value of soil moisture before freezing and pavement temperature are required for each depth. Meanwhile, based on the results observed in this study, when the semi-logarithmic function is applied to a specific pavement, it needs to be calibrated by soil type, which also requires measurements from the specific pavement. Therefore, the aim of this study is to demonstrate that the machine learning model is a powerful method to predict moisture content in unbound material layers and it could be a new option for future research.

While it is true that existing software, like MATLAB, can be used to evaluate machine learning models, the application of these models to predict moisture content in base and subgrade layers is unique. The data set for this project is not only curated but also specific to the particular application, which means that a variety of methods can be used to analyse the data and extract meaningful insights. Furthermore, while a person with basic knowledge of data analysis or modelling could have implemented this project, the use of machine learning brings a new level of sophistication to the analysis. Machine learning algorithms can detect delicate patterns in the data that would otherwise be difficult to detect and can provide more accurate and reliable predictions. Therefore, we believe that this project has significant scientific merit and would be a worthwhile addition to the existing literature.

8.7. CONCLUSION

This study focused on applying machine learning to predict the seasonal fluctuations in the moisture content of unbound materials. A series of machine learning models were implemented based on field data collected at the IRRF test road in Edmonton, Alberta between 2013 and 2018. The environmental data were collected from the Environment Canada weather station (Oliver AGDM). Machine models were implemented for the five depths across the roadway. An rational quadratic GPR model obtained based on three parameters of pavement temperature, day of the year and depth showed the best performance. Therefore, pavement temperature, depth and one time-based parameter (day of the year) were used as inputs to implement machine learning models for the prediction of moisture content at different locations. All the machine learning models showed high accuracy during training and validation, R^2 values were above 0.97 and RMSE values were smaller than 0.013.

The rational quadratic GPR model based on these three input parameters was compared with one existing literature model for the determination of unfrozen moisture content in winter. The

model developed by Teltayev and Suppes (2019) used initial moisture content and temperature (below 0°C) to predict moisture content in winter. Although the semi-logarithmic function performed well in the context of the previous studies, the accuracy of the moisture content values obtained using this model was low when it was applied for the determination of moisture content at the IRRF test road. The semi-logarithmic function overestimates the moisture content of the IRRF test road in winter, which is significantly affected by soil type and pavement structure, so calibration may be required. Meanwhile, the moisture content was influenced by depth. The semi-logarithmic function showed lower accuracy when applied to deeper locations in the literature, and its R^2 dropped to 0.48 when applied to the IRRF test road at a depth of 1.80 m. However, the machine learning model remained at a much higher accuracy when applied to the same depth, with an R^2 of 0.79. It was found that the machine learning model can improve the R^2 values by 4% to 65% and decrease RMSE values by 74% to 92% for predicting moisture content of the base and subgrade layers, compared to the model developed by Teltayev and Suppes (2019). Thus, in this context, the machine learning model outperformed this literature model. This indicates that, provided that measured data is available, machine learning models could provide a practical and flexible method to predict the seasonal variations in moisture content in pavement base and subgrade layers.

CHAPTER 9.MODEL DEVELOPMENT FOR SIMULTANEOUS PREDICTION OF TEMPERATURE AND MOISTURE CONTENT

This section has been submitted to Journal of Testing and Evaluation on March 2023 as Huang, Y., Molavi Nojumi, M., Hashemian, L. and Bayat, A. Integrating Machine Learning for Improved Prediction of Temperature and Moisture in Pavement Granular Layers.

9.1. ABSTRACT

Pavement temperature and moisture content within the base and subgrade layers affect the load-bearing capacity of the pavement and dominate the pavement performance in cold regions. Accurately predicting pavement temperature and moisture content can improve pavement design and management. Conventional approaches, including numerical and statistical models, have been implemented to predict pavement temperature and soil moisture content. However, they have weaknesses, such as being only suitable for warm regions or only for predicting pavement temperature within the asphalt layer. Furthermore, none of them can simultaneously predict the pavement temperature and moisture content. To address this issue, data collected from an instrumented test road in Alberta, Canada, were used to train a model to predict the daily average pavement temperature and moisture content at various depths through three parameters, namely depth, day of the year, and air temperature. MATLAB toolbox, Neural Network Fitting, was used, and the performance of three built-in algorithms, Levenberg-Marquardt, Bayesian regularization, and Scaled conjugate gradient backpropagation, was compared. The model with Bayesian regularization showed the highest accuracy, with an R^2 value of 0.99 and an RMSE of 1.49ºC for pavement temperature prediction, and an R^2 value of 0.95 and an RMSE of 0.025 m^3/m^3 for moisture content prediction. The model developed in this research is the first to simultaneously estimate pavement temperature and moisture content, so its performance was separately compared with two existing models in the literature. The

Artificial Neural Network (ANN) model shows higher accuracy than the two existing models, so it was found that the ANN could be a robust method for pavement temperature and moisture content prediction at various depths.

Keywords: pavement temperature prediction, moisture content prediction, artificial neural network, time domain reflectometers

9.2. INTRODUCTION

Cold climate negatively affects flexible pavements, and, in Canada, 75% of flexible pavement degradation is caused by climatic factors (Doré et al., 2005). Differential frost heave in winter, thaw weakening in spring, and freeze-thaw cycling lead pavements in cold regions to show premature distress, lower load capacity, structural deterioration, and high maintenance costs (Smith, 2006; Tighe et al., 2006). The temperature and moisture content of base and subgrade layers have been shown to affect the load-bearing capacity of the pavement and dominate the pavement performance in cold regions (ARA., 2004; Bayat, 2009; Bohra et al., 1999; Haghi et al., 2016; Hall and Rao, 1999; Olidis and Hein, 2004; Popik et al., 2005; Utilities, 1997), and there is a high correlation between them (Bayat, 2009). The lower base and subgrade temperature in winter results in higher modulus of the base and subgrade layers, but with the increase of base and subgrade temperature in late winter and early spring, the base and subgrade moisture content reaches its maximum value, and the load-bearing capacity of pavements drops to the minimum throughout the year value (Bayat, 2009; Haghi et al., 2016b). To protect pavements in cold regions, many North American authorities have even decided to reduce the maximum axle load of trucks or ban heavy traffic during the thaw-weakening season (Asefzadeh et al., 2016). Therefore, an in-depth understanding of the temperature and moisture content of the base and subgrade layers can improve pavement design and maintenance.

Although base and subgrade temperatures have a significant impact on pavement performance, the current research on them is limited, and the existing studies mainly focus on the study of the temperature of the road surface or asphalt layer (Asefzadeh et al., 2017; Liu et al., 2018; Molavi Nojumi et al., 2022; Qin, 2016; Qiu et al., 2020). The enhanced integrated climate model (EICM) (ARA., 2004) can be applied to predict pavement temperature. However, it has its shortcomings. First, the accuracy of EICM is highly dependent on the accuracy of the input and requires a lot of input, including boundary conditions and material properties for which accurate values are difficult to obtain. Furthermore, the EICM assumes the heat capacity and thermal conductivity of the unbound materials are constant. Only one statistical model has been found in the literature for base and subgrade temperature prediction. Heydinger (2003b) has proposed a sinusoidal function to predict temperature within the pavement structure, the parameters of which need to be determined from the pavement temperature measured at each depth. The model assumes that the temperature change is completely sinusoidal, but this does not match what is observed in the actual field, especially at shallower locations.

Numerous studies have been done to predict the moisture content of the base and subgrade layers, however, each existing methods have its limitations (Croney and Coleman, 1948). For example, a theoretical approach base on principles of thermodynamics has been to assess the moisture content of the pavement, however, it assumes that the temperature beneath the pavement is constant (Croney and Coleman, 1948). Teltayev and Suppes (2019) have proposed a statistical model to estimate moisture content within pavement structures in warm regions. However, previous studies have shown that moisture content changes differently in warm and cold regions (Teltayev and Suppes, 2019), so models built for warm regions cannot be used to estimate moisture content in cold regions. In the warm region, where the temperature beneath the pavement keeps above 0°C, the moisture content variation is dominated by time and precipitation (Hedayati and Hossain, 2015; Heydinger, 2003a). However, in cold regions, due

to extreme weather, the prediction of moisture content is a more complex issue. The penetration of frost into the pavement structure will cause changes in the water state in the pavement structure, that is, part of the water is liquid and part of the water freezes (Bayat, 2009; Kozlowski, 2007). At the same time, many factors such as soil type, capillary action, and surface effect affect the amount of liquid water in the soil (Jin et al., 2020; Stein and Kane, 1983). In early spring, water content increases due to the presence of ice in the subgrade which reduces its drainage capacity. The EICM can also be used to predict moisture content, but studies have shown that it is hard to match the measured values with values predicted by the EICM (Bulut et al., 2013; Oh et al., 2006). Thus, it is hard to predict the moisture content of the base and subgrade layers in cold regions.

Recently, artificial intelligence has gained more and more attention and has been applied to predict pavement temperature. Xu et al. (2017) have accurately predicted the pavement temperature for the next three hours by an improved Back Propagation neural network model. Milad et al. (2021) have applied four deep learning-based regression models to predict asphalt pavement temperature, and Bidirectional Long Short-Term Memory outperforms other algorithms. Molavi Nojumi et al. (2022) have applied a machine learning model to predict daily average, maximum and minimum pavement temperature within the asphalt layer, and R^2 values are higher than 0.95. Tabrizi et al. (2021) have employed the Convolutional Neural Network to predict hourly pavement surface temperature, and predictions are close to measured values. Although all the work has predicted the pavement temperature and showed high accuracy, they all focus on the pavement temperature within the asphalt layer.

Meanwhile, machine learning and deep learning models have also been used to predict soil water content, but the number of existing studies is limited, and none of them have predicted simultaneously pavement temperature and moisture content of the base and subgrade layers. Chen et al. (2021) have used a long short-term memory model to predict subgrade material

moisture, and this model predicts the dynamic characteristic of the subgrade moisture content. Artificial neural networks have also been applied to predict soil moisture content by analyzing ground-penetrating radar signals (D'Amico et al., 2010) and remote satellite images (Xing et al., 2017). However, those artificial neural networks have been designed for general soil and the influence of pavement has not been taken into account.

The performance of a pavement is largely influenced by the temperature and moisture content of its granular layers (ARA., 2004; Bayat, 2009; Bohra et al., 1999; Haghi et al., 2016; Hall and Rao, 1999; Olidis and Hein, 2004; Popik et al., 2005; Utilities, 1997). However, the current models available are unable to accurately estimate both variables simultaneously. To overcome this limitation, this study aims to apply deep learning to build an artificial neural network (ANN) model to predict pavement temperature and moisture content of the base and subgrade layers, simultaneously. To study the influence of environmental factors on flexible pavement, the Integrated Road Research Facility (IRRF) test road has been built in Edmonton, Alberta, and sensors have been installed in base and subgrade layers to monitor pavement performance. Time-domain reflectometers (TDRs) have been used to collect pavement temperature and volumetric soil water content (VWC) of the base and subgrade layers, and previous studies have proved that TDRs can detect unfrozen moisture content in winter (ROTH et al., 1992; Skierucha et al., 2012; Watanabe and Wake, 2009; Zhou et al., 2014). Environmental factors have been collected from the nearest weather station, Oliver AGDM. The Toolbox, Neural Network Fitting, in MATLAB was used to train, test and validate the model. Three built-in algorithms, Levenberg-Marquardt, Bayesian regularization and Scaled conjugate gradient backpropagation, have been used and the best-performing algorithm has been selected for comparison with two existing models.

9.3. THE INTEGRATED ROAD RESEARCH FACILITY TEST ROAD

The IRRF test road is a fully instrumented road that studies the effects of the environment and traffic on pavement performance. As shown in Figure 9-1, a 0.25 m hot mix asphalt (HMA) layer is on top of a 0.45 m granular base course (GBC) layer, and the CS650 time domain reflectometers (TDRs, Campbell Scientific Canada) were installed in the IRRF test road in the middle of the lane. Two TDRs are located in the base layer, at depths of 0.50 m, and 0.70 m relative to the pavement surface. Two TDRs are located at depths of 0.80 m and 1.80 m. Pavement temperature and moisture content were collected every fifteen minutes by a CR-1000 data logger from Campbell Scientific Canada.

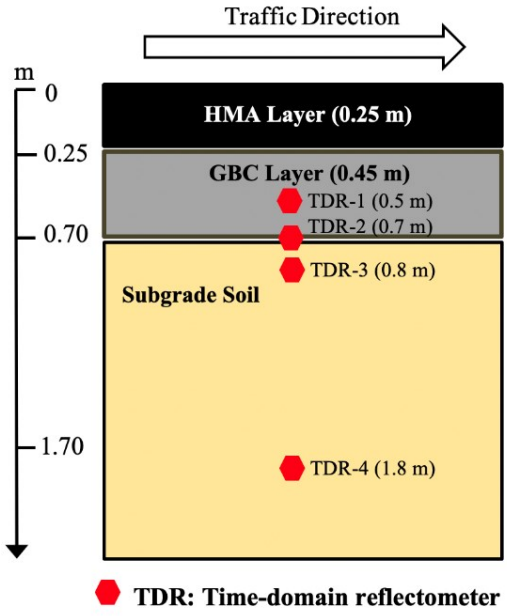

Figure 9-1: Cross-section of pavement layers and location of TDR embedded in the base and subgrade layers

TDR is an instrument for indirectly measuring soil moisture content by calculating the dielectric constant based on the Topp equation (Topp et al., 1980). The dielectric constant is influenced by temperature, water content, and soil type (Watanabe and Wake, 2009), so moisture content data collected by TDRs were calibrated in the laboratory of the University of

Alberta (Haghi, 2019). When pavement temperature is below 0°C, there is a mixture of ice and water, and TDR has been proven to detect unfrozen water using the Topp equation (Kahimba and Ranjan, 2007; Patterson and Smith, 1980; Stein and Kane, 1983). Some data has been lost due to technical issues with the data collection system. Table 9-1 shows all available data for model development.

Table 9-1: Availability of data for model development.

Depth (m)	Start date	End date	No. of measurements	No. of daily data points
0.5	9-Nov-2013	23-Mar-2016	83040	586
0.7	1-Nov-2013	5-Mar-2016	82080	430
0.8	8-Jan-2013	9-Apr-2015	78816	693
1.8	8-Jan-2013	25-Jan-2018	176928	1010

Figure 9-2 shows the grain size distribution of the granular base course and subgrade soil. The granular base course is well-graded gravel and the subgrade soil is clayey sand, according to the ASTM C 136-06 and the Unified Soil Classification System. About 27% and 21% of subgrade soil by weight passed the 0.075 mm sieve and the 0.02 mm sieve, respectively. The liquid limit of the subgrade soil is 25%, and the plastic index is 9%. The density of the granular base course is 2.10 ton/m^3, and the density of subgrade soil is 1.85 ton/m^3. The coefficient of permeability of subgrade soil is 0.03 cm/s. For more detailed information on IRRF roads, please refer to the published literature (Molavi Nojumi et al., 2022; Haghi, 2019), which will not be repeated here.

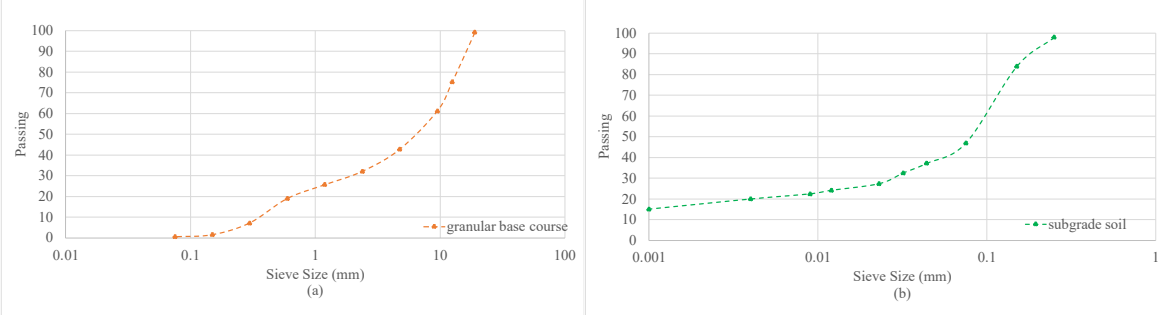

Figure 9-2: Grain size distribution of the (a) granular base course and (b) subgrade soil

9.4. METHODS

Pavement temperature and moisture content of the base and subgrade layers recorded at the IRRF were used as two outputs of the ANN models. The environmental parameter, air temperature, collected from the weather station, Oliver AGDM, was used as input parameters. The weather station is 6 km away from the IRRF test road. MATLAB_R2017a was used to train models for pavement temperature and moisture content prediction, and Neural Network toolbox 10.0 was employed.

Figure 9-3 shows the model development process. Irrelevant data and outliers were removed during data preprocessing. At the same time, since the moisture content was calibrated by the pavement temperature collected by the same sensor, if the pavement temperature was not available, the moisture content data were also removed. The data recorded every fifteen minutes were then converted to daily average values, so if data for the whole day were not available, data for that day were deleted, too.

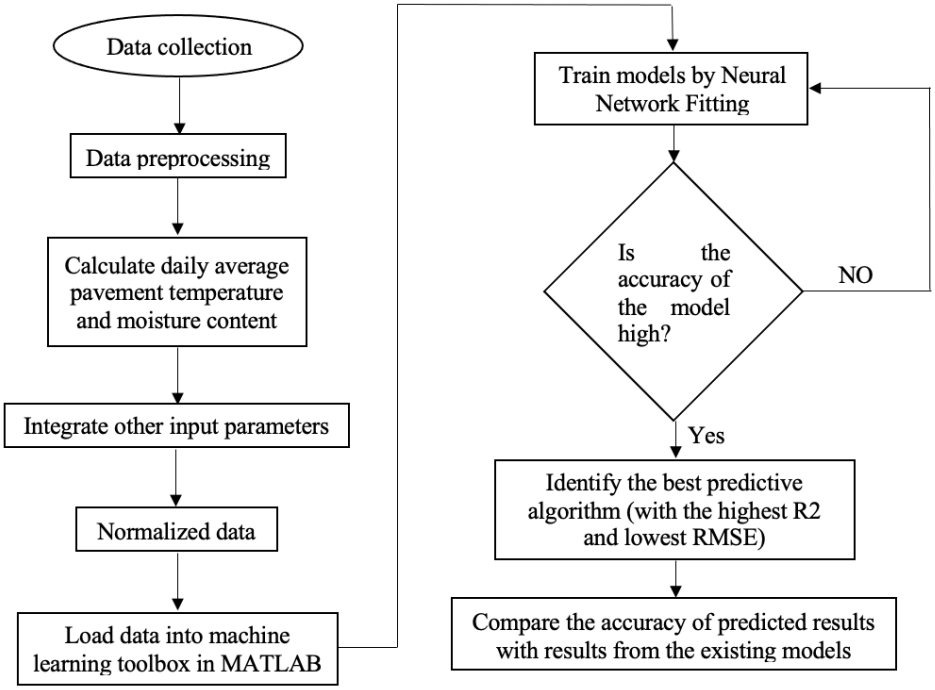

Figure 9-3: Flowchart for training models to predict pavement temperature and moisture content

The study by Molavi Nojumi et al. (2022) showed that the variation of pavement temperature within the asphalt layer was dominated by day of the year (DOY), air temperature and solar radiation. DOY is a time-dependent parameter. January 1st corresponds to the 1st day, and December 31st corresponds to the 365th day in a year. The moisture content change in the base and subgrade layers was affected by air temperature and depth. However, all the data used in this work were away from the road surface. The influence of solar radiation on the variation of pavement temperature and moisture content was limited, so only depth, DOY and air temperature were chosen as input parameters and discussed below. Because the variables have different scales such as pavement temperature varies from -20 to 30°C, while moisture content varies from 0.03 to 0.4 m^3/m^3, all inputs and outputs were then normalized to values between 0 and 1 by Equation 9-1, which is expressed as.

$$X' = \frac{X - X_{min}}{X_{max} - X_{min}} \qquad \text{Equation 9-1}$$

where X' is the normalized value, X is the data value, and X_{min} and X_{max} are the minimum and maximum values of the data.

Then, all data were loaded into MATLAB. Two-layer feed-forward network with sigmoid hidden neurons and linear output neurons was used for the modelling (default setting of the Neural Network toolbox 10.0). The tangent sigmoid transfer function is expressed as Equation 9-2.

$$f(x) = \frac{2}{(1 + e^{-2x})} - 1 \qquad \text{Equation 9-2}$$

As shown in Figure 9-4, there are three types of layers in a neural network: the input layer, the hidden layer, and the output layer. One hidden layer is included in the ANN model. Since this study used the toolbox, Neural Net Fitting, in MATLAB_R2017a to train the ANN models, the number of layers is fixed and the ANN model performed very well. Therefore, the ANN models with two layers were developed. Each layer is made up of several neurons. The number of hidden neurons is determined by the network performance. The default number of hidden neurons in the Neural Network Fitting toolbox of MATLAB_R2017a is 10, and the ANN model had been trained with 10, 20, 30, and 40 hidden neurons. The network performance did not improve when the number of hidden neurons was increased to 40, thus 30 hidden neurons were used in this study. The input layer takes in data from outside the network, the hidden layer processes the data, and the output layer produces the results of the neural network. To predict the temperature and moisture content simultaneously, temperature and moisture content measurements were both used as outputs, as shown in Figure 9-4. Data were randomly divided into three groups for model training, validation and testing. Finally, the performance of the model is based on the results of the three groups. The default setting for data grouping was used in this work, 70% of the data was used for model training, 15% for validation, and 15% for model testing. The training subset is a set of input-output pairs to train the network. The

input-output pairs are fed into the network, and the network adjusts its weights and biases to minimize the error between its predicted output and the actual output. The validation subset is used to measure network generalization, and to halt training when generalization stops improving. The testing group is independent and does not affect model training. The testing group is used to evaluate the model's performance during and after training. The model testing avoids overfitting of the ANN models. MATLAB chooses the regression (R) to evaluate the correlation between the target and output. The coefficient of determination (R^2) and root mean square error (RMSE) were used to assess the performance of the models. R^2 and RMSE were calculated using Equation 9-3 and 9-4.

$$R^2 = 1 - \frac{\sum_{i=1}^{n}(y_i - f_i)^2}{\sum_{i=1}^{n}(y_i - \bar{y})^2} \qquad \text{Equation 9-3}$$

$$RMSE = \sqrt[2]{\frac{\sum_{i=1}^{n}(y_i - f_i)^2}{n}} \qquad \text{Equation 9-4}$$

where y_i is the measured value, f_i is the predicted value, $\bar{y}$ is the mean of the measured values, and n is the number of the dataset. If the results of the model are not satisfactory, the model needs to be trained repeatedly until the R-value does not increase. Because different initial conditions and sampling lead to different results. The model with the highest R^2 and lowest RMSE was carried forward to compare with other existing models.

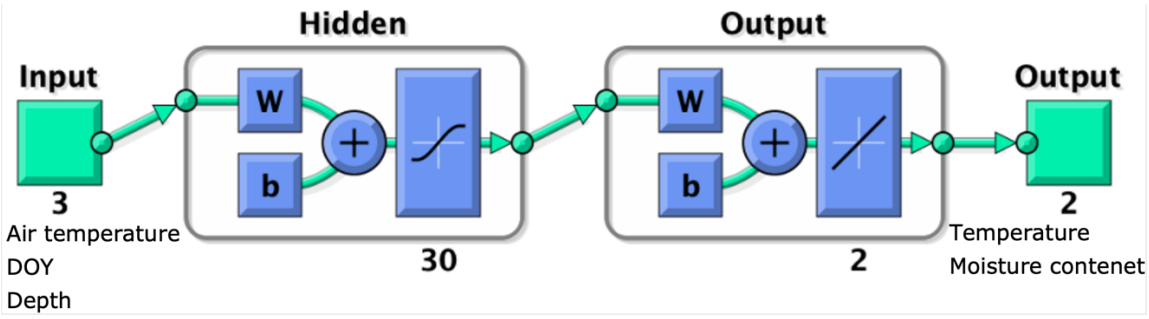

Figure 9-4: The neural network diagram used in this model development

9.4.1. Algorithms

Neural Net Fitting provides three built-in training algorithms, Levenberg-Marquardt, Bayesian regularization, and Scaled conjugate gradient backpropagation. Levenberg-Marquardt is generally the fastest of the three algorithms (Hagan and Menhaj, 1994; Marquardt, 1963). Bayesian regularization updates weights and bias values according to Levenberg-Marquardt optimization, and is good at dealing with noisy or small datasets, but usually takes a long time (Foresee and Hagan, 1997; MacKay, 1992). Scaled conjugate gradient backpropagation is recommended for large data sets (Moller, 1993). More details can be found in the literature (Foresee and Hagan, 1997; Hagan and Menhaj, 1994; MacKay, 1992; Marquardt, 1963; Moller, 1993), and a detailed discussion of the three algorithms is out of the scope of this research.

9.4.2. Statistical Analysis of Pavement Temperature and Moisture Content

Statistical analysis was conducted to show how the pavement temperature and moisture content change with depth and layer Table 9-2 shows the statistical parameters of pavement temperature and moisture content for each depth. Minimum (*min*), maximum (*max*), mean and standard deviation (*SD*) of the entire data used for ANN model development have been summarized in Table 9-2. The mean values of the pavement temperature at different depths are close, but the minimum and maximum values of the pavement temperature change significantly along the depths. Meanwhile, the *SD* values are much larger at shallower locations than that at deeper locations, thus depth dominates the pavement temperature variation. For moisture content variation, it was observed that soil type influenced the moisture content variation. The maximum, mean and *SD* values of data collected from the same soil layer are similar, and these values calculated from the subgrade layer are higher than those of the GBC layer. However, as explained above, the data were randomly divided into three groups for training, validation, and testing by MATLAB, so the statistical parameters of the training, validation and testing datasets are unknown.

Table 9-2: Statistical parameters for pavement temperature and moisture content.

Depth (m)	Layer	Pavement temperature (°C)				Moisture content (m^3/m^3)			
		min	***max***	**mean**	***SD***	***min***	***max***	**mean**	***SD***
0.5	GBC	-16	34	8	12	0.022	0.161	0.109	0.047
0.7	GBC	-11	30	9	12	0.049	0.210	0.139	0.051
0.8	Subgrade	-11	29	9	11	0.027	0.386	0.272	0.109
1.8	Subgrade	-3	21	8	8	0.031	0.364	0.233	0.099

9.4.3. Model Development

Models have been developed to predict pavement temperature and moisture content in the base and subgrade layers at various depths. As shown in Figure 9-4, three inputs, namely depth, DOY, and air temperature, were used as input parameters, and thirty hidden neurons were used in the hidden layer to predict pavement temperature and moisture content. *R* was also used to evaluate the relationship between inputs and outputs, and Figure 9-5 showed the results at a depth of 0.5 m. The process was repeated for each depth and similar results were observed, thus only results at a depth of 0.5 m were shown. Figure 9-5 (a) showed the relationship between the moisture content and air temperature. Because there was a mixture of ice and water when the pavement temperature was below 0°C, the data were divided into two parts, below 0°C and above 0°C. Correlation coefficients were found to be 0.54 for the pavement below 0°C, and 0.22 for the pavement above 0°C. Figure 9-5 (b) indicated the correlation coefficients between the moisture content and day of the year. The whole year was divided into three parts (DOY was smaller than 100, DOY was between 100 and 300, and DOY was larger than 300) because the moisture content showed different trends. Correlation coefficients were 0.73, -0.67 and -0.82 for the three parts, respectively. Although there was a correlation between moisture content and air temperature and day of the year, the correlation was not so strong and higher correlation coefficients were observed between pavement temperature and air temperature and day of the year. Meanwhile, different trends were observed for the first and second parts of the

year, so the whole year was divided into two parts (DOY was smaller than 180 and DOY was bigger than 180). Correlation coefficients were found to be 0.91, 0.90 and -0.97 for the air temperature, day of the year (DOY was smaller than 180), and day of the year (DOY was larger than 180), respectively, indicating a strong correlation.

Three different algorithms have been trained, respectively. Figure 9-6 shows the results of the model with the algorithm Levenberg-Marquardt. As mentioned above, the data were randomly divided into three groups, 70% of the data was used for training, 15% of the data was used for validation, and 15% was used for testing, and the final result was calculated based on the model training, validation and testing results. The same model training procedure has been repeated to develop models with Bayesian regularization and Scaled conjugate gradient backpropagation. Table 9-3 shows the ANN model's training results. Bayesian regularization does not allow for validation because the usual validation process involves monitoring the error on the validation set as training progresses. If the error worsens, training is halted. However, the Bayesian error is not solely dependent on the model's performance on the dataset, but also on the magnitude of its weights. As the weights increase, so does the error. Therefore, during training, if validation is enabled, it may prevent the network from exploring larger weights, which could potentially lead to the global minimum (Foresee and Hagan, 1997; MacKay, 1992). It was observed that Bayesian regularization showed the highest R^2 value and lowest RMSE value during model testing, thus only the results of Bayesian regularization have been used to compare with existing models.

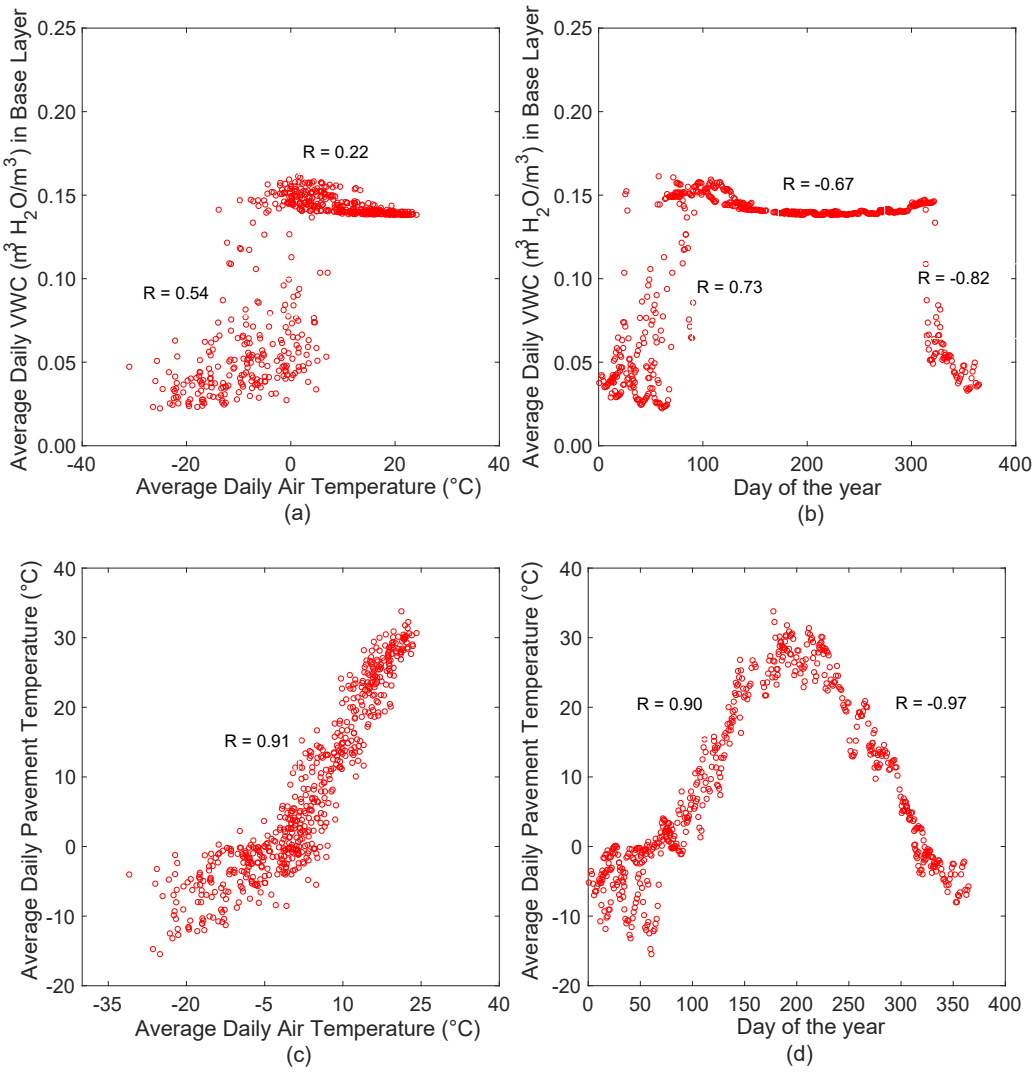

Figure 9-5: Correlation between inputs and outputs at a depth of 0.50 m (a) moisture content vs. air temperature, (b) moisture content vs. day of the year, (c) pavement temperature vs. air temperature, and (d) pavement temperature vs. day of the year

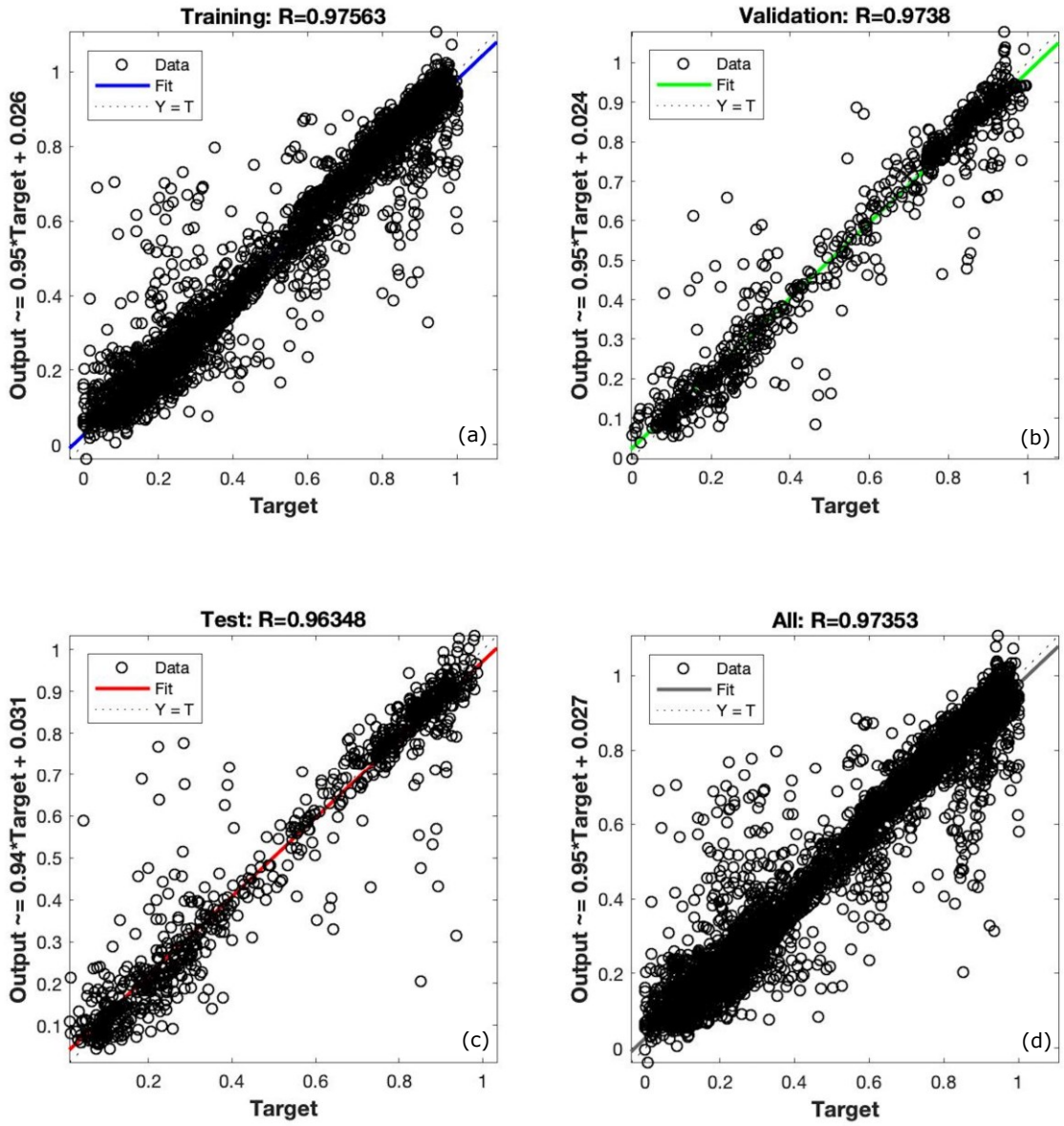

Figure 9-6: Results of the model with Levenberg-Marquardt algorithm (a) training results, (b) validation results, (c) test results, and (d) overall results

Table 9-3: ANN model's training results.

Algorithm	**Performance**					
	Training		**Validation**		**Testing**	
	R^2	**RMSE**	R^2	**RMSE**	R^2	**RMSE**
Levenberg-Marquardt	0.95	0.070	0.95	0.073	0.93	0.076
Bayesian regularization	*0.95*	*0.070*	*na*	*na*	*0.95*	*0.072*
Scaled conjugate gradient	0.93	0.083	0.91	0.094	0.92	0.087

Note: na = not applicable.

The R^2 and RMSE values have been calculated for pavement temperature and moisture content prediction, respectively. Table 9-4 summarizes the performance of three algorithms. It is observed that all three algorithms provide good predictions of pavement temperature, with R^2 values higher than 0.96. However, Levenberg-Marquardt and Bayesian regularization can improve predictions of moisture content. The highest accuracy was obtained using Bayesian regularization with an R^2 of 0.99 and an RMSE of 1.49 ºC for predicting pavement temperature, and an R^2 of 0.95 and an RMSE of 0.025 m^3/m^3 for predicting moisture content. Thus, Bayesian regularization demonstrates proficiency in predicting both pavement temperature and moisture content simultaneously.

Table 9-4: Performance of different algorithms for predicting pavement temperature and moisture content.

Algorithm	**Performance**			
	Pavement temperature		**Moisture content**	
	R²	**RMSE (ºC)**	***R²***	**RMSE (m^3/m^3)**
Levenberg-Marquardt	0.98	1.54	0.94	0.026
Bayesian regularization	***0.99***	***1.49***	***0.95***	***0.025***
Scaled conjugate gradient	0.96	2.14	0.91	0.033

9.5. RESULTS AND DISCUSSION

The model developed by the Neural Network Fitting toolbox simultaneously predicts pavement temperature and water content at various depths, which cannot be achieved by existing models. Therefore, to evaluate the performance of the ANN model, the temperature prediction and moisture content prediction results have been compared with the existing models, respectively.

9.5.1. Average Daily Pavement Temperature Prediction

To evaluate the performance of the ANN model, the predictions obtained using the Bayesian regularization algorithm are compared against a statistical model that is proposed by Heydinger (2003b). This statistical model is represented in Equation 9-5:

$$T(t) = A + Bsin[\omega(t - \phi)] \quad \text{Equation 9-5}$$

where t is the day of the year, A is the mean temperature (°C), B is the temperature amplitude (°C), ω is the normalized frequency (i.e. $\omega = 2\pi/365.25$), and ϕ is the time shift. The statistical model does not include depth as a predictor, but A, B and ϕ are calculated based on measured pavement temperature at each depth (Heydinger, 2003b).

Figure 9-7 compares the measured temperature against the predicted temperature obtained using ANN, and the predicted temperature obtained using the statistical model (Heydinger, 2003b), and Table 9-5 summarizes the comparison results at various depths. The ANN model showed high accuracy at predicting temperature in the base and subgrade layers (i.e. R^2 is larger than 0.98 and RMSE is lower than 1.88°C), and performance got better at greater depth (i.e. R^2 increases to 0.99 and RMSE decreases to 0.75°C). However, the statistical model showed lower accuracy, especially at a shallower depth (i.e. the depth of 0.50 m). The R^2 values obtained from ANN results were 40%, 15%, 13%, and 2% higher than those obtained from the statistical model for depths of 0.50 m, 0.70 m, 0.80 m, and 1.80 m, respectively. The RMSE values in ANN results were 72%, 64%, 58%, and 62% lower compared to the statistical model for depths of 0.50 m, 0.70 m, 0.80 m, and 1.80 m, respectively.

The statistical model (Heydinger, 2003b) assumes that the base and subgrade temperatures follow a sinusoidal variation, which is inconsistent with field measurements as shown in Figure 9-7. For example, at a depth of 0.50 m (Figure 9-7 (a)), the lowest temperature measured in winter 2014 was on March 2, 2014, while the lowest temperature using the statistical model

happened on January 12, 2014, namely in the middle of winter. Pavement temperature was dominated by air temperature and depth, and the influence of air temperature was more significant at shallower locations, however, the statistical model ignored the influence of the air temperature. Therefore, at shallower depths, the greater the difference between the measured temperature and the sinusoidal variation, the accuracy of the statistical model was lowest at the depth of 0.50 m.

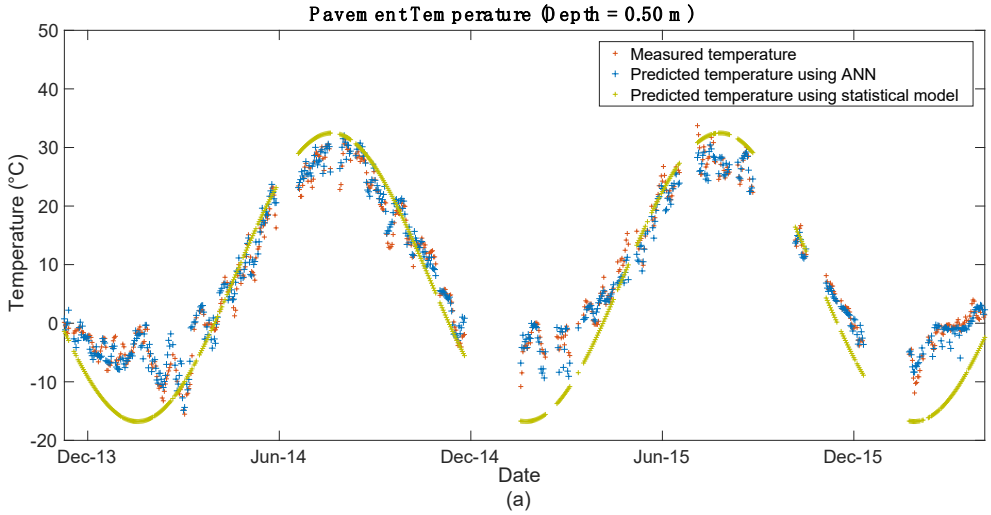

(a)

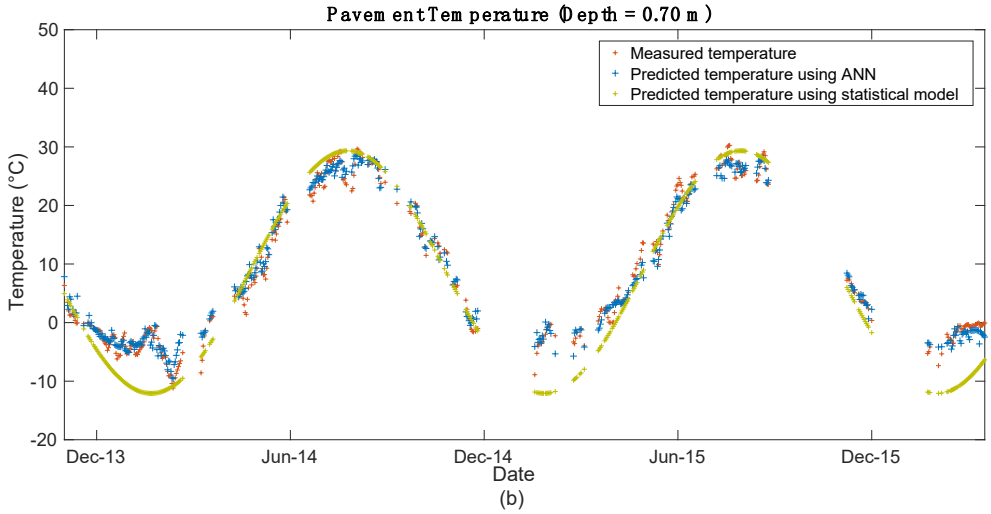

(b)

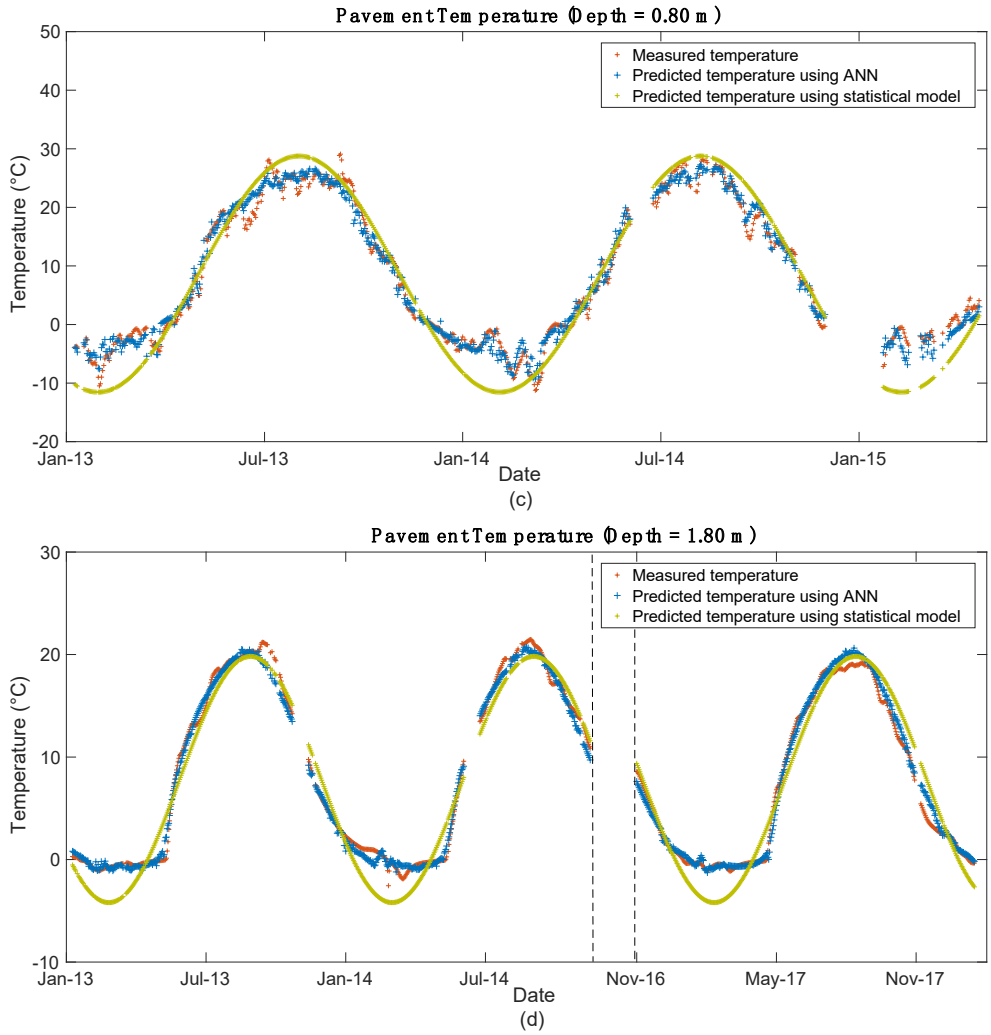

Figure 9-7: Average daily pavement temperature predicted results comparison at (a) 0.5 m, (b) 0.7 m, (c) 0.8 m, and (d) 1.8 m

Table 9-5: Pavement temperature performance comparison between ANN and the statistical model.

Depth (m)	ANN models		$T(t) = A + Bsin[\omega(t-\phi)]$(Heydinger, 2003b)				
	R^2	RMSE (°C)	R^2	RMSE (°C)	A (°C)	B (°C)	ϕ (day)
0.50	0.98	1.88	0.70	6.81	7.84	24.63	108
0.70	0.98	1.69	0.85	4.74	8.63	20.71	112
0.80	0.98	1.77	0.87	4.21	8.60	20.15	120
1.80	0.99	0.75	0.97	1.96	7.81	12.01	146

Figure 9-8 compares the pavement temperature predicted by the ANN model and statistical model. It is evident that the temperature predicted by the ANN model is in good agreement with the measured temperature, while the difference between the measured temperature and

the predicted temperature by the statistical model is large, especially when the pavement temperature is below 0°C. When the pavement temperature is negative, R^2 of the ANN model was 0.69 and RMSE was 1.60°C, while, R^2 of the statistical model was -3.86 and RMSE was 6.33°C. A negative value of the R^2 means the accuracy of the statistical model dropped significantly and there was a big difference between the measure values and predicted values. Because the difference between the measured value and the predicted value of the statistical model was too large, resulting in negative R^2 values, and negative R^2 values demonstrate that the model has very bad predictions (i.e., $\sum_{i=1}^{n}(y_i - f_i)^2$ was larger than $\sum_{i=1}^{n}(y_i - \bar{y})^2$). When the temperature dropped from 0°C to -20°C, it was found that the resilient modulus of soil increased significantly (Simonsen et al., 2002). Statistical models may lead designers to overestimate the elastic modulus of winter pavements, thereby reducing road life, while the ANN model can accurately predict pavement temperatures within the base and subgrade layers. Thus, the ANN model is a more powerful prediction method.

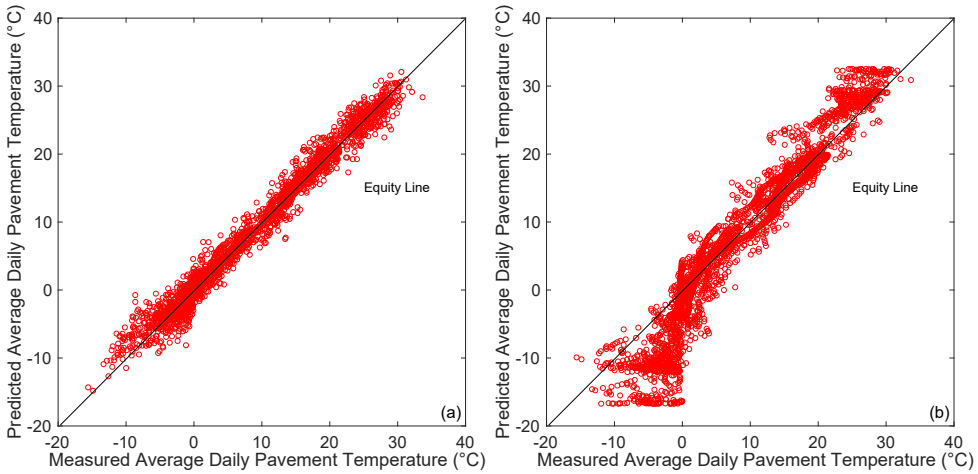

Figure 9-8: Pavement temperature predicted using (a) the ANN model and (b) the statistical model

9.5.2. Average Daily Moisture Content Prediction

When pavement temperature is below 0°C, there is a mixture of water and ice. Previous studies have proved that TDR detects unfrozen moisture content when pavement temperature is below

0°C (Kahimba and Ranjan, 2007; Patterson and Smith, 1980; Stein and Kane, 1983). Teltayev and Suppes (2019) have proposed a semi-logarithm model to predict unfrozen moisture content when pavement temperature is negative. To evaluate the ANN model's performance against other existing models, the predicted moisture content obtained using the ANN model was compared with the semi-logarithm model developed by Teltayev and Suppes (2019). The semi-logarithm model is based on initial soil moisture content, and absolute negative pavement temperature, as represented in Equation 9-6.

$$W_{uf} = 0.911 + 0.634W_0 - 0.552ln|T| - 0.067W_0 ln|T| \quad \text{Equation 9-6}$$

where W_{uf} is the unfrozen soil moisture content (%), W_0 is the initial moisture content when the pavement temperature becomes negative (%), and T is the negative pavement temperature (°C). The moisture content detected by TDR is the volumetric moisture content (m^3/m^3), and the moisture content calculated by Equation 9-6 is given in a weight percentage, so values obtained by Equation 9-6 have been converted to volumetric moisture content by Equation 9-7:

$$\theta = W_{uf} \times \rho_{water} / \rho_{soil} \quad \text{Equation 9-7}$$

where θ is the volumetric moisture content (m^3/m^3), ρ_{water} is the density of water (kg/m^3), and ρ_{soil} is the soil density (kg/m^3).

Figure 9-9 visualizes the moisture content prediction results using the ANN model and the semi-logarithmic model. TDR detects the total moisture content in the warm season and unfrozen moisture content in the cold season (Kahimba and Ranjan, 2007; Patterson and Smith, 1980; Stein and Kane, 1983). Because the semi-logarithmic model requires initial moisture content and some measurements are missing from January 2016 at a depth of 0.70 m and January 2013 at a depth of 0.80 m, it is not possible to predict unfrozen moisture changes in these two winters. In general, the predicted values using the ANN model are in good agreement with the measured values, but in late fall and late winter, when the moisture content starts to

decrease and increase, the ANN model overestimates the unfrozen moisture content. The predicted values using the semi-logarithmic model have a consistent trend with the observed values. But the semi-logarithmic model overestimates the moisture content, and there is a considerable difference between predictions and measured values.

Table 9-6 summarizes the performance of the ANN model and the semi-logarithmic function. The ANN model maintains high accuracy through three inputs to predict the moisture content at different depths, with R^2 greater than 0.90 and RMSE less than 0.033 m^3/m^3. The RMSE values of the ANN model were between 38% to 65% lower than for the semi-logarithmic function. The predicted values using the semi-logarithmic function show a reasonable correlation with the measured values. The distribution of unfrozen moisture content is influenced by soil type (Anderson and Tice, 1972), and the soil types used to develop the semi-logarithmic model and ANN model are different, thus the semi-logarithmic model may need to be calibrated by soil type.

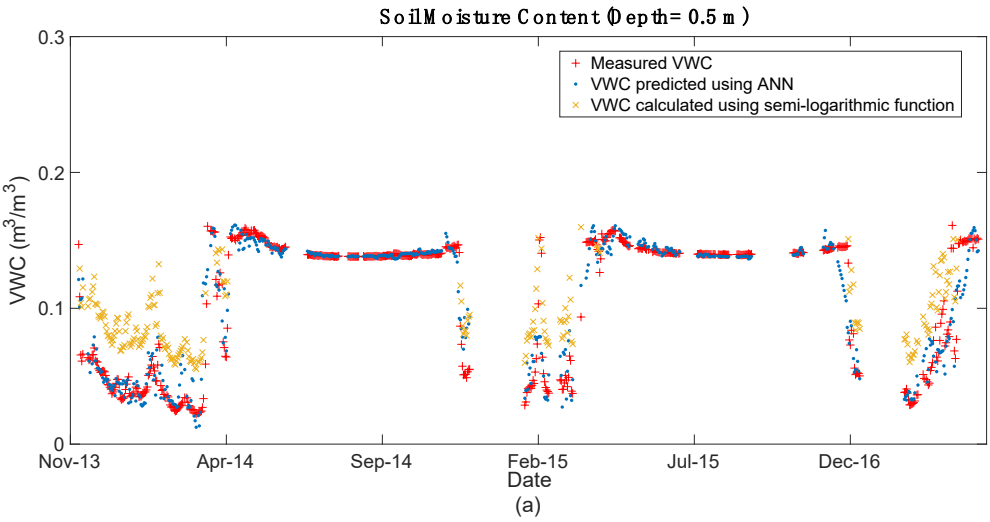

(a)

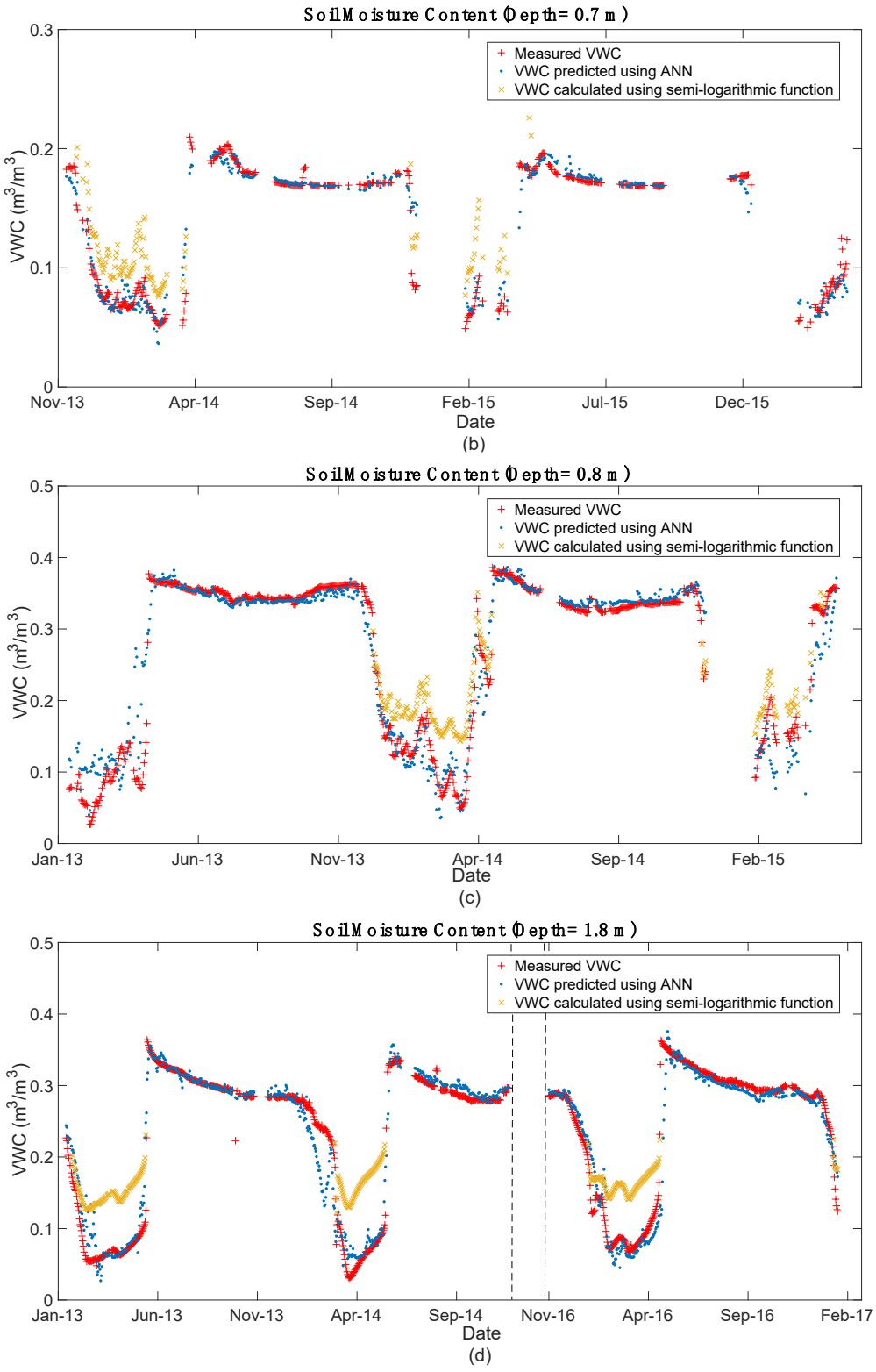

Figure 9-9: Average daily moisture content predicted results comparison at (a) 0.5 m, (b) 0.7 m, (c) 0.8 m, and (d) 1.8 m

Table 9-6: Moisture content prediction performance comparison between ANN and the statistical model

Depth (m)	ANN model		$W_{uf} = 0.911 + 0.634W_0 - 0.552ln\|T\| - 0.067W_0ln\|T\|$(Teltayev & Suppes, 2019)	
	R^2	RMSE (m^3/m^3)	R^2	RMSE (m^3/m^3)
0.50	0.90	0.015	-1.37	0.040
0.70	0.93	0.013	-1.10	0.035
0.80	0.91	0.033	0.32	0.053
1.80	0.93	0.027	-4.41	0.078

9.5.3. Limitation of the Proposed ANN Model

The ANN model predicts pavement temperature and moisture content in base and subgrade layers simultaneously through three parameters and shows higher accuracy than the existing models. The three parameters used, namely air temperature, depth and DOY, are readily available. This greatly increases the generality of the model. This study shows that the ANN model could be a powerful approach for pavement temperature and moisture content prediction. However, the current ANN model developed in this study is only trained on the data collected from the IRRF test road and only works on the IRRF test road. Meanwhile, the ANN model has only been trained for one pavement structure, one GBC type and one subgrade soil type, thus the number of layers and soil properties were not taken into account. If the ANN model can be trained with data collected from other pavements (including more different pavement structures and soil types), more parameters, such as the number of layers and soil parameters, can be used as input parameters and improve the generality of the ANN model. However, such an expansive data set is not available. If the pavement temperature and moisture content measurements, and environmental factors are available for other locations, the ANN model could be developed to predict the pavement temperature and moisture content. In different climatic regions and pavement structures, different parameters, such as precipitation, solar

radiation, etc., may be required to predict pavement temperature and moisture. But this also provides more choices for future model selection. Even the two aforementioned existing models are still inseparable from field-measured data and field corrections, especially for moisture content that is highly dependent on soil type.

9.6. CONCLUSIONS

The ANN model was trained to predict pavement temperature and moisture content within the base and subgrade layers simultaneously through three input parameters. Data collected from the IRRF test road from January 2013 to January 2018 were used, and the environment input parameter, air temperature, was collected from the closest weather station. Three algorithms – including Levenberg-Marquardt, Bayesian regularization, and Scaled conjugate gradient backpropagation – were then implemented for model training. The model with the highest R was kept, and R^2 and RMSE for pavement temperature and moisture content prediction were calculated, respectively. The Bayesian regularization model showed the highest R^2 and lowest RMSE, so its results were compared with two other existing models for pavement temperature prediction and moisture content prediction, respectively.

It was found that the ANN model can improve the R^2 values by 2% to 40% and decrease RMSE values by 58% to 72% for predicting daily average pavement temperature within the base and subgrade layers, compared to the statistical model proposed by Heydinger (2003b). The semi-logarithmic function (Teltayev and Suppes, 2019) only works when the initial moisture content is available and the pavement temperature is negative, and overestimated the moisture content of the IRRF test road, resulting in negative R^2 values. The ANN model improved the quality of the daily moisture content predictions within the base and subgrade layers, with R^2 greater than 0.90 and RMSE less than 0.033 m^3/m^3.

The resilient modulus of the pavement is influenced by the pavement temperature and moisture content, so the accurate prediction of pavement temperature and moisture content within the base and subgrade layers can, in turn, improve pavement design and management. Based on the results of this work, the ANN approach can be a robust method for simultaneous pavement temperature and moisture content prediction at various depths.

CHAPTER 10.CHANGES IN STRUCTURAL CAPACITY AFTER FIVE YEARS OF OPERATION

This section has been published as Huang, Y., Moghaddam, T. B., Hashemian, L. and Bayat, A., 2023. Structural Capacity of Sections Constructed with Different Waste and Recycled Embankment and Insulation Materials at the Integrated Road Research Facility Test Road after Five Years of Operation. Transportation Research Record, 03611981231159874.

10.1.ABSTRACT

The Integrated Road Research Facility test road was constructed in 2012 to study the application of waste and recycled materials in road construction in cold regions. Bottom ash (BA) and polystyrene board were used in test sections as insulation materials. Tire-derived aggregate (TDA) from passenger and light-truck tires (PLTT), off-the-road (OTR) tires, and a mixture of TDA from PLTT and soil were used as embankment fill materials in three additional test sections. Two control sections were used to evaluate the performance of the test sections. To compare the long-term impact of these materials on the load-bearing capacity of the pavement, falling weight deflectometer (FWD) tests were conducted after five years of operation. FWD data were used to back-calculate the subgrade modulus, effective modulus, and effective structural number. It was found that although embankments backfilled with TDA from PLTT and OTR gave an initial improvement in the load-bearing capacity of the pavement, a significant loss in load-bearing capacity of pavements with TDA embankments was observed after five years. In contrast, the test section with an embankment backfilled with a mixture TDA from PLTT and soil performed close to the control section, and no significant loss in load-bearing capacity was observed during this study. The test section insulated with polystyrene showed lower load-bearing capacity and a higher loss in load-bearing capacity

after five years of operation. However, the test section insulated with BA performed close to the control section and had a lower loss in load-bearing capacity than the control section.

Keywords: tire-derived aggregate, bottom ash, polystyrene board, falling weight deflectometer, and load-bearing capacity

10.2. INTRODUCTION

Pavement structures in cold regions such as Canada, which are exposed to extremely low temperatures in winter, freeze–thaw cycles, and frost heave, often show premature failure, low lifespan, and high maintenance costs, among other issues (Salem, 2004; Tighe et al., 2006). Road performance is mainly affected by environmental factors: a study conducted by Dore´ et al. (2005) showed that, considering environmental factors and traffic loading, up to 70% of pavement deterioration is caused by environmental factors. Thus, the performance of pavement structures in cold regions cannot be fully correlated with studies done in warm or moderate regions (Hashemian and Bayat, 2016). The Integrated Road Research Facility (IRRF) test road was constructed in 2012 in Edmonton, Alberta, to investigate the application of waste and recycled materials as embankment backfill and insulation layers in cold regions. Edmonton is located in a freezing climatic region. Based on air temperature data from 2012–2020, the average air freezing index (the sum of degree-days with a daily air temperature below 0°C during a given time period) during the freeze–thaw period was 1177°Cday at the IRRF test road. Similarly, the average air thawing index (sum of degree-days above 0°C for the air temperature during the freeze–thaw period) was 662°Cday over the same time period (Huang et al., 2021; National Snow and Ice Data Center, 2022).

In the pavement sections designed to test different insulation materials, extruded polystyrene board and bottom ash (BA) have been studied as insulation layers at the IRRF test road. Polystyrene board is a traditional insulation material and has been used since 1967 to protect

pavement structures against frost damage (Penner, 1967). Several studies have shown that polystyrene boards can reduce thaw depth and protect the subgrade from frost heave (Huang et al., 2021; Haghi et al., 2014; Tatarniuk and Lewycky, 2011). BA is one by-product of coal combustion. As of 2019, 36% of electricity in Alberta was generated from coal, Alberta still produces a considerable amount of BA every year (*Provincial and Territorial Energy Profiles – Alberta*, 2019). Previous studies have shown that the physical properties of BA make it a high-quality base material (Forteza et al., 2004; López et al., 2015). BA acts as an insulation layer to protect the subgrade from frost in winter (Huang, 1990; Huang et al., 2021; Haghi et al., 2014). Haghi et al. (2014, 2016, 2018, 2019) found that polystyrene and BA protected the subgrade layer from frost. However, the polystyrene layer led to higher temperatures in hot mix asphalt (HMA) and base layers during summer and lower HMA and base layers temperatures during winter (Haghi et al., 2014). Analysis of falling weight deflectometer (FWD) test results one year after the completion of the construction of the IRRF test road showed that the IRRF test section insulated with BA exhibited a load-carrying capacity similar to the control section (CS; without insulation), while the polystyrene section showed a significant reduction in the load-bearing capacity of the pavement (Haghi et al., 2016). Furthermore, the section insulated with BA showed similar viscoelastic behavior as the CS; however, the pavement insulated with polystyrene was more prone to damage in summer because of the higher HMA temperature (Haghi et al., 2019). Huang et al. (2021) compared the pavement temperature and moisture content six years after the completion of road construction. The researchers found that the pavement insulated with polystyrene showed less moisture variation than pavement insulated with BA; however, again the polystyrene section was shown to have a much lower base layer temperature than the CS in winter, which may make the polystyrene section more prone to low-temperature damage. While these initial

results have been published, there is still a lack of long-term results on the effect of polystyrene and BA insulation layers on the load-bearing capacity of pavement in cold regions.

Monitoring also continues at several test sections used to evaluate the performance of tire-derived aggregate (TDA) from waste tires as an embankment fill material. Millions of tires are disposed of every year, and these tires pose many health risks, including acting as mosquito breeding sites, being fire hazards, and more (Alberta Recycling Management Authority, accessed July 13, 2022). In Alberta, 131.3 million scrap tires have been recycled since 1992, and 53 million tires have been processed into TDA for civil engineering projects since 1996 (Alberta Recycling Management Authority, accessed 2022). In 2020/2021, 64,881 tonnes of tires were recycled, including 4099.7 tonnes of passenger and light-truck tires (PLTT), designed for use on passenger cars, light trucks, and multipurpose passenger vehicles, and 450.4 tonnes of off-the-road (OTR) tires, designed for use in construction, road building, forestry, mining, oil exploration, and other industries (Alberta Recycling Management Authority, accessed July 13, 2022; Alberta Recycling Authority, accessed November 19, 2022). TDA derived from PLTT and OTR has been used as a lightweight, free-draining fill embankment material in the IRRF test road. Visual inspection of samples during TDA production showed that the TDA made from PLTT consisted of mostly thin, plate-like granules, while the TDA produced from OTR tires gave granules that were thicker and mostly irregular in shape. Nassiri et al. (2013) used FWD test results to investigate the uniformity of the subgrade layer containing the TDA layers after construction. Meles et al. (2014) studied the compression behavior and performance of TDA as an embankment fill material for highway embankments and found that TDA derived from PLTT is more compressible than TDA derived from OTR tires and TDA–soil mixtures. Hashemian and Bayat (2018) investigated the load-bearing capacity of pavements with TDA embankments after two years of construction. Although the pavements with TDA embankments showed a lower resilient modulus, their load-

bearing capacity was greater than that of a CS constructed without a TDA embankment. Kang et al. (2021) modeled TDA from OTR tires under compression using the discrete element method and found that it had a high elastic modulus in warmer temperatures, and a larger strain was observed in summer than in winter. However, the difference between the summer and winter strain values was only 0.4%. Although these studies have been conducted to analyze the performance of TDA materials as embankment backfill, the long-term effects of TDA embankments on the bearing capacity of the pavement after five years of operation have not been documented.

The main objective of this study is to investigate how the use of (i) polystyrene and BA as insulating layers and (ii) TDA derived from PLTT, OTR, and PLTT–soil mixtures as embankment fill affect the load-bearing capacity of roads in cold regions after five years of operation. FWD testing was conducted at the IRRF test road on August 18 2015 and August 20 2020. These data were used to back-calculate the resilient modulus of the subgrade, the effective modulus of the pavement, and the structural number. Temperature and moisture content distribution in the base and subgrade layers were available for the same days. The results of the back-calculation were analyzed using the adjacent CS as a baseline.

10.3. INTEGRATED ROAD RESEARCH FACILITY TEST ROAD

The IRRF test road was constructed as part of a program launched to study the potential for use of recycled tires and waste materials in road construction and was completed in October 2013. The road opened to public traffic in the middle of October 2015. The IRRF test road is a 500-m, two-lane access road to the Edmonton Waste Management Center (EWMC). The IRRF test road is divided into two parts. The first portion was designed to study the effect of cold weather and insulation materials. The other was designed to study the use of TDA from waste tires as a lightweight embankment fill. There are two CSs—constructed without the use of any

recycled or waste materials—to evaluate the performance of the test sections (insulation and embankment fill), as shown in Figure 10-1. Data from the data logger at the IRRF test road are sent to the University of Alberta for analysis.

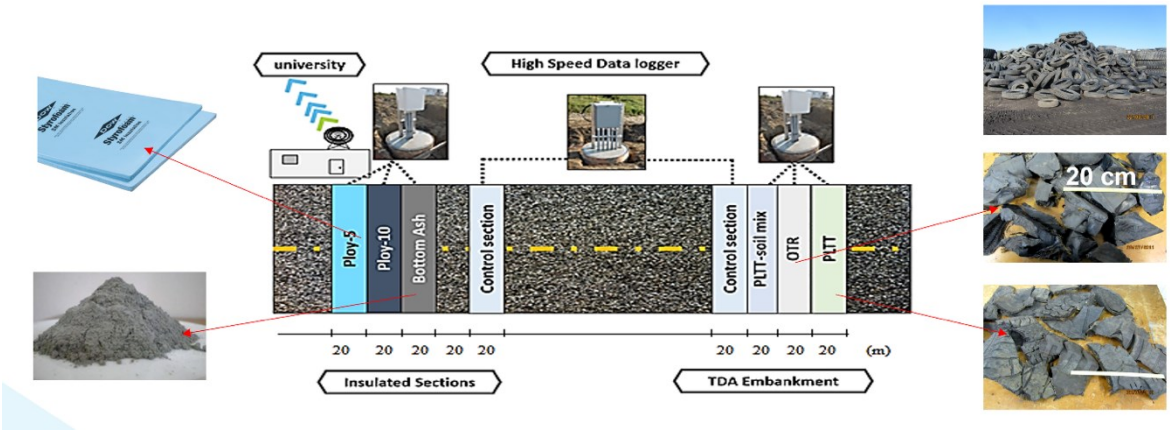

Figure 10-1: Test and control sections in the Integrated Road Research Facility test road

Note: Poly-5 = 0.05-m thick polystyrene board; Poly-10 = 0.10-m thick polystyrene board; PLTT = passenger and light-truck tires; OTR = off-the-road; TDA = tire-derived aggregate.

As shown in Figure 10-2, the pavement consisted of a 0.25-m HMA layer on a 0.45-m granular base course (GBC). A weigh-in-motion (WIM) system was installed to record traffic information, and according to WIM data from 2016 to 2019, an average of 368 garbage trucks per day drive on the test road. The test road is divided into eight sections of 20 m: two CSs (CS1 and CS2), three sections with tire embankment, and three sections with different insulation layers (Figure 10-2). In CS2, CS650 time domain reflectometers (TDRs; Campbell Scientific) are used to collect temperature and moisture content data in the GBC and subgrade layers, and a 109 AM-L thermistor (installed at a depth of 0.09 m) is used to monitor HMA layer temperature. Five TDRs were installed in the GBC and subgrade layers of the CS2 at depths of 0.50, 0.70, 0.80, 1.80, and 2.70 m below the road surface. Meanwhile, thermistors installed in three TDA embankment sections and two insulation sections are used to monitor the temperature of the base and subgrade layers.

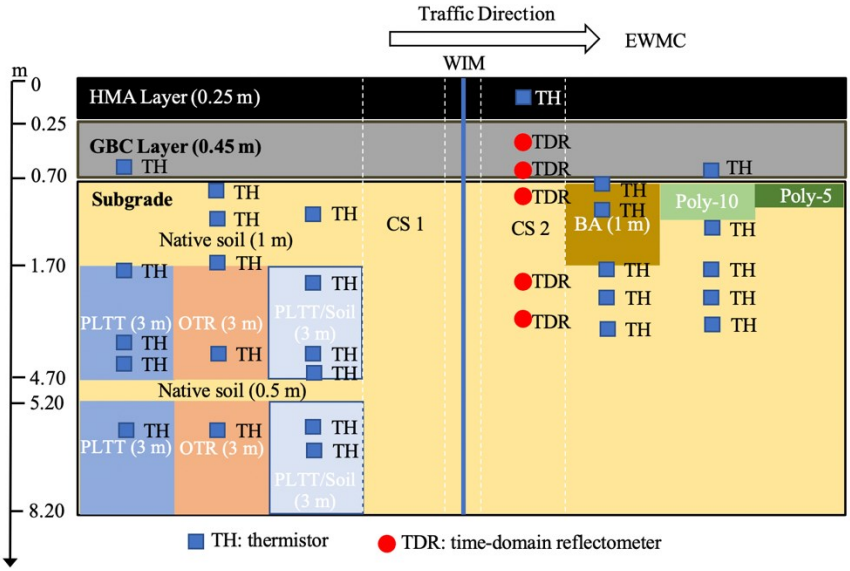

Figure 10-2: Cross-section of the Integrated Road Research Facility test road showing test and control sections and sensor placement

Note: EWMC = Edmonton Waste Management Center; WIM = weigh-in-motion; HMA = hot mix asphalt; GBC = granular base course; CS = control section; Poly-5 = 0.05-m thick polystyrene board; Poly-10 = 0.10-m thick polystyrene board; PLTT = passenger and light-truck tires; OTR = off-the-road.

To test the performance of recycled tires as pavement embankment materials, TDA derived from PLTT, TDA derived from OTR, and a mixture of TDA from PLTT and soil were used as embankments in three sections of the test road (Figure 10-2). During construction, the PLTT and soil were mixed onsite in a volume ratio of 50:50. All TDA backfill materials were wrapped in a nonwoven geotextile, so they would not mix with the surrounding soil. To prevent internal heating of the TDA, a 0.5-m layer of native soil was placed between the two 3-m TDA layers. After three years of monitoring, no internal heating was observed in the tire layers (Hashemian and Bayat, 2018). At that time, a 1-m layer of native soil was placed on top of the TDA layer.

Three sections containing insulation layers were also constructed at the IRRF test road. In the first insulated test section, a 1-m layer of BA was placed between the GBC and subgrade layers (with the BA wrapped in a geotextile material to avoid mixing with native soil). In the two other sections, 0.10-m thick polystyrene board (Poly-10) and a 0.05-m polystyrene board (Poly-5) were placed between the GBC and subgrade layers.

Additional details related to the IRRF test road construction and configuration are available in the literature (Nassiri et al., 2013; Haghi et al., 2014; Hashemian and Bayat, 2016, 2018; Haghi et al., 2018, 2019).

10.4. FALLING WEIGHT DEFLECTOMETER TESTING

FWD testing has been used extensively at the IRRF test road. The advantage of FWD testing is that it is nondestructive. The FWD test simulates the dynamic loading of a moving vehicle and records the deformations of the road surface at various distances from the load plate. A study by Tholen et al. (1985) indicates that FWD testing result was consistent with actual pavement loading and behavior, and can be applied to a wide range of pavements. FWD results have been commonly used to backcalculate the structural bearing capacity of pavement, one of the main factors that determine pavement performance. A pavement with a lower structural bearing capacity does not provide adequate support for traffic loading. In the case of inadequate support, the asphalt layer bends more, so a lower road bearing capacity leads to a higher risk of crocodile cracks and lateral cracks, and a shorter pavement life (Dong and Huang, 2015).

The subgrade modulus is dominated by subgrade moisture content. The IRRF test road is located in a region where pavements undergo freeze–thaw cycles and weakening of the subgrade during the spring thaw every year. In winter, as the temperature drops, the moisture inside the soil freezes. Then, in early spring, the pavement temperature begins to rise (from top to bottom), and water accumulates in the subgrade because of the low permeability of the sublayer. The soil moisture content is higher at this time than at any other time in the year, resulting in a low soil modulus. According to previous observations at the IRRF test road, excess water in the subgrade was drained in summer (Haghi et al., 2016; Hashemian and Bayat, 2018). Therefore, the FWD test results obtained in summer were deliberately chosen for this study, to exclude the influence of soil water accumulation on the results. FWD testing has been

conducted monthly at the IRRF test road, with similar results obtained when comparing FWD data collected on other dates. Thus, for ease of comparison and to reduce the amount of data presented, only one test per year was selected to give representative results.

FWD data were collected on all sections of the IRRF test on August 18 2015 and August 20 2020. These data were used to determine the loss in load-bearing capacity of the pavement sections after five years of use. A FWD with a nine-sensor configuration (0, 200, 300, 450, 600, 900, 1200, 1500, and 1800 mm from the center of the load plate) was used with three stress levels (26.7, 40.0, and 53.5 kN). The load was applied every 5 m on the inner and outer wheel paths. To compare the FWD test results, all deflections were normalized to a target load of 40.0 kN. All deflections were checked based on the method reported by Xu et al. (2002) and no irregularities were identified.

10.5. ENVIRONMENTAL FACTORS

Pavement temperature and moisture content collected on August 18 2015 and August 20 2020 from TDRs and thermistors embedded in the test road were compared. As shown in Figure 10-3 (a), in 2020, the temperature of the HMA and GBC was 2.7°C higher than that recorded in 2015, and the difference in subgrade temperature was about 1.3°C. The HMA layer temperature recorded at a depth of 0.09 m was used to adjust the maximum deflection (D_0) directly below the load plate. The temperature of the HMA layer was 22.95°C on August 18 2015 and 25.69°C on August 20 2020. Although a temperature difference of 1.3°C in the subgrade layer was observed in the CS (CS2), the differences in temperature of the subgrade layer were smaller in the BA and Poly-10 sections (0.5°C and 0.1°C, respectively). The difference in subgrade layer temperature in the three tire sections was small and varied from 0.06°C to 0.46°C. The temperature of the subgrade layer of the OTR section (above 3 m) was higher than those of the other two tire sections. Although the moisture content affects the

subgrade modulus (Bohra et al., 1999), the measurements of moisture content were very close for the two days when FWD testing was done (Figure 10-4), and thus the effect of the moisture content can be ignored.

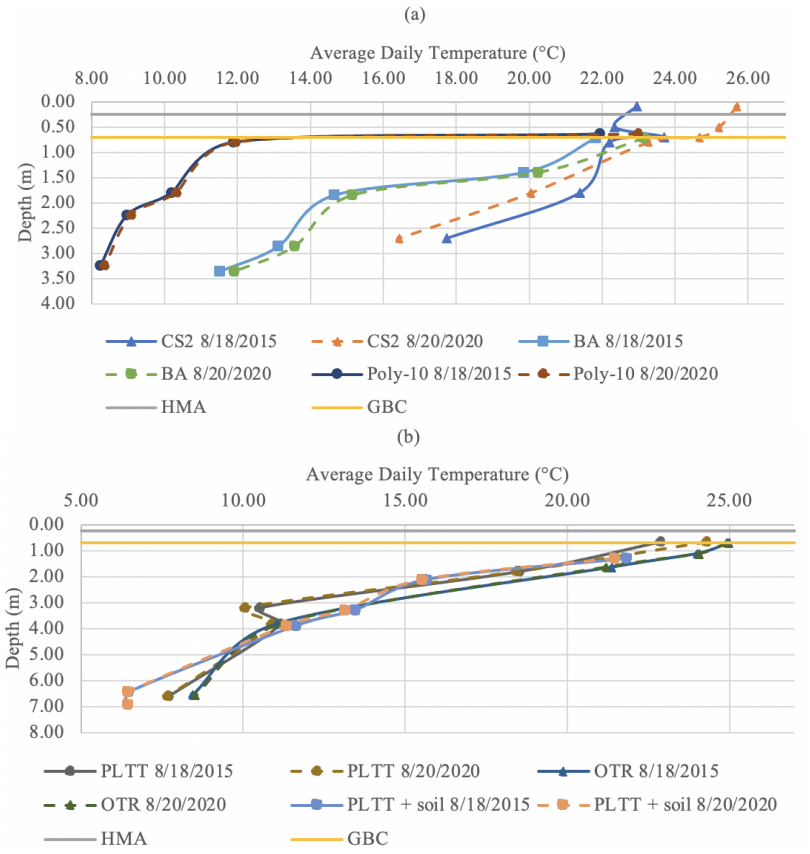

Figure 10-3: Variation in pavement temperature with depth in the (a) insulation section and (b) tire section

Note: CS = control section; Poly-10 = 0.10-m thick polystyrene board; BA = bottom ash; HMA = hot mix asphalt; GBC = granular base course; PLTT = passenger and light-truck tires; OTR = off-the-road.

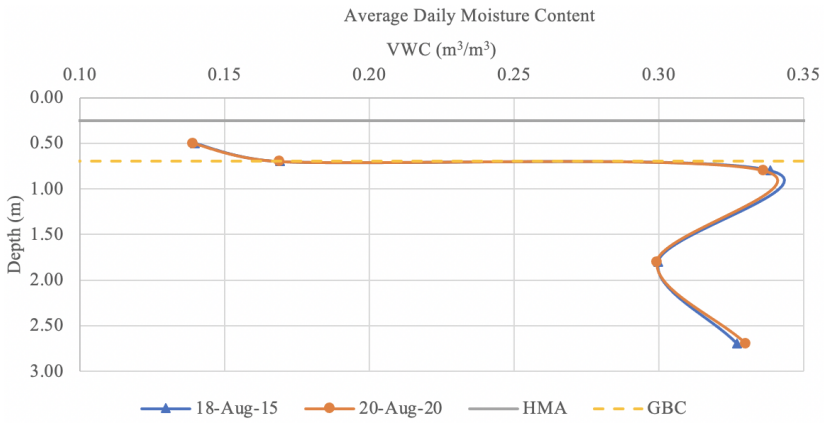

Figure 10-4: Pavement moisture content with depth for CS2

Note: CS = control section; HMA = hot mix asphalt; GBC = granular base course; VWC = volumetric water content.

10.6. RESULTS AND DISCUSSION

10.6.1. Deflection Bowls

On August 20 2020, the HMA layer temperature was 25.69°C. Figures 10-5 and 10-6 compare the FWD results of the deflection bowls for all sections tested. The deflection of the pavement with the TDA derived from PLTT and soil embankment was similar to the CS (CS1) (Figure 10-5). However, FWD results for the sections backfilled with TDA from PLTT and TDA from OTR tires showed less deflection than the CS when the distance between the geophone and load plate was less than 900 mm. In the insulation sections, the FWD test results indicate that the test section insulated with BA performed similarly to the CS (CS2). However, the two sections insulated with polystyrene showed higher deflection than the CS. The Poly-10 section also showed higher deflection than the Poly-5 section when the load plate and geophone were in the same spot (0 mm separation).

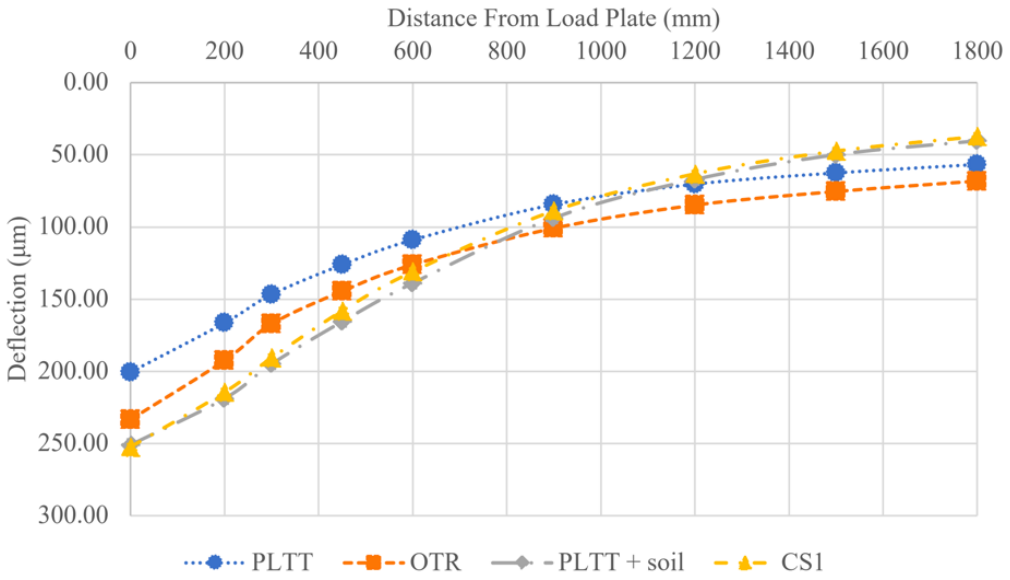

Figure 10-5: Deflection measured by all nine geophones for tire embankment sections backfilled with tire-derived aggregate (TDA) from passenger and light-truck tires (PLTT), TDA from off-the-road (OTR), and PLTT/soil mixture, as well as the control section (CS1) August 20 2020

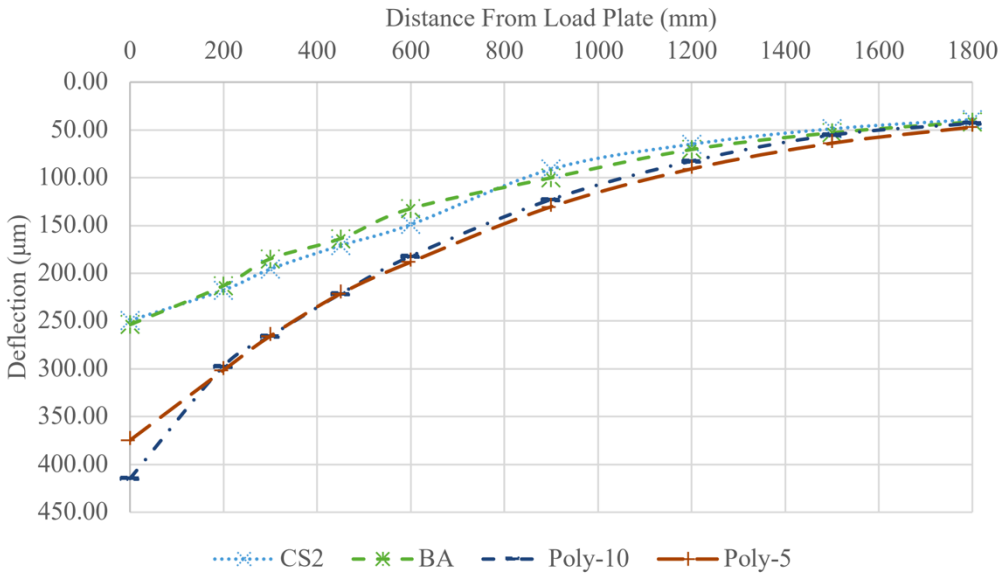

Figure 10-6: Deflection measured by all nine geophones for sections containing different insulation layers (bottom ash, 10 cm polystyrene [Poly-10], and 5 cm polystyrene [Poly-5], as well as the control section) for August 20 2020

Note: CS = control section; BA = bottom ash.

10.6.2. Maximum Deflection

Figure 10-7 shows the maximum deflection (D_0) measured directly below the load plate and the HMA layer temperature for each day data was collected. All D_0 values showed the same trend in 2015 and 2020. For the embankment sections, the section with the embankment backfilled using TDA derived from PLTT had the lowest D_0 value, while the CS (CS1) had the highest D_0 value. The section backfilled with the mixture of TDA from PLTT and soil performed very close to the CS. Compared to the D_0 values observed on August 18 2015, D_0 increased by 47%, 61%, 32%, and 36% for the TDA from PLTT, TDA from OTR, TDA from PLTT and soil mixture, and CSs, respectively. The highest change of D_0 was observed for the test section with the embankment backfilled with TDA from OTR.

For the insulation sections, the section insulated with Poly-10 had the highest D_0 values in 2015 and 2020. The performance of the two CSs was very similar. The performance of the section insulated with BA was very close to that of the CS. Higher D_0 values were observed in 2020 for the insulation sections. Compared to the values in 2015, D_0 increased by 32%, 22%, 73%,

and 60% for the CS2, BA, Poly-10, and Poly-5 sections, respectively. The greatest increase in deflection was observed for the pavement sections insulated with polystyrene board. There is a high correlation between the D_0 value and the temperature of the HMA layer (Haghi et al., 2016; Hashemian and Bayat, 2018). Polystyrene board leads to a higher HMA layer temperature in summer and lower HMA layer temperature in winter (Huang et al., 2021), and thus increases the likelihood of pavement damage (Haghi et al.,, 2019; Huang et al., 2021). This fits with the higher deflection values observed for the pavements insulated with polystyrene board after five years of operation. In 2020, the maximum deflection (D_0) of the sections insulated with polystyrene was also much higher than the BA and CS, which could be related to the reduction in load-bearing capacity of the sections insulated with polystyrene.

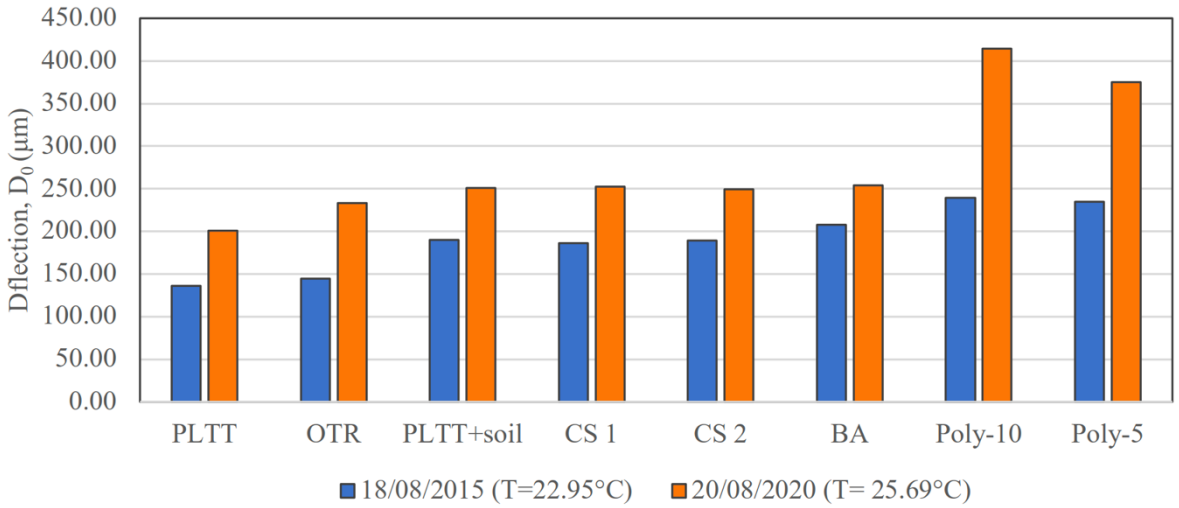

Figure 10-7: Maximum deflection D_0 measured 0 mm from the load plate

Note: CS = control section; Poly-10 = 0.10-m thick polystyrene board; Poly-5 = 0.05-m thick polystyrene board; BA = bottom ash; PLTT = passenger and light-truck tires; OTR = off-the-road.

Figure 10-8 indicates the maximum deflection (D_9) at 1800 mm from the load plate and the HMA layer temperature. For the three sections with embankments constructed using TDA materials, all test sections showed higher D_9 values than the CS (CS1). For the three insulation sections, the section insulated with BA showed the highest D_9 values in 2015; however, the sections insulated with 10 cm polystyrene and 5 cm polystyrene showed higher D_9 values in

2020 than the BA and CSs. Compared to the D_9 values measured in 2015, the 2020 D_9 values increased by 20%, 21%, 1%, 12%, 6%, 5%, 19%, and 23% for the PLTT, OTR, PLTT/soil, CS1, CS2, BA, Poly-10, and Poly-5 sections, respectively. The D_9 values measured in the PLTT, OTR, Poly-10, and Poly-5 sections increased more than that of the CSs after five years of operation. However, the BA section showed a similar percentage of increased D_9 values as that of the CS. The test section with the embankment backfilled with a mixture of TDA from PLTT and soil was found to be the most stable section, with the lowest change in deflection (D_9) after five years.

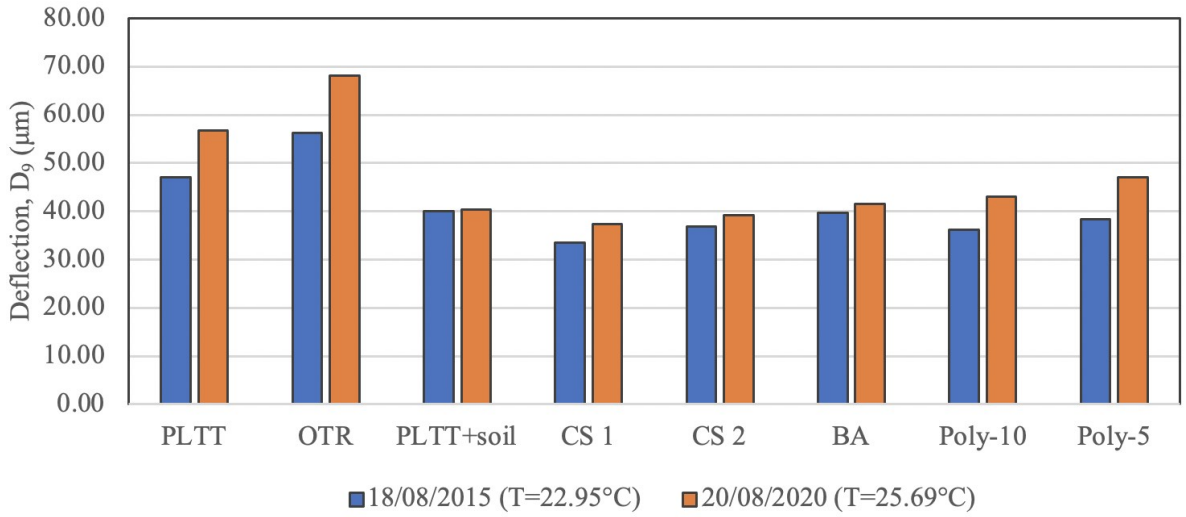

Figure 10-8: Maximum deflection D_9 measured 1800 mm from the load plate

Note: CS = control section; Poly-10 = 0.10-m thick polystyrene board; Poly-5 = 0.05-m thick polystyrene board BA = bottom ash; PLTT = passenger and light-truck tires; OTR = off-the-road.

10.6.3. Back-Calculated Subgrade Modulus

The subgrade modulus was back-calculated from FWD data according to the American Association of State Highway and Transportation Officials (AASHTO) 1993 pavement design guide (AASHTO, 1993). Equation 10-1 was expressed as follows:

$$M_R = \frac{0.24 \times P}{D_r \times r} \qquad \text{Equation 10-1}$$

where M_R is the resilient modulus of the subgrade (kg/cm^2), P is the target load (kg), D_r is the deflection at a distance r from the loading plate (cm), and r is the distance of the selected geophone from the loading plate (cm).

To estimate the subgrade modulus, the deflection used should be far enough away from the load plate so that it is not affected by other pavement layers. According to the AASHTO 1993 pavement design guide (AASHTO, 1993), the distance between the loading plate and the selected geophone should be higher than the value of $0.7 \times a_e$, with a_e (the radius of the stress bulb at the subgrade–pavement interface [cm]) calculated as in Equation 10-2:

$$a_e = \sqrt{[a^2 + (D\sqrt[3]{\frac{E_P}{M_R}})^2]} \qquad \text{Equation 10-2}$$

where a is the load plate radius (cm), D is the total thickness of the pavement layers above the subgrade (cm), and E_P is the effective modulus of the pavement above the subgrade (kg/cm^2). Based on the results of this calculation, D_9 (with a separation of 1800 mm) meets this requirement for all sections.

Table 10-1 presents the back-calculated subgrade modulus for all the test sections and the change in subgrade modulus after five years of operation. As expected, the test sections with the embankments composed of TDA derived from PLTT and OTR, which had higher values of D_9, showed a lower subgrade modulus in 2015 and 2020 than the section with the embankment backfilled with a mixture of TDA derived from PLTT and soil and the CS (CS1). These two sections with TDA-derived embankments also exhibited high rates of subgrade modulus loss, 17% in the section with TDA derived from PLTT and 18% in that with TDA from OTR. These results show that after five years of operation, these two sections with TDA embankments (OTR and PLTT) have undergone a larger loss of subgrade modulus than the CS (CS1), which may lead to a high degree of road settlement, with the road section consisting of

TDA embankments (OTR and PLTT) prone to damage. The test section with the embankment backfilled with a mixture of TDA from PLTT and soil had a lower subgrade modulus after five years than the CS, and the subgrade modulus loss was much smaller, at 1%.

Table 10-1: Back-calculated subgrade moduli for the various IRRF test road sections.

	TDA Embankment Sections				**Insulated Sections**			
	PLTT	**OTR**	**PLTT/soil**	**CS1**	**CS2**	**BA**	**Poly-10**	**Poly-5**
18/08/2015 (MPa)	113.31	94.91	133.36	159.39	144.60	134.54	147.40	139.20
20/08/2020 (MPa)	94.08	78.19	132.27	142.88	136.11	128.23	123.77	113.26
Change Ratio(%)	17	18	1	10	6	5	16	19

Note: TDA = tire-derived aggregate; PLTT = passenger and light-truck tires; OTR = off-the-road; CS = control section; BA = bottom ash; Poly-10 = 0.10-m thick polystyrene board; Poly-5 = 0.05-m thick polystyrene board.

The change in subgrade modulus is expected to be related to the effect of the thermal insulation material used to protect the subgrade. The results indicate that the subgrade modulus and change ratio of the test section insulated with BA were similar to that of the CS (CS2), so the influence of the BA layer on the subgrade modulus was insignificant. Although polystyrene board also proved to be an effective insulation material in limiting the frost above the subgrade, the test sections insulated with polystyrene did show high subgrade modulus loss after five years of the test road being in operation. In 2015, when the test road opened, the subgrade moduli of the test sections insulated with Poly-10 and Poly-5 were similar to the subgrade modulus of the CS (CS2). However, by 2020, the subgrade moduli of the test sections insulated with Poly-10 and Poly-5 had decreased by 16% and 19%, respectively, resulting in a lower subgrade modulus than that of the CS. With respect to the subgrade moduli, BA performed better than polystyrene board.

10.6.4. Back-Calculated Effective Modulus of Pavement

The method given in AASHTO 1993 (AASHTO, 1993) was applied to back-calculate the effective modulus of the pavement, as in Equation 10-3:

$$D_0 = 1.5pa\left\{\frac{1}{M_r\sqrt{1+(\frac{D}{a}\sqrt[3]{\frac{E_P}{M_r}})^2}}+\frac{\left[1-\frac{1}{\sqrt{1+(\frac{D}{a})^2}}\right]}{E_P}\right\} \quad \text{Equation 10-3}$$

In this equation, D_0 is the deflection measured directly below the load plate (cm) (adjusted to a standard temperature of 20°C before calculation), p is the load plate pressure (kg/cm^2), a is the load plate radius (cm), M_R is the subgrade modulus (kg/cm^2), D is the total thickness of the pavement layers above the subgrade (cm), and E_p is the effective modulus of all pavement layers above the subgrade (kg/cm^2).

Table 10-2 summarizes the effective moduli of the pavement for all sections. The effective moduli of the two CSs (CS1 and CS2) showed a reduction of 33% and 32%, respectively, over the five years (2015–2020). The reduction in effective moduli was attributed to deterioration caused by environmental factors and traffic loading. Although the test sections with embankments backfilled with TDA derived from PLTT and OTR had a higher effective modulus than the CS (CS1) in 2015, there was a greater reduction in effective modulus than that of the CS (CS1) in 2020, 41% and 50%, respectively. This indicates that backfilling the embankment with TDA from PLTT and OTR results in a larger reduction in effective modulus than in the CS. However, the effective modulus of the pavement with the embankment backfilled with a mixture of TDA from PLTT and soil was similar to that of the CS. Although the effective modulus of the test section with TDA from PLTT and soil was not as high as those

of the other two test sections backfilled with TDA in 2015, no significant decrease in effective modulus was observed in the test section with TDA from PLTT and soil in 2020.

Table 10-2: Back-calculated effective moduli of the pavement for the various sections.

	TDA Embankment Sections				Insulated Sections			
	PLTT	**OTR**	**PLTT /soil**	**CS1**	**CS2**	**BA**	**Poly-10**	**Poly-5**
18/08/2015 (MPa)	2163	2237	1121	1056	1080	971	758	798
20/08/2020 (MPa)	1270	1117	742	712	740	741	381	450
Change Ratio(%)	41	50	34	33	32	24	50	44

Note: TDA = tire-derived aggregate; PLTT = passenger and light-truck tires; OTR = off-the-road; CS = control section; BA = bottom ash; Poly-10 = 0.10-m thick polystyrene board; Poly-5 = 0.05-m thick polystyrene board.

The results in Table 10-2 show that the effective modulus of the BA section has the smallest decrease in the three insulated sections after five years of operation, while the Poly-10 and Poly-5 sections have much larger changes in effective modulus. In 2015, the effective modulus of the two sections insulated with polystyrene board was lower than that of the CS (CS2). After five years of operation of the IRRF test road, the effective modulus of the Poly-10 section had dropped by 50%, and in 2020, the ratio of the effective modulus of the Poly-10 section to the CS (CS2) was 0.51. The effective modulus of the Poly-5 section in 2020 was found to have decreased by 44% compared with that in 2015. This suggests that while both BA and polystyrene act as insulating layers to protect the subgrade, the polystyrene may result in a huge loss in effective modulus after many years of operation. The loss in load-bearing capacity in the Poly-10 and Poly-5 sections can be explained by two possible reasons. Firstly, the effective moduli of the test sections insulated with polystyrene were already lower in 2015 when the road was opened, so these sections insulated with polystyrene board were prone to traffic loading. Then, since the polystyrene board leads to higher HMA and base temperatures in summer and lower HMA and base temperatures in winter than the CS (AASHTO, 1993),

the test sections insulated with polystyrene are also more prone to damage in summer and winter. Thus, these results indicate that BA not only protects the subgrade from frost but also results in a much smaller loss in effective modulus than the polystyrene board.

10.6.5. Structural Number

The effective structural number of the different test and CSs can be calculated using the effective modulus, as in the method outlined in AASHTO 1993 (AASHTO, 1993). The structural number is calculated using Equation 10-4:

$$SN_{eff} = 0.0045D\sqrt[3]{E_P} \qquad \text{Equation 10-4}$$

where SN_{eff} is the effective structural number of the existing pavement, D is the total thickness of all pavement layers above the subgrade (cm), and E_P is the effective modulus of the pavement layers above the subgrade (kg/cm^2).

The effective structural number can be used to compare the total effect of the moduli of the different layers on the test and CSs and also be used as an indicator of how the TDA embankment and insulation layers influence the total structural capacity of the pavement. Table 10-3 shows that the sections with embankments backfilled with TDA derived from PLTT and OTR did have a higher structural bearing capacity of the pavement in 2015; however, the structural bearing capacity decreased faster and showed a higher change ratio than the CS (CS1). The section backfilled with a mixture of TDA from PLTT and soil performed similarly to the CS (based on analysis of the data in 2015 and 2020). The use of BA and polystyrene as insulation layers did reduce the structural number of the pavement; however, the sections insulated with Poly-10 and Poly-5 showed a much higher change ratio than the CS (CS2). Although the structural number of the BA section was lower than that of the CS (CS2) in 2015, in 2020, the structural number of the BA section was found to be similar to that of the CS, because of the low change ratio of the BA section.

Table 10-3: Structural numbers of the various sections.

	TDA Embankment Sections				Insulated Sections			
	PLTT	**OTR**	**PLTT/soil**	**CS1**	**CS2**	**BA**	**Poly-10**	**Poly-5**
18/08/2015	8.43	8.52	6.77	6.64	6.69	6.45	5.94	6.04
20/08/2020	7.06	6.76	5.90	5.82	5.89	5.90	4.72	4.99
Change Ratio (%)	16	21	13	12	12	9	21	17

Note: TDA = tire-derived aggregate; PLTT = passenger and light-truck tires; OTR = off-the-road; CS = control section; BA = bottom ash; Poly-10 = 0.10-m thick polystyrene board; Poly-5 = 0.05-m thick polystyrene board.

Long-term monitoring of the IRRF test road has been ongoing since the road opened to public traffic in 2015. Although the FWD test results for the test sections obtained in August 2015 and 2020 were different and the test sections insulated with Poly-10 and Poly-5 showed lower effective moduli than other sections after five years of operation, in 2020, the IRRF test road had only been open to traffic for five years. No visible damage was found in 2020. The long-term monitoring of the IRRF test continues and more research will be conducted to assess the effect of TDA and BA on the structural capacity after years of operation.

10.6.6. Analysis of Variance

Analysis of variance (ANOVA) was used to statistically evaluate the differences in structural capacity. A two-factor ANOVA without replication was applied to understand the significance of the inclusion of waste and recycled materials in the test sections in the subgrade modulus, effective modulus, and structural number for various sections. The significance level utilized in this analysis was 0.05. Table 10-4 presents the ANOVA results for the subgrade moduli (back-calculated from FWD data) for the different test sections. Taking the subgrade modulus of the TDA sections as an example, the value of F (10.426) was greater than the value of F-

crit (10.128), and the *p*-value (0.048) was smaller than 0.05. Thus, it can be concluded that the impact of TDA materials on the back-calculated subgrade moduli was significant. The same analysis procedure was repeated to analyze the effect of TDA and insulating material on the subgrade modulus, effective modulus, and structural number of the IRRF test road. The study found that, except for the insulated material having no significant effect on the subgrade moduli, the types of TDA had a significant effect on the subgrade moduli, effective moduli, and structural number, and the types of insulation materials had a significant effect on the effective moduli and structural numbers of the IRRF test road. Meanwhile, the time has no significant effect on the subgrade modulus of the insulated sections and the effective modulus of the TDA sections.

Table 10-4: Analysis of variance results for the integrated road research facility test road.

Calculated Parameter	Variables	TDA Sections			Insulated Sections		
		F	*P*-value	*F*-crit	*F*	*P*-value	*F*-crit
Subgrade Modulus	Material	10.4265	0.0483	10.1280	10.1103	0.0501	10.1280
	Time	48.7031	0.0048	9.2766	1.4137	0.3914	9.2766
Effective modulus	Material	12.6886	0.0378	10.1280	100.8154	0.0021	10.1280
	Time	5.6457	0.0945	9.2766	27.1064	0.0113	9.2766
Structural number	Material	29.0397	0.0125	10.1280	38.6677	0.0084	10.1280
	Time	13.3558	0.0306	9.2766	10.6001	0.0418	9.2766

Note: TDA = tire-derived aggregate.

10.7. SUMMARY AND CONCLUSIONS

The IRRF test road has been open to public traffic since mid-October 2015. The loss of bearing capacity because of the combined effect of environmental factors and five years of traffic loading (2015–2020) was monitored using a FWD for the test sections with different embankment and insulation materials as well as the CSs. To quantify the load-bearing capacity loss of the pavements, FWD data from tests conducted on the IRRF test road on August 18

2015 and August 20 2020 were analyzed. The subgrade modulus, effective modulus of the pavement, and effective structural number were back-calculated based on the maximum deflections D_0 and D_9. The results are summarized as follows.

- The temperature distribution of the insulation CS (CS2) on the two monitoring days showed that in 2020, the temperature of the HMA layer was 3°C higher than in 2015. Moisture content readings from the TDRs indicated that the moisture content of the base and subgrade layers was similar when FWD tests were conducted in 2015 and 2020.
- For the three test sections constructed with TDA embankments, the section with the embankment of TDA from PLTT showed the smallest maximum deflection D_0, followed by the section with TDA from OTR. However, after five years, it was found that D_0 increased by 47% for the test section with TDA from PLTT and increased by 61% for the test section with TDA from OTR. The D_0 values of the test section with the embankment backfilled with a mixture of PLTT and soil were close to that of the CS for both 2015 and 2020.
- For the test sections insulated with different materials, although the BA test section had a larger D_0 than the CSs in 2015, D_0 increased by 22% in 2020, which was lower than both CSs (32% for CS1 and 36% for CS2). The pavements insulated with polystyrene board showed a much higher D_0 in 2015 and a much higher change ratio in 2020. The D_0 measured in the Poly-10 test section increased by 73% from 2015 to 2020.
- The maximum deflection, D_9, was used to back-calculate the subgrade modulus. The embankment section filled with TDA from OTR tires showed the highest D_9 values, with an increase of 21% from 2015 to 2020. The embankment test section backfilled with a mixture of PLTT and soil performed similarly to the CS and showed the lowest change (1%) between 2015 and 2020.

- In 2015, the maximum deflection, D_9, of the three sections with different insulation layers was very close. However, the change ratio of D_9 was higher for the test sections insulated with polystyrene board (19% for the Poly-10 section and 23% for the Poly-5 section) from 2015 to 2020.
- The subgrade modulus was lower in the test sections with TDA embankments compared to the CS, and from 2015 to 2020 the PLTT and OTR sections showed high change ratios (17% and 18%, respectively). However, the change ratio for the test section with the embankment backfilled with a mixture of TDA from PLTT and soil section was 1% less than that of the CS. In the insulation sections, the test section insulated with BA had a similar subgrade modulus and change ratio as the CS (5% for BA, 10% for CS1, and 6% for CS2). Although the pavements insulated with polystyrene board showed a similar subgrade modulus to the CS in 2015, the subgrade modulus values were lower than the CS in 2020 because of much higher change ratios (16% for the Poly-10 section and 19% for the Poly-5 section).
- The effective modulus of the CSs dropped by 32% and 33% from 2015 to 2020. Each of the test sections with TDA embankments had a higher effective modulus than the CS in 2015 and 2020, and the change ratios for the embankment test sections filled with TDA from PLTT and TDA from OTR tires were as high as 41% and 50% from 2015 to 2020. However, the effective modulus of the test section with the embankment backfilled with a mixture of TDA from PLTT and soil only decreased by 34% in the same five years. The inclusion of insulation materials in the test sections led to a lower effective modulus, particularly the Poly-10. The test section insulated with Poly-10 showed the highest change ratio in the effective modulus (50%) after five years of operation. However, in comparison, the effective modulus of the BA section only dropped by 24% from 2015 to 2020.

- The structural numbers of these two CSs both dropped by 12% from 2015 to 2020. All the test sections with TDA embankments showed a higher effective structural number than the CS. Similarly, they all showed a higher loss in structural capacity from 2015 to 2020 (16% for the test section with TDA from PLTT, 21% for the test section with TDA from OTR tires, 13% for the test section backfilled with a mix of TDA from PLTT and soil, and 12% for the CS).
- The inclusion of insulation layers reduced the structural capacity of the pavement. All the test sections with insulation layers, regardless of the material, showed a lower structural number than the CS in 2015 and 2020. After five years, the pavements with polystyrene boards showed a high change ratio (21% for the Poly-10 section and 17% for the Poly-5 section). However, for the BA section, the structural number only decreased by 9% from 2015 to 2020.

Based on these results, it can be concluded that although the embankments with TDA from PLTT and TDA from OTR initially improved the load-bearing capacity and structural capacity of the IRRF test road compared to the CS, these embankments resulted in a higher change ratio of the subgrade modulus, effective modulus, and structural number than the CS. In contrast, the section with an embankment backfilled with a mixture of TDA from PLTT and soil performed close to the CS, with no significant drop in load-bearing or structural capacity observed after five years of operation. Thus, if TDA from PLTT is used as an embankment fill material, mixing it with soil is recommended based on these results.

With respect to the evaluation of polystyrene board and BA insulation layers on road performance, a significant drop in the load-bearing and structural capacity was observed for the pavements constructed with polystyrene board in 2020 (after five years of operation). This could be because of the higher temperature variation in the HMA layer and the lower initial effective modulus of the polystyrene sections. However, the test section insulated with a layer

of BA showed a higher load-bearing and structural capacity in 2015, as well as a lower change ratio after five years. Thus, based on this research, BA is recommended over polystyrene as an insulation layer within pavements in cold climates.

CHAPTER 11. APPLICAION OF THE MACHINE LEARNING MODEL TO DETERMINE SPRING LOAD RESTRICTIONS AND WINTER WEIGHT PREMIUM

This section has been submitted to the Journal of the Transportation Research Board July 2023 as Huang, Y., Moghaddam, T. B., Hashemian, L. and Bayat, A. Application of the Machine Learning Method to Determine Spring Load Limits and Winter Weight Premium.

11.1. ABSTRACT

Freight is important to sustaining the Canadian economy. However, heavy truck transportation also put enormous pressure on roadway networks. To minimize road damage caused by heavy traffic, Spring Load Restrictions (SLR) are implemented to minimize road damage caused by heavy traffic during the thaw-weakening season, and Winter Weight Premium (WWP) is used to reduce the impact of SLR on trucking operations by allowing higher axle loads in winter. However, existing policies apply fixed dates each year for these restrictions, irrespective of the actual structural capacity of the pavement. The objective of this study is to explore the practical implementation of machine learning models for accurately determining the start and end dates of SLR and WWP. Some methods were proposed to improve the application of SLR and WWP. However, existing methods rely mainly on indirect indices, such as the cumulative thawing index and cumulative freezing index, which pose challenges in their calculation. This study directly derives the start and end dates of SLR and WWP from frost and thaw depths in the pavement structure which are determined by pavement temperature and moisture content. In contrast to previous studies that neglected the influence of soil moisture content on determining the start and end dates of SLR and WWP, this study examines the variation in soil moisture content to evaluate the validity of existing theories. The findings reveal a high level of

agreement between the machine learning model's estimations of frost and thaw depths and the measured values, with R^2 values exceeding 0.91.

Keywords: Spring Load Restrictions, Winter Weight Premium, frost depth, thawing depth, machine learning

11.2. INTRODUCTION

Freight transport plays a crucial role in sustaining Canada's economy, but the substantial volume of heavy truck traffic places immense pressure on the country's roadway networks. This pressure leads to premature failure, extensive pavement damage, the need for costly road maintenance, and other related issues. Furthermore, Canada's cold regions present additional challenges for roadways, including frost heave, freeze-thaw cycles, and thawing weakening. In late winter and early spring, the temperature of the pavement structure rises from top to bottom, resulting in the upper soil layer thawing and the lower layer remaining frozen, leading to limited drainage capacity. The water in the subgrade layer cannot be discharged in time, resulting in a significant increase in water content. Moisture content influences the density and modulus of both the soil and bound materials, ultimately impacting the overall performance of the pavement (ARA., 2004; Bohra et al., 1999; Christopher et al., 2006; Haghi et al., 2016; Huang et al., 2021; Janoo and Shepherd, 2000). Soil reaches its maximum density at an optimum moisture content. If all other conditions remain the same, both coarse-grained and fine-grained materials can significantly increase their modulus when dry, often by more than five times. Thus, the high moisture content in the spring can cause a decrease in the stiffness of the subgrade. On the other hand, excess water can lead to the separation of the asphalt binder from the aggregate, resulting in long-term effects on the structural integrity of the cementitious material. As a result, roadways become more vulnerable to the detrimental effects of heavy

truck traffic, further exacerbating the strain on the infrastructure (Al-Qadi et al., 2008; Bayat, 2009; Haghi, 2019).

To mitigate the damage caused by excessive truck loads to roads during the thaw-weakening season, authorities in North America employ Spring Load Restrictions (SLR) to impose load limits on roads. However, the use of SLR poses economic challenges for the local freight transportation industry. To address the economic difficulties faced by the trucking industry during the thaw-weakening period, the Winter Weight Premium (WWP) has been introduced. This involves increasing the maximum allowable axle load during the freezing period. Many authorities apply a fixed date every year; however, the fixed-date approach fails to consider the actual load-carrying capacity of the pavement, potentially resulting in inefficient restrictions or inadequate protection for the roads (Canada Cartage Group of Companies, 2021). Asefzadeh et al. (2016) conducted a study in which they collected two years' pavement temperatures from a test road in Edmonton, Alberta, and calculated the actual frost and thaw depths. The results indicated variations in the frost progress and thawing duration between the two years, highlighting the year-to-year variability of the start and end dates of SLR and WWP. These findings underscore the need for a dynamic approach that replaces the traditional fixed-date approach.

Previous studies (Bradley et al., 2012; Mahoney et al., 1987; Minnesota Department of Transportation, 2014) have relied on indirect parameters, such as cumulative thawing index (CTI) and cumulative freezing index (CFI) to estimate the start and end dates of SLR and WWP. These indices reach a threshold, triggering the application of SLR or WWP. However, these studies lack a clear definition of the end date of SLR, and the calculation of the CTI and CFI poses significant challenges (Asefzadeh et al., 2016). Determining the start date of the CTI calculation is difficult due to unexpected increases in winter air temperature (e.g., in January

and February). Moreover, the CTI and CFI calculations require calibration with a reference temperature specific to each location.

Asefzadeh et al. (2016) utilized three existing models to measure the CTIs and estimate the start and end dates of SLR for a test road in Alberta. The predicted start dates of SLR showed a variation of two to four days among the models. However, the differences in the predicted end dates of SLR were unacceptably large, exceeding one and a half months. Additionally, all three existing methods suggest removing SLR before the soil moisture content recovers from the high-water levels.

Baïz et al. (2008) and Bao et al. (2019, 2021) proposed theories to determine the start and end dates of SLR and WWP based on frost and thaw depths. However, these depths were also calculated using freezing and thawing indices. Moreover, the existing pavement temperature prediction models in the literature (Chen et al., 2019; Li et al., 2018; Milad et al., 2021; Tabrizi et al., 2021) are limited to the asphalt layer. The proposed theories (Baïz et al., 2008; Bao et al., 2019, 2021) also failed to consider the soil moisture content. To date, no research has addressed the direct estimation of SLR and WWP application and removal dates through pavement temperature. Thus, a new method that dynamically determines the start and end dates of SLR and WWP based on frost and thaw depths derived from pavement temperature can improve road management.

In recent years, machine learning (ML) models have gained popularity for estimating environmental factors of pavement structure, including pavement temperature (Abo-hashema, 2013; Huang et al., 2023b; Huang et al., 2023; Milad et al., 2021; Molavi Nojumi et al., 2022; Qiu et al., 2020; Tabrizi et al., 2021) and moisture content (Huang et al., 2023a) at different depths using available inputs. Building on this trend, the primary objective of this study is to introduce a dynamic approach that utilizes a machine learning model to determine the start and end dates of SLR and WWP. The machine learning model was developed by pavement

temperatures collected from the Integrated Road Research Facility (IRRF) test road from January 2013 to December 2020.

Additionally, this study aims to assess the validity of existing theories that determine the start and end of SLR and WWP based on frost-and-thaw depths by comparing the model's outcomes with changes in moisture content in the subgrade. To achieve this, pavement temperatures and moisture content measured from the IRRF test road during specific periods, including November 2013 to August 2014 and November 2016 to August 2017, were utilized. By employing this dynamic approach, the research seeks to enhance the accuracy and effectiveness of SLR and WWP implementation, enabling road authorities to make informed decisions based on real-time data and subgrade conditions. The comparison between the machine learning model and water content variations in the subgrade provides valuable insights into the applicability and reliability of existing theories in determining the appropriate timing for implementing and lifting SLR and WWP. This analysis contributes to advancing our understanding of the factors influencing road damage during the thaw-weakening season and aids in the development of more robust and efficient policies for managing truck transportation. Ultimately, by refining the methodologies for determining SLR and WWP dates, this research aims to promote sustainable freight transport practices and minimize the negative impacts of low-load structural capacity during the thawing-weakening period on roadway networks.

11.3. MACHINE LEARNING MODEL DEVELOPMENT

The Integrated Road Research Facility test road, located in Edmonton, Alberta, serves as an advanced instrumented test road designed to investigate the environmental influence on pavement structure performance. Construction of the IRRF test road commenced in 2012 and was completed in 2013, and opened to public traffic in 2015. Figure 11-1 (a) illustrates the composition of the test road, which comprises a 0.25 m layer of hot mix asphalt (HMA) placed

on top of a 0.45 m granular base course (GBC). Table 11-1 provides the grain size specifications for the GBC and subgrade soil. The GBC is composed of well-graded gravel, with a maximum particle size of 0.019 m and a density of 2.10 ton/m^3. The subgrade soil, classified as clayed sand, has a maximum particle size of 0.0005 m and a density of 1.85 ton/m^3.

Pavement temperature and moisture content data were collected using CS650 time domain reflectometers (TDRs, Campbell Scientific), as shown in Figure 11-1 (b). The TDRs recorded the pavement temperature and volumetric water content (VWC) at depths of 0.50, 0.70, 0.80, 1.80, and 2.70 m below the road surface at five-minute intervals. The TDRs employed the Topp equation (Topp et al., 1980) to calculate VWC based on the bulk dielectric permittivity of the soil (K_α):

$$VWC = -5.3 \times 10^{-2} + 2.92 \times 10^{-2} K_a - 5.5 \times 10^{-4} K_a^2 + 4.3 \times 10^{-6} K_a^3 \qquad \text{Equation 11-1}$$

where VWC (m^3/m^3) is the volumetric water content, and K_α is the bulk dielectric permittivity of the soil. The speed of wave propagation depends on the dielectric permittivity of the porous medium. Increasing the water content reduces the speed of propagation or increases the time it takes for an electromagnetic wave to travel from one pole to another. This dependence has led to naming the probe the "Time Domain Reflectometer." Laboratory tests were conducted to calibrate the VWC using soil samples collected from the IRRF test road. The permittivity of water is influenced by temperature and water is the main contributor to soil permittivity, so the soil permittivity is temperature dependent. Equation 11-2 (Haghi, 2019) was used to eliminate the temperature dependency of the measured results:

$$VWC_{21} = VWC/(0.0084(T - 21) + 0.9936) \qquad \text{Equation 11-2}$$

where 21°C was used as the base point to calibrate the permittivity, VWC_{21} (m^3/m^3) represents the soil permittivity without the effect of temperature, and T (°C) is the temperature of the sample. Meanwhile, soil permittivity is influenced by soil type and the compaction of the soil.

Calibration was also performed for the granular base course and subgrade materials using Equations 11-3 and 11-4 (Haghi, 2019).

$$VWC_{GBC} = 1.338VWC - 0.0901 \quad \text{Equation 11-3}$$

$$VWC_{subgrade} = 1.1619VWC - 25.296 \quad \text{Equation 11-4}$$

where VWC_{GBC} (m^3/m^3) is the volumetric moisture content of the GBC layer and $VWC_{subgrade}$ (m^3/m^3) is the volumetric moisture content of the subgrade layer. It is important to note that the TDRs only captured variations in liquid water content during winter (Huang et al. 2023a).

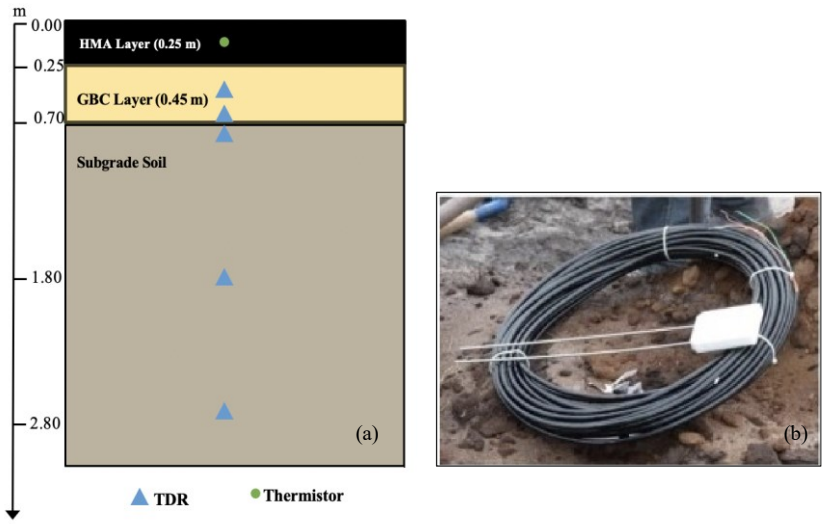

Figure 11-1: (a) Cross-section of the IRRF test road, and (b) CS 650 TDR

The machine learning model was developed using the average daily pavement temperature data collected from the IRRF test road, as shown in Figure 11-2. Pavement temperature data was collected from January 2013 to December 2020, and the details are provided in Table 11-2. The environmental parameters — such as average air temperature, solar radiation, and other relevant factors — were collected from the nearest Environment Canada weather station, Oliver AGDM.

A sensitivity analysis was conducted to assess the correlation between the pavement temperature and different parameters, and the performance of various parameter combinations was compared. Among the analyzed parameters, the best combination identified for input

parameters was average air temperature, day of the year, and depth. Day of the year serves as a time-related parameter ranging from 1 to 365, with January 1st corresponding to a value of 1. Depth is used to locate the sensors.

Table 11-1: Grain size distribution of GBC and subgrade soil used in IRRF test road.

GBC		**Subgrade Soil**	
Grain Size (mm)	**Percent Passing (%)**	**Grain Size (mm)**	**Percent Passing (%)**
19.000	99.15	0.250	98.0
12.500	75.17	0.150	83.9
9.500	61.23	0.075	46.9
4.750	42.73	0.044	37.1
2.380	32.08	0.032	32.5
1.190	25.61	0.023	27.3
0.595	18.93	0.012	24.1
0.297	7.09	0.009	22.4
0.149	1.46	0.004	19.9
0.075	0.51	0.001	15.0

For the model's development, the machine learning toolbox regression learner, in MATLAB version R2017a, was utilized. All five machine learning algorithms available in the toolbox, namely regression trees, support vector machines, Gaussian process regression models, ensembles of trees, and linear regression models were employed to train the models. The performance of the machine learning models was evaluated using the coefficient of determination (R^2) and the root mean square error (RMSE). Equations 11-5 and 11-6 were used to calculate R^2 and RMSE:

$$R^2 = 1 - \frac{\sum_i (x_i - f_i)^2}{\sum_i (x_i - \bar{x})^2} \qquad \text{Equation 11-5}$$

$$RMSE = \sqrt{\frac{\sum_{i=1}^{N}(x_i - f_i)^2}{N}}$$ Equation 11-6

where x_i represents the actual value, f_i represents the predicted value, $\bar{x}$ is the mean value of the entire dataset, and N is the total number of data points.

Among the machine learning algorithms used, most demonstrated excellent performance achieving R^2 values above 0.95, except for the linear regression model. The linear regression model is a widely used algorithm, but it assumes a linear relationship between input parameters and the target variable, which does not hold for pavement temperature prediction.

The Gaussian process regression machine learning model stood out as the top performer, exhibiting the highest accuracy with an impressive R^2 of 0.99 and an RMSE of 1.45°C. Gaussian process regression is a nonparametric Bayesian method that employs Gaussian processes for regression. Gaussian process regression calculates the probability distribution over all acceptable functions that can fit the given data. The superiority of Gaussian process regression models in estimating pavement temperature can be attributed to their ability to capture complex relationships without relying on strong assumptions, handle small or sparse datasets effectively, and provide uncertainty estimates. The flexibility, probabilistic nature, and ability to handle uncertainty make Gaussian process regression models well-suited to the specific task of pavement temperature estimation (Bonaccorso, 2018; Schulz et al., 2018). Cross-validation was employed to validate the performance of the machine learning model, with the data randomly divided into five groups. All the estimated pavement temperatures used in this study were calculated by the Gaussian process regression machine learning model (Li et al. 2018).

Table 11-2: Performance of the ML model developed.

Depth (m)	Start date	End date	Machine learning	
			R^2	RMSE (°C)
0.50	January 2013	June 2020	0.98	1.70
0.70	January 2013	July 2020	0.98	1.80
0.80	January 2013	December 2020	0.98	1.62
1.80	February 2020	August 2020	0.98	1.20
2.70	January 2013	December 2017	0.98	0.76

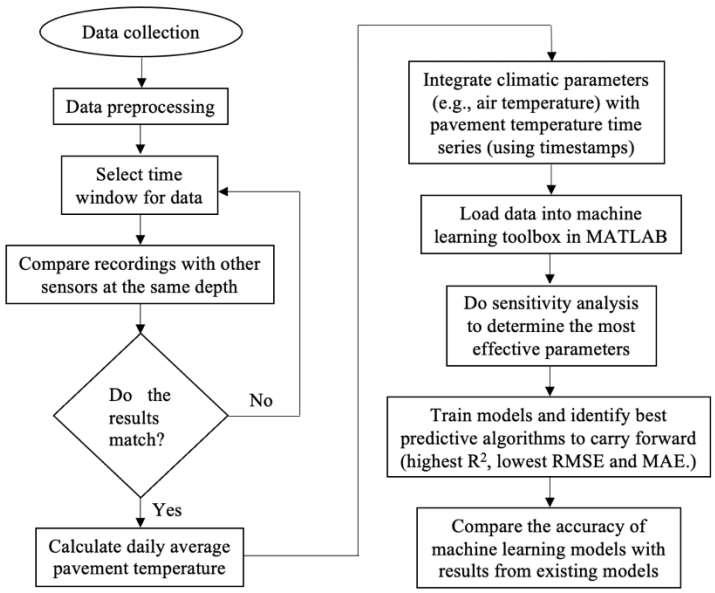

Figure 11-2: Procedure for developing machine learning predictive models (Huang et al., 2023a; Huang et al., 2023)

11.4. AIR TEMPERATURE

Air temperatures were collected from the Oliver ADGM weather station. Figure 11-3 (a) represents the average daily air temperature, while Figure 11-3 (b) shows the average monthly air temperature. The data covers the period from November to May for the years 2013 to 2014 and 2016 to 2017.

In the winter of 2013 to 2014, the average daily air temperature dropped below 0°C from 3 November 2013. The lowest average daily air temperature recorded during this period was -

30.9°C on 6 December 2013. The average daily air temperature remained below 0°C until 9 March 2014, with occasional days in December and January when the average daily air temperature reached above 0°C. The average monthly air temperature for February 2013 was -16.4°C, indicating consistently cold temperatures during that month.

Comparatively, the winter of 2016 to 2017 experienced milder weather. The average daily air temperature remained above 0°C until 15 November 2016, and then stabilized below 0°C from 18 March 2017. In November 2016, the average monthly air temperature was still above 0°C, whereas in 2013 the average monthly air temperature was -7.1°C. From December to April, the average monthly air temperature remained below 0°C although the average monthly air temperature values for December, February, and March in 2017 were higher than those recorded in 2014.

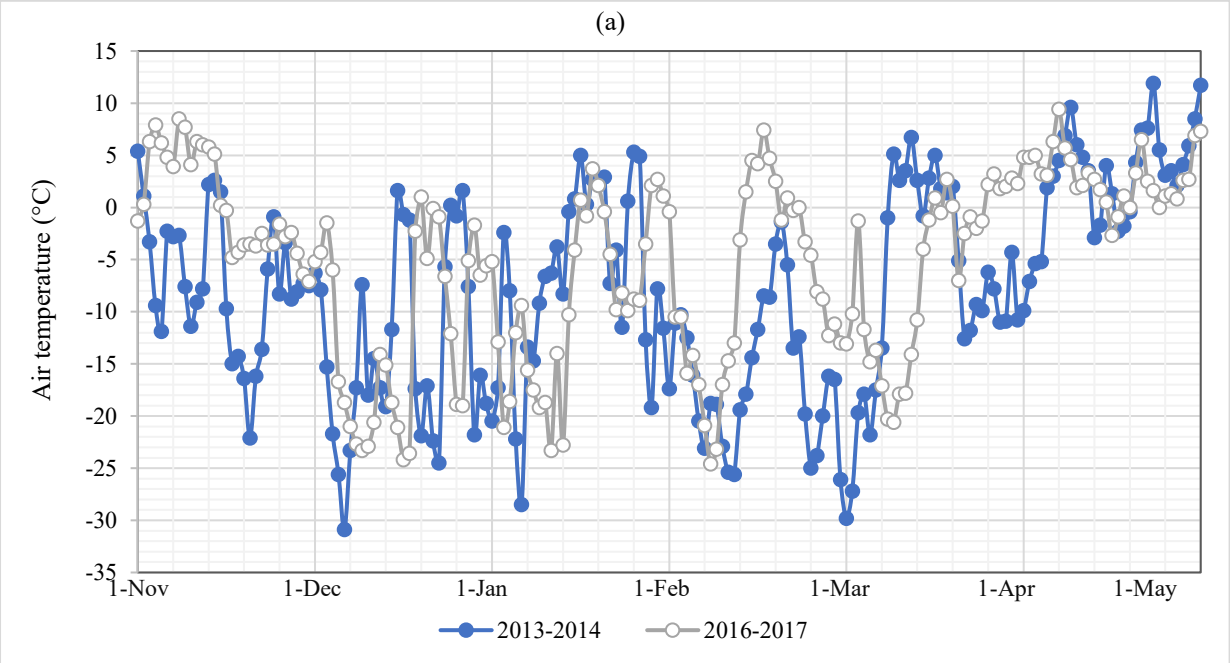

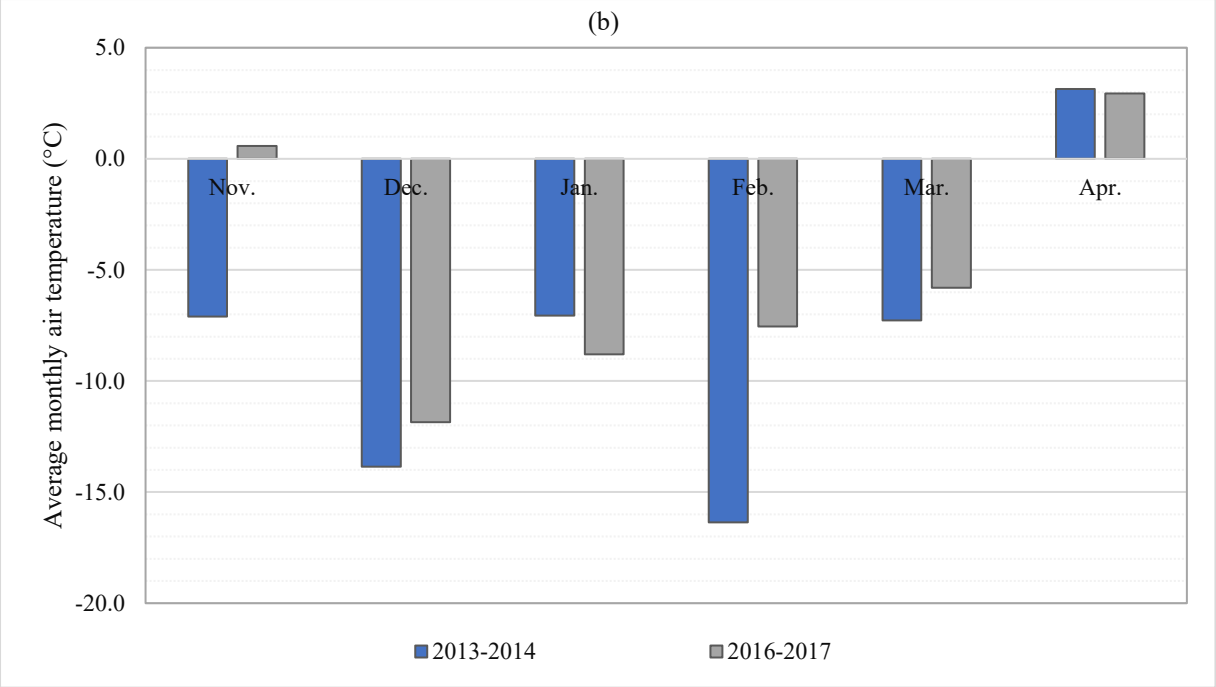

Figure 11-3: (a) Average daily air temperature and (b) average monthly air temperature

11.5. COMPARISON OF MEASURED AND ESTIMATED FROST AND THAWING DEPTHS

In the frost and thaw depth analysis, interpolation is based on measured and estimated temperatures at different depths. Figure 11-4 compares the measured frost and thaw depths obtained from sensors installed in the test road with the estimated frost and thaw depths calculated using the Gaussian process regression machine learning model.

Figure 11-3 (a) shows that the air temperature was above 0°C for a few days in January, February, and March 2014, but was not consistently above freezing. Therefore, the calculation of the thaw depth for 2014 and 2017 started in March. The predicted frost and thaw depths obtained from the Gaussian process regression machine learning model show good agreement with the measurement results, with the R^2 value being 0.93 for 60 frost depth samples and 0.91 for the 16 thaw depth samples. The predicted trends align well with the measured trends.

Based on the pavement temperature recordings, in the period from 2013 to 2014, the frost reached the GBC layer on 10 November 2013 and reached the subgrade layer on 28 November 2013. Thawing began on 12 March 2014, and the frost and thaw depth met on 6 April 2014. Even though the temperature, at a depth of 1.80 m below the road surface, remained at 0°C until 25 April 2014, it did not affect the end date of the thawing process. Previous studies (Baïz et al., 2008; Bao et al., 2021) have shown that once the frost and thaw depths meet, the freeze-thaw cycle is considered complete for that year. In the period from 2016 to 2017, the frost reached the GBC layer on 24 November 2016 and reached the subgrade layer on 3 December 2016. Thawing began on 18 March 2017, and the frost and thaw depths met on 8 April 2017.

According to the estimated results of the machine learning model, the frost started on 9 November 2013, and the frost depth reached the subgrade layer on 27 November 2013. Thawing began on 10 March 2014, and the frost depth and thaw depth met on 10 April 2014. For the winter from 2016 to 2017, the frost reached the base layer on 23 November 2016. Thawing began on 15 March 2017. Then, the frost and thaw depths met on 5 April 2017. The difference between the measured data and the estimated dates from the Gaussian process regression model estimated date was within four days. The Gaussian process regression model demonstrated high accuracy in predicting frost and thaw depths for other years as well. To provide representative results and facilitate comparison, only the results obtained from November 2013 to April 2014 and November 2016 to April 2017 were selected.

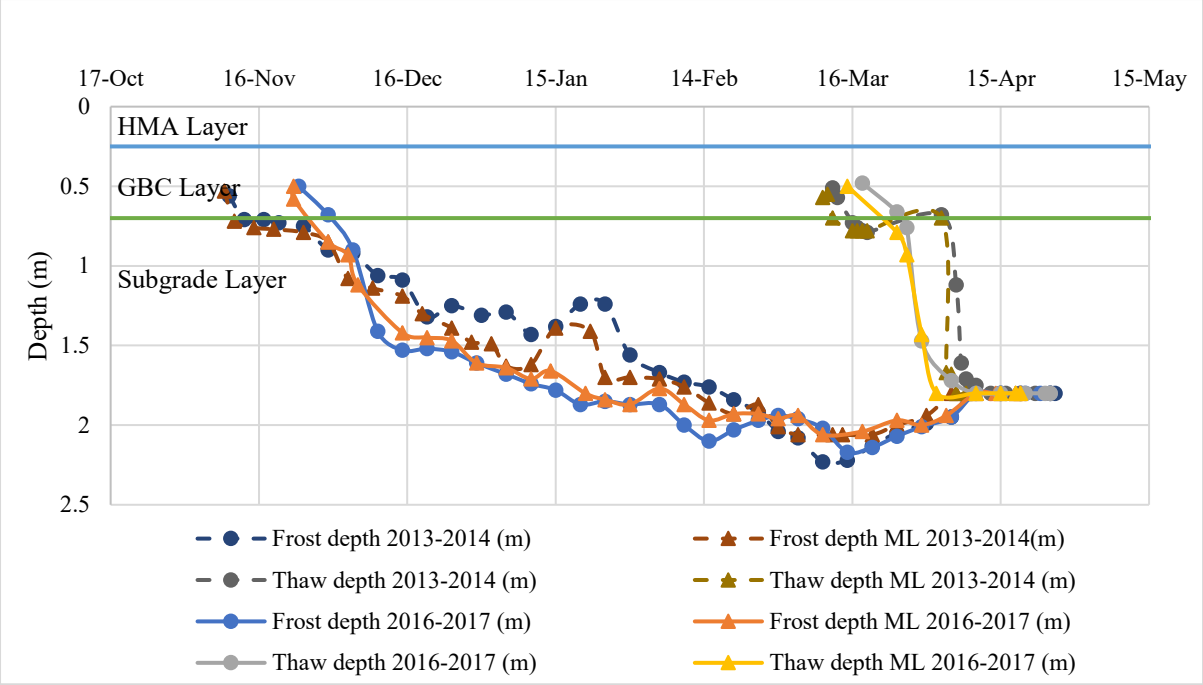

Figure 11-4: Measured and estimated frost and thaw depths from 2013 to 2014 and 2016 to 2017

11.6. MOISTURE CONTENT VARIATION OF BASE AND SUBGRADE

Figure 11-5 illustrates the variation in moisture content during the same freeze-thaw period for the subgrade layers. The moisture content at the top of the subgrade layer started to drop on 21 November 2013 and 26 November 2016, respectively. The decrease in moisture content occurred approximately one week after the frost reached the subgrade layer. At a depth of 0.80 m, the moisture content started to increase on 4 March 2014. However, as shown in Figure 11-3 (a), the average daily air temperature dropped below 0°C again from 20 March to 3 April 2014. Consequently, the moisture content decreased from 0.34 to 0.22 m^3/m^3 on 2 April 2014. The moisture content at the depth of 1.8 m began to decrease on 7 January 2014 and 12 December 2016, respectively, following the changes in moisture content at shallower depths. Even though at a depth of 2.7 m the pavement temperature never dropped below 0°C, the

moisture content at the same depth started to drop on 12 January 2014 and 13 January 2017. This reduction in moisture content below the frozen layer can be attributed to the migration of unfrozen water into the frozen layer (Hoekstra, 1967).

The moisture content collected by the TDR installed at a depth of 0.8 m was sensitive to temperature changes, resulting in sudden increases in January and February when the temperature rose. However, the moisture content collected at deeper locations only exhibited seasonal variation and did not increase with short-term temperature rises.

During the spring, the moisture content at a depth of 0.8 m was higher compared to other seasons, reaching its peak values for the entire year. Maximum values of 0.39 m^3/m^3 and 0.38 m^3/m^3 were observed on 6 April 2014 and 16 April 2017, respectively. According to the study by Asefzadeh et al. (2016), the subgrade soil takes approximately 120 days to recover from the high-water level. Therefore, the subgrade soil would recover from the high-water level on 6 August 2014 and 16 August 2017, respectively.

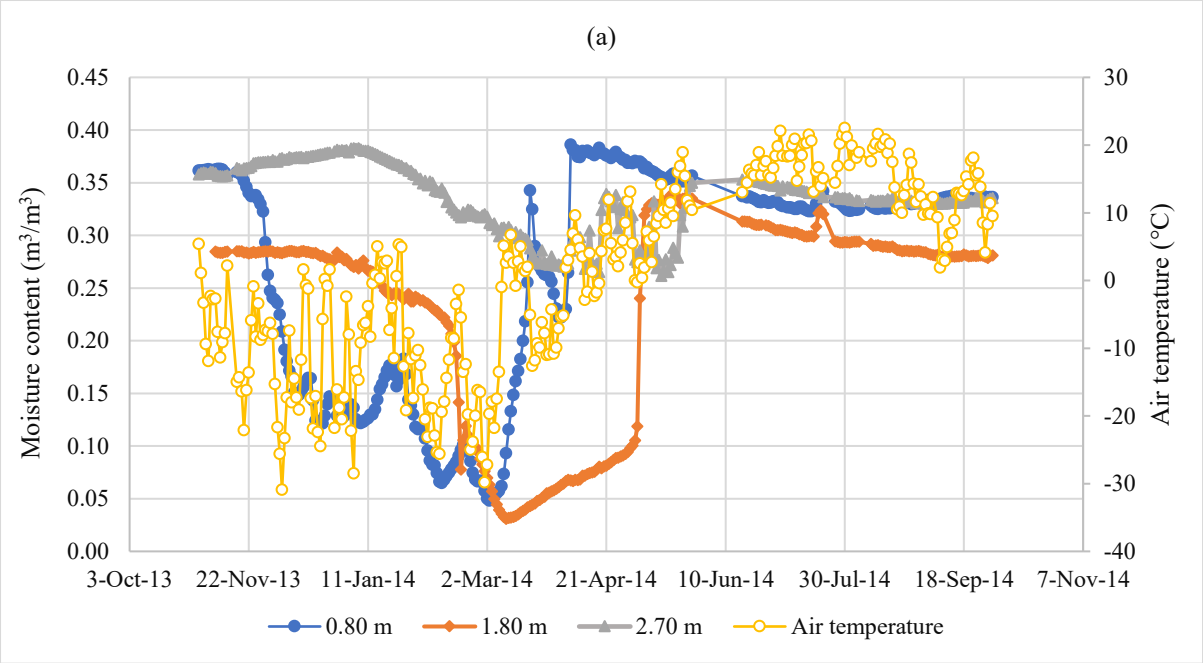

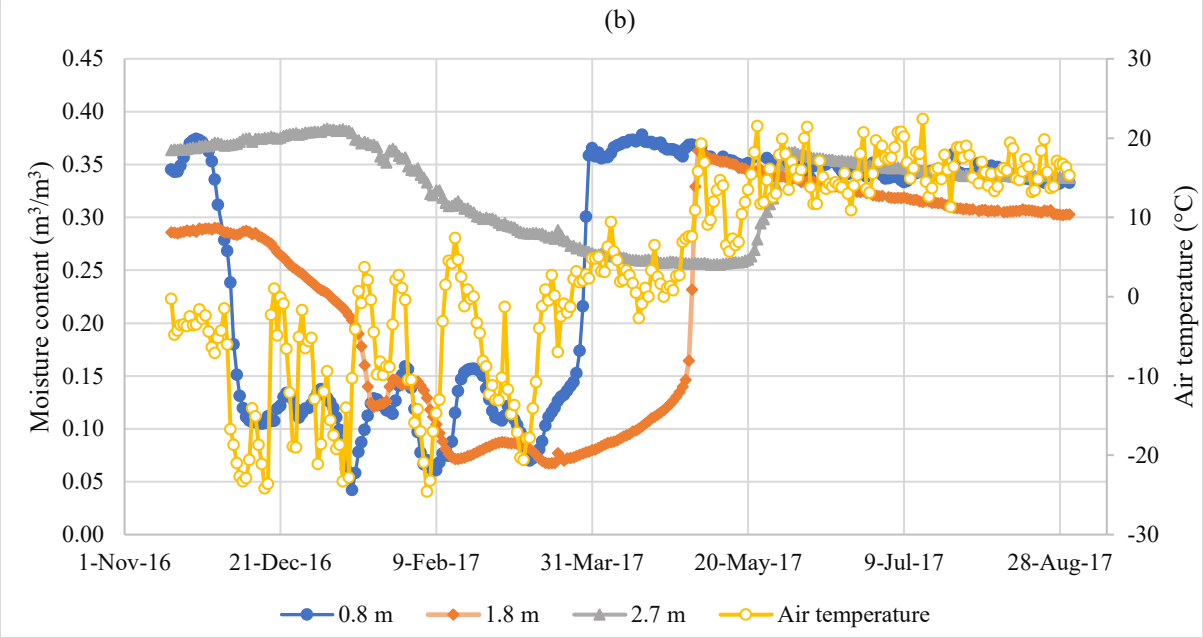

Figure 11-5: Average daily moisture content variation in the pavement structure from (a) 2013 to 2014 and (b) 2016 to 2017

11.7. DISCUSSION

11.7.1. Actual Start and End Dates of WWP and SLR

Based on the theory proposed by Baïz et al. (2008), the actual start and end dates of the SLR and WWP periods were determined based on the frost and thaw depths reaching specific thresholds and exhibiting continuous trends. The critical contact stress depth, which is the depth where the maximum traffic-induced vertical stress in the subgrade layer becomes less than 1% of the tire-pavement contact stress, was used to determine the start date of the WWP. According to previous research by Asefzadeh et al. (2016), this critical depth is 1.05 m below the road surface in the IRRF test road. In alignment with the Alberta regulations, the WWP should start when the frost depth reaches 1.00 m (Bradley et al., 2012). In this study, the WWP was considered to start when the frost depth reached a depth of 1.00 m below the road surface. Based on Alberta Transportation regulations, the WWP should end and the SLR should begin when the thaw depth reaches 0.25 m (2023 Government of Alberta, n.d.). The shallowest TDR was installed at a depth of 0.50 m below the road surface, so the SLR was considered to start

and the WWP was considered to end when the thaw depth continuously exceeded 0 m (reaching the GBC layer). The SLR was considered to end when the frost depth met the thaw depth, indicating the completion of the freeze-thaw cycle (Bao et al., 2021).

Table 11-3 presents the comparison of the actual start and end dates of the WWP between the winters of 2013 to 2014 and 2016 to 2017. Despite the winter of 2013 to 2014 being colder than the winter of 2016 to 2017, the WWP lasted longer in the winter of 2016 to 2017 (102 days) than in the winter of 2013 to 2014 (94 days). The WWP started on 8 December 2013 and ended on 12 March 2014, while it started on 6 December 2016 and ended on 18 March 2017.

Table 11-3: Measured and estimated start and end dates of WWP.

Data type	**WWP start date**		**WWP end date**	
	2013 to 2014	**2016 to 2017**	**2013 to 2014**	**2016 to 2017**
Measurements	8 December	6 December	12 March	18 March
Machine learning	4 December	5 December	10 March	15 March
Difference	4 days	1 day	2 days	3 days
Actual duration	94 days	102 days		
Estimated duration	96 days	100 days		

Table 11-4 demonstrates the measured and estimated start and end dates of the SLR. Although the monthly average air temperature in March 2014 was lower than that in March 2017, the SLR started six days earlier in 2014. The SLR started on 12 March 2014 and on 18 March 2017, and ended on 6 April 2014 and 8 April 2017. It lasted 25 days in the winter of 2013 to 2014 and 21 days in the winter of 2016 to 2017.

The differences between the measured and estimated results in both years were within four days. This demonstrates the high accuracy of the Gaussian process regression model, indicating that the machine learning model can be a practical method for determining the start and end dates of the WWP and SLR. Through the Gaussian process regression model, the estimated results indicate that the WWP lasted for 96 days from 2013 to 2014 and 100 days from 2016

to 2017. Additionally, the SLR was found to last for 31 days from 2013 to 2014 and 21 days from 2016 to 2017.

Table 11-4: Measured and estimated start and end dates of SLR.

Data type	SLR start date		SLR end date	
	2013 to 2014	2016 to 2017	2013 to 2014	2016 to 2017
Measurements	12 March	18 March	6 April	8 April
Machine learning	10 March	15 March	10 April	5 April
Difference	2 days	3 days	4 days	3 days
Actual duration	25 days	21 days		
Estimated duration	31 days	21 days		

11.7.2. Observed Moisture Content at the Start and End of the Day for WWP and SLR

In this study, the moisture content at a depth of 0.80 m below the road surface was utilized to analyze the triggering and lifting of the SLR and WWP. This depth was chosen because the moisture content at this level exhibited a strong correlation with air temperature and was less influenced by other factors due to its distance from the road surface.

The observed moisture content at a depth of 0.80 m indicated the initiation of the WWP. In 2013, the moisture content started to decrease on 21 November 2013 and reached a value of 0.18 m^3/m^3 on 8 December 2013. Similarly, in 2016, the moisture content began to decrease on 29 November 2016 and dropped to 0.18 m^3/m^3 on 6 December 2016. The decrease in the soil moisture content corresponds to an increase in the soil resilient modulus (ARA., 2004; Haghi, 2019), allowing for higher maximum axle loads on trucks. Therefore, the start date of the WWP aligned with the observed moisture content variation in the soil.

During the SLR period, the moisture content at a depth of 0.80 m showed an increasing trend. From 12 March to 8 April 2017, the moisture content increased from 0.07 to 0.37 m^3/m^3, with

the highest value of 0.38 m^3/m^3 observed on 16 April 2017. A similar trend occurred in 2014, where the moisture content began to increase from 0.07 m^3/m^3 on 9 March and reached its highest value of 0.39 m^3/m^3 on 6 April. Despite the frost depth and thaw depth meeting on 6 April 2014, the accumulated water in the soil could not drain from the subgrade layer. This is problematic because high soil moisture content combined with heavy truck traffic can lead to significant pavement damage (Haghi, 2019).

Based on Alberta Transportation regulations, the thawing period should end around 16 June (with a possible variation of one week earlier or later) (2023 Government of Alberta, n.d.). On 16 June 2017, the moisture content was measured at 0.35 m^3/m^3. After 120 days from 16 April 2017, the moisture content decreased to 0.34 m^3/m^3 on 17 August 2017, which was selected as the moisture content base point. In 2014, the moisture content dropped to 0.34 m^3/m^3 on 17 June, and in 2017, it dropped to the same value on 25 June. It took 97 days in 2014 and 99 days in 2017 for the moisture content at a depth of 0.80 m to return to 0.34 m^3/m^3, indicating the discharge of accumulated water from the start date of the SLR. These observations indicate that frost and thawing depths can be utilized to estimate the start date of WWP and SLR. However, determining the end of the SLR should be based on a combination of frost and thaw depths along with the moisture content in the subgrade layer.

11.7.3. Limitations of the Machine Learning Models

The main limitation of the machine learning models used in this study, specifically the Gaussian process regression model, is their reliance on the training data and the consequent lack of generalizability of the data. In this case, the model was trained using pavement temperature data collected specifically from the IRRF test road. Therefore, its applicability to other road surfaces or geographical locations may be limited.

The accuracy and performance of machine learning models heavily depend on the quality, diversity, and representativeness of the training data. If the model is trained on a narrow or biased dataset, it may not capture the full range of variations and patterns present in different scenarios. This lack of generalizability can result in reduced accuracy and reliability when applied to new or unseen data.

To overcome this limitation, it would be beneficial to train the machine learning model using a larger and more diverse dataset that includes pavement temperature data from various locations and road types. This would enhance the model's ability to generalize and provide accurate predictions in different contexts. Additionally, considering other relevant factors, such as the properties of pavement materials, the number of layers, and so on, could further improve the model's performance and broaden its applicability.

11.8. CONCLUSION

The study utilized a machine learning model to determine the start and end dates of SLR and WWP by directly calculating the frost and thaw depths from the pavement temperature. Pavement temperatures collected from the IRRF test road from January 2013 to December 2020 were used to develop machine learning models. Air temperature, day of the year, and depth were used as the input parameters. The Gaussian process regression model performed the best with an R^2 of 0.99 and an RMSE of 1.45°C. Pavement temperatures collected from November 2013 to April 2014 and November 2016 to April 2017 were used to discuss the accuracy of the machine learning prediction. Furthermore, the study discussed some existing theories that proposed to determine the start and end dates of the WWP and SLR directly by frost and thaw depths. Moisture content is a dominant factor in the structural capacity of the soil. However, these existing theories did not consider the soil’s moisture content. This study used moisture content collected from the IRRF test road during the same period to discuss the

validity of these existing theories. The following conclusions were made based on a detailed analysis of measured and estimated results, and moisture content variation.

- The Gaussian process regression model demonstrated high accuracy in estimating frost and thaw depths (R^2 of 0.93 and 0.91 for the frost and thaw depths, respectively), making it a practical method for determining the start and end dates of WWP and SLR in pavement structures.
- A comparison with measured results showed good agreement, with differences in start and end dates of WWP and SLR occurring within four days.
- The soil moisture content at a depth of 0.80 m below the pavement exhibited significant changes corresponding to the start of WWP and SLR, validating the existing theories. However, when the frost depth met the thaw depth, the accumulated moisture content in the subgrade layer could not effectively discharge, leading to prolonged high moisture content levels in the soil beyond the end date for SLR.
- The subgrade layer required approximately 120 days to discharge excess water, but it actually took fewer days (97 days in 2014 and 99 days in 2017), which emphasized the need to consider soil moisture content when determining the end date of SLR.

In conclusion, the machine learning model could be a practical method to determine the start and end dates of the WWP and SLR; however, the excess water could not discharge when the frost depth and thaw depth met, and the high moisture content with truck transportation on the road may lead to serious damage to the pavement. Therefore, it is necessary to consider the soil moisture content when determining the end date of the SLR.

Moreover, if more input parameters are used, such as the properties of pavement materials, the number of layers, and so on, the generalizability of the model could improve. However, such expansive data is not currently available. Although the generalizability of the machine learning

model is limited and a dataset collected from the specific projects is necessary, machine learning models provide a robust option to improve road management.

CHAPTER 12.CONCLUSIONS AND RECONMMENDATIONS

12.1.CONCLUSIONS

In conclusion, this thesis has focused on addressing the challenges faced by pavements in cold regions, particularly regarding pavement temperature, moisture content, and structural capacity. By leveraging artificial intelligence techniques, specifically machine learning models, we have demonstrated their effectiveness in predicting pavement temperature and moisture content at multiple depths. These models outperformed existing models in terms of accuracy, showcasing their potential for improving pavement design and management in cold regions.

In light of the predetermined research objectives, the following conclusions have been derived:

- Based on years of pavement temperature and moisture content collected from sensors installed in the IRRF test road, the long-term effects of bottom ash as insulation layers on the pavement temperature and moisture content was described in **Chapter 4**, and the following findings were noted:
    - Both bottom ash and polystyrene effectively protect the subgrade from frost, preventing frozen water from forming in this layer.
    - The temperature gradient and rate of temperature change in the bottom ash section closely resemble those of the control section, indicating similar performance.
    - The 10 cm polystyrene insulation layer significantly reduces frost depth by 70% and minimizes moisture content variations in the subgrade layer at a depth of 1.80 meters. However, it is noteworthy that this section experiences lower base temperatures in winter, potentially increasing susceptibility to low-temperature cracking.
- Machine learning models, as discussed in **Chapters 5** and **6**, were employed to predict pavement temperatures in the HMA, base, and subgrade layers, revealing the following:

- Machine learning models emerged as a potent method for accurately predicting pavement temperatures at various depths within pavement structures, surpassing existing models in terms of performance.
- The combination of air temperature, day of the year, and depth proved to be the most effective set of input parameters.

- **Chapter 7** illustrates the training of machine learning models to predict the temperatures of base and subgrade layers, considering the presence of special insulation materials like the bottom ash layer and polystyrene board. This chapter highlights the practical applicability of machine learning models in this context.
- A machine learning model was developed to predict moisture content in the base and subgrade layers, with the most effective input parameters being pavement temperature, day of the year and depth. These findings were summarized in **Chapter 8**.
- In **Chapter 9**, an Artificial Neural Network (ANN) model was employed to predict pavement temperature and moisture content simultaneously. Remarkably, this ANN model with Bayesian regularization achieved high accuracy using only three input parameters: air temperature, day of the year, and depth. The details of this comparison are elaborated in **Chapter 9**.
- In **Chapter** 10, the FWD test results from 2015 and 2020 were used to compare structural variations in different test sections. The following findings were observed:
  - Although pure tired sections exhibited higher effective modulus in 2015, they showed lower subgrade resilient modulus in 2015 and much higher effective modulus change ratios in 2020 than that in the control section.
  - The embankment backfilled with a mixture of tire-derived aggregate from passenger and light-truck tires and soil closely matched the performance of the

control section and exhibited a higher subgrade modulus than the pure tire section in 2020.

- The polystyrene section showed much lower effective modulus and higher change ratios in 2020 than the control section.
- The bottom ash section performed similar to the control section and it even showed lower change ratios after five years operation.

- In **Chapter 11**, the machine learning model was utilized to directly determine the start and end dates of the SLR and WWP based on frost and thaw depths, with its performance compared to measured results. Validation of this method was carried out using moisture content variations in the subgrade layer, leading to the following findings:
  - A comparison between the predicted and measured results showed good agreement, with differences in start and end dates of WWP and SLR occurring within four days.
  - The soil moisture content within the pavement exhibited significant changes corresponding to the start of WWP and SLR, validating the existing theories.
  - However, when the frost depth met the thaw depth, the accumulated moisture content in the subgrade layer could not effectively discharge, leading to prolonged high moisture content levels in the soil beyond the end date for SLR.

Overall, this thesis has not only advanced our understanding of cold region pavement challenges but also demonstrated the potential of machine learning models for improved pavement design and management.

12.2. ACADEMIC AND INDUSTRY CONTRIBUTIONS

12.2.1. Academic Contributions

Based on the conclusions and findings presented, the academic contributions of this research can be summarized as follows:

- This research significantly contributes to academic knowledge by enhancing the understanding of the complex challenges faced by pavements in cold regions. It delves into critical aspects such as pavement temperature, moisture content, and structural capacity, shedding light on previously underexplored areas.
- The study demonstrates the practical application of artificial intelligence techniques, particularly machine learning models, in predicting pavement temperature and moisture content at various depths within pavement structures. This academic contribution showcases the potential of machine learning as a powerful tool for addressing and solving cold region pavement issues.
- The research provides valuable insights into the long-term effects of insulation materials, including bottom ash and polystyrene, on pavement temperature and moisture content. This knowledge is essential for informed decision-making in pavement design and can drive advancements in the field.
- The identification of the most effective input parameters, including air temperature, day of the year, and depth, for accurate pavement temperature predictions contributes to the academic understanding of pavement modeling and its practical application.
- Chapter 6 highlights the practical applicability of machine learning models in predicting temperatures of base and subgrade layers, even in the presence of special insulation materials. This insight contributes to academic discussions on real-world pavement engineering.

- The development of a machine learning model for predicting moisture content in base and subgrade layers, along with the identification of optimal input parameters, advances academic knowledge in pavement moisture management.
- The research introduces an Artificial Neural Network (ANN) model capable of simultaneously predicting pavement temperature and moisture content with high accuracy. This model's performance offers a practical tool for pavement engineers.
- Chapter 9 compares structural variations in different test sections, providing insights into the performance of various pavement configurations, including the impact of tire-derived aggregate, polystyrene, and bottom ash on structural capacity.
- Chapter 10 presents a novel method for directly determining the start and end dates of seasonal policies using machine learning and frost/thaw depths. This contribution has practical implications for road management in cold regions.

12.2.2. Industry Contributions

Drawing from the presented conclusions and findings, the practical implications for the industry can be summarized as follows:

- The research introduces the practical application of machine learning models for predicting pavement temperature and moisture content in base and subgrade layers. This industry contribution offers a valuable tool for pavement engineers and practitioners involved in real-world projects.
- The development of a machine learning model for predicting moisture content in base and subgrade layers contributes to improved moisture management practices in pavement construction and maintenance, benefiting the industry.
- While existing software like MATLAB can evaluate machine learning models, this research brings a new level of sophistication to pavement moisture content analysis.

The industry can benefit from the advanced algorithms employed, which can detect subtle data patterns and provide more accurate predictions.

- Chapter 9's comparative analysis of different test sections offers valuable insights into the structural performance of various pavement configurations. This information can guide industry professionals in making informed decisions regarding pavement design and construction.
- Chapter 10's novel method for determining the start and end dates of seasonal policies through machine learning and frost/thaw depths has practical implications for road management in cold regions. This industry contribution can optimize road policies and enhance pavement performance.
- The research promotes data-driven decision-making in pavement engineering, empowering industry professionals to make more informed choices regarding materials, insulation strategies, and moisture management practices.

12.3. LIMITATIONS

The study primarily focuses on unfrozen moisture content (liquid water) and does not account for solid moisture content (ice). Although unfrozen moisture content correlates with the resilient modulus of the subgrade layer, the absence of ice-related data limits the comprehensive understanding of moisture content changes in the base and subgrade layers during the entire year.

The machine learning models developed in this research are trained exclusively using data from the IRRF test road. As a result, their generality is limited, and their applicability is specific to this particular pavement structure and the two unbound materials used. Expanding the generality of these models would require a more diverse dataset, incorporating data from

different pavement structures, material properties, climatic regions, and additional input parameters such as layer thickness and material properties.

The construction of more generalized machine learning models necessitates a comprehensive dataset that currently remains unavailable. This dataset would ideally include measurements from various pavement structures, materials, and climatic regions. Input parameters would need to adapt to the specific attributes of each pavement structure, further emphasizing the need for measured data.

12.4. RECOMMENDATIONS

In light of the significant contributions and findings presented in this research, several recommendations can be made to enhance the design, construction, and management of pavements in cold regions. These recommendations aim to leverage the insights gained from the study and further advance the field of cold region pavement engineering. The following key recommendations are offered for consideration:

- Based on the results obtained, it is recommended to consider mixing Tire-Derived Aggregate from Passenger and Light-Truck Tires with soil when using it as an embankment fill material. This practice has shown promise in maintaining structural integrity.
- When selecting insulation materials for pavements in cold climates, bottom ash is recommended over polystyrene. The research indicates that bottom ash provides effective protection against frost and moisture content variations.
- In anticipation of future advancements, it is advisable to gather more comprehensive datasets, including a wider range of parameters as inputs. This expanded data collection would enhance the generality and applicability of machine learning models for pavement prediction.

- Although the Gaussian process regression models developed in this study performed the best, when new dataset was included, the performance of different machine learning algorithms needs to discuss again. Meanwhile, when applying the models to different climates, it may be necessary to incorporate different environmental factors.
- Due to the limited data in the IRRF test road, the cost of computation of the machine learning models has not been included in this research. If the machine learning models were applied to a larger dataset, the cost of computation should be taken into account.
- To improve the accuracy of determining the end date for Spring Load Restrictions, it is advisable to incorporate moisture content variation data into the decision-making process. This consideration will provide a more holistic approach to pavement management in cold regions.

BIBLIOGRAPHY

AASHTO. (2008). *Mechanistic Empirical Pavement Design Guide: A manual of practice*. American Association of State Highway and Transportation Officials, Editor.

Abo-Hashema, M. A. (2013). Modeling pavement temperature prediction using artificial neural networks. In *Airfield and highway pavement 2013: Sustainable and efficient pavements*(pp. 490-505).

Adwan, I., Milad, A., Memon, Z. A., Widyatmoko, I., Zanuri, N. A., Memon, N. A., & Yusoff, N. I. M. (2021). Asphalt pavement temperature prediction models: A review. *Applied Sciences, 11*(9), 3794. https://doi.org/10.3390/app11093794

Aidara, M. L. C., Ba, M., & Carter, A. (2015). Measurement of Dynamic Modulus and Master Curve Modeling of Hot Mix Asphalt from Senegal (West Africa). *Studies in Engineering and Technology*, *2*(1), 124. https://doi.org/10.11114/set.v2i1.936

Alavi, M.Z., Pouranian, M.R., & Hajj, E.Y. (2014). Prediction of asphalt pavement temperature profile with finite control volume method. *Transportation Research Record*, *2456*(1), 96-106.

Alberta Recycling Authority. https://www.albertarecycling.ca/programs/tires/. Accessed November 19, 2022.

Alberta Recycling Management Authority. 2020-21 Progress Report. https://www.albertarecycling.ca/about/reports/. Accessed July 13, 2022.

Al-Qadi, I. L., Wang, H., Yoo, P. J., & Dessouky, S. H. (2008). Dynamic analysis and in situ validation of perpetual pavement response to vehicular loading. *Transportation research record*, *2087*(1), 29-39.

American Association of State Highway and Transportation Officials, (1993). *AASHTO Guide for Design of Pavement Structures*, Vol. 1. AASHTO, Washington, D.C.

Anderson, D. M., & Tice, A. R. (1972). Predicting unfrozen water contents in frozen soils from surface area measurements. *Highway research record*, *393*(2), 12-18.

ARA, Inc., ERES Consultants Division. (2000). Guide for mechanistic–empirical design of new and rehabilitated pavement structures. Appendix DD–1: Resilient modulus as function of soil moisture – Summary of predictive models. Final Report. NCHRP Project. A-37A.

ARA, Inc., ERES Consultants Division. (2004). Guide for mechanistic–empirical design of new and rehabilitated pavement structures. Final Rep., NCHRP Project 1-37A.

Arellano, D. (2007). Consideration of Differential Icing Conditions in the Design of Pavement Systems Overlying Geofoam. In *Proc., 86th Annual Meeting. Transportation Research Board*. Washington, DC: Transportation Research Board.

Asefzadeh, A., Hashemian, L., & Bayat, A. (2017). Development of statistical temperature prediction models for a test road in Edmonton, Alberta, Canada. *International Journal of Pavement Research and Technology*, *10*(5), 369–382. https://doi.org/10.1016/j.ijprt.2017.05.004

Asefzadeh, A., Hashemian, L., Haghi, N. T., & Bayat, A. (2016). Evaluation of spring load restrictions and winter weight premium duration prediction methods in cold regions according to field data. *Canadian Journal of Civil Engineering*, *43*(7), 667–674. https://doi.org/10.1139/cjce-2015-0554

Bai, B.C., Park, D.W., Vo, H.V., Dessouky, S., & Im, J.S. (2015). Thermal properties of asphalt mixtures modified with conductive fillers. *Journal of Nanomaterials*, 2015.

Baïz, S., Tighe, S. L., Haas, C. T., Mills, B., & Perchanok, M. (2008). Development of frost and thaw depth predictors for decision making about variable load restrictions. *Transportation Research Record*, *2053*, 1–8. https://doi.org/10.3141/2053-01

Bao, T., Azmoon, B., & (Leo) Liu, Z. (2021). Freeze-thaw depth prediction with constrained optimization for spring load restriction. *Transportation Geotechnics*, *26*. https://doi.org/10.1016/j.trgeo.2020.100419

Bao, T., Liu, Z., & Bland, J. (2019). A multivariate freezing-thawing depth prediction model for spring load restriction. *Cold Regions Science and Technology*, *167*. https://doi.org/10.1016/j.coldregions.2019.102856

Barber, E. S. (1957). Calculation of maximum pavement temperatures from weather reports. *Highway Research Board bulletin*, *168*.

Baştanlar, Y., & Özuysal, M. (2014). Introduction to machine learning. *Methods in Molecular Biology USA*, 105–128. Totowa, NJ: Humana Press. https://doi.org/10.1007/978-1-62703-748-8_7

Bayat, A. (2009). *Field and Numerical Investigation to Determine the Impact of Environmental and Wheel Loads on Flexible Pavement*. Doctoral thesis. University of Waterloo, Canada.

Birgisson, B., Ovik, J., & Newcomb, D.E. (2000). Analytical predictions of seasonal variations in flexible pavements: Minnesota road research project site. *Transportation research record*, *1730*(1), 81-90.

Bohra, N. C., Altschaeffl, A. G., Drumm, E. C., Reeves, J. S., Madgett, M. R., & Trolinger, W. D. (1999). Subgrade resilient modulus correction for saturation effects. *Journal of Geotechnical and Geoenvironmental Engineering, 125*(3), 233–235. https://doi.org/10.1061/(ASCE)1090-0241(1999)125:3(233)

Bonaccorso, G. (2018). *Machine Learning Algorithms: Popular algorithms for data science and machine learning*. Packt Publishing Ltd.

Bradley, A. H., Ahammed, M. A., Hilderman, S., & Kass, S. (2012). Responding to climate change with rational approaches for managing seasonal weight programs in Manitoba. In *Cold Regions Engineering 2012: Sustainable Infrastructure Development in a Changing Cold Environment*(pp. 391-401).

Bulut, R., Muraleetharan, K. K., Zaman, M., Yue, E., Soltani, H., & Hossain, Z. (2013). Evaluation of the Enhanced Integrated Climatic Model for modulus-based construction specification for Oklahoma pavements (No. OTCREOS11. 1-10-F). Oklahoma Transportation Center.

Canada Cartage Group of Companies. (2021, February 26). 2021 CANADIAN SPRING THAW REGULATIONS (UPDATED). Available from: https://www.canadacartage.com/2021-canadian-spring-thaw-regulations/ [Accessed 31 May 2022].

Canada Energy Regulator. Provincial and Territorial Energy Profiles – Alberta. https://www.cer-rec.gc.ca/en/data-analysis/energy-markets/provincial-territorial-energy-profiles/provincial-territorial-energy-profiles-alberta.html. Accessed July 13, 2022.

Chao, W. L. (2011). *Machine learning tutorial*. Digital Image and Signal Processing. National Taiwan University, Taiwan.

Chen, J., Wang, H., & Xie, P. (2019). Pavement temperature prediction: Theoretical models and critical affecting factors. *Applied Thermal Engineering*, 158, 113755. https://doi.org/10.1016/j.applthermaleng.2019.113755

Chen, L., Chen, J., Wang, C., Dai, Y., Guo, R., & Huang, Q. (2021). Modeling of moisture content of subgrade materials in high-speed railway using a deep learning method. *Advances in Materials Science and Engineering*, *2021*, 1-9.

Christopher, B. R., Schwartz, C. W., & Boudreau, R. L. (2010). *Geotechnical aspects of pavements: Reference manual.* US Department of Transportation, Federal Highway Administration.

Christopher, B. R., Schwartz, C., & Boudreau, R.(2006). *Geotechnical aspects of pavements (ReportNo.FHWANHI-05-037).* US Department of Transportation, Federal Highway Administration.

Chuvilin, E. M., Sokolova, N. S., Bukhanov, B. A., Istomin, V. A., & Mingareeva, G. R. (2020).

Determination of the freezing point of soils based on measurements of pore water potential.

Earth's Cryosphere, *24*, 9-16.

City of Edmonton Transportation, Canada. (2012). Roadway Design Standard Construction Specifications. <http://www.edmonton.ca/city _government/documents/RoadsTraffic/Volume_2_-_Roadways_May _2012.pdf> (March 1, 2015)

Cortes, C., Vapnik, V., & Saitta, L. (1995). Support-Vector Networks Editor. *Machine Leaming*, 20, pp. 273-297. https://doi.org/10.1007/BF00994018

Côté, J., & Konrad, J. M. (2002). A Field Study of Hoarfrost Formation on Insulated Pavements. *Canadian Geotechnical Journal*, *39*(3), 547–560. https://doi.org/10.1139/t02-007

Côté, J., & Konrad, J. M. (2005). A Numerical Approach to Evaluate the Risk of Differential Surface Icing on Pavements with Insulated Sections. *Cold Regions Science and Technology*, *43*(3), 187–206. https://doi.org/10.1016/j.coldregions.2005.05.004

Côté, J., & Konrad, J. M. (2006). Granular Protection Design to Minimize Differential Icing on Insulated Pavements. *Canadian Geotechnical Journal*, *43*(3), 260–272. https://doi.org/10.1139/t06-002

Côté, J., & Konrad, J. M. (2005). Thermal conductivity of base-course materials. *Canadian Geotechnical Journal, 42*(1), 61–78.

Cristianini, N., & Shawe-Taylor, J. (2000). *An introduction to support vector machines and other kernel-based learning methods.* Cambridge university press.

Croney, D., & Coleman, J. D. (1948). Soil Thermodynamics Applied to the Movement of Moisture in Road Foundations. *Transportation Research Board*, Washington, D.C. https://trid.trb.org/view/125294

D'Amico, F., Guattari, C., & Benedetto, A. (2010, June). GPR signal processing in frequency domain using artificial neural network for water content prediction in unsaturated subgrade. In *Proceedings of the XIII Internarional Conference on Ground Penetrating Radar*,1–6. https://doi.org/10.1109/ICGPR.2010.5550076

Dong, Q., and Huang, B. (2015). Failure Probability of Resurfaced Preventive Maintenance Treatments: Investigation into Long-Term Pavement Performance Program. *Transportation Research Record*, 2481(1), 65–74.

Doré, G., Drouin, P., Pierre, P., & Desrochers, P. (2005). *Estimation of the Relationships of Road Deterioration to Traffic and Weather in Canada.* Transport Canada, Final Report. BPR inc., Québec, QC.

Dumais, S., & Doré, G. (2016). An albedo based model for the calculation of pavement surface temperatures in permafrost regions. *Cold Regions Science and Technology*, *123*, 44–52.

Edgar, T., Mathis, R., & Potter, C. (2015). Injection of Structural Polymer Foam to Control Highway Frost Heave. Presented at Airfield and Highway Pavements 2015, Miami, FL.

El-Maaty, A. E. A. (2017). Temperature Change Implications for Flexible Pavement Performance and Life. *International Journal of Transportation Engineering and Technology*, *3*(1), 1. https://doi.org/10.11648/j.ijtet.20170301.11

Elseifi, M. A., Al-qadi, I. L., Asce, F., & Yoo, P. J. (2006). Viscoelastic Modeling and Field Validation of Flexible Pavements. *Journal of Engineering Mechanics*, *132*(2), 172–178. https://doi.org/10.1061/(ASCE)0733-9399(2006)132

Esch, D. C. (1972). *Control of Permafrost Degradation Beneath a Roadway by Subgrade Insulation*. Alaska Department of Transportation and Public Facilities, Juneau, AK.

Fathi, A., Mazari, M., Saghafi, M., Hosseini, A., & Kumar, S. (2019). Parametric study of pavement deterioration using machine learning algorithms. In *Airfield and Highway Pavements 2019: Innovation and Sustainability in Highway and Airfield Pavement Technology* (pp. 31–41). American Society of Civil Engineers Reston, VA: ASCE.

Field, D. A., Ruban, T., Johnston, A., Dixon, D., & Lewycky, D. (2011). Edmonton experience with bottom ash and other insulating materials for mitigation of frost heave induced damage

in pavements. In *2011 Conference and Exhibition of the Transportation Association of Canada. Transportation Successes: Let's Build on them. 2011 Congress et Exhibition de l'Association des Transports du Canada. Les Succes en Transports: Une Tremplin vers l'AvenirTransportation Association of Canada (TAC).*

Foresee, F. D., & Hagan, M. T. (1997, June). Gauss-Newton approximation to Bayesian learning. In *Proceedings of international conference on neural networks (ICNN'97)* (Vol. 3, pp. 1930-1935). IEEE.

Forteza, R., Far, M., Seguı, C., & Cerdá, V. (2004). Characterization of Bottom Ash in Municipal Solid Waste Incinerators for Its Use in Road Base. *Waste Management*, *24*(9), 899–909.

Fredlund, D. G., Bergan, A. T., & Wong, P. K. (1977). Relation between resilient modulus and stress conditions for cohesive subgrade soils. *Transportation Research Record*, *642* (Aug): 73–81.

Fujita, Y., Shimada, K., Ichihara, M., & Hamamoto, Y. (2017). A method based on machine learning using hand-crafted features for crack detection from asphalt pavement surface images. *Thirteenth International Conference on Quality Control by Artificial Vision 2017*, *10338*, 103380I. https://doi.org/10.1117/12.2264075

Government of Alberta. (2023). Road restrictions and bans – Overview. [online]. Available from: https://www.alberta.ca/road-restrictions-and-bans-overview.aspx#jumplinks-2 [Accessed 31 May 2022].

Gungor, O. E., and Al-Qadi, I. L. (2018). Developing Machine-Learning Models to Predict Airfield Pavement Responses. *Transportation Research Record*, *2672*(29), 23–34. https://doi.org/10.1177/0361198118780681

Hagan, M. T., & Menhaj, M. B. (1994). Training feedforward networks with the Marquardt algorithm. *IEEE Transactions on Neural Networks*, *5*(6), 989–993.

Haghi, N. T., Ahmadian, N. M. M., Hashemian, L., & Bayat, A. (2019). Capital Cost Comparison of Pavements Comprised of Insulation Layers: Case Study in Edmonton, Canada. *Journal of Construction Engineering and Management*, *145*, 1–8.

Haghi, N. T., Hashemian, L., & Bayat, A. (2016). Effects of seasonal variation on the load-bearing capacity of pavements composed of insulation layers. *Transportation Research*

Record: Journal of the Transportation Research Board, 2579(1), 87–95. https://doi.org/10.3141/2579-10

Haghi, N. T., Hashemian, L., & Bayat, A. (2018). The Effect of Insulation Layers on Pavement Strength During Non-Freeze–Thaw Season. *International Journal of Pavement Engineering*, *19*, 543–552.

Haghi, N. T., Hashemian, L., & Bayat, A. (2019). Seasonal response and damage evaluation of pavements comprised of insulation layers. *International Journal of Pavement Research and Technology, 12*(2), 170–177. https://doi.org/10.1007/s42947-019-0022-3

Haghi, N. T., Nassiri, S., Shafiee, M. H., & Bayat, A. (2014). Using field data to evaluate bottom ash as pavement insulation layer. *Transportation Research Record: Journal of the Transportation Research Board, 2433*(1), 39–47. https://doi.org/10.3141/2433-05

Haghi, N.T., Hashemian, L., & Bayat, A. (2016). Effects of seasonal variation on the load-bearing capacity of pavements composed of insulation layers. *Transportation Research Record*, *2579*(1), 87-95.

Haghi, N.T., Nassiri, S., Shafiee, M. H., & Bayat, A. (2014). Using field data to evaluate bottom ash as pavement insulation layer. *Transportation Research Record*, *2433*(1), 39-47.

Haghi, S. N. T. (2019). *Use of waste/recycled material as insulation in road construction* [doctoral thesis]. University of Alberta. University of Alberta Library.

Hall, K. D., & Rao, S. (1999). Predicting subgrade moisture content for low-volume pavement design using in situ moisture content data. *Transportation Research Record*, *2*(1652), 98–107. https://doi.org/10.3141/1652-47

Hashemian, L., & Bayat, A. (2016). Three Years' Monitoring of Instrumented Test Road. *Proc., International Conference on Accelerated Pavement Testing (APT),* San Jose, Costa Rica.

Hashemian, L., & Bayat, A. (2018). Field Evaluation of Load-Bearing Capacity of Tire Fill Embankment Pavements. *Journal of Testing and Evaluation*, *46*(5), 1901–1910. https://doi.org/10.1520/JTE20160667.

Hayden, R. L., & Swanson, H. N. (1972). *Styrofoam Highway Insulation on Colorado Mountain Passes.* Report CDOH-P&R-R&SS-72-6. Colorado Division of Highways, Denver, CO.

Hazen, A. (1892). *Some Physical Properties of Sands and Gravels*. 24th Annual Report of the State Department of Health of Massachusetts. State Board of Health of Massachusetts, Boston, MA.

Hedayati, M., & Hossain, S. (2015). Data based model to estimate subgrade moisture variation case study: Low volume pavement in North Texas. *Transportation Geotechnics, 3*, 48–57. https://doi.org/10.1016/j.trgeo.2015.03.001

Hedayati, M., Hossain, M. S., Mehdibeigi, A., & Thian, B. (2014). Real-time modeling of moisture distribution in subgrade soils. *Geo-Congress 2014: Geo-Characterization and Modeling for Sustainability*, 3015–3024.

Hermansson, A. (2000). Simulation model for calculating pavement temperatures including maximum temperature. *Transportation Research Record*, *1699*, 134–141. https://doi.org/10.3141/1699-19

Hermansson, Å. (2004). Mathematical model for paved surface summer and winter temperature : comparison of calculated and measured temperatures. *Cold Regions Science and Technology, 40*, 1–17. https://doi.org/10.1016/j.coldregions.2004.03.001

Heydinger, A. G. (2003a). Evaluation of Seasonal Effects on Subgrade Soils. *Transportation Research Record*, *1821*, 47–55. https://doi.org/10.3141/1821-06

Heydinger, A. (2003b). *Monitoring seasonal instrumentation and modeling climatic effects on pavement at the ohio/shrp test road*. Report No. FHWA/OH-2003/018. U.S. Department of Transportation.

Hoekstra, P. (1967, September 25–7 October). *Moisture movement to a freezing front*. International Union of Geodesy and Geophysics.

Hou, Y., Li, Q., Zhang, C., Lu, G., Ye, Z., Chen, Y., Wang, L., & Cao, D. (2021). The state-of-the-art review on applications of intrusive sensing, image processing techniques, and machine learning methods in pavement monitoring and analysis. Engineering, 7(6), 845–856. https://doi.org/10.1016/j.eng.2020.07.030

Huang, W. H. (1990). *The Use of Bottom Ash in Highway Embankment and Pavement Construction.* Doctoral dissertation. Purdue University, West Lafayette, Indiana.

Huang, Y., M. Molavi Nojumi, M., Hashemian, L., & Bayat, A. (2021). Performance Evaluation of Different Insulating Materials using Field Temperature and Moisture Data.

Transportation Research Record: Journal of the Transportation Research Board, *2675*(9): 595–607.

Huang, Y., Molavi Nojumi, M., Ansari, S., Hashemian, L., & Bayat, A. (2023a). Evaluating the use of machine learning for moisture content prediction in base and subgrade layers. *Road Materials and Pavement Design*, 1-19.

Huang, Y., Molavi Nojumi, M., Ansari, S., Hashemian, L., & Bayat, A. (2023b). Evaluation of machine learning approach for base and subgrade layer temperature prediction at various depths in the presence of insulation layers. *International Journal of Pavement Engineering*, *24*(1), 2180640.

Huang, Y., Molavi Nojumi, M., Hashemian, L., & Bayat, A. (2023). Evaluation of a machine learning approach for temperature prediction in pavement base and subgrade layers in Alberta, Canada. *Journal of Transportation Engineering, Part B: Pavements, 149*, 04022076. https://doi.org/10.1061/JPEODX.PVENG-1010

Inkoom, S., Sobanjo, J., Barbu, A., & Niu, X. (2019). Prediction of the crack condition of highway pavements using machine learning models. *Structure and Infrastructure Engineering*, *15*(7), 940–953. https://doi.org/10.1080/15732479.2019.1581230

Islam, M. R., Ahsan, S., & Tarefder, R. A. (2015). Modeling temperature profile of hot-mix asphalt in flexible pavement. *International Journal of Pavement Research and Technology*, *8*(1), 47–52.

Janoo, V., & Shepherd, K. (2000). Seasonal variation of moisture and subsurface layer moduli. *Transportation research record*, *1709*(1), 98-107.

Jin, X., Yang, W., Gao, X., Zhao, J. Q., Li, Z., & Jiang, J. (2020). Modeling the unfrozen water content of frozen soil based on the absorption effects of clay surfaces. *Water Resources Research, 56*(12), 1–16. https://doi.org/10.1029/2020WR027482

Justo-Silva, R., Ferreira, A., & Flintsch, G. (2021). Review on machine learning techniques for developing pavement performance prediction models. *Sustainability, 13*(9), 5248. https://doi.org/10.3390/su13095248

Kahimba, F. C., & Ranjan, R. S. (2007). Soil temperature correction of field TDR readings obtained under near freezing conditions. *Canadian Biosystems Engineering, 49*,1.

Kang, C., Huang, S., & Bayat, A. (2021). Compressibility Characteristics of TDA from OTR (off-the-Road) Tires: A Numerical Approach. *Transportation Geotechnics*, *29*, 100561.

Klein, R., Nestle, N., Niessner, R., & Baumann, T. (2003). Numerical modelling of the generation and transport of heat in a bottom ash monofill. *Journal of hazardous materials*, *100*(1-3), 147-162.

Kozlowski, T. (2007). A semi-empirical model for phase composition of water in clay–water systems. *Cold Regions Science and Technology, 49*(3), 226–236. https://doi.org/10.1016/j.coldregions.2007.03.013

Lei, S., Daniels, J. L., Bian, Z., & Wainaina, N. (2011). Improved soil temperature modeling. *Environmental Earth Sciences*, *62*(6), 1123–1130. https://doi.org/10.1007/s12665-010-0600-9

Li, Y., Liu, L., & Sun, L. (2018). Temperature predictions for asphalt pavement with thick asphalt layer. *Construction and Building Materials*, *160*, 802–809. https://doi.org/10.1016/j.conbuildmat.2017.12.145

Liu, B., Yan, S., You, H., Dong, Y., Li, Y., Lang, J., & Gu, R. (2018). Road surface temperature prediction based on gradient extreme learning machine boosting. *Computers in Industry*, *99* (Aug), 294–302. https://doi.org/10.1016/j.compind.2018.03.026.

López, E. L., Vega-Zamanillo, Á., Pérez, M. A. C., & Hernández-Sanz, A. (2015). Bearing Capacity of Bottom Ash and Its Mixture with Soils. *Soils and Foundations*, *55*(3), 529–535.

MacKay, D. J. C. (1992). Bayesian interpolation. *Neural Computation*, *4*(3), 415–447.

Mahoney, J. P., Rutherford, M. S., & Hicks, R. G. (1987). *Guidelines for spring highway use restrictions* (No. FHWA-TS-87-209).

Marcelino, P., M. D. L. Antunes, E. Fortunato, & M. C. Gomes. (2019). Machine learning approach for pavement performance prediction. . *International Journal of Pavement Engineering*, *22* (3): 341–354. https://doi.org/10.1080/10298436.2019.1609673.

Marquardt, D. W. (1963). An algorithm for least-squares estimation of nonlinear parameters. *Journal of the Society for Industrial and Applied Mathematics*, *11*(2), 431–441.

Meles, D., Bayat, A., Shafiee, M. H., Nassiri, S., & Gul, M. (2014). Investigation of Tire Derived Aggregate as a Fill Material for Highway Embankment. International Journal of

Geotechnical Engineering, *8*(2), 182–190. https://doi.org/10.1179/1939787913Y.0000000015.

Milad, A. A., Adwan, I., Majeed, S. A., Memon, Z. A., Bilema, M., Omar, H. A., Abdolrasol, M. G. M., Usman, A., & Yusoff, N. I. M. (2021). Development of a Hybrid Machine Learning Model for Asphalt Pavement Temperature Prediction. *IEEE Access*, *9*, 158041–158056. https://doi.org/10.1109/ACCESS.2021.3129979

Milad, A., Adwan, I., Majeed, S. A., Yusoff, N. I. M., Al-Ansari, N., & Yaseen, Z. M. (2021). Emerging Technologies of Deep Learning Models Development for Pavement Temperature Prediction. *IEEE Access*, *9*, 23840–23849. https://doi.org/10.1109/ACCESS.2021.3056568

Miller, H. J., Cabral, C., Kestler, M. A., & Berg, R. (2015). Aurora SPR-3 (042), Phase 1: Review of Seasonal Weight Restriction Models for Comparison and Demonstration Project. Presented at 94th Annual Meeting of the Transportation Research Board, Washington, D.C.

Miller, H., Cabral, C., Kestler, M., Berg, R., & Eaton, R. (2012). Calibration of a freeze-thaw prediction model for spring load restriction timing in northern New England. *In: Cold Regions Engineering 2012: Sustainable Infrastructure Development in a Changing Cold Environment*, 19-22 August 2012 Quebec. American Society of Civil Engineers, 369-379.

Minhoto, M. J. C., Pais, J. C., Pereira, P. A. A., & Picado-santos, L. G. (2005). Predicting Asphalt Pavement Temperature with a Three-Dimensional Finite Element Method. *Transportation Research Record. 1919* (1): 96–110. https://doi.org/10.1177/0361198105191900111.

Minnesota Department of Transportation. (2014). *Policy and Process for Seasonal Load Limit Starting and Ending Date*.

Mohamed, H. (2014). *Quantification of Environmental Impacts on the Performance of Asphalt Pavements.* Doctoral dissertation. University of Idaho, Moscow.

Mohammed, S.A., & Karim, M.R. (2017, June). Application of coal bottom ash as aggregate replacement in highway embankment, acoustic absorbing wall and asphalt mixtures. *In: IOP Conference Series: Materials Science and Engineering*. IOP Publishing.

Mohseni, A. (1998). *LTPP seasonal asphalt concrete (AC) pavement temperature models*. United States. Federal Highway Administration. Office of Engineering Research and Development.

Molavi Nojumi, M., Huang, Y., Hashemian, L., & Bayat, A. (2022). Application of Machine Learning for Temperature Prediction in a Test Road in Alberta. *International Journal of Pavement Research and Technology*, *15*(2), 303–319. https://doi.org/10.1007/s42947-021-00023-3

Møller, M. F. (1993). A scaled conjugate gradient algorithm for fast supervised learning. *Neural networks*, *6*(4), 525-533.

Mrawira, D. M., & Luca, J. (2002). Thermal properties and transient temperature response of full-depth asphalt pavements. *Transportation Research Record*, *1809*, 160–171. https://doi.org/10.3141/1809-18

Nassiri, S., Bayat, A., & Skirrow, R. (2013). Integrated Road Research Facility (IRRF): An Alberta Research Initiative. *In: 2013 conference and exhibition of the transportation association of Canada-transportation: better-faster-safer,* 22-25 September 2013 Winnipeg. 1-18.

National Snow & Ice Data Center. Air Freezing Index. https://nsidc.org/learn/cryosphere-glossary/air-freezing-index. Accessed November 19, 2022.

Nitsche, P., Stütz, R., Kammer, M., & Maurer, P. (2014). Comparison of machine learning methods for evaluating pavement roughness based on vehicle response. *Journal of Computing in Civil Engineering, 28* (4): 4014015. https://doi.org/10.1061/(ASCE)CP.1943-5487.0000285.

Nivedya, M. K., & Mallick, R. B. (2020). A multi-structure multi-run range (MSMRR) approach for using machine learning with constrained data in pavement engineering. *SN Applied Sciences*, *2*(3). https://doi.org/10.1007/s42452-020-2233-2

Nojumi, M. M., Huang, Y., Hashemian, L., & Bayat, A. (2021). Application of machine learning for temperature prediction in a test road in Alberta. *International Journal of Pavement Research and Technology*, *15* (2): 303–319. https://doi.org/10.1007/s42947-021-00023-3.

Oh, J., Ryu, D., Fernando, E. G., & Lytton, R. L. (2006). Estimation of expected moisture contents for pavements by environmental and soil characteristics. *Transportation Research Record*, *1967*(1), 134–147.

Olidis, C., & Hein, D. (2004, September). Guide for the mechanistic-empirical design of new and rehabilitated pavement structures materials characterization: Is your agency ready. In *2004 annual conference of the transportation association of Canada*.

Patterson, D. E., & Smith, M. W. (1980). The use of time domain reflectometry for the measurement of unfrozen water content in frozen soils. *Cold Regions Science and Technology, 3*(2-3), 205–210. https://doi.org/10.1016/0165-232X(80)90026-9

Penner, E. (1967). Experimental pavement structures insulated with a polyurethane and extruded polystyrene foam. *Physics of Snow and Ice: Proceedings*, *1*(2), 1311-1322.

Popik, M., Olidis, C., & Tighe, S. (2005). "The effect of seasonal variations on the resilient modulus of unbound materials." In *Proc., TAC/ATC 2005-2005 Annual Conf. and Exhibition of the Transportation Association of Canada: Transportation—Investing in Our Future*, 3–5. Calgary, AB, Canada: Transportation Association of Canada.

Qin, Y. (2016). Pavement surface maximum temperature increases linearly with solar absorption and reciprocal thermal inertial. *International Journal of Heat and Mass Transfer*, *97*, 391–399. https://doi.org/10.1016/j.ijheatmasstransfer.2016.02.032

Qiu, X., Hong, H., Xu, W., Yang, Q., & Xiao, S. (2020). August. Surface temperature prediction of asphalt pavement based on APRIORI-GBDT. *In: International Conference on Transportation and Development 2020*. Reston, VA: American Society of Civil Engineers, 200-212.

Qiu, X., Xu, W. Y., Zhang, Z. H., Li, N. N., & Hong, H. J. (2020). Surface Temperature Prediction of Asphalt Pavement Based on GBDT. *IOP Conference Series: Materials Science and Engineering*, *758*(1). https://doi.org/10.1088/1757-899X/758/1/012031

Roth, C. H., Malicki, M. A., & Plagge, R. (1992). Empirical evaluation of the relationship between soil dielectric constant and volumetric water content as the basis for calibrating soil moisture measurements by TDR. *Journal of Soil Science*, *43*(1), 1-13.

Saarelainen, S. (1996). Pavement design applying allowable frost heave. In *Cold regions engineering: The cold regions infrastructure – An international imperative for the 21st century*, 890–898.

Sarkar, R., & Dawson, A. R. (2017). Economic assessment of use of pond ash in pavements.

International Journal of Pavement Engineering, 18(7), 578-594.

Salem, H. M. A. (2004). *Quantification of Environmental Impacts on the Performance of Asphalt Pavements.* Doctoral dissertation. University of Idaho, Moscow, ID.

Salour, F. A. (2015). *Moisture Influence on Structural Behaviour of Pavements*. Doctoral thesis. School of Architecture and the Built Environment, Royal Institute of Technology, Stockholm, Sweden.

Salour, F., & Erlingsson, S. (2013). Investigation of a pavement structural behaviour during spring thaw using falling weight deflectometer. *Road Materials and Pavement Design*, *14*(1), 141–158.

Schulz, E., Speekenbrink, M., & Krause, A. (2018). A tutorial on Gaussian process regression: Modelling, exploring, and exploiting functions. *Journal of Mathematical Psychology*, *85*, 1-16.

Simonsen, E., Janoo, V. C., & Isacsson, U. (2002). Resilient properties of unbound road materials during seasonal frost conditions. *Journal of Cold Regions Engineering*, *16*(1), 28–50.

Skierucha, W., Wilczek, A., Szypłowska, A., Sławiński, C., & Lamorski, K. (2012). A TDR-based soil moisture monitoring system with simultaneous measurement of soil temperature and electrical conductivity. Sensors, 12(10), 13545-13566.

Smith, B. S. (2006). *Design and construction of pavements in cold regions: state of the practice*. Thesis (Master). Brigham Young University.

Solaimanian, M., & Kennedy, T. W. (1993). Predicting Maximum Pavement Surface Temperature Using Maximum Air Temperature and Hourly Solar Radiation. *Transportation Research Record*, *1417*, 1–11. http://onlinepubs.trb.org/Onlinepubs/trr/1993/1417/1417-001.pdf

Stein, J., & Kane, D. L. (1983). Monitoring the unfrozen water content of soil and snow using time domain reflectometry. *Water Resources Research, 19*(6), 1573–1584. https://doi.org/10.1029/WR019i006p01573

Swiler, L., Gulian, M., Frankel, A., Safta, C., & Jakeman, J. (2020). A survey of constrained Gaussian process regression: Approaches and implementation challenges. *Journal of Machine Learning for Modeling and Computing*, *1*(2), 119-156. DOI: 10.1615/JMachLearnModelComput.2020035155

Tabrizi, S. E., Xiao, K., Thé, J. V. G., Saad, M., Farghaly, H., Yang, S. X., & Gharabaghi, B. (2021). Hourly road pavement surface temperature forecasting using deep learning models. *Journal of Hydrology*, *603*, 126877.

Tatarniuk, C., & Lewycky, D. (2011). A Case Study on the Performance of High Load Polystyrene as Roadway Insula-tion in Edmonton, Alberta, Canada. *Proc., Annual Conference of Transportation Association of Canada*, Alberta, Canada.

Teltayev, B. B., & Suppes, E. A. (2019). Temperature in pavement and subgrade and its effect on moisture. *Case Studies in Thermal Engineering, 13*, 1–11. https://doi.org/10.1016/j.csite.2018.11.014

Tholen, O., J. Sharma, & R. L. Terrel. Comparison of Falling Weight Deflectometer with Other Deflection Testing Devices. *Transportation Research Record: Journal of the Transportation Research Board*, 1985. 1007: 20–26.

Thompson, M. R., Dempsey, B. J., Hill, H., & Vogel, J. (1987). Characterizing Temperature Effects for Pavement Analysis and Design. *Transportation Research Record: Journal of the Transportation Research Board*, *1121*, 14–22.

Tighe, S. L., Cowe Falls, L., Haas, R., & MacLeod, D. (2006). Climate Impacts and Adaptations on Roads in Northern Canada. Presented at 55th Annual Meeting of the Transportation Research Board, Washington, D.C.

Tighe, S. L., Cowe Falls, L., Haas, R., & MacLeod, D. (2006). *Climate impacts and adaptations on roads in northern Canada*. In *Proc., Transportation Research Board 85th Annual Meeting,* Washington, DC: Transportation Research Board.

Topp, G. C., Davis, J. L., &Annan, A. P. (1980). Electromagnetic determination of soil water content: Measurements in coaxial transmission lines. *Water Resources Research, 16*(3), 574–582. https://doi.org/10.1029/WR016i003p00574

Utilities, A. T. and. (1997). Pavement design manual. *Alberta Transportation and Utilities*.

Uzarowski, L., Rizvi, R., Krzewinski, T. G., Ulring, J. D., & Maher, M. L. J. (2013). Maher. Runway Pavement Rehabilitation Design and Construction in Remote Areas in the North–Case Study. Presented at ISCORD 2013: Planning for Sustainable Cold Regions, Alaska. AASHTO. (2008). Mechanistic Empirical Pavement Design Guide: A Manual Practice. In *American Association of State Highway and Transportation Officials* (Issue July).

Watanabe, K., & Wake, T. (2009). Measurement of unfrozen water content and relative permittivity of frozen unsaturated soil using NMR and TDR. *Cold Regions Science and Technology, 59*(1), 34–41. https://doi.org/10.1016/j.coldregions.2009.05.011

Witczak, M. W., Andrei, D., & Houston, W. N. (2000). Guide for mechanistic-empirical design of new and rehabilitated pavement structures. Appendix DD-1: Resilient modulus as function of soil moisture—Summary of predictive models. *Final report to National Cooperative Highway Research Program, Report*, (1-37A).

Xing, C., Chen, N., Zhang, X., & Gong, J. (2017). A machine learning based reconstruction method for satellite remote sensing of soil moisture images with in situ observations. *Remote Sensing, 9*(5), 484. https://doi.org/10.3390/rs9050484

Xu, B., Dan, H. C., & Li, L. (2017). Temperature prediction model of asphalt pavement in cold regions based on an improved BP neural network. *Applied Thermal Engineering*, *120*(Mar), 568–580. https://doi.org/10.1016/j.applthermaleng.2017.04.024

Xu, B., Ranjithan, S. R., & Kim, Y. R. (2002). New Condition Assessment Procedure for Asphalt Pavement Layers, Using Falling Weight Deflectometer Deflections. *Transportation Research Record: Journal of the Transportation Research Board*, *1806(*1): 57–69.

Zach. (2021). RMSE vs. R-Squared: Which Metric Should You Use? [online] Statology Study. Available from: https://www.statology.org/rmse-vs-r-squared/ [Accessed 1 December 2021].

Zapata, C. E., & Houston, W. N. (2008). *Calibration and validation of the enhanced integrated climatic model for pavement design*. Transportation Research Board.

Zeiada, W., Dabous, S. A., Hamad, K., Al-ruzouq, R., & Khalil, M. A. (2020). Machine Learning for Pavement Performance Modelling in Warm Climate Regions. *Arabian Journal for Science and Engineering*, *45*(5), 4091–4109. https://doi.org/10.1007/s13369-020-04398-6

Zeng, A., Ho, H., & Yu, Y. (2020). Prediction of building electricity usage using Gaussian Process Regression. *Journal of Building Engineering, 28*, Article 101054. https://doi.org/10.1016/j.jobe.2019.101054

Zhang, J., Little, D. N., Hariharan, N.,& Kim, Y. R. (2019). Prediction of climate specific vertical movement of pavements with expansive soils based on long-term 2D numerical

simulation of rainwater infiltration. *Computers and Geotechnics*, *115,* Article 103172. https://doi.org/10.1016/j.compgeo.2019.103172

Zheng, J., & Zhang, R. (2013). Prediction and application of equilibrium water content of expansive soil subgrade. In *IACGE 2013: Challenges and Recent Advances in Geotechnical and Seismic Research and Practices*, 754–761. https://doi.org/10.1061/9780784413128.087

Zhou, X., Zhou, J., Kinzelbach, W., & Stauffer, F. (2014). Simultaneous measurement of unfrozen water content and ice content in frozen soil using gamma ray attenuation and TDR. *Water Resources Research*, *50*(12), 9630–9655. https://doi.org/10.1002/2014WR015640

Zhou, Z., Li, G., Shen, M., & Wang, Q. (2022). Dynamic responses of frozen subgrade soil exposed to freeze-thaw cycles. *Soil Dynamics and Earthquake Engineering, 152*, Article 107010. doi:10.1016/j.soildyn.2021.107010